NUREG/CR-5694

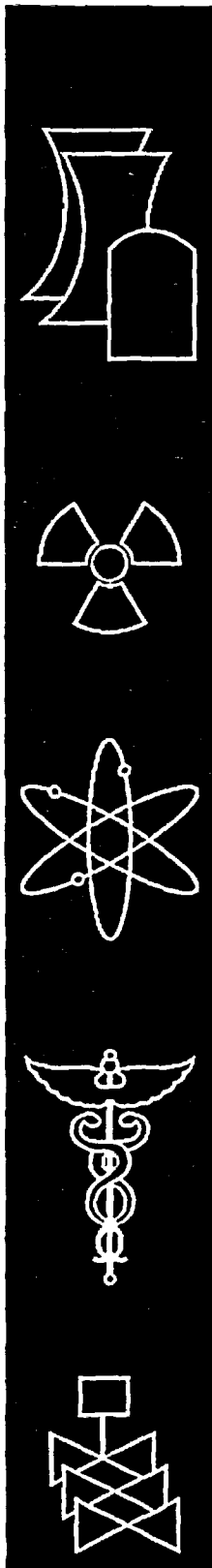

Results of Field Studies at the Maricopa Environmental Monitoring Site, Arizona

University of Arizona

U.S. Nuclear Regulatory Commission
Office of Nuclear Regulatory Research
Washington, DC 20555-0001

AVAILABILITY NOTICE

Availability of Reference Materials Cited in NRC Publications

NRC publications in the NUREG series, NRC regulations, and *Title 10, Energy,* of the *Code of Federal Regulations,* may be purchased from one of the following sources:

1. The Superintendent of Documents
   U.S. Government Printing Office
   P.O. Box 37082
   Washington, DC 20402–9328
   <http://www.access.gpo.gov/su_docs>
   202–512–1800

2. The National Technical Information Service
   Springfield, VA 22161–0002
   <http://www.ntis.gov/ordernow>
   703–487–4650

The NUREG series comprises (1) brochures (NUREG/BR-XXXX), (2) proceedings of conferences (NUREG/CP-XXXX), (3) reports resulting from international agreements (NUREG/IA-XXXX), (4) technical and administrative reports and books [(NUREG-XXXX) or (NUREG/CR-XXXX)], and (5) compilations of legal decisions and orders of the Commission and Atomic and Safety Licensing Boards and of Office Directors' decisions under Section 2.206 of NRC's regulations (NUREG-XXXX).

A single copy of each NRC draft report is available free, to the extent of supply, upon written request as follows:

Address: Office of the Chief Information Officer
Reproduction and Distribution
Services Section
U.S. Nuclear Regulatory Commission
Washington, DC 20555–0001
E–mail: <DISTRIBUTION@nrc.gov>
Facsimile: 301–415–2289

A portion of NRC regulatory and technical information is available at NRC's World Wide Web site:

<http://www.nrc.gov>

All NRC documents released to the public are available for inspection or copying for a fee, in paper, microfiche, or, in some cases, diskette, from the Public Document Room (PDR):

NRC Public Document Room
2120 L Street, N.W., Lower Level
Washington, DC 20555–0001
<http://www.nrc.gov/NRC/PDR/pdr1.htm>
1–800–397–4209 or locally 202–634–3273

Microfiche of most NRC documents made publicly available since January 1981 may be found in the Local Public Document Rooms (LPDRs) located in the vicinity of nuclear power plants. The locations of the LPDRs may be obtained from the PDR (see previous paragraph) or through:

<http://www.nrc.gov/NRC/NUREGS/SR1350/V9/lpdr/html>

Publicly released documents include, to name a few, NUREG-series reports; *Federal Register* notices; applicant, licensee, and vendor documents and correspondence; NRC correspondence and internal memoranda; bulletins and information notices; inspection and investigation reports; licensee event reports; and Commission papers and their attachments.

Documents available from public and special technical libraries include all open literature items, such as books, journal articles, and transactions, *Federal Register* notices, Federal and State legislation, and congressional reports. Such documents as theses, dissertations, foreign reports and translations, and non-NRC conference proceedings may be purchased from their sponsoring organization.

Copies of industry codes and standards used in a substantive manner in the NRC regulatory process are maintained at the NRC Library, Two White Flint North, 11545 Rockville Pike, Rockville, MD 20852–2738. These standards are available in the library for reference use by the public. Codes and standards are usually copyrighted and may be purchased from the originating organization or, if they are American National Standards, from—

American National Standards Institute
11 West 42nd Street
New York, NY 10036–8002
<http://www.ansi.org>
212–642–4900

NUREG/CR-5694

Results of Field Studies at the Maricopa Environmental Monitoring Site, Arizona

Manuscript Completed: May 1999
Date Published: June 1999

Prepared by
M. H. Young*
P. J. Wierenga, A. W. Warrick, L. L. Hofmann**
S. A. Musil, M. Yao, C. J. Mai, Z. Zou**
B. R. Scanlon***

**Department of Soil, Water and Environmental Science
University of Arizona
Tucson, AZ 85721

Subcontractor:
***Bureau of Economic Geology
University of Texas at Austin
Austin, TX 78713

T. J. Nicholson, NRC Project Manager

Prepared for
Division of Risk Analysis and Applications
Office of Nuclear Regulatory Research
U.S. Nuclear Regulatory Commission
Washington, DC 20555-0001
NRC Job Code W6151

*Currently at School of Civil and Environmental Engineering
Georgia Institute of Technology
Atlanta, GA 30332-0512

ABSTRACT

The purpose of this study was to evaluate issues related to alternative monitoring strategies for sites containing low level radioactive wastes. The study consisted of a theoretical evaluation of monitoring strategies and field studies. This NUREG reports on the field activities and the results of the field experiments.

A field site, located at the Maricopa Agricultural Center (Maricopa, AZ) was designed for conducting controlled water flow and solute transport studies, and for testing the strengths and weaknesses of four monitoring strategies designated as 1) Monitoring Trench, 2) Monitoring Island, 3) Borehole Monitoring, and 4) Geophysical Monitoring. Field instrumentation was extensive, and designed to support alternative monitoring strategies. Two experiments were conducted at the site covering the time frame from Spring 1997 through Summer 1998. During Experiment 1, water was applied at an average flux of 1.85 cm d^{-1} to the 50 m by 50 m field plot for 24 days, with bromide tracer added for the first 15 days. The water application period was followed by a redistribution period of 69 days. During Experiment 2, water was applied at an average rate of 1.97 cm d^{-1} for 33 days with a redistribution period of 177 days. Field experiments ended officially on July 1, 1998.

Water movement across the plot was spatially variable during Experiment 1, due mostly to variability in the initial water content, and thus, the soil's hydraulic properties. The results of intrusive and non-intrusive instruments showed that 1) water movement in the western portion of the site was faster than the eastern portion; 2) a zone of more rapid water flow was observed near the northern and central areas of the plot, as confirmed using several types of instruments; and 3) the variability of water movement, as measured using a neutron probe, decreased with increasing depth. During Experiment 2, spatial variability of water movement was significantly reduced in surface soils (< 1.5 m), from a CV = 41.8 % to 4.7 % between Experiments 1 and 2, respectively. The reduced variability was observed because the flux-controlled water application led to more uniform hydraulic property fields, and thus, more uniform water movement. Most of the monitoring systems performed well during the field experiments. Though some data were lost (or considered unreliable) due to electrical problems with the AC power supply and corrosion of electrical connections, an extensive data set was compiled and found useful for comparing monitoring strategies.

CONTENTS

LIST OF FIGURES

TABLES

EXECUTIVE SUMMARY

U.S. Nuclear Regulatory staff identified a need for research to better assess unsaturated zone monitoring techniques and strategies applicable to LLW disposal facilities. The need was later expanded to include facilities designated under the Site Decommissioning Management Plan (SDMP). This research project originated from the need to evaluate a wide variety of issues related to alternative monitoring strategies, which could be used in long-term monitoring programs at disposal sites, and thus reviewed by NRC staff during the licensing process. Thus, field implementation and evaluation of alternative strategies were important and necessary components of this research project. The purpose of this NUREG is to report on the field activities and the results of the field experiments; a companion NUREG (NUREG/CR-5698, Young et al., 1999) directly compares the strengths and weaknesses of the monitoring strategies.

Goals of the research were to: 1) assess capabilities, limitations, and usefulness of alternative techniques for monitoring water movement and contaminant transport in the unsaturated zone of humid and arid areas; 2) provide the technical bases for identifying and evaluating appropriate techniques for unsaturated zone monitoring at LLW and SDMP sites; 3) develop guidance on the design, installation, use, and decommissioning of unsaturated zone monitoring systems; 4) examine the issue of whether and how unsaturated zone monitoring systems may compromise the performance of natural and engineered barriers at LLW facilities and how to eliminate or mitigate such compromises; and 5) test monitoring strategies and instrumentation on a variety of field scales using actual water and solute tracer application rates and geometries.

To achieve these goals, a field site was designed for conducting controlled water flow and solute transport studies, and for testing the strengths and weaknesses of four monitoring strategies. The site is located at the Maricopa Agricultural Center, Maricopa, AZ, a research facility which is located about 42 km southwest of Phoenix and operated by the University of Arizona. The field was extensively instrumented using commercially-available monitoring systems. The monitoring systems overlap each other considerably, permitting them to support more than one monitoring strategy. Briefly described, the strategies are: 1) Monitoring Trench strategy - a 60 m trench excavated to 1.5 m depth, into which 13 instrumentation clusters were installed at 5 m lateral spacing; 2) Monitoring Island strategy - two vertical culverts (1.55 m diameter) drilled to 3 m depth with monitoring instruments installed radially around the islands into undisturbed soil; 3) Borehole Monitoring strategy - vertical and horizontal access tubes (120 total), into which permanently-installed (tensiometers and solution samplers) or portable sensors (neutron probe) were inserted for taking measurements; and 4) Geophysical Monitoring strategy - incorporated permanently-installed (ERT; 12 locations) and portable (EM-31, EM-38; 90 locations each) sensors for monitoring changes in bulk electrical conductivity and resistivity.

Two experiments were conducted at the site covering the time frame from Spring 1997 through Summer 1998. During Experiment 1, water at an average flux of 1.85 cm d^{-1} was applied to the 50 m by 50 m field plot for 24 days for a total application of 44.4 cm. Bromide was added as a tracer for the first 15 days. Redistribution occurred for 69 days before the experiment ended. During Experiment 2, water at an average rate of 1.97 cm d^{-1} was applied to the soil for 33 days for a total application of 64.82 cm. Redistribution occurred for 177 days before field experiments at the site ended officially on July 1, 1998. Data were collected manually and through a series of data acquisition systems.

Water movement through the subsoil of the plot was spatially variable during Experiment 1, due mostly to variability in the initial water content, and thus, the hydraulic properties. The results of the intrusive and non-intrusive instruments, many of which provided redundant measurements of performance measures (e.g., water content, water tension, solute transport), showed that 1) water movement in the western portion of the site was faster than the eastern portion, due most likely to soil texture and structure; 2) a zone of rapid water flow was observed near the northern and central areas of the plot, as confirmed using several types of instruments; and 3) the variability of water movement, as measured using neutron probe, decreased with increasing depth, when the effective thickness of the soil profile was increased. Spatial variability of water movement was significantly reduced in surface soils (< 1.5 m), from a CV = 41.8 % to 4.7 % between Experiments 1 and 2, respectively. The reduced variability was observed because the flux-controlled water application led to more uniform hydraulic property fields, and thus, more uniform water movement. A flood or

sprinkler method of water application probably would have resulted in higher variability than we observed, because of the dependence of infiltration rates on the hydraulic conductivity of surface soils, an aspect of the field site that would be very difficult to characterize or monitor. Given application probably would have resulted in higher variability than we observed, because of the dependence of infiltration rates on the hydraulic conductivity of surface soils, an aspect of the field site that would be very difficult to characterize or monitor. Given that most infiltration in nature occurs under non-flood conditions (e.g., rainfall rate < soil hydraulic conductivity), the boundary conditions used during the experiments were realistic and easily monitored.

Most of the monitoring systems performed well during the field experiments, and the report presents and describes the data collected for each of the systems use. However, some data collected from the tensiometers were lost (or considered unreliable) due to corrosion of electrical connections where wire leads were spliced together with connectors. In fact, all pressure transducers installed in the trench tensiometers were replaced before Experiment 2 because of corrosion problems, and some units were still problematic. Tensiometers installed in the deep boreholes operated very well during Experiment 1, but many of them failed during Experiment 2. Over-designing these connections, to withstand the harsh ambient conditions, likely would have reduced some of this data loss. We noticed a significant amount of feedback through the AC power system that led to larger variability in the TDR readings, especially during Experiment 1. We solved the problem by modifying the TDR cable testers so that all data would be collected using the backup battery. Data from most of the other monitoring systems exhibited some effects from the large changes in ambient temperature and humidity, requiring some secondary post-processing. For example, the neutron probe meter was effected by temperature fluctuations, requiring the collection of standard counts at least twice per day, and subsequent testing to ensure that the standard counts were within the 95% confidence interval established for each probe.

FOREWORD

This technical report was prepared by the Department of Soil, Water and Environmental Science at The University of Arizona (UAZ), and the Bureau of Economic Geology at the University of Texas at Austin, under its research project with the Radiation Protection, Environmental Risk and Waste Management Branch in the Office of Nuclear Regulatory Research (Contract No. NRC 04-95-046). The research objectives were to: assess capabilities, limitations, and usefulness of alternative techniques for monitoring moisture movement and contaminant transport in the unsaturated zone; provide technical bases for identifying and evaluating appropriate techniques for unsaturated zone monitoring; and test monitoring strategies and instrumentation on a variety of field scales using actual water and tracer applications and geometries. The research was requested by the Office of Nuclear Material Safety and Safeguards to provide technical information and bases for licensing reviews.

This report presents the results of a field study conducted at the Maricopa Environmental Monitoring site for assessing state-of-the-art monitoring systems that are currently being used, or proposed for use, at low-level radioactive waste (LLW) disposal facilities and decommissioned facilities designated under the Site Decommissioning Monitoring Plan (SDMP). The field study included the instruments and installation similar to those that could be used today for monitoring radioactive disposal sites.

This report describes the results of Experiments 1 and 2. Both experiments focused on water application to soil, with and without tracers. Monitoring systems installed in the field were then used to detect water and tracer arrival. This report, NUREG/CR-5694, presents the results of those field studies. A companion report, NUREG/CR-5698 (Young et al., 1999), compares four monitoring strategies at the site, and relies heavily on the information and data contained herein.

Information in both NUREG/CR-5698 and this report may be useful to those involved in designing or reviewing monitoring programs for water and contaminant movement at LLW and decommissioning facilities. Two workshops were conducted by the UAZ investigators: a "hands-on" technology transfer workshop held at the Maricopa field site in February 1998; and a "lessons learned" seminar held at NRC Headquarters auditorium in July 1998. Agreement State regulators and their contractors were notified of the workshops, and attended along with scientists from other Federal agencies, DOE national laboratories, universities and industry.

NUREG/CR-5694 is not a substitute for NRC regulations, and compliance is not required. The approaches and /or methods described in this NUREG/CR are provided for information purposes only. Publication of this report does not necessarily constitute NRC approval or agreement with the information contained herein.

ACKNOWLEDGMENTS

This research was supported by the U.S. Nuclear Regulatory Commission, under Contract No. 04-95-046. Numerous persons were involved in the field construction and data collection. They include John Fleming, Geof Moss, Christina Betz, David Moore, Ted Angle, Bill Laughlin, Gaylen Bennett and Barry Anthis. The authors would also like to thank peer reviewers Glendon Gee, Phil Meyer, and Mark Rockhold of Pacific Northwest National Laboratory for their insights, discussions and comments during the development and operation of the field project.

LIST OF ABBREVIATIONS

ANOVA	Analysis of Variance
AZMET	Arizona Meteorological Network
AC	Alternating Current
BTC	Breakthrough curve
C/Co	Relative Concentration
CAP	Central Arizona Project
CFR	Code of Federal Regulations
CPN	Campbell Pacific Nuclear, Inc.
CR	Count Ratio
CSI	Campbell Scientific, Inc.
CV	Coefficient of Variation
D/C	Direct Current
E-W	East-West
EC	Electric conductivity
EC_a	Apparent Electrical Conductivity
EM	Electromagnetic Induction
ERT	Electroresistive Borehole Tomography
HDPE	High Density Polyethylene
HDS	Heat Dissipation Sensors
ID	Inside Diameter
LLW	Low-level waste
MAC	Maricopa Agricultural Center
MEM	Maricopa Environmental Monitoring
N-S	North-South
NRC	U.S. Nuclear Regulatory Commission
OD	Outer Diameter
PT	Pressure Transducer
PVC	Polyvinyl Chloride
RMSE	Root Mean Squared Error
SE	Standard Error
TCP	Thermocouple Psychrometer
TDR	Time Domain Reflectometry
TTC	Temperature Thermocouple
ΔT	Change in Temperature
ΔZ	Change in Depth
θ_v	Volumetric water content

1.0 INTRODUCTION AND OBJECTIVES

In September, 1994, the U.S. Nuclear Regulatory Commission (NRC) issued a Request for Proposal (RFP) to assess unsaturated zone monitoring techniques and strategies applicable to low-level radioactive waste (LLW) disposal facilities. The research was later expanded to include decommissioned facilities designated under the Site Decommissioning Monitoring Plan (SDMP). The RFP stemmed from a request by NRC staff for additional information on monitoring systems and strategies that could be used for evaluating future disposal site applications.

Monitoring of disposal sites is required by NRC, who state that the site "shall be capable of being characterized, modeled, analyzed, and monitored." (Subpart D of 10 CFR Part 61, § 61.53; Ofc. Fed. Reg., 1990). The applicant must design and install an environmental monitoring system that is "capable of providing early warning of releases of radionuclides from the disposal site before they leave the site boundary." A monitoring system must be installed prior to site construction, and be maintained throughout the life of the facility, including the post-closure phase. Though the overall environmental monitoring system of a LLW or SDMP site may encompass many parameters, such as flora and fauna (Shum et al., 1989), the present report focuses on monitoring the unsaturated zone.

Unsaturated zone monitoring to detect releases of radionuclides is an important issue at LLW disposal facilities and SDMP sites. The unsaturated zone is a primary component that isolates near surface waste from underlying ground-water systems. Monitoring can be used to show that facilities are operating safely during waste emplacement and after site closure. Effective unsaturated zone monitoring requires choosing instruments and installation procedures, and integrating them into an overall program that incorporates: 1) the results of site characterization, 2) operational limits for each device, 3) frequency of data collection, and 4) the need for performance confirmation of the site. As stated by the National Research Council (1995), integration of site characterization, monitoring and performance assessment should be an iterative process, one that relies on feedback from each of these phases.

The field project designed and implemented for this research focused on both monitoring strategies and the systems which support these strategies. A further goal of the project was to improve subsurface monitoring by emphasizing redundancy of measurements, which, in this context, means a series of instruments for measuring different soil conditions (e.g., water content, water tension, tracer concentrations), each of which provide information on water movement. This concept was implemented into the different monitoring strategies that were studied. The redundancy approach makes integration of site characterization and monitoring much more feasible.

There were three broad goals for the field study portion of this contract: 1) to construct a field site in which monitoring strategies could be evaluated through a series of water flow and solute transport experiments; 2) to evaluate the use of several strategies for monitoring flow and transport in the unsaturated zone at both arid and humid sites; and 3) to be able to address the specific objectives as listed below:

1. Assess capabilities, limitations, and usefulness of alternative techniques for monitoring water movement and contaminant transport in the unsaturated zone of humid and arid areas.

2. Provide the technical bases for identifying and evaluating appropriate techniques for unsaturated zone monitoring at LLW sites.

3. Develop guidance on the design, installation, use, and decommissioning of unsaturated zone monitoring systems.

4. Examine the issue of whether and how unsaturated zone monitoring systems may compromise the performance of natural and engineered barriers at LLW facilities and how to eliminate or mitigate such compromises.

5. Test monitoring strategies and instrumentation on a variety of field scales using actual water and solute tracer application rates and geometries.

The original field testing plan (Young et al., 1996) described some of the supporting factors that we considered during the design phase of this project. The experimental design and many of the monitoring instruments described in this study could be used at SDMP facilities, though little

direct experience is available on long-term monitoring of SDMP disposal sites. Many of the strategies are being used or proposed for use at existing or future disposal sites. By including them in our field study, we would be able to evaluate their advantages and disadvantages during controlled experiments.

The proposed study site was watered at a rate that is much higher than natural rainfall in the United States. This was done so that the experiments could be completed, and the results would become available, in a timely manner. Because of the relatively high rates of water application used, the results can be applied to sites with high rainfall conditions, such as those in Ohio and Pennsylvania, where many SDMP sites are found. Because the study concentrates on developing monitoring strategies which can be used for a variety of LLW and SDMP conditions, significant effort was spent on studying commercially available monitoring instruments suitable for unsaturated and saturated soils. The present report describes the materials and methods used during site construction, the experimental design for Experiments 1 and 2, and the experimental results. It focuses on descriptions of the various monitoring strategies and the hardware installation used to support them. A companion NUREG/CR-5698 (Young et al., 1999) describes application of the results to developing better monitoring strategies.

2. MATERIALS AND METHODS

2.1 Site Location and General Information

Field activities are conducted on Field-115 (F-115), a 0.9 hectare field at the Maricopa Agricultural Center (MAC), Maricopa, AZ. This complex, located about 90 miles northwest of Tucson and 25 miles southwest of Phoenix, is in the northwestern portion of Section 20, Township 4 South, Range 4 East, in western Pinal County, Arizona. The facility is owned and operated by The University of Arizona and comprises 770 hectares (Figure 2.1-1).

Broad valleys surrounded by mountains of moderate height characterize the region. The mountains range in age from Precambrian (granite and schist dominated) to Tertiary (andesite dominated) (Soil Conservation Service, 1974). The valley floor is covered with material eroded from these mountains, placed in thick alluvial deposits up to several hundred feet thick. The alluvial deposits exhibit characteristic depositional variability with lenses of material ranging from gravelly to clayey textures. The deep, well-drained soils in the valley floor are nearly level or gently sloping with slopes of less than 1 percent (Soil Conservation Service, 1991). The Santa Cruz Wash, an intermittent river, which flows through the Maricopa Agricultural Center is, located about 400 m from the plot. The Santa Cruz Wash has experienced extreme flood events (some as recently as 1981 and 1985), and as a result, the subsurface soil at the site is heterogeneous.

Most of this research is conducted on a 50 m by 50 m plot located within Field F-115. The irrigated plot on F-115 is bordered to the south and east by irrigation return canals, to the west by a support zone and access road and to the north by a flood-irrigated alfalfa field maintained by the U.S. Dept. of Agriculture. AC power was made available by trenching and placing electrical lines, in conduit, across the field, then installing outlet boxes at four locations.

Water for irrigation was available at the western edge of F-115. More information about the irrigation system is found below.

2.2 General Overview of Plot Design

A combination of four monitoring strategies, instrumentation, and experimental methodologies were selected to meet the objectives.

The Maricopa site was designed so that both large- and small-scale soil water processes could be monitored simultaneously. Large-scale processes were studied by monitoring hydrological conditions across the entire 50 m by 50 m irrigated plot. Small-scale processes were studied by monitoring multiple instruments within monitoring strategies on a spatial scale of several meters. Instruments used to monitor processes at smaller scales provided data and information on limitations of specific monitoring instruments and by redundant comparisons of instruments that monitor similar hydrologic parameters.

The first strategy, called Monitoring Trench, consisted of a 65 m long buried trench, into which monitoring instruments were installed in clusters at a consistent depth at 10 m intervals. By studying responses in each cluster along the transect, we were able to infer water movement and solute transport rates, as well as the behavior of the instruments. Instruments chosen for the trench provide redundant measurements of hydrologic parameters, or performance confirmations. The clusters contained instruments to measure soil water tension (tensiometers, psychrometers, and heat dissipation sensors), soil water content (neutron probe, time domain reflectometry probes), and tracer concentration (solution samplers).

The second monitoring strategy, called Monitoring Islands, was used to monitor water movement and solute transport in localized areas with greater vertical resolution. A major advantage of the monitoring islands is ease of access for servicing or replacing instruments. Two monitoring islands, each consisting of 1.82 m diameter highway culverts placed vertically within boreholes, were advanced to 3 m depth. The islands were equipped with ladders and standing areas

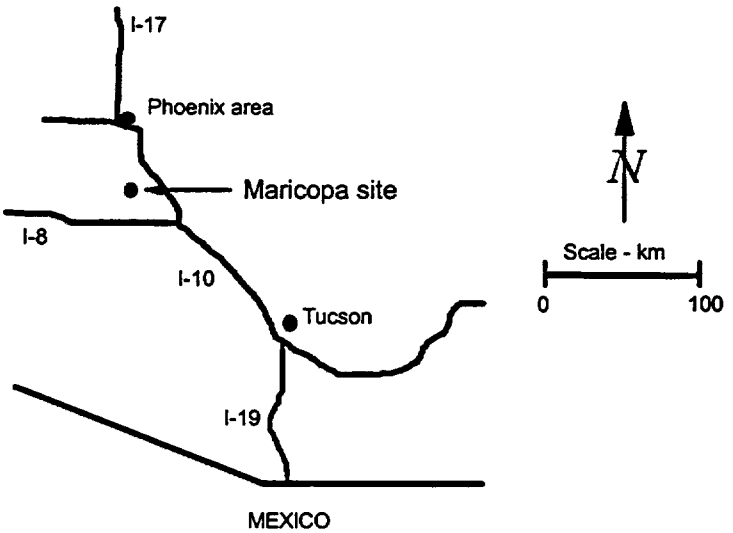

Figure 2.1-1. Map of Maricopa site.

to facilitate the installation and measurement processes. One island was equipped with a rubber skirt (or flange) to shunt water away from the backfilled annular space around the monitoring island culvert, in hopes of reducing the potential for preferential flow. Instruments were installed at 0.5 m depth increments to 3.0 m to facilitate vertical resolution of hydrological processes.

The third monitoring strategy, called Borehole Monitoring, consisted of neutron probe access tubes, tensiometers, and solution samplers, systematically spaced throughout the plot. Neutron probe moisture meters were used extensively during these experiments for monitoring changes in water content. Both horizontally- and vertically installed access tubes were used. The series of vertical neutron probe access tubes, allows for spatial monitoring of water movement at both plot and subplot scales. Three horizontal neutron probe access tubes were to quantify spatial trends of water content changes along linear transects in both disturbed and undisturbed areas of the experimental plot.

The fourth monitoring strategy, called Geophysical Monitoring, consisted of surface and subsurface geophysical techniques. Non-intrusive (electromagnetic induction) and intrusive (borehole tomography) geophysical techniques were used to monitor large-scale water content changes. Results obtained with these techniques were compared with results from more commonly used methods of measuring water content (i.e., neutron probe).

Several smaller-scale monitoring techniques were implemented in this study. Atmospheric effects were studied to evaluate the extent to which barometric pumping could increase downward movement of gaseous tracers in the subsurface in areas where LLW disposal sites are proposed. A series of pneumatic pressure tests, performed on boreholes located a considerable distance from the irrigated plot, were used to verify the presence or absence of potential fast pathways for gas transport.

The following sections discuss site construction; instrument development and installation; system installation, and experimental procedures in full detail.

2.3 Site Construction and Layout

The plot surface was graded and smoothed, to facilitate drainage of rainwater, before any system construction or instrument installation. Soil was scraped from the north and south edges of the field until a 0.6% grade was obtained. The plot crown was thus oriented east-west. This very shallow grade was considered adequate to shunt rainwater away from the plot and into drainage channels that lined three sides of the plot. This was especially important after Hypalon pond-liner material was installed on the plot surface.

2.3.1 Buried Trench Monitoring Strategy

a. Construction

Excavation for the trench monitoring strategy was completed in early October, 1996. The trench, used to monitor changes in soil water conditions at 1.5 m depth across a 55 m long, instrumented transect, extended 7 m on either side of the irrigated area, oriented north-south (Figure 2.3-1). The trench was excavated by first cutting a slot using a trencher, 1 m deep and 15 cm wide, ensuring a smooth face for installing instruments. An excavator with a 91 cm wide blade was used immediately afterwards to remove soil along the transect. Care was taken to avoid contact between the excavator blade and the smooth side of the trench face. Excavated soil was stockpiled into two different piles, depending on the depth of collection. The interface of silt loam and coarser sandy material was found through previous soil sampling to exist at about 1 meter depth. Surface soil collected to this depth was kept on one side of the trench, and soil collected from 1 to 1.5 meter depth was kept on the other side. As the trench was excavated, grab soil samples were collected in the trench at 1 meter depth, at 5 meter intervals, to be analyzed for texture and water content. The operator was then instructed to continue excavating to 1.5 meter at that location. Tarpaulin material was used to cover the trench floor to avoid drying immediately after the proper depth was reached. The excavator operator was unable to remove soil to the exact target depth in most areas, because calcified soil was difficult to excavate. Soil was rarely excavated from the profile deeper than 1.6 meters.

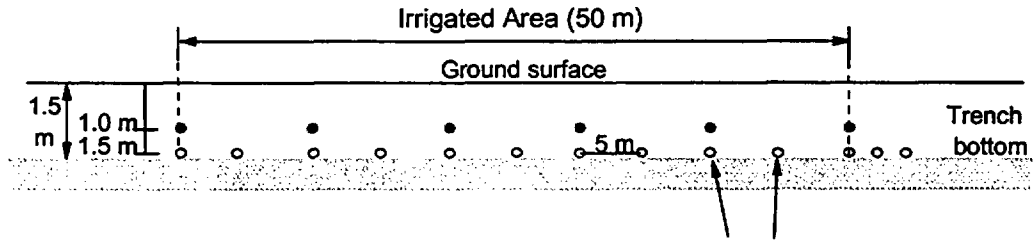

Total Number of Instruments In Trench Transect

Thermocouple Psychrometer	13
Tensiometer	19
TDR Probe	13
Heat Dissipation Sensor	13
Stainless Steel Solution Sampler	13

At 1 m have tensiometers only

Figure 2.3-1. Monitoring instruments installed at buried trench transect.

After excavation was completed, 13 instrument clusters were selected along the transect, spaced 5 m apart. Locations were marked for sampler installation using the global coordinate system established for the plot. The exact depth from ground surface was found by laying a large level across the trench and measuring downward to 1.5 m, ensuring that the tube was resting on the true soil surface and not on excavated soil. The center of each sampling cluster was marked with a nail and flagging tape, and the entire transect was then strung with kite string so that all the instruments would be installed at the same depth relative to ground surface. As the instruments were being installed, a survey crew from the Environmental Research Laboratory (University of Arizona) established a benchmark for the site, using existing benchmarks previously established on the MAC farm. The western side of the trench, used for the horizontal neutron probe access tube, was surveyed carefully to 1.5 m depth, requiring hand excavation and repacking of soil in some places.

b. Installation of Instruments

Access ports into the trench face were made by using either an impact drill for circular ports or an impact hammer for rectangular ports. Circular access ports used for tensiometers and solution samplers were created using an impact drill and a 2.54 cm diameter drilling bit welded to an extension rod. A jig was used to ensure that holes for the tensiometers and solution samplers were advanced at an angle of 10 degrees from horizontal, normal to the trench face. Access holes for the thermocouple psychrometers (TCP) and heat dissipation sensors (HDS) were advanced horizontal to ground surface and normal to the trench face, also using the impact drill. Prolonged use of the drilling bit in the calcified soil led to numerous failures of the welded connection between the bit and extension rods. We found that tapping a 2.54 cm diameter aluminum tube into the soil with a small sledgehammer also provided a useful way of creating access ports, so this method was used as well.

At each of the 13 locations, thermocouple psychrometers (TCP), heat dissipation sensors (HDS), tensiometers, time domain reflectometry (TDR) probes, and solution samplers were installed (in that order), from north to south, except at one location. At the cluster located at Y = 55 m (northern most cluster), the TDR probe was placed to the north of the psychrometer. Each instrument was installed so that the end of the instrument terminated 50 cm into undisturbed soil. Instruments were installed 15 cm apart from one another within each cluster. Additional clusters were installed 2.5 and 5 m outside the irrigated area on the southern end of the trench to permit monitoring of any lateral movement of water and tracers.

The instruments were installed similar to that described by Vinson et al. (1997). Native soil excavated from the trench was sieved through a screen with 104 μm openings and mixed into a heavy slurry. The slurry was then sucked into a plastic tube and placed carefully into the back of the access port. The instruments were then placed into the access port so that the slurry would cover the porous material of the instruments. This method ensured a better hydraulic connection between the porous material and the soil material. Native, moistened soil passed through a 2 mm screen was used to backfill the access tube to the trench face.

Electrical wiring for the TCP, HDS, and tubing for the solution samplers were brought from the base of the trench to ground surface in PVC conduit. Lead wires for the TCP and HDS were routed to multiplexers near the center of the plot. Lead wiring for the pressure transducers was spliced to 22 AWG, two-pair wire using Molex type connectors. The connection was placed in conduit from a different access point in the main conduit (Figure 2.3-2), and then fed through conduit and wired directly to the data logger at the southern end of the plot. Figure 2.3-3 is a schematic of placement of all conduits installed at the site. TDR coaxial cables were brought to the surface without conduit because the RG-8 cable has a much thicker outer shield, capable of withstanding any environmental conditions expected during the experiments. The TDR coaxial cable was also brought to a central location at the center of the plot, where the multiplexer, cable tester and portable computer were housed. All electrical wiring and instruments were tested by connecting a data logger (model 21X) to individual instruments, and checking to see that reasonable values were obtained before the trench was backfilled.

Backfilling of the trench commenced after the horizontal

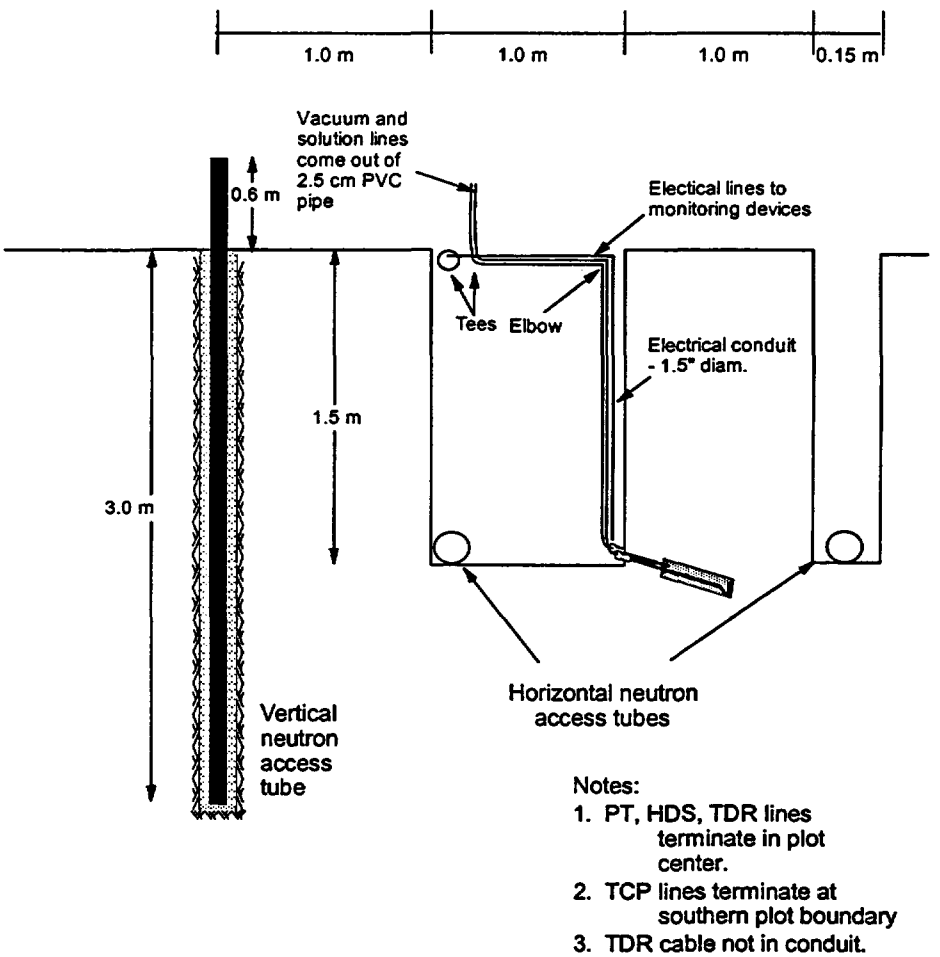

Figure 2.3-2. Schematic of completion of trench.

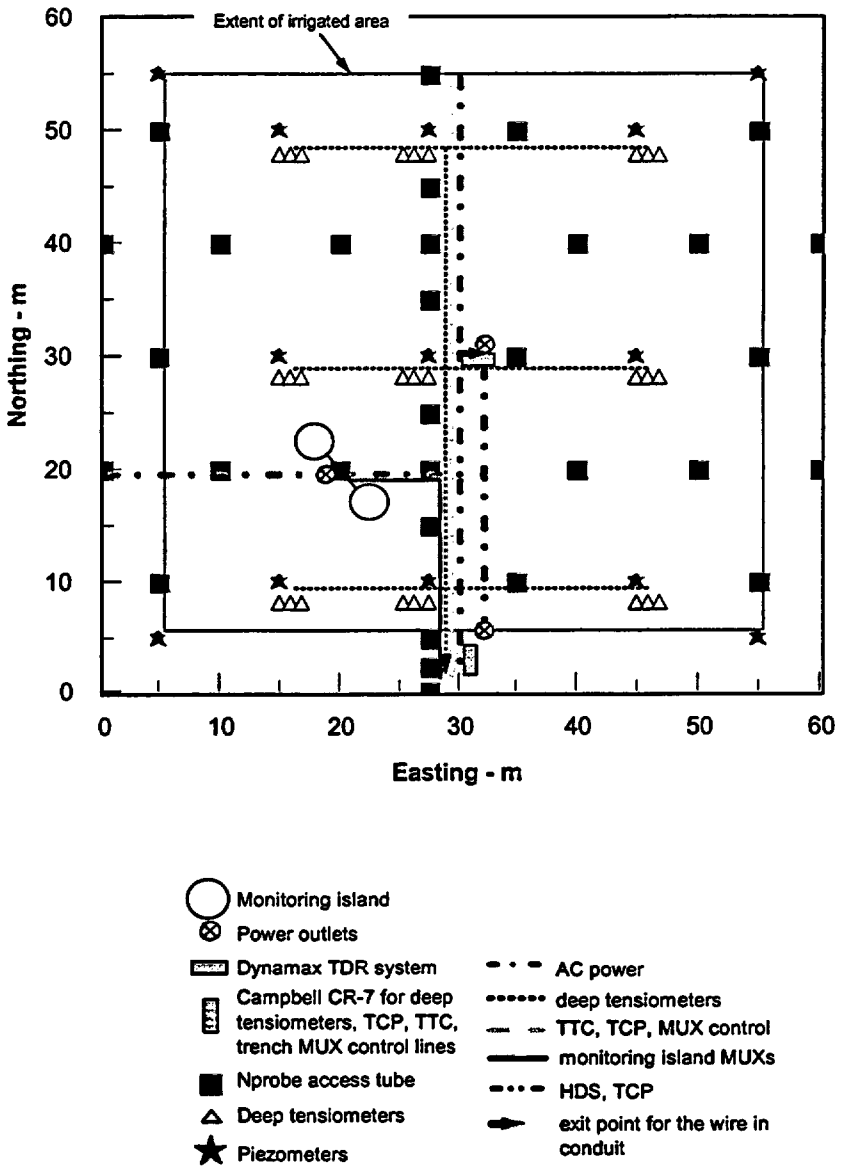

Figure 2.3-3. Map showing locations of conduits, field utilities and instrumentation.

neutron probe access tube was installed in the trench. A large backhoe was brought to the site and the stockpiled material was returned to the trench in the same order as it was removed. Two mechanical tampers were used to compact the soil after placement in the trench. The soil was not moisture treated before placement and compaction. Soil was carefully compacted, mostly by hand tamping, immediately around the instrument clusters to avoid snagging or crushing any wiring or conduits. Soil was placed in layers less than 30 cm thick prior to compaction, and every reasonable effort was made to avoid leaving cavities or large soil blocks before placing the next layer. After backfilling the trench so that the new surface was approximately 5 cm below the true soil surface (leaving room for placement of the conduits just below ground surface), only a small amount of the stockpiled soil remained, indicating that close to the same mass of soil was replaced as was excavated.

Appendix 1 contains a table of coordinates for all monitoring instruments installed in the trench.

2.3.2 Monitoring Islands Strategy

a. Construction

Monitoring islands can allow deep access into soil profiles adjacent to, or within, disposal cells. The present monitoring island strategy consisted of two, 1.53 m diameter by 3.5 m long, corrugated steel, highway culverts. Access ports were added to both culverts, before installation, using a cutting torch. The ports were added in 0.5 m increments from 0.5 m to 3.0 m distance along opposite sides of each island. Ports were also added at 1, 2, and 3 m depth at 90 degrees to the other ports (15 sets of access ports total for each island). Access ports for the tensiometers, HDS, and solution samplers were each 3.8 cm (1.5 inch) in diameter, spaced 15 cm apart. The rectangular ports for the TDR probe were 10 cm by 5 cm in size. A ladder was bolted to the inside of the culvert for complete access to the island, and a shelf was also added at 1.75 m depth so that workers could sample and service the instruments safely.

The culverts were placed 3.62 m apart, center to center, close enough to relate soil properties found at the locations, yet far enough apart to avoid interference from installation. The culverts were installed by augering a 1.68 m diameter borehole, lowering the culvert into the borehole, and backfilling the annular space with sieved native material. We designated the two islands as being either the north or south islands. The north island was outfitted with a rubber skirt designed to shunt water away from the wall and annular space areas; the south island was installed without the skirt. The base of the skirt was placed 15 cm below the soil surface, extending 25 cm from the outer wall of the island. The top of the skirt was attached to the outside of the island above the soil surface using large hose clamps and sealed using silicon caulking. The skirt sloped away from the annular space, so no ponding of water on the rubber material should have occurred. Soil material, excavated from around the monitoring island, was used to backfill above the skirt material.

b. Installation of Instruments

Monitoring instruments were installed during the Summer of 1996 in the same way as described above in the buried trench transect. We did not need to use an impact drill for the access holes because the soil material was soft enough to use a regular rotary drill. Access holes on the east and west side of the islands were advanced so that the end of each instrument terminated in a straight line, oriented north-south (Figure 2.3-4). This also allowed us to orient the instruments along a north-south transect from the west side of the south island and the east side of the north island, with the neutron probe access tube between the two islands. The instruments were not installed normal to the island wall, because they would no longer be 15 cm apart, nor would they exist along a north-south transect. Instruments were also installed in the backfill material in the annular space of each island to observe whether water preferentially moved in the annular space. Excavation of backfill for these access holes did not extend beyond the backfill material itself.

Monitoring instruments installed in the backfill were modified slightly from those installed in the undisturbed soil. The tensiometers were assembled with very short tube lengths (assembly of tensiometers discussed below). TDR waveguides were shortened to 10 cm length so that the measurement zone of influence would take place primarily

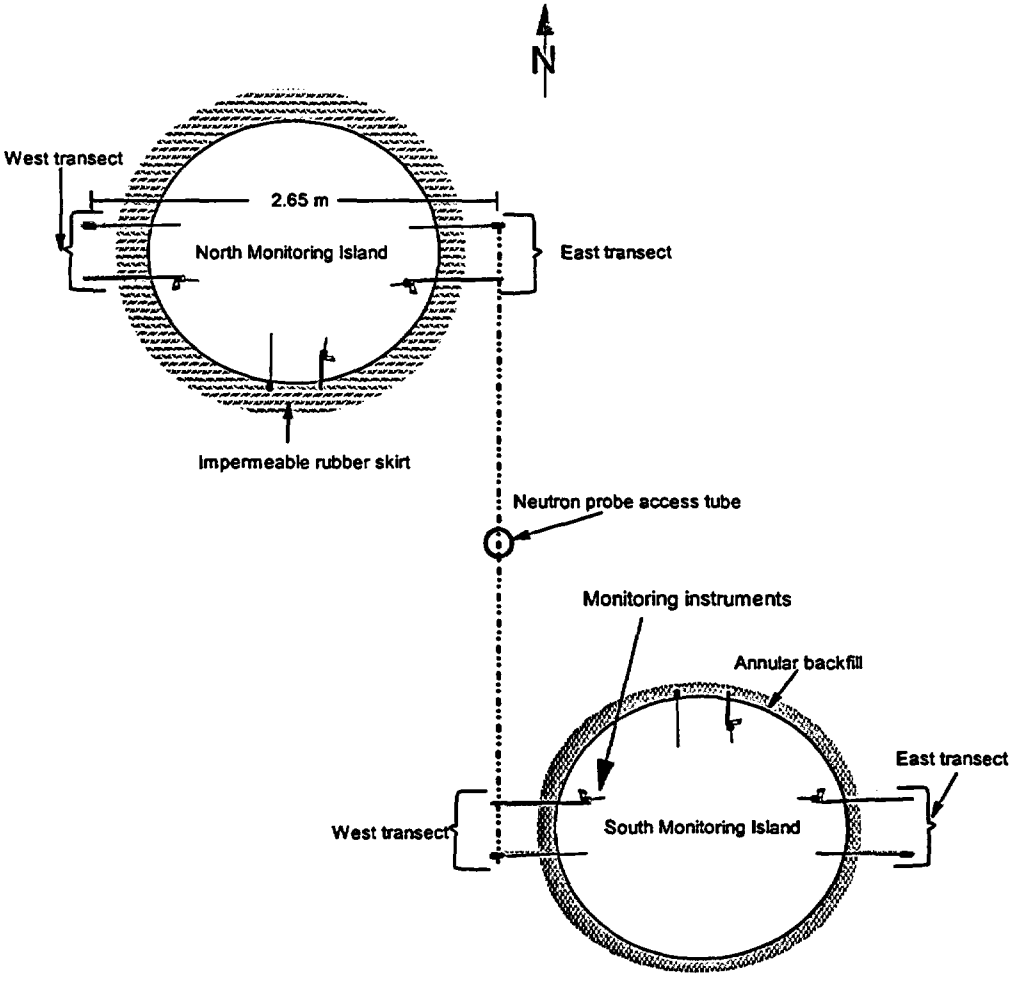

Figure 2.3-4. Monitoring island and instrument orientation.

in the backfill material. All other design features were the same.

Plywood covers (3/4" thick) were made for both islands reinforced with square tubing welded together into a lattice. A door was added for personnel access into the islands. The plywood and door were covered with Hypalon pond-liner for weather proofing.

2.3.3 Borehole Monitoring Strategy

a. Location and Construction of Vertical Access Tubes

To observe infiltration of water into soil on a scale that approximates a future LLW site, a network of vertical neutron probe access tubes and other monitoring instruments was installed at regular intervals throughout the plot. This network complements the instruments installed in the trench transect and monitoring islands, and provides a better understanding of responses to infiltration of water across a much broader portion of the site. Figure 2.3-5 is a schematic of the borehole locations used for neutron probe access tubes, tensiometers and solution samplers.

All boreholes were machine drilled by HF Drilling, Inc. (Phoenix, AZ) during the period of 12 November through 13 December 1996. Boreholes advanced without discreet soil sampling were installed by advancing a 10.2 cm diameter solid-stem auger to target depths of 3, 5, 10 or 15 m, depending on the location and purpose of the borehole (see Figure 2.3-5). All neutron probe access tubes were constructed of Schedule 40 PVC tubes, 5.0 cm ID, and sealed at the bottom with PVC caps. They were placed in the boreholes and backfilled to ground surface with native soil material which had passed a 3 mm screen. The material was slowly poured down the annular space between the outside of the neutron probe access tubes and the borehole walls, ensuring that material did not bridge, by compacting the backfill material in lifts to ground surface. Of the 10 access tubes advanced to 15 m depth, nine were screened at the lower 4.3 m (15 feet) using a manufactured screen with a 0.25 mm (0.01 inch) slot size. The upper 10.7 m consisted of solid PVC pipe. The lower portion of these access tubes were screened so that the tube could also be used for monitoring groundwater levels and tracer concentration. The one unscreened 15 m deep borehole was located at X = 15, Y = 10 (#402).

Three additional boreholes (#802, #803, #804) were advanced to 15 m depth using the hollow-stem auger, at the NW, NE and SE corners of the irrigated plot. Each of these three boreholes were completed as traditional monitoring wells; e.g., the screened interval was packed using 10/20 sand, followed by 60 cm of powdered bentonite, and then backfilled to ground surface using grout cement. The monitoring wells were constructed using 5 cm ID Schedule 40 PVC. Soil samples were collected during construction of the three boreholes, every 1.53 m (5 feet) using a 60 cm split spoon sampler. Originally, we intended to collect samples in brass rings, each 15 cm long. However, it was often difficult to advance the split spoon the full 60 cm, leaving a portion of the sleeves unfilled and subject to cave-in. We found that collecting grab samples for textural analysis, rather than attempting to retrieve undisturbed samples, was sufficient for our purposes.

b. Location and Construction of Horizontal Access Tubes

To study spatial variability of wetting front arrival along a linear transect at a specific depth, three horizontal neutron probe access tubes were installed at approximately 1.5 m depth (Figure 2.3-5). The first access tube, placed within the west side of the buried trench, was composed of 7.6 cm inside diameter HDPE pipe and is located at X = 28.5 m. This access tube hereafter will be referred to as the disturbed N-S access tube. The trench bottom onto which the access tube was placed, was accurately surveyed so that it would be at a consistent 1.5 m depth. During installation of the access tube, a small kink developed which could have impeded the movement of the neutron probe. To avoid this possibility, the kinked portion was removed, and the two pieces were spliced together with a PVC compression fitting at Y = 36.75 m. Three markers, composed of two additional layers of HDPE, 0.5 m long, were placed around the access tube at Y = -0.5, 30.25, and 57.0 m. The purpose of the markers is to accurately determine the location of the neutron probe source in relation to the plot coordinates as the neutron source is pulled through the tube. The second access tube, hereafter referred to as the "undisturbed" N-S tube, also was composed of 7.6 cm HDPE, and installed at

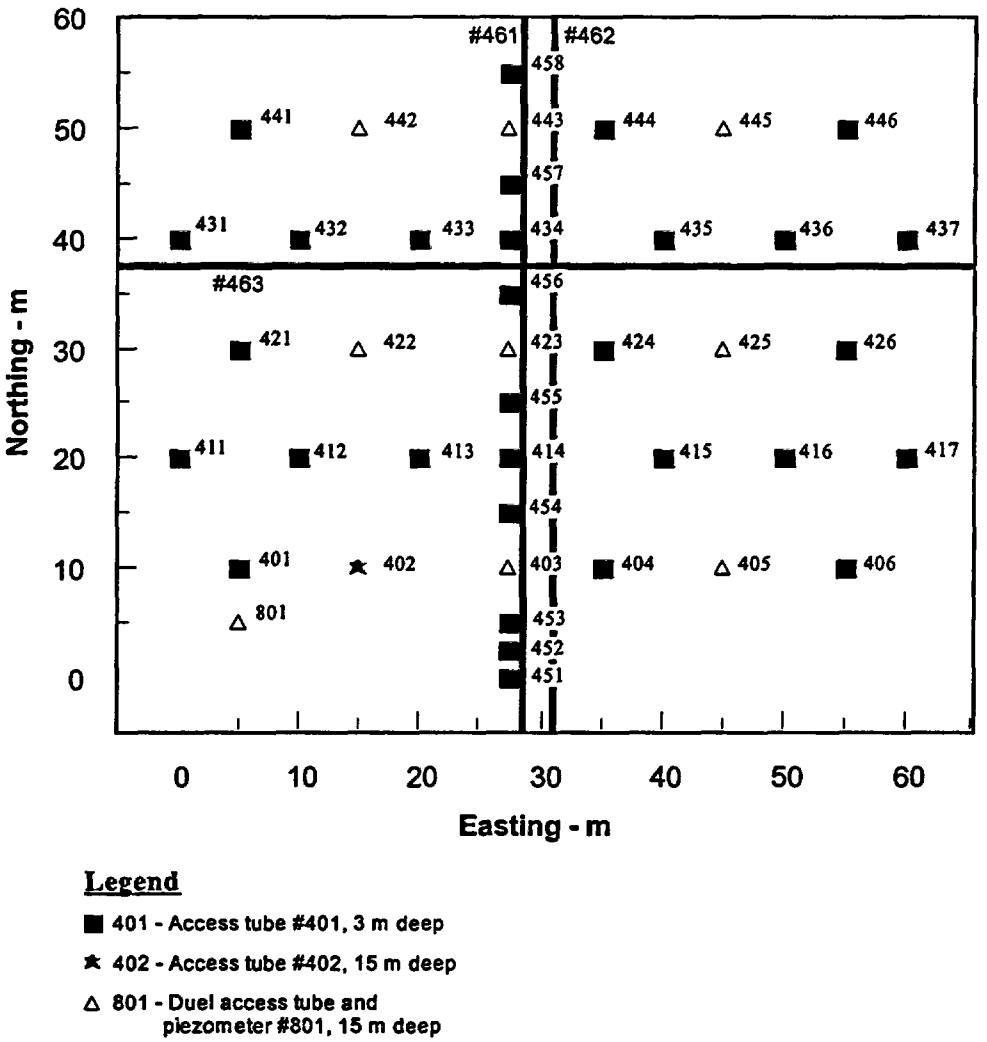

Figure 2.3-5. Numbering key for vertical neutron probe access tubes. Lines show locations of horizontal neutron probe access tubes.

approximately 1.5 m depth using a single cut (15 cm wide) from a Ditch Witch at X = 31 m.. Markers were also added to the access tube and are found at Y = -1.5, 30.00, and 57.25 m. Slight imperfections at the soil surface caused the depth of excavation to vary slightly along the transect. Table 2.3-1 lists the depths to the top of the access tube as measured from the soil surface.

The third access tube, was composed of 10.2 cm diameter, Sch. 40 PVC well pipe. Each length of pipe (3.1 m) was connected using threaded fittings with o-rings to eliminate leakage. The access tube (hereafter referred to as the undisturbed E-W tube) was lowered to a depth of 1.67 m in a trench (15 cm wide) using a Ditch Witch at Y = 37.5 m. This tube was equipped with paraffin markers, which were attached with duct tape. The markers are located at X = 0.75, 30.5, and 60.25 m, and the depths to the top of the access tube are listed in Table 2.3-1.

The access tubes were sampled using a model 503DR moisture meter (CPN/Boart Longyear, Pacheco, CA) in 25 cm intervals using 16 second counts. The base of the probe itself was equipped with an eye hook installed by the instrument manufacturer. The probe cable was marked in 25 cm increments using stick-on numbers. The entire length of the probe cable was contained in clear shrinkable tubing to secure the numbers and to provide resistance against wear.

Each of the three horizontal access tubes were equipped with a galvanized woven draw cable (1/8" diameter), terminated with hooks at either end. Prior to data collection or when necessary, the access tube was cleared of moisture, windblown sand, or other debris, by first pulling through a mop head attached to a leader cable. Cable spools at both ends of the open access tube were secured with WorkMate benches, to wind and unwind the steel cable. During data collection, the probe was attached to the draw cable inside the access tube. The probe was then pulled through the access tube, along with the probe cable, as the draw cable was retrieved. After the probe had passed the measurement starting point, the operator simply pulled back the probe until the zero mark was reached, and began logging.

2.3.4 Geophysical Monitoring Strategy

This monitoring strategy encompasses two systems: electroresistive tomography (ERT) and electromagnetic induction (EM). Only ERT required construction, specifically subsurface drilling. All ERT points were constructed by installing electrodes (copper plates, 30 cm in height) onto the outside of Schedule 40 PVC tubes, 2.5 cm OD, at 1 m offsets beginning at 1 m depth. All electrode leads were brought to ground surface inside the PVC tube. The leads were terminated at a single multi-pin connector that was environmentally sealed to reduce corrosion. Each electrode was sealed to the PVC tube using electrical tape and silicon sealant.

A total of 12 boreholes were constructed for the ERT monitoring system (Figure 2.3-6). All boreholes were machine drilled by HF Drilling, Inc. (Phoenix, AZ) during the same period as the boreholes for the Borehole Monitoring Strategy. Boreholes were advanced without discreet soil sampling using a 10.2 cm diameter solid-stem auger to a target depth of 15 m. After reaching the target depth, the electrode string was lowered into the borehole, and held in place while backfill material was slowly poured down the annular space between the outside of the tube and the borehole walls. Care was taken to ensure that material did not bridge.

No construction was necessary for the EM measurements. EM is a non-invasive technique that required no installation of access holes. A total of 90 positions were surveyed and marked with spray paint on the cover over the plot prior to Experiment 1. Monitoring positions were offset by approximately 9 m (Figure 2.3-7). At some positions the EM readings were affected by near surface AC power lines, and the metal conduit from the monitoring islands. They were removed from the data set.

Table 2.3-1. Depth to top of casing of horizontal neutron probe access tubes.

Neutron Probe Type	x† (m)	y (m)	z (m)
N-S disturbed (#461)	-0.5	28.5	1.50
"	30.25	28.5	1.50
"	58	28.5	1.50
N-S undisturbed (#462)	2.5	31.0	1.40
"	5.0	31.0	1.41
"	10	31.0	1.41
"	15	31.0	1.43
"	20	31.0	1.40
"	25	31.0	1.39
"	30	31.0	1.40
"	35	31.0	1.37
"	40	31.0	1.39
"	45	31.0	1.39
"	50	31.0	1.42
"	55	31.0	1.37
E-W undisturbed (#463)	37.5	0.75	1.67
"	37.5	29.75	1.67
"	37.5	60	1.67

† - x and y are the distances (m) in the x and y direction of the points where depth measurements (z) were taken. z is the depth below ground surface.

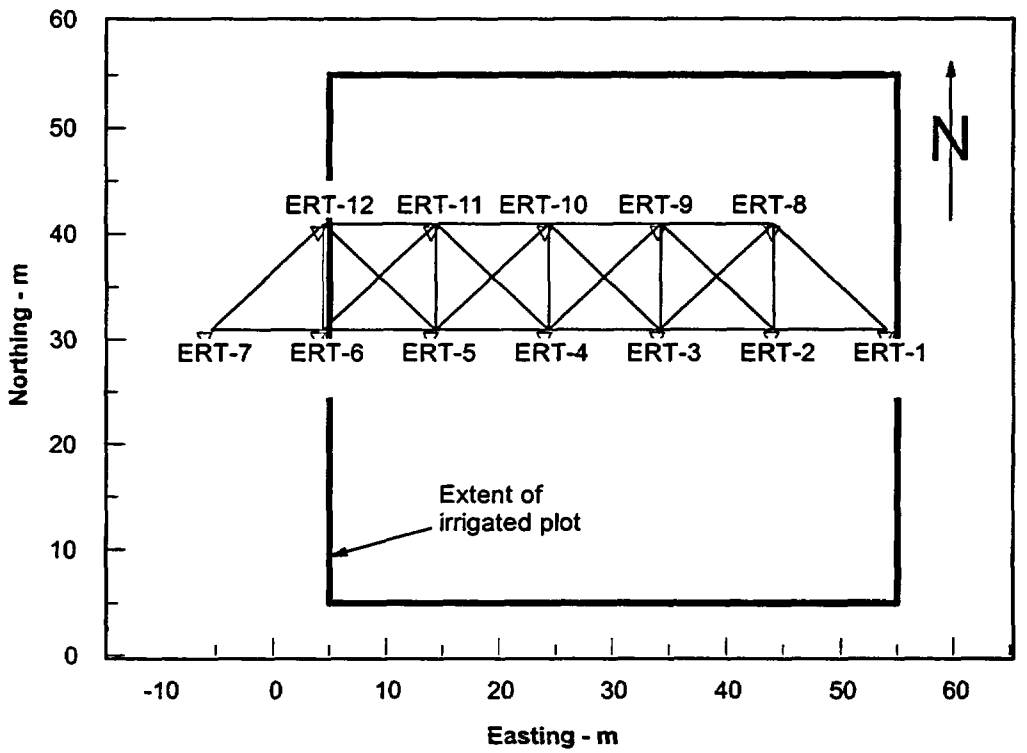

Figure 2.3-6. Plan view of ERT borehole locations. Lines represent planes of data collected.

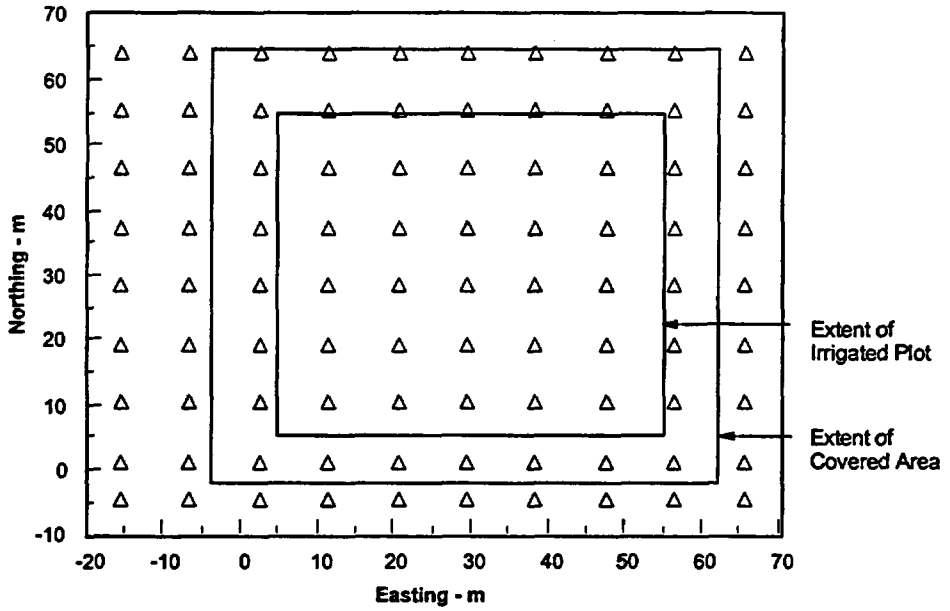

Figure 2.3-7. Locations for electromagnetic induction surveys.

2.4 Description of Individual Monitoring Instruments

2.4.1 Time Domain Reflectometry

The TDR system used in the monitoring islands consisted of a cable tester (model 1502C, Tektronix, Beaverton, OR), TDR probes with 30 cm long waveguides (model CS 610), multiplexers, (model SDMX50), and a data logger (model CR10), which were obtained from Campbell Scientific Inc., Logan, UT. All coaxial cable used in the TDR system was RG-8 type (model 9914, Belden Wire and Cable, Carmel, IN). Three 1:8 multiplexers were installed inside the south island along with the data logger and cable tester, and two other multiplexers were installed in the north island. The first level multiplexer was used only to split the electromagnetic signal to one of the four second-level units. Given that 15 probes were installed in each island, all but one of the second-level ports were used for directly querying probes. The data logger was powered using a deep-cell marine battery connected to a trickle-battery charger. An AC power outlet installed between the two monitoring islands powered the battery charger. After Experiment #1, the TDR cable tester was modified to accept D/C power from the battery.

The TDR probes used in the trench were purchased with 2 m long coaxial cable (type RG-58U) and male BNC connectors. We chose to extend these cables toward a central multiplexer in the center of the irrigated plot, using RG-8 cable with a single 10 AWG conductor (model 9914, Belden Wire and Cable, Carmel, IN). The connection between the two cables was made using female splice and twist-type BNC connectors, which were weather-proofed using shrinkable tubing, reinforced with silicon sealant.

Collection, storage, and analysis of trench TDR data were performed using 20 cm long TDR probes (model TR-100, Dynamax, Inc., Houston, TX), a 1502C cable tester (Tektronix, Inc., Beaverton, OR) and the Vadose TDR Soil Moisture System (Dynamax, Inc., Houston, TX). The computer and TDR multiplexer were placed inside an instrument shelter near the center of the plot. The long distances from the probe to the multiplexer (up to 27.5 m) necessitated the use of high quality coaxial cable to extend the 2 m long coaxial cable that came stock with the probe.

Access holes for the TDR probes, used in both the monitoring islands and buried trench, were excavated using a cutting tool (8.5 cm wide by 4.0 cm high by 10.5 cm deep) connected to an impact hammer (Art's Manufacturing and Supply, American Falls, ID). The access hole excavated in the monitoring island was oriented at approximately 8° to the right of normal to keep all the instruments parallel to each other. The impact hammer was used to pound the cutting tool to a distance of either 20 cm (monitoring island) or 30 cm (buried trench) into the undisturbed soil, horizontal to ground surface. The cutting tool was then replaced by a probe insertion tool, onto which the TDR probe was inserted, and tapped into the undisturbed soil the remaining 20 cm. The probe was tested during the installation process by connecting it directly to a cable tester, where the waveform could be monitored while the probe was slowly inserted into the soil. The waveform was analyzed manually to determine estimates of the dielectric constant and water content. We checked specifically for unusual-looking waveforms that could indicate failure of the waveguides during installation (e.g., shorting of probes, multiple inflections, etc.). A small number of probes appeared problematic and these were replaced with new probes.

2.4.2 Tensiometers

a. Trench and Monitoring Island Tensiometers

Each tensiometer was constructed by cutting a section of 1/2" Sch. 80 PVC pipe and acrylic tubing according to the lengths listed in Table 2.4-1. A thin layer of epoxy was applied to the end of each ceramic porous cup, which was inserted into the 1/2" Sch. 80 PVC pipe. One end of each section X (as depicted on Figure 2.4-1) was drilled to a length of approximately 5 cm with a 1/2" cylindrical ball nose bit, to increase the ID of the PVC. The same end of the pipe was drilled out with a 3/4" countersink (82°) to allow a closer fit of the ceramic cup to the end of the PVC pipe. The ceramic cup was epoxied to the fitted ends of

Table 2.4-1. Tensiometer dimensions† as used in the trench and monitoring islands (See Fig. 2.4-1 for definition of X, Y and Z).

Section	Trench 1 m depth 6 installed	Trench 1.5 m depth 13 installed	Mon. Island Long tensiometer 24 installed	Mon. Island Short tensiometer 6 installed
Y	73.0	125.0	8.0	8.0
X	48.0	48.0	52.0	15.0
Acrylic	6.4	6.4	6.4	6.4
Z	5.1	5.1	5.1	5.1

† - all lengths have dimensions of cm.

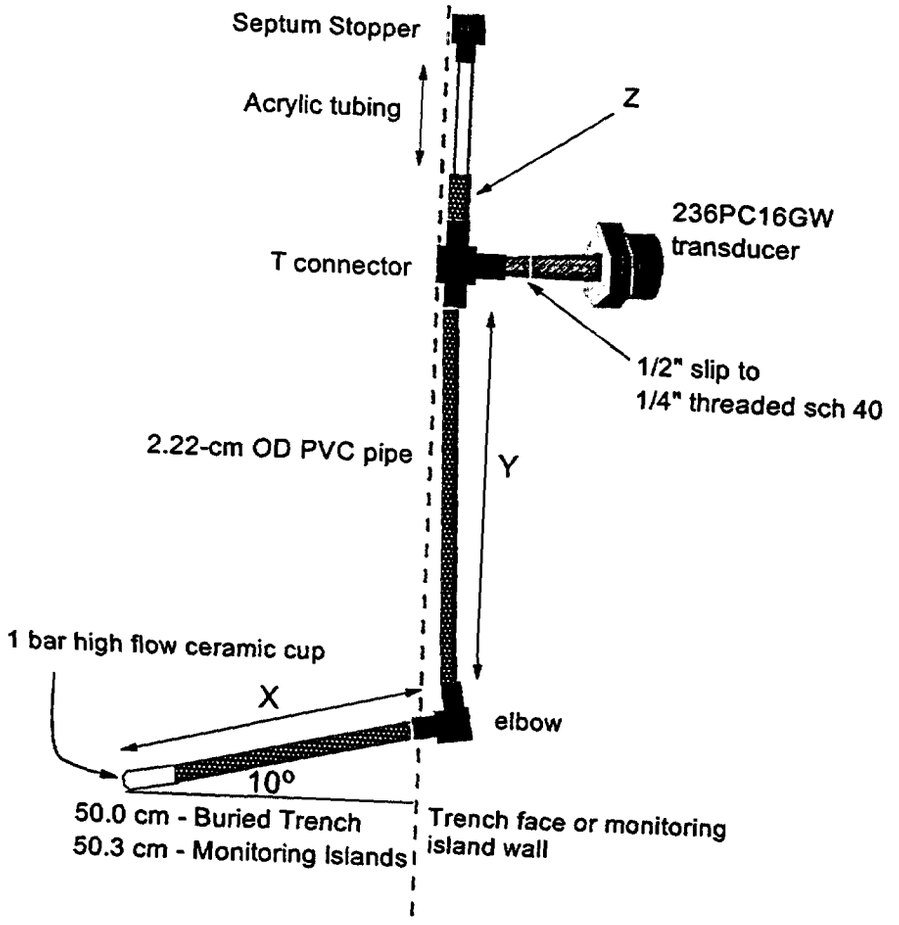

Figure 2.4-1. Schematic of shallow tensiometer.

section X and allowed to dry with the porous cup facing down for 24 hours. Section Z was drilled out with the 21/32" drill bit to a length of 1.3 cm. The acrylic section was then epoxied into the drilled end of section Z and allowed to dry for 24 hours. All other lengths of PVC tubing were cut as required on Table 2.4-1. Each section was then solvent welded using PVC primer and cement to the specifications listed in Figure 2.4-1. The significant difference between tensiometers in the monitoring island and those used in the trench was the length of riser tubing that brought the top of the tensiometer to ground surface for servicing.

Each tensiometer was checked for leaks by placing the welded connections under water and pressurizing the tensiometer body. Leaks would be seen from air bubbles coming out of the connections.

To install the tensiometers, a jig (Figure 2.4-2) was held either to the sidewall (for the buried trench) or the culvert (for the monitoring island), to ensure proper angle (10°) and orientation during installation. Using a 1.25 cm diameter drill bit and the rotary drill, the access hole was advanced 50 cm into the undisturbed soil, ensuring that the cuttings were removed. The 1.25 cm diameter bit was replaced with a 2.54 cm diameter bit, and the entire length of the access hole was reamed to the proper diameter. A heavy slurry was made consisting of native material sieved through a screen with 104 μm openings and tap water. The slurry was sucked into a 1.25 cm ID pipe, inserted into the back of the access hole, and blown out of the pipe into place. Without touching the porous material itself, the tensiometer cup was inserted into the access hole and placed so that the plastic tubing (Y and Z in Figure 2.4-1) was vertical. The tensiometers were backfilled with sieved native material (sieve size of 540 μm).

The top of each tensiometer was sealed using a septum stopper and silicon sealant. The septum stopper was used for manual measurements with a Tensimeter (Soil Measurement Systems, Tucson, AZ). Trench tensiometer lengths were cut so that the septum stopper would be just below ground surface and easily accessible to the Tensimeter. Pressure transducers (model 236PC15GW, MicroSwitch, Freeport, IL), screwed into the T-connector, were approximately 5 cm below the top of the acrylic tubing, usually at or near the base of the box that covered the assembly. Electrical wiring for the three southernmost pressure transducers (Y = 0, 2.5, and 5 m) installed on tensiometers were routed directly to the CR7 found at the south end of the trench. The remaining transducers installed on trench tensiometers were wired into a 16-channel AM416 multiplexer positioned near the center of the plot. Common multiplexer leads were routed to the CR7 at the south end of the trench. Pressure transducers used inside the monitoring island were operated using multiplexers mounted inside each island. The multiplexers were operated from the CR7 data logger located at the south end of the trench.

b. Deep Borehole Tensiometers

Tensiometers were also installed in the 10.2 cm diameter boreholes and completed at depths of 3, 5, and 10 m. These deep tensiometers were developed by Dr. J. Buck Sisson at the Idaho National Engineering Laboratory (Figure 2.4-3). The tensiometer cups were attached to 2.54 cm ID Class 200 PVC pipe for lowering into the borehole. Three tensiometers, separated horizontally from one another by 1 m, were installed in nine clusters of three each (27 tensiometers total).

After the borehole was advanced to the final depth, the tensiometer cup was lowered to the proper depth, and held in place while sieved native material was slowly poured around the cup. Water was added to the dry sieved soil to improve the contact between the soil and the ceramic cup. The remainder of the borehole was then backfilled using sieved native material, compacted as described above.

Tensiometer pressure transducer strings were constructed by permanently soldering two-pair 22 AWG wire to the pressure transducer (model 26PCCFA1G, MicroSwitch, Freeport, IL) contacts and terminated with a Molex connector. The soldered connections were isolated with shrinkable tubing. The pressure transducers were attached to a stopper assembly using 1/4" vacuum tubing. Stopper assemblies consisted of 1/4" OD stainless steel tubing inserted through a #2 stopper epoxied to a 1" Schedule 40 PVC plug and secured with a nut on the threaded lower end

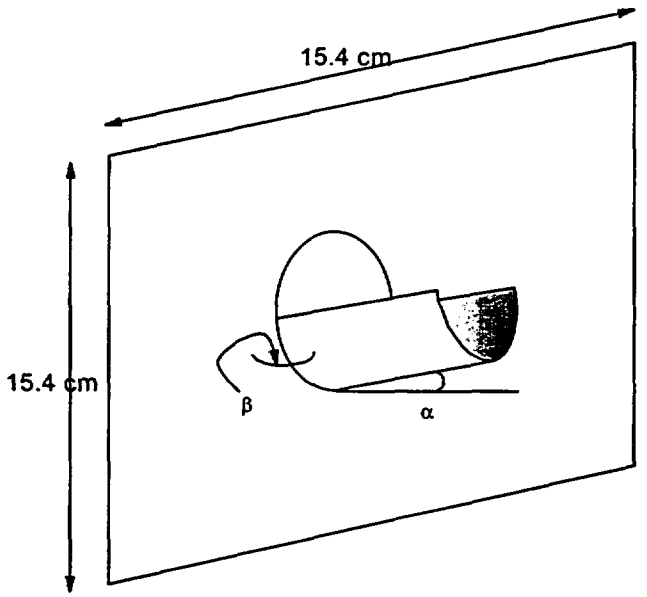

Purpose	Angle down - α	Angle left/right - β
solution sampler - trench	10°	0°
solution sampler - island	10°	8° left
heat dissipation sensors - trench	0°	0°
heat dissipation sensors - island	0°	3° left
tensiometers - trench	10°	0°
tensiometers - island	10°	3° right

Figure 2.4-2. Template for drilling guide holes to install monitoring instruments.

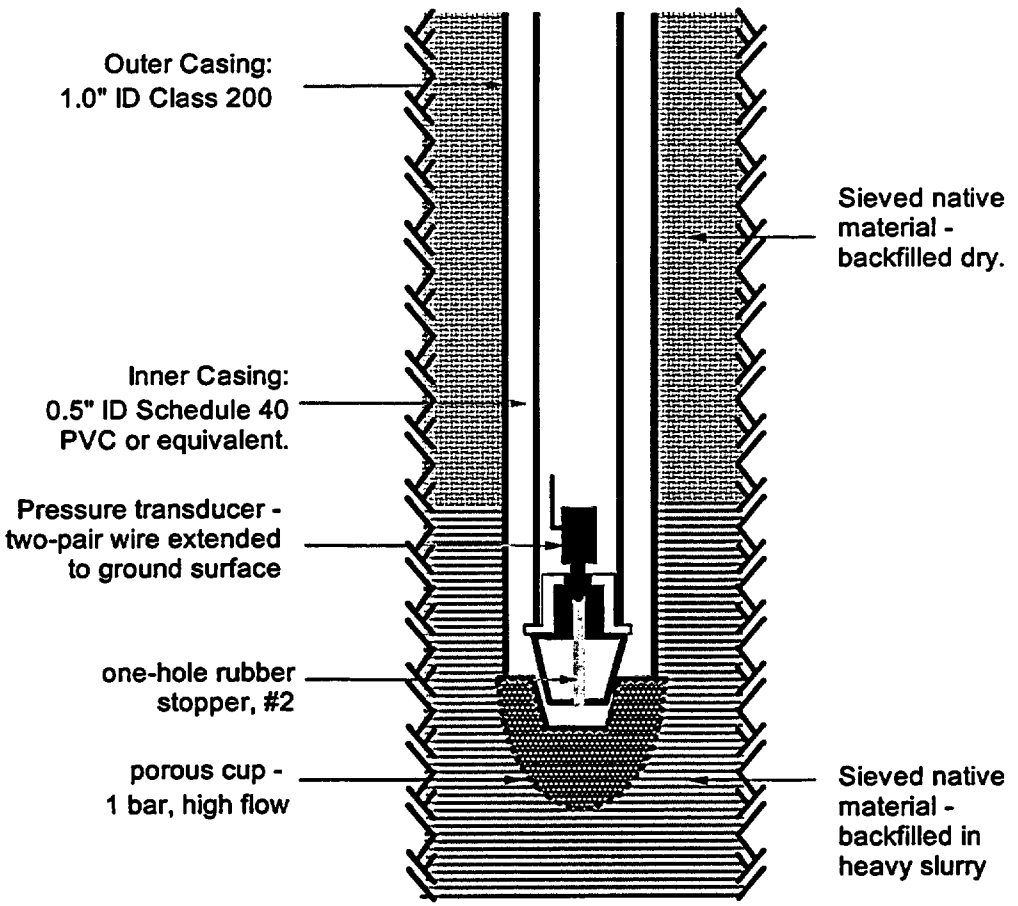

Figure 2.4-3. Schematic of deep tensiometers.

of the stainless steel tubing. The pressure transducer wire was fed through a 1" HDPE tubing, long enough to extend above the soil surface, which was sealed around the stopper assembly with silicon sealant.

Final assembly required servicing the tensiometer by pouring 150 ml of water into the tensiometer cup, enough to completely fill the cup, and inserting the pressure transducer. A very light coating of vacuum grease was applied to the #2 stopper before the pressure transducer was lowered into the borehole, forming an air-tight seal between the stopper and ceramic cup. Splicing with the Molex clip allowed us to remove the pressure transducer string for future servicing and/or repair. Wire leads from all 27 tensiometers were routed through conduit to a second-level CR7 at the south end of the plot.

2.4.3 Heat Dissipation Sensors

Heat dissipation sensors (model 229, Campbell Scientific, Inc., Logan, UT) were installed at both the buried trench (13 total) and monitoring islands (30 total) for measuring soil water tension. Because the HDS and tensiometers both require contact between the ceramic material and host soil, installation was virtually identical to the installation procedure used for the tensiometers. The description can thus be found above.

All HDS were calibrated independently by using a series of soil bins (Figure 2.4-4). Before beginning calibration, they were submerged in water for a minimum of 24 hours. A known amount of soil material (Berino loamy fine sand, fine-loamy, mixed, thermic, typic Haplargid) was moistened to a corresponding soil water tension and packed into plastic soil bins at equal bulk densities. Several HDS sensors were then placed into the soil, the bin was sealed, and the units were allowed to equilibrate with the soil. Tensiometers were installed in each bin and sampled using a Tensimeter (Soil Measurement Systems, Tucson, AZ), providing an independent tension reading. Three bins were used and maintained at tensions of 50, 100, and 200 cm of water. Generally, the units equilibrated in 3-5 days. Afterwards, the units were removed from the soil bin and transferred to the next drier bin. When the units were fully tested in the bins, they were embedded in silica flour and placed inside a pressure plate apparatus on 15 bar ceramic plates (Soilmoisture Equipment, Inc., Santa Barbara, CA) and brought to pressures of 1 and 5 bar. This procedure provided independent readings for each HDS sensor from near saturated to very dry conditions. Calibration curves were then determined according to Reese (1996).

The multiplexer for the HDS sensors installed in the trench, was located near the center of the irrigated plot, while one multiplexer was installed in each of the monitoring islands. All multiplexers were controlled using the CR7 data logger and model CE8 constant current interface (Campbell Scientific, Inc.) at the southern end of the trench. Uncorrected HDS data were converted to tensions in the site database using individual calibration curves.

2.4.4 Solution Samplers

Two types of solution samplers were used during this research: single- and dual-chamber models. The single-chamber samplers were installed in the trench and monitoring islands, and the dual-chamber samplers were installed in the deep boreholes. All samplers were constructed of stainless steel.

a. Installed in Trench and Monitoring Islands

All samplers installed in the trench and monitoring islands were composed of porous stainless steel tubing (20.3 cm long by 2.54 cm OD) with attached stainless fluid retrieval tubes (0.32 cm OD). Figure 2.4-5 shows how the vacuum and fluid retrieval tubes are terminated inside the sampler. All samplers were cleaned and checked for bubbling pressure before field installation. Samplers were cleaned by soaking in isopropyl alcohol. Alcohol was pulled inside the samplers under vacuum to ensure that all steel pores were cleaned. Afterward, pulling water into and pushing water out of the sampler under vacuum and pressure, respectively, displaced the alcohol.

In the buried trench, these steel tubes were connected to polypropylene tubing (0.64 cm OD) through compression fittings (Kynar PVDF model 0607-031, JACO). The polypropylene tubing was brought to ground surface inside the same conduit used for HDS and TCP wiring, and was

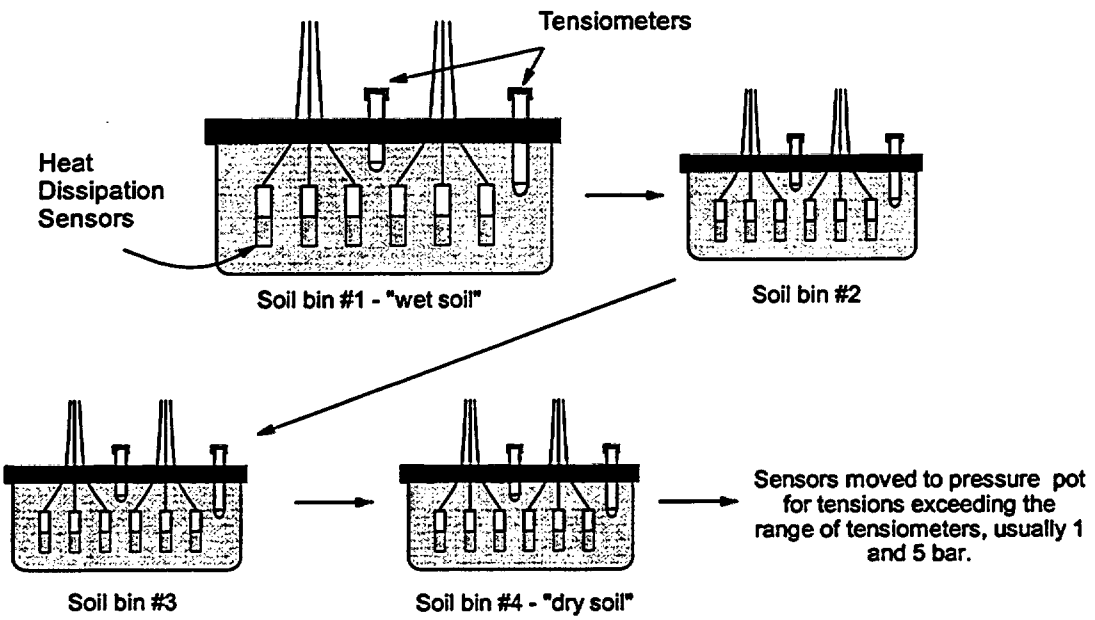

Figure 2.4-4. Calibration of heat dissipation sensors as they are moved to successively drier soil.

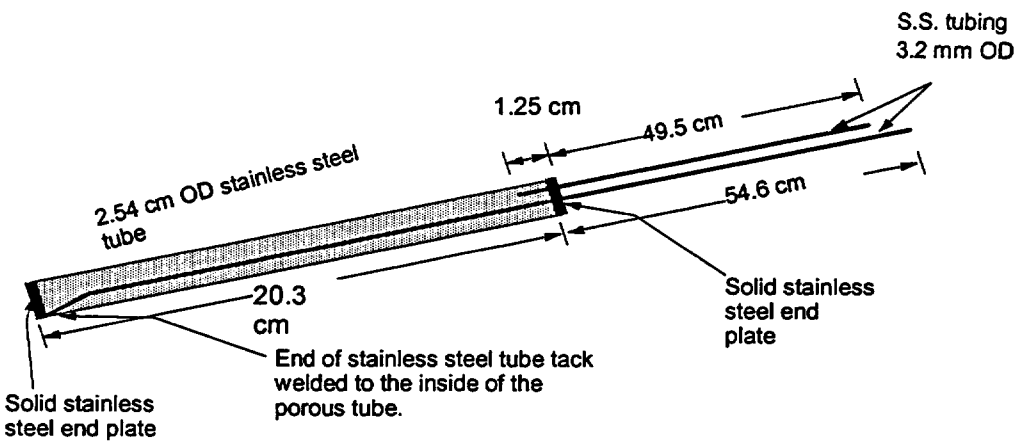

Figure 2.4-5. Schematic for single chamber stainless steel solution sampler.

terminated to the east of the wooden walkway. The vacuum line was closed off using a short piece of rubber tubing and a plastic tube clamp. The fluid retrieval line was connected to plastic vials using a two-hole stopper and a short piece of polypropylene tubing connected to quick-disconnect couplings. Vacuum was applied to the samplers using a single manifold constructed along the entire length of the buried trench. The manifold was equipped with one port for each sampler, and a final port for connection to a portable vacuum pump. Vacuum was regulated by opening and closing the tubing clamp found at the southernmost port on the plot (e.g., Y = 0 m). The manifold was vacuum tested prior to beginning the experiment and was found to hold vacuum quite well.

In the monitoring islands, connections from the stainless steel tubing to the polypropylene tubing were done using the same compression fittings as described above. Vacuum manifolds were constructed so that all 15 samplers in each island could be sampled at the same time. The manifold was made of PVC pipe and connected together using pneumatic tubing. Each solution sampler was connected to the manifold using quick-disconnect couplings and polypropylene tubing. Only those samplers used on any particular day would be connected to the manifold. Ports not used were automatically closed off with the normally-closed couplings.

Vacuum levels applied to the solution samplers in both the trench and monitoring islands depended on the wetness of the soil. During the infiltration phase of the experiments, water contents were higher so that adequate amounts of fluid could be retrieved without applying a vacuum in excess of 200 cm. As the soil drained after ceasing irrigation, vacuum was increased to a maximum level of 500 cm of water.

b. Installed in Deep Boreholes

The dual-chamber solution samplers (Figure 2.4-6) were completed using sieved native material in the same way as described above. The vacuum/pressure line and fluid return lines were connected to polypropylene tubing (0.64 cm OD) through compression fittings (Kynar PVDF model 0607-031, JACO). The polypropylene lines were marked appropriately, and fed through the Class 200 pipe to ground surface. A one-by-three manifold was constructed using PVC pipe, quick-disconnect couplings (models 0855-103 and 0751-124, Ryan-Herco Products) and Masterflex tubing, so that each of the three solution samplers could be pressurized and sampled contemporaneously using a portable vacuum pump.

2.4.5 Temperature Thermocouples

A total of 10 temperature thermocouples were used to measure temperature changes with depth. Two vertical transects, located at X = 29 m, and Y = 10 and 20 m, were chosen. Five thermocouples were installed in each transect, at 0.05, 0.10, 0.25, 0.50 and 1.0 m depth.

The thermocouples were made by stripping approximately 6.4 mm of the outer cover away from both the copper (blue) and constantin (red) wires (model TT-T-24, Omega Engineering, Stamford, CT). The two wires were tightly twisted together and tinned using a soldering iron. Then epoxy was placed on the bare portion of the sensor to prevent shorting due to contact with infiltrating water during the experiments. When the epoxy was dry, a razor blade was used to trim away any excess epoxy from the bare portion of the TTC sensor. The thermocouple junctions were tested by placing the sensors and a mercury thermometer in a bucket of ice water and comparing the temperatures.

2.4.6 Thermocouple Psychrometers

The thermocouple psychrometers (model 74-XV, JRD Merril Specialty Equipment, Logan, UT, where X represents lead length in meters) were ordered with lead lengths capable of reaching the CR7 data logger at the south end of trench with model A3497 cooling current interface (Campbell Scientific, Inc., Logan, UT). One unit was installed at each of the 13 instrument clusters located along the buried trench. Psychrometers were calibrated in the laboratory following the method of Brisco (1984) and Rawlins and Campbell (1986). Saline (NaCl) solutions were prepared in volumetric flasks at concentrations corresponding to tensions ranging from 2.3 to 70 bar. Calibration curves were generated for each unit

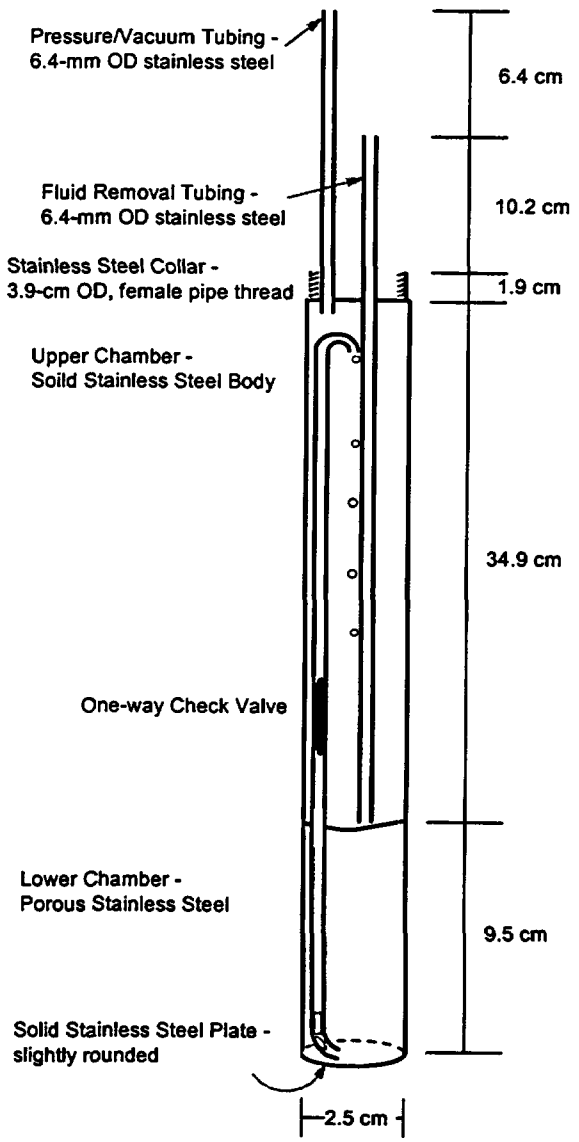

Figure 2.4-6. Schematic for dual chamber stainless steel solution sampler.

independently, which were then placed in the database for post-processing. Instruments were installed by advancing the access hole 50 cm into the undisturbed soil, placing the psychrometers at the back of the hole, and backfilling the hole to the trench wall with moistened, sieved native material. Wire leads were fed into conduit and terminated at the CR7 data logger.

2.4.7 Surface Electromagnetic Induction

Surface, non-invasive geophysical techniques were used to detect changes in the apparent electrical conductivity (EC_a), from which water content changes could be inferred (Sheets and Hendrickx, 1995). Models EM-31 and EM-38 (Geonics Ltd., Mississauga, Ontario, Canada) were used during the experiment. Penetration depth depends mostly on the height of the unit above the soil surface and instrument orientation. For Experiment #1, we placed the units on the soil surface to obtain readings to optimal soil depths. The depth of penetration is 0.75 and 1.5 m for horizontal and vertical orientations using the EM-38, and 3.0 and 6.0 m for horizontal and vertical orientations using the EM-31 (McNeill, 1992).

Data were collected during Experiment 1 approximately daily for the EM-38, which has a shallower penetration depth, until the wetting front was observed to migrate deeper than 2.0 m. At this time, it was assumed that the soil water storage would be at steady state and that changes in EC_a would stabilize. Data collection using the EM-31 commenced with measurements taken approximately every two to three days depending on availability of field personnel. All data were recorded by hand during the experiment.

During Experiment 2, the sampling program was optimized slightly. The two westernmost N-S transects, as shown on Figure 2.3-7, were not used for measurement because they were far from the irrigated plot and did not contribute useful information for our purposes. We also included site specific depth profiling at four locations on the irrigated plot to verify theoretical inverse calculations made by Borchers et al. (1997). This was done by placing the EM instrument onto a wooden rack and raising the meter above ground surface to various levels while collecting the EC_a reading. A different rack was used for each EM instrument. The EM-38 was raised by 0.10 m increments to 1 m, and the EM-31 was raised by 0.20 m increments to 2 m. These readings were taken at five locations daily until the wetting front reached the depth of penetration of the instrument, as signaled by the lack of change of EC_a reading in the field.

2.4.8 Electroresistive Borehole Tomography

A total of 12 boreholes were constructed for performing Electroresistive Borehole Tomography (ERT) measurements. ERT is a borehole D/C electrical method which uses a dipole-dipole configuration with dipole lengths of 3 m (3 times the electrode spacing). ERT boreholes were completed using 5 cm ID Schedule 40 PVC. Sources and detectors were spaced every 1 m to 15 m depth, with all electrical wiring for the sources/detectors contained inside the casing. Wire leads from the boreholes to the data acquisition system were placed in conduit on the soil surface.

During data collection, 150 volts was placed across the transmitter dipole to produce a near steady-state current of about one amp (Stubben and LaBreque, 1998). The induced voltage was measured across a receiver dipole. Using many different combinations of transmitter and receiver dipoles at different separation distances in the same two boreholes, a 3-D inversion algorithm provided an image of the 3-D resistivity within the area bounded by the boreholes. The algorithm was run several times prior to beginning Experiment 1 to get baseline readings. During the experiments, more data were collected, and subtracted from the baseline readings. The resultant values provided changes in resistivity, from which changes in water content could be inferred.

2.4.9 Gas Transport Experiments

A total of six boreholes were drilled for soil gas studies at the Maricopa site. Two boreholes were used to monitor subsurface gas pressures in response to barometric pressure fluctuations, one inside (MAM1) and the other outside (MAM2) the irrigated plot. The remaining four boreholes were drilled outside the irrigated plot for pneumatic pressure tests.

The monitoring boreholes were drilled using a hollow stem auger (diameter: 17.8 cm [7 inch]) to a depth of 11 m. Soil samples were collected during borehole construction at 0.3 m depth intervals for analysis of texture and water content. Bulk density samples also were collected at 0.9 to 1.5 m depth intervals. Gas ports, consisting of slotted stainless steel screens (2.54 cm outside diameter, 30 cm long), were installed at 2.5 m intervals to 10 m (Figure 2.4-7). A YSI (Yellow Springs, OH) thermistor was installed with each gas port to monitor temperature change at depth. The gas ports were connected to the surface using nylon tubing (0.635 cm outside diameter). The borehole was backfilled with sand 13 cm below and above the screens and a 50:50 sand/bentonite mixture to form a seal and to prevent preferential flow in the borehole.

The data logging system consisted of a CR10X data logger (Campbell Scientific, Inc.) that controlled solenoid valves, a pressure transducer, a barometer, and thermistors. Each gas port was connected to a dedicated solenoid valve. An extra solenoid valve was included to used as an atmospheric vent. A solenoid, connected to a manifold, allowed measurement of air pressure at four depths with a single differential pressure transducer (Model 239, SETRA, Acton, MA) at the surface. The solenoid valves were opened and closed by a Campbell CD16AC switching unit which received commands from the CR10X. A Setra 270 Barometer was included to monitor barometric pressure fluctuations. Surface and subsurface gas pressures and temperatures were logged every 15 min to evaluate attenuation and phase lag of pressure fluctuations with depth.

Four boreholes were drilled to conduct pneumatic pressure tests. An injection/extraction borehole (designated MI1) was drilled to 7.5 m depth and 3 monitoring boreholes (designated MP1, MP2, and MP4) to 10 m depth at distances of 1, 2, and 4 m from the injection/extraction borehole. Sediment samples were collected at 0.3 m intervals to total depth for texture and water content analyses in all boreholes. A PVC screen (5 cm diameter with 0.25 mm slots) was installed at the base of the injection/extraction well (MI1). A PVC pipe of similar diameter was used to connect the screen to the surface. Sand (20/40) was used to complete the boreholes around the screens and the remainder of the borehole was completed with grout to land surface.

Gas ports were installed at 2.5 m intervals in each of the monitoring boreholes. The gas ports consisted of 3 mm copper tubing at the desired test depth with a 3 cm slotted section at the base. Thermistors were placed at each depth in MP2 to record temperature fluctuations during testing.

The pneumatic test was conducted using a high volume, low pressure blower to inject/extract air into MI1. A ROTRON Model EN6F5L blower was used with a 1.80 m section of flexible hose (5 cm diameter) attached to a 3 m section of pipe to establish laminar flow. At the end of the pipe a thermistor, an Omega flow meter, and a 15 psi pressure transducer was used to measure the air temperature, flow rate, and injection pressure respectively. A second section of flexible hose connected the pipe to the PVC well head on MI1. A Campbell CR10X data logger was used to monitor pressures and temperatures. A Campbell AM416 multiplexer was used to switch between 12 pressure transducers and 4 thermistors used during testing. Data required for analysis included flow rate from the air pump, temperature and pressure of injected or extracted air, pressure at all monitored depths in all monitored boreholes and temperature measurements from one borehole. Injection tests were conducted at 50.8, 101.6, 152.5, and 203.3 cm water pressure. Each test was run until no observable change occurred in the farthest most pressure transducer (MP4, 10 m depth). Extraction tests were conducted at 101.6 cm water.

2.5 Methods of Instrument Calibration

2.5.1 Neutron Probe

It should be mentioned here that two probes were used during the field experiment: the #66 and the #18 probes, named for the serial number of each unit. The #66 probe was used for scanning vertical access tubes only and the #18 probe was used for the horizontal tubes only. Thus we calibrated each probe to match the specific tube type during the experiment.

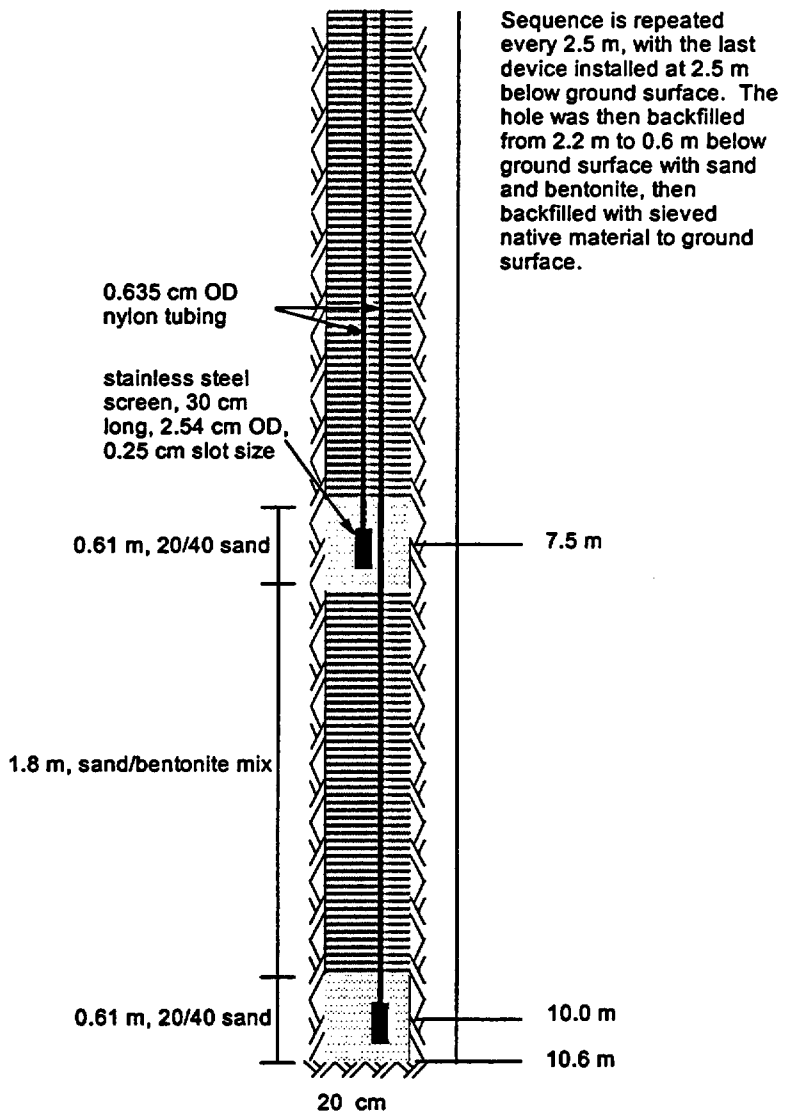

Figure 2.4-7. Borehole schematic for pneumatic monitoring boreholes (not to scale).

2.5.1.1 Steady-state Method

The steady-state method was carried out approximately 20 m west of the irrigated plot, adjacent to the standard borehole used during Experiments 1 and 2. The calibration area was installed in a 12.2 by 6.1 m area. A total of three access tubes were installed to a depth of 3 m. Each access tube (5 cm ID PVC, 10 cm PVC, and 7.5 cm HDPE) represented tube material and diameters used during the field experiments. Undisturbed soil cores were collected using a Giddings probe (4 cm ID) in 6 boreholes total inside the calibration area, two each adjacent to the different access tubes. Samples were then extracted from the sampling tube and measured for volumetric water content using the thermogravimetric method. Netafim irrigation line was installed at the same 30 cm offset as used in the field plot, after which the area was covered with pond liner to prevent evaporation. Water was applied to the area for 6 days at a rate of 3 cm d^{-1}, and allowed to redistribute. Both neutron probes (e.g., #66 and #18) were then calibrated in the same boreholes as used during the field experiments: #66 was used for measuring water content in the 5 cm ID PVC boreholes, and the #18 probe was used in the 10 cm PVC, and 7.5 cm HDPE tubes. All readings were taken at 0.25 cm depth increments using 16 second counts, the same as done during the field experiment. The probe source was pushed against the side of the borehole for the 7.5 and 10 cm boreholes, to simulate field conditions when the probe is pulled through the access tube. After each data collection period, the Giddings probe immediately was used to collect additional soil cores for water content analysis. In this way, neutron probe readings and water content samples were obtained at increasingly drier soil conditions, providing a wider range of field conditions for the calibration curve.

2.5.1.2 Transient Method

The alternative method for calibrating the neutron probe was first proposed by Carneiro and de Jong (1985), which they called the "volumetric technique." Similar to their method, we summed specific volumes of water added to the soil and calculated the change in soil water storage at the immediate vicinity of the access tubes. Changes in count ratios obtained by the neutron probe were integrated over depth, and then compared to changes in soil water storage, as known from the water additions. The relationship between these two changing parameters is the slope of the calibration curve. This method is limited to the slope only, however, because we were unable to collect a sufficient numbers of samples during the field work to characterize the water content across the plot. However, this method has the advantage of involving soil from the entire profile, rather than in discrete portions. A complete description of the method is found in Young et al. (1998a).

A total of 24 access tubes were used for the analysis. During the experiment, water movement rates varied somewhat across the field, and these different rates needed to be considered in this analysis. Thus, a time series of neutron probe readings was developed for each depth and spatial location across the site. Arrival time, T_a, is defined as the time, t, at which the rate of change in neutron probe count ratio, CR, during a measurement interval, Δt, is largest:

$$T_a \equiv \left(t \left| \frac{CR_{t+\Delta t} - CR_t}{\Delta t} \equiv t_{max} \right. \right) \qquad (2\text{-}1)$$

CR can be either the neutron probe count ratio or water content, and t is time in days from beginning of the experiment (Young et al., 1998b).

Initial count readings were subtracted from daily readings during the experiment and then converted to CR. Change of soil water storage for each day, n, (referred to as SWS_{cn}) was estimated by summing the product of the CR and data collection interval (25 cm) throughout the profile to a final depth of 300 cm. The first reading used (z = 25 cm) was multiplied by 37.5 cm to account for loss of neutrons through the soil surface. The last reading taken at each borehole (z = 300 cm) was multiplied by 12.5 cm, because we are interested in soil water storage to 300 cm, not 312.5 cm as would otherwise be the case.

Parameter b was allowed to vary such that the RMSE was minimized:

$$RMSE = \left(\sum_{i=1}^{n} \frac{(\Delta SWS_m - \Delta SWS_{cn}(b))^2}{n-1} \right)^{1/2} \qquad (2\text{-}2)$$

The resulting scatterplot has a single minima located where the slope value provides the closest comparison to SWS_m. This procedure was carried out for each of the 24 access tubes, yielding a different calibration slope for each position on the field plot. Using these different slopes would be tedious in practice, thus we investigated the possibility of averaging the slopes, which also provides an estimate of deviation and uncertainty in the slope and hence the water content values. The fitted slopes were checked for normality using the Shapiro-Wilk statistic (SPSS software, release 8.00), the presence of outliers, and then spatial interdependence (Geo-EAS, version 1.2.1), steps similar to those taken by Grismer et al. (1995). Finally, we fitted all the data simultaneously, such that one value of the slope parameter and standard error would be generated. One advantage of the transient method, aside from the fact that it can be done contemporaneously with the infiltration experiment, is that location error in the neutron probe readings can be quantified. The sources of error in the measurements made using the neutron probe will be discussed below.

2.5.2 Time Domain Reflectometry

TDR probes were calibrated using the upward infiltration method (Young et al., 1997). Experiments were conducted using Casa Grande soil from the site and probes from both Dynamax, Inc. and Campbell Scientific, Inc. However, only probes from Dynamax Inc. are reported by Young et al. (1997).

2.5.3 Pressure Transducers Used with Tensiometers

Both pressure transducer models used during the field experiment (#236PC15GW and #26PCCFA1G) were calibrated using a water/mercury manometer and a vacuum system in the Soil Physics Laboratory at the University of Arizona. Transducers were calibrated using the same CR7 data logger as installed in the field, whenever possible. A manifold was constructed so that up to 16 transducers could be calibrated simultaneously. Eight vacuum steps were used in the process: 0, 5, 10, 25, 50, 100, 250, and maximum vacuum. Individual calibration curves were generated for each unit and stored in the site database. Those units found to be outside the factory specification for either linearity or offset, were recalibrated. If the results continued to be outside the factory specification, the units were returned to the manufacturer.

2.5.4 Heat Dissipation Sensors

Forty three heat dissipation sensors (229-L, Campbell Scientific Instruments, Logan, UT) were calibrated at soil pressures ranging from -50 to -5000 cm water. All sensors were pre-treated by submergence in water for 24 hours minimum, the same sensor pre-treatment used before field installation. Two different calibration apparati were used to expedite calibration by increasing the number of sensors that could be processed at one time and to minimize equilibration time. One setup involved compacting variably wetted soil in 25 x 25 x 10 cm water-tight plastic containers to obtain soil pressures of -50, -100, and -200 cm water which will be called calibration tubs. Berino loamy fine sand (fine-loamy, mixed, thermic, Typic Haplargid) was used as the calibration medium. Calibration tubs were constructed by adding appropriate quantities of water to separate batches of soil. They were allowed to equilibrate for 24 hours, and compacted to a 6 cm thickness at a 1.67 g cm^{-3} bulk density. A #7 cork borer was used to cut guide holes in the soil slightly smaller in diameter than the HDS ceramic plug to maximize ceramic plug/soil contact. The sensors were inserted into the holes so the porous ceramic was a minimum 2 cm below soil surface. HDS wire leads were routed through holes cut into the container lid and wired to a multiplexer relay (model AM416, Campbell Scientific, Inc. Logan, UT), CE8 constant current interface (model CE8, Campbell Scientific, Inc. Logan, UT), and data logger (model CR7). Lid holes were plugged with rubber stoppers and duct tape to minimize water loss. Two tensiometers, used for independently measuring soil water tension, were inserted into the soil at the same depth as the HDS plug. Soil tension measurements were made with a Tensimeter (Soil Measurement Systems, Tucson, AZ) using the double-puncture method (Cresswell, 1993) to correct for air compression of septum/water column head space. Tensiometer measurements were averaged and used as the independent variable for generating the calibration curves.

Heat dissipation sensors were sampled by the data logger

every 4 hours. Sensor operation involved a 20 second excitation with the constant current interface to induce consistent heating input while temperatures were collected every second during heating. Change in temperature (ΔT) was the temperature difference between 20 and 1 second heating times. ΔT measurements were plotted against time to determine when the sensor had come into equilibrium with the calibration soil. The sensor was considered equilibrated when there was no change in ΔT for 24 hours (6 readings). After equilibration at a certain tension, the sensors were installed in the calibration tub with the next larger tension. Calibrations proceeded from -50 cm to -100 cm to -200 cm water.

Calibration pressures of -1000 and -5000 cm were obtained using a 5000 cm (5 bar) pressure apparatus similar to that described by Fredlund and Wong (1989). The sensors were positioned in a 7.35 cm diameter by 3.5 cm tall acrylic retaining ring sitting on a 15 bar ceramic plate. One pressure plate apparatus with a 6 sensor capacity was used for calibration. A slurry consisting of 0.005 M $CaSO_4$ solution and 325 mesh silica flour was poured into the retaining ring completely encasing the sensor. HDS wire leads were routed through ¼ inch compression fittings sealed with nylon ferrules to prevent cutting the leads. All sensors could be wired into the data logger and constant current interface outside of the pressure pot. Calibration values were collected when ΔT measurements remained unchanged for 24 hours and ceramic plate outflow had ceased. Calibration pressure was recorded with a Norgren 0 to 15000 cm pressure gauge. Least squares regression was used to fit the calibration data to the form of:

$$\Delta T = b_0 + b_1 \ln(\psi) \qquad (2\text{-}3)$$

where ψ is the soil water pressure measured with the Tensimeter, and b_0 and b_1 are calibration coefficients.

2.5.5 Thermocouple Psychrometers

Psychrometers were calibrated in the laboratory following the method of Brisco (1984) and Rawlins and Campbell (1986). Saline (NaCl) solutions (0.05, 0.02, 0.97, and 1.5 M) were prepared in volumetric flasks at concentrations corresponding to tensions of 2.3, 9.0, 45.7, and 70.2 bar, respectively. Measurements were made in a calibration chamber (model 81-500, J.R.D. Merrill Specialty Equipment, Logan, UT), where the ambient temperature was carefully monitored and then normalized for 20 °C. Cooling excitation at the thermocouple junction was maintained at -2029 μV (5 mA) using a Cooling Current Interface (model A3497, Campbell Scientific, Inc., Logan, UT) for a duration of 26 second. Wet bulb measurements were then made at 1.425 second intervals for approximately 40 seconds, and were recorded on the CR7 data logger in units of μV.

Calibration curves were generated for each unit independently using simple linear regression, with the wet bulb measurements (in units of μV) and the equivalent tension (in units of bar) designated as the independent and dependent parameters, respectively. The regression data were then transferred to the database and used for post-processing of the raw data collected during the field experiments.

2.6 Water Application System

2.6.1 General Requirements

The water application system was designed to address several requirements. First, the system needed to be capable of delivering sufficient quantities of water at adequate flux rates. Second, the system needed to have insignificant hydraulic and manufacturing variability, where hydraulic variability is the reduction of emitter rate with increasing distance from the pressurized manifold and manufacturing variability is the inherent variability in the drip emitters themselves. Third, the system needed to be flexible enough to allow premixing of tracer prior to injection in the main irrigation system. And fourth, the application system needed to be designed so that specific zones of the field could be isolated for future experiments.

2.6.2 Design

The water application system was designed into the existing irrigation system at the Maricopa Agricultural Center. Two

reservoirs, approximately 0.5 km from the experimental plot, are kept full from either ground water or the Central Arizona Project (CAP) system. Water from both reservoirs was fed via gravity to an irrigation pumping building, which is located SE of the plot.

Water was routed from the farm reservoirs and pumped into two water tanks each with a capacity of about 25,000 liters. Both tanks, used previously for storing petroleum products, were thoroughly cleaned before being transported to the site. The tanks were positioned just west of the irrigation pumping building and placed onto railroad ties. The tanks were plumbed together at the base of the tanks using 10 cm ID Schedule 40 PVC well pipe and a flexible rubber connector. A translucent standpipe to be used for manually observing the water level in both tanks was then threaded into the PVC well pipe. Irrigation water for the plot could be delivered from either of the two tanks, or it could be sent directly from the farm reservoirs to the plot by turning a valve inside the pumping house. All water was pumped through a sand filter using a high-capacity water pump (model 3796, Goulds Pumps, Seneca Falls, MY) before delivery to the plot. The sand filter (model TR-100 HD, Triton), was flushed out at least every other day to ensure adequate filtering and pressurization of the irrigation system.

A field gate valve was situated at the western edge of the support zone of F-115, approximately 50 m from the irrigated portion of the field. Water flow from this gate valve was recorded using two totalizing flow meters (model MT-100, McCrometer, Hemet, CA), placed in series. The two meters were designated as Meter #1 and Meter #2. The water line was trenched across the support zone, then split into six separate irrigation stations (Figure 2.6-1) plumbed in parallel. A ball valve was installed behind the main line to sample the solution for laboratory measurements of tracer concentrations during the field experiments. Four of the stations (1-4) were equipped with 27 irrigation lines and two (stations 5 and 6) had 28 lines, yielding a total of 164 irrigation lines. Each irrigation string was connected to the main manifold by flexible fire hose to account for possible expansion and contraction of the irrigation lines. Water control was achieved using a 5 cm reducing valve (model 600, Wilkens, Inc., Paso Robles, CA) and solenoid valve (model 700 series, Hardy) immediately before water entered the individual header pipes. The solenoids were activated and deactivated by a central timer and controller. The controller was also wired directly to the water pump inside the irrigation building, allowing us to control starting and stopping of the water pump from the field. The system was wired in such a way that the pump would not turn on unless one of the solenoids was activated; otherwise, back-pressure in the irrigation building would cause failure of the sand filter. Gauges were installed on both manifolds installed on either side of the field to monitor drip-line pressures.

Self-cleaning precision emitter drip-line (0.6 gallon/hour, Netafim Techline, Fresno, CA) was used for the irrigation system. Each of the 164 lines were spaced 30 cm apart, the same spacing as drip-line emitters, providing just under 27000 emitters for the 2500 m^2 area of the plot. Each line was cut to the same length, walked out onto the field and oriented so that the emitter direction would be horizontal to the soil surface. Considerable effort was spent to ensure that each line would remain parallel to each other during the experiment. Specifications for the Techline indicated that the material had a coefficient of expansion of 2%. Thus, we expected that the length of each line would be 50 m ± 50 cm. If the lines overlapped one another during the higher, daytime temperatures, then water application could easily become non-uniform. To guard against this from occurring, each irrigation line was staked at an interval of 2.25 m across the length of the field.

During the field experiments, the irrigation system was pressurized three times per day, and allowed to run for 14 minutes per event, each time delivering approximately 0.66 cm to the field. If the system was programmed to deliver the full amount of water during one event, the application rate would have corresponded to approximately 68.6 cm d^{-1}. This high flow rate would have exceeded the saturated hydraulic conductivity of the surface soil, resulting in ponding and poor control. It was therefore necessary to balance the need for uniformity along the drip lines by reducing the number of pressurizing events, with the need to reduce the chances of ponding.

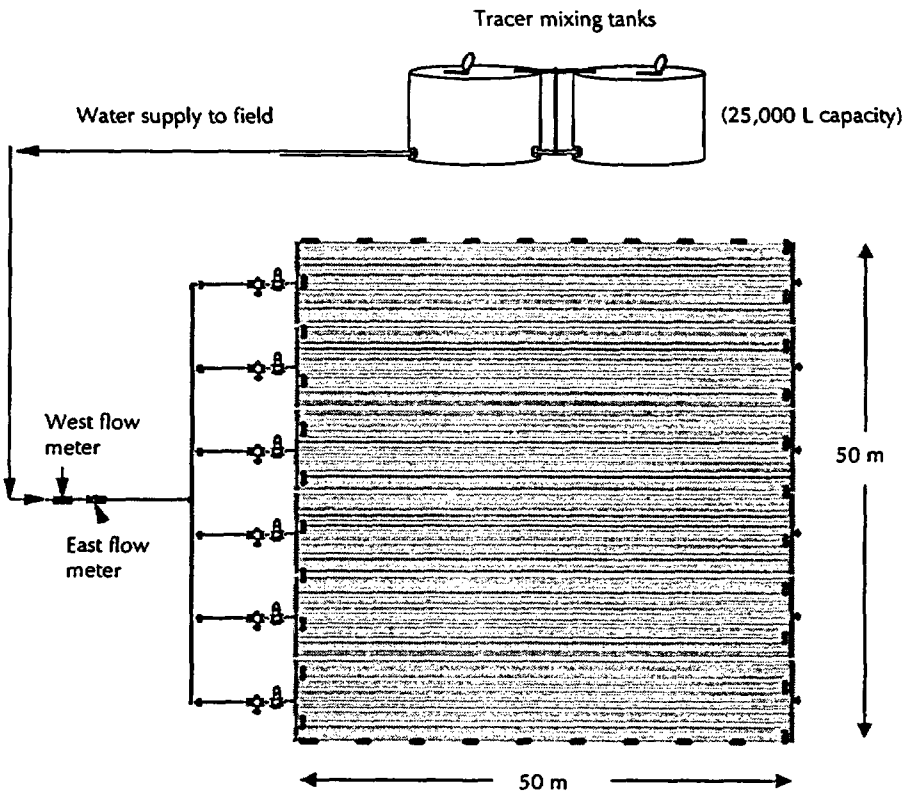

Figure 2.6-1. Diagram of water application system consisting of six independently operated stations.

2.6.3 Calibration and Field Testing

2.6.3.1 Calibration Method

A total of seven uniformity tests were run on a prototype irrigation system that consisted of 27 lines each 50 m long. This was the identical setup for one irrigation station at the Maricopa site. The goal was to determine if the discharge amounts were independent of the distance to the header pipe (i.e., insignificant hydraulic variation). Independence of distance would indicate that water will be evenly distributed across the field at the site. If the discharge amounts are found to be dependent on distances to the header, then one part of the field could receive more water than the other, biasing our experimental results. A modification of the irrigation system design would be required so that both ends of the irrigation system would be pressurized simultaneously.

Five of the tests (designated herein as Tests 1 - 5) were run by choosing eight locations for collecting water at increasing distances from the header. Water was collected in troughs constructed with a 10 foot length of 10 cm ID PVC pipe, and an outlet for draining the trough after testing. The trough was placed beneath ten drip emitters, normal to the direction of the drip line (10 different lines). The system was pressurized and the test ran for 8 minutes (we found that the header pipe pressure decreased after about 5 minutes of operation, likely because the farm's potable water supply was de-pressurizing from the high flow rate). In these cases, the test was terminated when the pressure dropped below 7 psi, the minimum rating for the Netafim drippers. We used two statistical tests to analyze the data: the Kolmogorov-Smirnov (K-S) for testing normality and the Pearson Product Moment Correlation for testing correlation between distance and discharge. The Pearson test measures the strength of association between two variables without specifying which is the dependent or independent variable.

The remaining two tests were run to quantify the manufacturers variability (designated herein as Tests 6 - 7). Our goal in running these tests was to quantify the manufacturer's variation of the drippers and compare them to the factory rating supplied by Netafim. An unacceptably high variability would indicate poor manufacturing of the drip line. The tests involved choosing and collecting water from 24 individual drippers using 23 by 23 cm pans, and weighing the amount of water collected during a specific time period. In Test 6, we randomly chose the drippers and in Test 7, we randomly chose one drip line and equally spaced 24 pans along the line. We determined the mean, standard deviation and coefficient of variability (CV) of the water collected in each pan (we discarded a small number of samples because of spillage), and then checked that against those found in CATI (1995). A linear regression test was also run using distance from header and discharge as the independent and dependent variables, respectively. Though the pans were randomly placed in Test 6, we sorted the discharge values according to distance from the header.

Mass balances were calculated for Tests 4-7. This was done by comparing the total amount of water collected as a percentage of that recorded on the water meter, with the percent of drippers monitored. Poor mass balance would indicate that some of the dripper lines could be leaking, or that we did not correctly collect water from drippers monitored in the field test.

2.6.3.2 Calibration Results

Figure 2.6-2 shows the discharge amounts as a function of distance to the header. Note that Tests 3 and 4 were run for the full 8 minutes because the system pressure dipped below 7 psi. Test 5 ran for 6 minutes because the system under-pressurized. We found a consistent 4 psi drop in pressure from the pressurized header pipe to the other end of the drip lines during the seven tests.

Results of the K-S analysis indicate that all five field tests passed the normality tests for a $P > 0.05$ (raw data not shown). The Pearson Product Moment Correlation, run for each test, showed that tests 1, 2, and 5 passed the correlation test ($P > 0.05$), indicating that the variables (e.g., distance to header, and discharge) are not associated. Tests 3 and 4 both failed. As stated above, these two field tests experienced line pressures below 7 psi, thus we would not expect the discharge amounts to be independent with distance from the header.

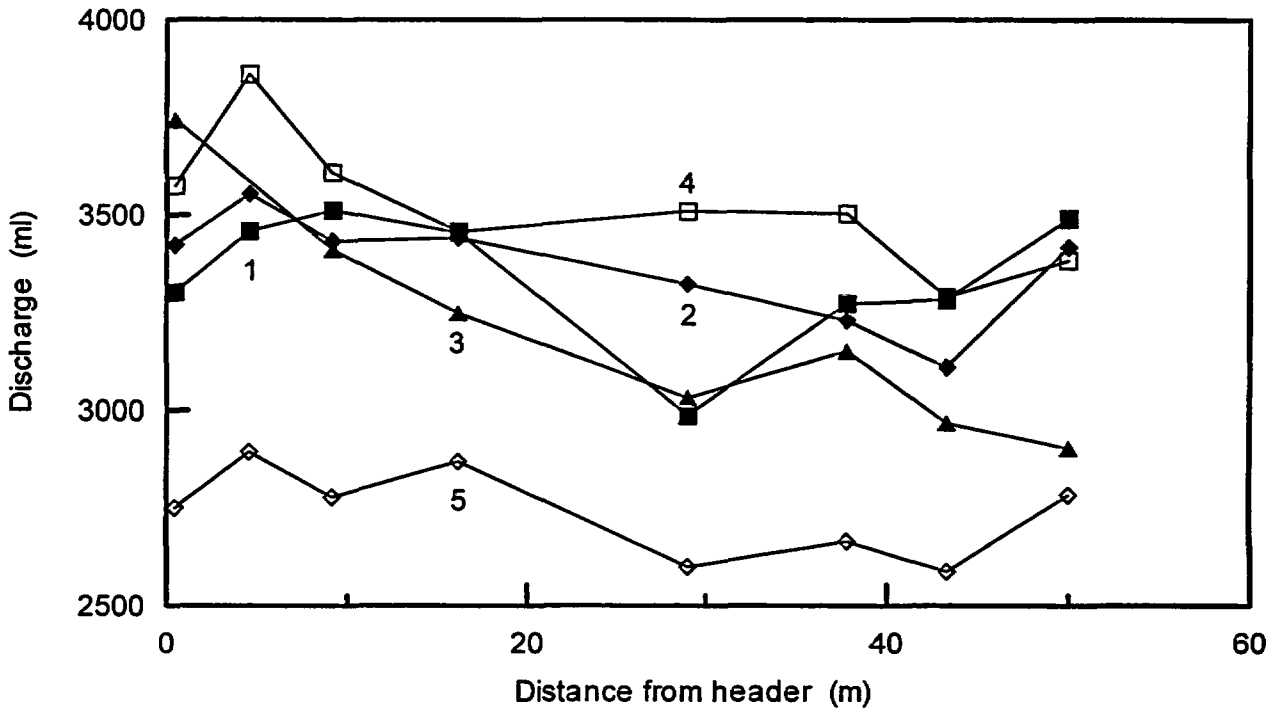

Figure 2.6-2. Results of uniformity testing of irrigation system.

Table 2.6-1 provides the results of statistical analyses for Field Tests 6 and 7. The differences in the mean values were caused by running Test 7 for one minute longer before the pressure in the potable system dropped below 7 psi. The CV was slightly higher than the factory rating of 0.036. The regression slope was less than zero in both cases, indicating a slight dependence of discharge on distance, but not statistically significant.

The mass balance analysis run on Tests 4 - 7 (see Table 2.6-2) shows that the percentage of water collected using both the pans and troughs was consistently less than the percentage of drippers used for collection. However, given the relatively large number of drippers on the station, comparisons between percent of water collected and percent of drippers monitored are good. The lower percentage of water collected indicates that 1) small leaks could be present in the system (though none were observed), 2) drippers not monitored could be systematically discharging more water than the drippers monitored, 3) water was not correctly dripping into the trough, or 4) the resolution of 10 gallons on the water meter was not sufficient for this type of test. The bottom three rows in Table 2.6-2 compare the emitter rate versus the entire station discharge. The values show that the average discharge rate of the emitters monitored was slightly less than the entire system, but still close. The small sample sizes for Tests 6 and 7 probably explain the larger differences between the average emitter rate from the entire station versus the emitters monitored.

Using the results of these seven tests, and the statistical analyses, the chosen design of the irrigation system (one pressurizing header) did provide uniform water application across the 50 m by 50 m plot. The results also illustrated the importance of maintaining adequate pressure throughout the 50 m length of the system. Though the statistics confirm that no association exists between distance to header and emitter discharge, visual inspection of Figure 2.6-2 indicates that a weak association potentially could be present between the two variables, but that it was not significant enough to warrant changing the irrigation design.

2.7 Final Site Preparation

After installation and in-place testing of the irrigation system, the field was prepared to be covered with pond liner. Drainage channels were cut into the north, east and south sides of the irrigated plot, sloping toward the east and south, and a sump pond was dug at the southeast corner of the plot for collecting rainwater. Anchoring trenches were dug on the back side of the drainage channels, and berms were textured to improve the installation of the cover.

In late March, 1997, 32 mil thick Hypalon pond liner was installed over the entire field plot, including the 50 m by 50 m irrigated plot, 5 m support zone outside of the irrigated plot, the drainage channels and the sump pond. Numerous holes were cut into the pond liner to accommodate the monitoring instruments and access tubes. Each hole was sealed as best as possible using a separate boot around each access port or tube. Silicon sealant also was used to reinforce the weld between the boot and cover itself (when necessary), and the boot and access tubes.

After the pond liner was installed wooden walkways were added to minimize disturbance to the soil during the experiments. Treated lumber (2x4 and 2x6 studs) were placed on the field and held together using wooden ties and wood screws. Each walkway was 25 cm (10 inches) wide, and placed so that each monitoring point would be accessed without stepping onto the soil surface directly (Figure 2.7-1).

2.8 Soil Sampling and Description

During excavation of the trench, and while it was open, soil sampling and profile description was performed. The purpose of these activities was to obtain information about the spatial variability of the soil properties along the transect to a depth of 1.5 m, to obtain hydraulic properties prior to the infiltration experiments, and to better simulate water flow and solute transport after the experiments. Sampling was divided into undisturbed core and grab sampling, depending on the location in the trench and the data required after analysis. Table 2.8-1 lists the sampling schedule for soil at the trench and the analysis for each

Table 2.6-1. Descriptive statistics from Tests 6 and 7 during calibration of irrigation system.

	Test 6†	Test 7‡
Mean (ml)	260	290
Standard Dev. (ml)	11.98	16.256
CV	.046	.056
regression slope	-0.175	-0.127
regression offset	272.7	299.5
r^2	0.43	0.13

† Test 6 - randomly placed pans throughout the station.

‡ Test 7 - equally spaced pans on one randomly-chosen line.

Table 2.6-2. Results of mass balance test for calibrating the irrigation system.

	Test 4	Test 5	Test 6	Test 7
Meter reading (gal)	430	330	345	380
Water collected (gal)	7.45	5.79	1.512	1.453
Water collected/meter reading (%)	1.73%	1.76%	0.44%	0.38%
Total emitters	4428	4428	4428	4428
Drippers monitored	80	80	22	19
Monitored/total (%)	1.81%	1.81%	0.50%	0.43%
Emit rate for emitters monitored (gal h^{-1})	0.70	0.72	.607	.612
Emit rate for station (gal h^{-1})	0.73	0.75	.687	.687
% difference in emit rate for emitters monitored versus entire station	4.29%	4.17%	13.18%	12.25%

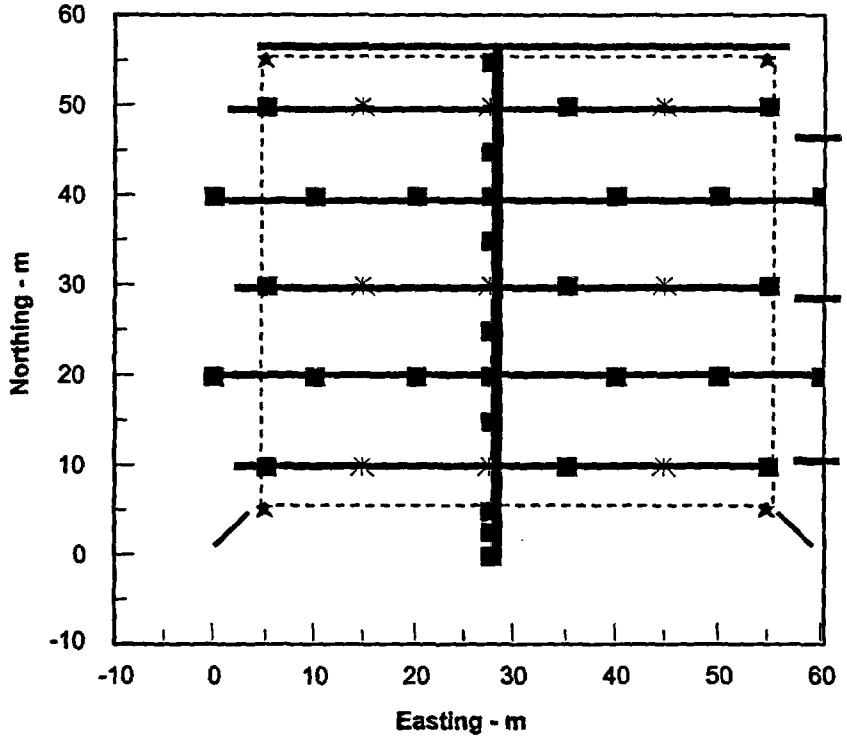

Figure 2.7-1. Location of wooden walkways placed on the covered plot.

Table 2.8-1 Compilation of soil sampling and analysis in buried trench transect.

A. Core Sampling		Number of samples
1	1.0 m depth, 2 cores at each of 6 sites with presence of tensiometers	12
2	1.5 m depth, 3 cores at each of 13 sites	39
3	special site, variable depth, 2 cores each strata, 2 sites, assume 4 strata	16
4	1.5 m depth, 3 cores to study analytical method variability	3
	Total	70
B. Grab Sampling		
1	composite sample collected every 25 cm depth to 175 cm, every 5.0 m	91
2	1.0 m depth, every other 5.0 m (no presence of tensiometer)	7
3	1.5 m depth, every 0.5 m	107
4	special site, very distinct layer at two sites, assume 4 strata	8
	Total	213
C. Analysis - categorized by sample type and location		
A1	upward infiltration, Ks, multistep outflow, and bulk density to determine hydraulic properties	
A2	same as A1 above	
A3	same as A1 above	
A4	same as A1 above	
B1	morphologic description (texture, color, EC, pH, aggregation, 1 and 15 bar tension)	
B2	texture, 1 and 15 bar tension	
B3	texture, 1 and 15 bar tension	
B4	texture, 1 and 15 bar tension, anion/cation, EC	
D. Other information		
1.	Core sampling to use 3.5" OD acrylic columns	
2.	Grab samples to contain 2.0 liters of soil	

sampling type. The methods used for sampling are found in Appendix 2. The soil profile along the entire length of the trench transect was described in October, 1996 by Mr. Guy Chammas, of the Department of Soil, Water and Environmental Science. Generally, the soil profiles in the trench were well developed in terms of calcium carbonate and clay accumulation (i.e., calcic or argillic horizons), and are in the Aridisol soil order. All profiles showed evidence of a plowed A (Ap) horizon between about 20 and 30 cm in depth. Below the Ap horizon, well-developed B horizons were present with calcium carbonate and/or clay accumulation. The B horizon was subdivided into two units at the southern end of the trench, usually according to changes in structure. In the southern area of the trench, the upper B horizon was found to have an angular to subangular structure, weakly graded. Differences in structure disappeared from Y = 20 m to the north, at which point these layers in the B horizon were lumped together into a single unit. The soil along the trench exhibited a very hard consistency and massive structure. The boundary between the B and C horizons was found to be abrupt and topographically smooth in the southern portion of the trench. Differences between the soil horizons were based on an increase in percent rock fragments (5-30%) and single-grained structure; however, these differences became indistinguishable north of approximately Y = 15 m, where the C horizon no longer was found.

Two representative pedons were identified along the trench so that undisturbed soil samples could be taken within morphologically distinct zones. One representative pedon was identified and located at Y = 5 m to depict the occurrence of a more gravelly and sandier 2C horizon at about 125 cm depth that tended to disappear below the trench toward the north. The other representative profile typifies the soil morphology for profiles from Y = 20 to the north.

3 RESULTS AND DISCUSSION

This section lists the results of laboratory and field calibration of instruments, and results of Experiments 1 and 2. The results of Experiments 1 and 2 are presented in the order of the monitoring systems used. This makes presentation of the results easier. A companion NUREG report (NUREG/CR-5698, Young, et al., 1999) provides comparisons of the different monitoring strategies considered for the site.

3.1 Calibration Results for Different Instruments

3.1.1 Neutron Probe

3.1.1.1 Steady-state Method

Neutron probe calibration sampling was conducted in April, 1998, four days after ending irrigation in the subplot. Dry bulk densities were determined for each of the samples collected in the subplot and are presented in Table 3.1-1. Substantial compaction occurred during the latest sampling, which was expected in the wetter soil. A small number of outliers at the 5 cm PVC access tube location were found at 40-60 and 90-110 cm depths. Mean bulk densities do not include these outliers. As mentioned above, the #66 probe was used in vertical access tubes only and the #18 probe was used for the horizontal tubes.

Figures 3.1-1 through 3.1-3 show the calibration results for the 5, 7.6, and 10 cm diameter access tubes, respectively. Calibration curves were generated using count ratio (CR) as the independent variable and volumetric water content as the dependent variable, which is more relevant to field applications. Note the drastic change in slope between the 5 cm diameter PVC versus the 10 cm PVC access tubes, reflecting the lower return of neutrons in the large diameter tube. All figures show some scatter around the regression line, but generally the representation is good. Correlation coefficients were above 80%, and close to 90% in the 7.5 cm HDPE tube.

3.1.1.2 Transient Calibration Method

Table 3.1-2 provides the results of the individual optimization for each of the 24 neutron probe access tubes located at least 5 m inside the irrigated plot. The slope values were shown be normally distributed using the Shapiro-Wilk test on all data (z=0.861; P=0.01). Two slope values were found to be outside the mean ± (2*standard deviation), and thus are considered to be outliers. This was observed to occur in access tubes #405 and #422, which experienced preferential wetting from a leak in the plastic cover prior to irrigation. This initial wetting led to smaller changes in water content (and hence CR) after irrigation began, thus leading to a higher calibration slope. The average standard error for estimating water content (e.g., last column in table) was less than 1.0 $m^3\ m^{-3}$, which was encouraging considering the variable texture at depth, the 25 cm collection interval and the 16 second count.

The data were checked for spatial interdependence using an omnidirectional semi-variogram, with a 90° tolerance and a search length of 12.5 cm (25% of the furthest well pair). Presence of spatial dependence would invalidate the random sampling required for the assumption of normality. The results of GeoEAS (version 1.2.1) showed no relationship between variance and lag distance with pure nugget variability of 5.52 cm (0.0184 $m^3\ m^{-3}$).

Figure 3.1-4 shows the scatterplot of RMSE versus slope for access tube #433, located close to the center of the plot. Note the distinct minimum error at slope = 24.3 CR^{-1}. The shape and behavior of the data from this access tube were very similar to those observed from the other access tubes, and is shown here as an example. The minimum RMSE, as stated above, occurred when the estimated soil water storage most closely matched the water applied to the soil. The unique solution provides some confidence that the slope was obtainable, and that the RMSE of water content was the error one can expect from using a particular slope at a particular location.

Table 3.1-3 shows the results of simultaneously fitting all data collected from the access tubes for depths at or less than 300 cm (n=2148). The results are presented for both unfiltered and filtered data (outliers removed). The RMSE for water content was considerably higher than the average value obtained from individually fitted slope values for other access tubes, reflecting the presence of location error

Table 3.1-1. Bulk densities from steady-state calibration of the neutron probe.

	5 cm ID PVC		7.6 cm ID HDPE		10 cm ID PVC			
Depth	#1	#2	#1	# 2	#1	#2	Mean	CV
cm	---------- g cm^{-3} ----------						%	%
15 to 35	1.79	1.79	1.66	1.89	1.74	1.73	1.77	3.9
40 to 60	1.77	1.44	1.71	1.64	1.68	1.60	1.64	6.4
65 to 86	1.81	1.84	1.73	1.76	1.71	1.75	1.77	2.5
90 to 110	1.69	2.03	1.64	1.89	1.43	1.74	1.74	10.9
115 to 135	1.68	1.81	1.63	1.83	1.53	1.65	1.69	6.1
140 to 160	1.65	1.96	1.55	1.85	1.66	1.84	1.75	7.9
165 to 185	1.70	1.69	1.72	1.81	1.69	1.72	1.72	2.4

Note: #1 and #2 indicate samples collected adjacent to one another.

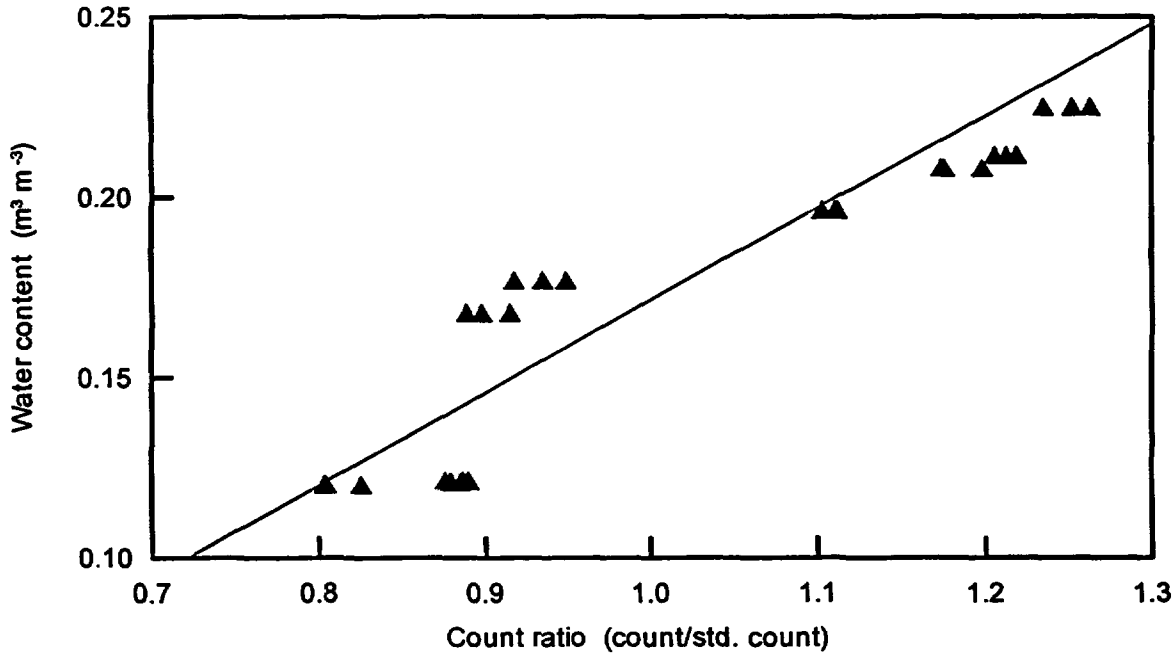

Figure 3.1-1. Calibration results of steady-state neutron probe for 5 cm access tube.

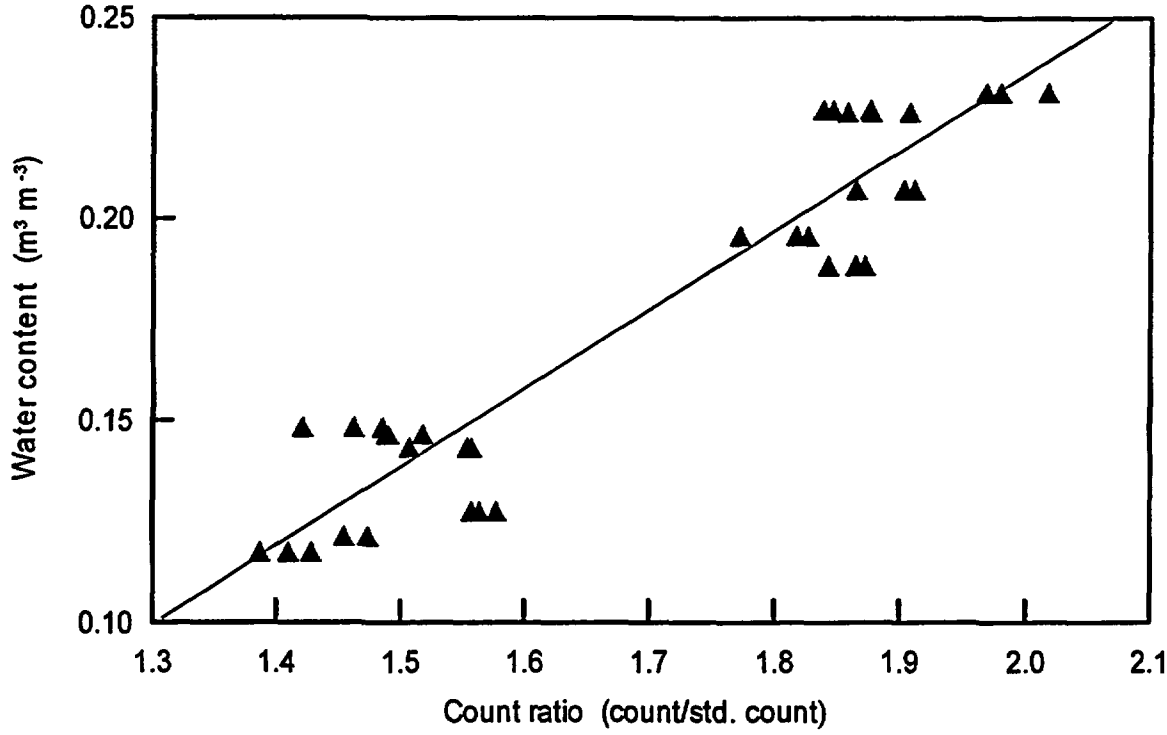

Figure 3.1-2. Calibration results of steady-state neutron probe for 7.6 cm access tube.

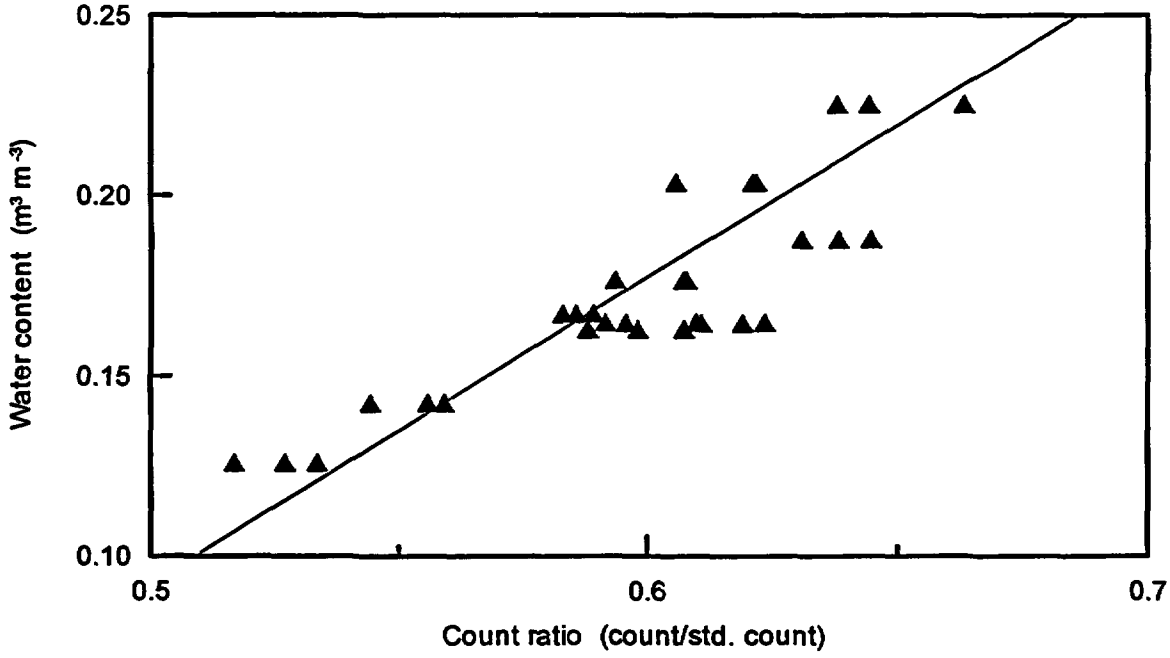

Figure 3.1-3. Calibration results of steady-state neutron probe for 10 cm access tube.

Table 3.1-2. Slopes, RMSE and SE of θ_v (volumetric moisture content) for calibration curves fitted to count ratio data from 24 neutron probe access tubes.

Borehole	Fitted Slope	RMSE	SE of θ_v
402	21.9	1.658	0.553%
403	25.4	1.882	0.627%
404	23.6	2.476	0.825%
405	36.9†	2.860	0.953%
412	20.5	1.307	0.436%
413	19.0	1.420	0.473%
414	20.7	1.923	0.641%
415	27.7	2.028	0.676%
416	23.1	1.609	0.536%
422	38.5†	2.181	0.727%
423	25.8	2.465	0.822%
424	20.8	2.550	0.850%
425	27.3	1.922	0.641%
432	21.3	1.780	0.593%
433	24.3	1.864	0.621%
434	24.9	1.931	0.644%
435	23.8	2.603	0.868%
442	25.5	2.285	0.762%
443	24.1	2.415	0.805%
444	24.4	2.209	0.736%
445	30.0	1.420	0.473%
454	19.9	2.758	0.919%
455	22.9	3.957	1.319%
456	29.6	3.602	1.201%
Mean	23.932	2.185	0.728%
Standard Dev.	2.935	0.645	0.215%

† - Values found to be statistical outliers. Mean and standard deviation are calculated without outliers.

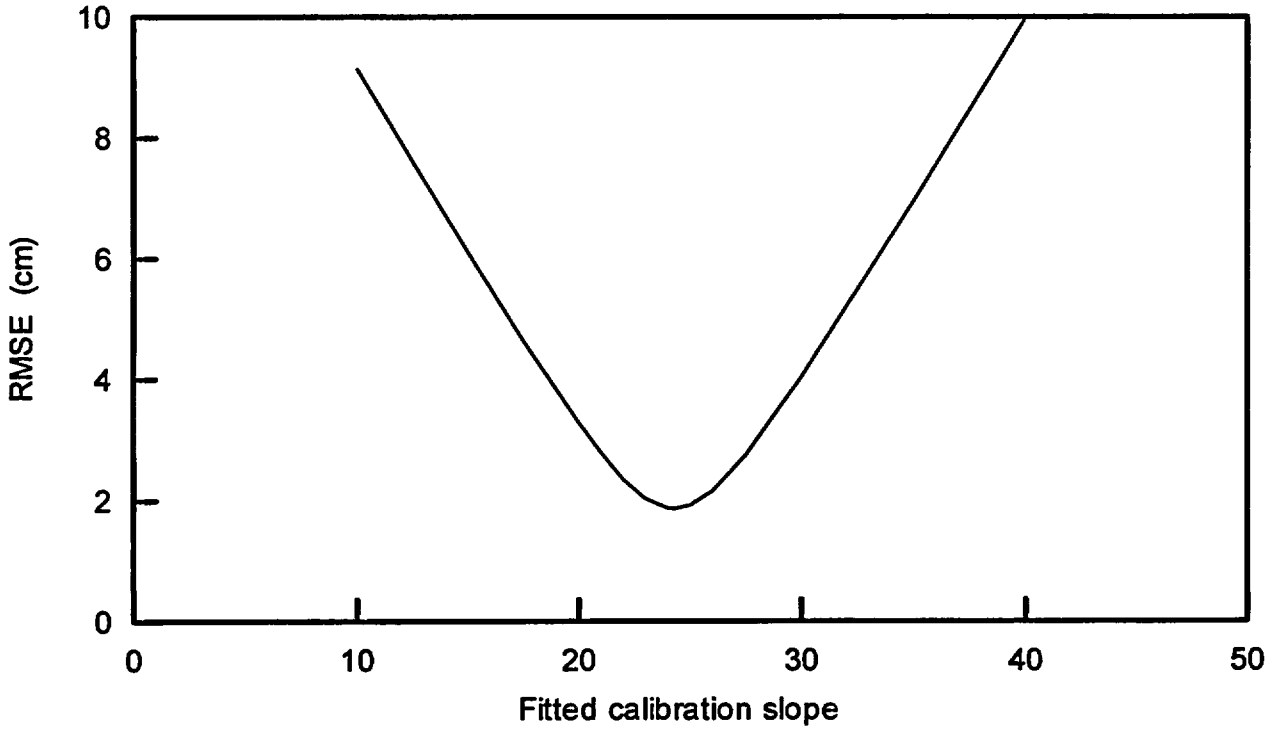

Figure 3.1-4. Scatterplot of RMSE versus slope for access tube #433, using transient neutron probe method.

Table 3.1-3 Results of simultaneously fitting all calibration data for depths at or less than 300 cm.

	Unfiltered data	Filtered data
Slope (CR^{-1})	23.8	23.6
RMSE of SWS_e (cm)	3.57	3.12
RMSE of θ_v ($m^3 - ^3$)	0.0119	0.0104

in the final estimate. Differences in the mean slope value between simultaneously and individually fitting the data, however, was not large (23.6 CR^{-1} versus 23.9 CR^{-1}, respectively), though it could be an important factor during field monitoring. We found that the location error represented 30% of the total error. This was a smaller contribution than found by others. Grismer et al. (1995) reported that $S_L^2(\theta)$ contributed more than 90% to the total error, though the magnitude of the location error was similar to ours.

The slope values obtained from steady-state and transient methods, for the 5 cm diameter access tubes, led to nominal errors in the change of water content as shown by Figure 3.1-5. During Experiment 1, for example, CR changes were less than about 0.5 throughout the plot and with depth. Volumetric water contents obtained using this change of CR, and the conventional and transient calibration curves, differ by only 2%. These differences, arising from the use of different calibration curves, were relatively small. However, given that the steady-state method was used to obtain slope and offset parameters for the three different access tubes, it was decided to use the steady-state results.

3.1.2 Time Domain Reflectometry

The TDR probes were calibrated in the laboratory (Young et al., 1997). The results will not be repeated here.

3.1.3 Pressure Transducers Used with Tensiometers

Pressure transducer (PT) calibration experiments were completed in July, 1996. Calibration parameters, correlation coefficients, standard errors and transducer locations are included in Table 3.1-4. Note the elevated offset values for transducer numbers corresponding to PT #s greater than 100 (model 26PCCFA1G). A different lot of transducers delivered by MicroSwitch were calibrated and found to exceed the factory calibration specification for offset value; they were subsequently returned and replaced with a new lot. After calibrating the second lot, and again discussing the elevated offset values with factory technicians, it was decided to use the transducers since the correlation coefficient was very close to unity.

3.1.4 Heat Dissipation Sensors

Calibration of all 43 HDS units used during the experiments required 155 days to complete. Sensor equilibration times varied depending upon calibration tension and degree of pre-treatment saturation for individual porous ceramic blocks. When sensor calibration proceeded sequentially from higher to lower soil pressures, equilibration times generally took 1 day or less at -50 cm, 3 days at -100 cm, 5.5 days at -200 cm, 3 days at -1000 cm, and 6 days at -5000 cm. The total amount of time needed to calibrate a set of 6 sensors was approximately 18.5 days. When the initial calibration pressure was -1000 cm after sensor pretreatment, a minimum of 6 days were needed before sensor equilibrium was achieved.

A scatter plot of the calibration data for the 43 sensors is presented in Figure 3.1-6. Regression parameter results are presented in Table 3.1-5. The standard error of estimate (s_{yx}) showed a reasonable range in predictive error considering the number of sensors calibrated. Median values are presented to illustrate the distribution symmetry of the slopes and intercepts.

Data from all the sensors were used simultaneously to generate a general calibration curve; the following calibration equation and statistics were obtained:

$$\Delta T = -0.345 + 0.282 \ln(\psi)$$
$$r^2 = 0.955,\ S_{xy} = 0.105,\ n = 208 \qquad (3\text{-}1)$$

with ψ the tension expressed as "cm" H_20. The data and fitted line in Figure 3.1-6 illustrate calibration symmetry of all sensors. The general calibration equation allowed calculation of the 95% confidence interval (CI) using equation 3-1 resulting in measurement uncertainty of ± 68 cm. The difference between maximum and minimum intercept values in Table 3.1-5 corresponds to a difference of 20 cm soil tension. Reece (1996) found that a common intercept could be used for a general calibration equation, but found that the slope values were unique at an $\alpha < 0.001$.

Because a 5-point calibration curve encompassing a tension range to -5000 cm water required considerable time to

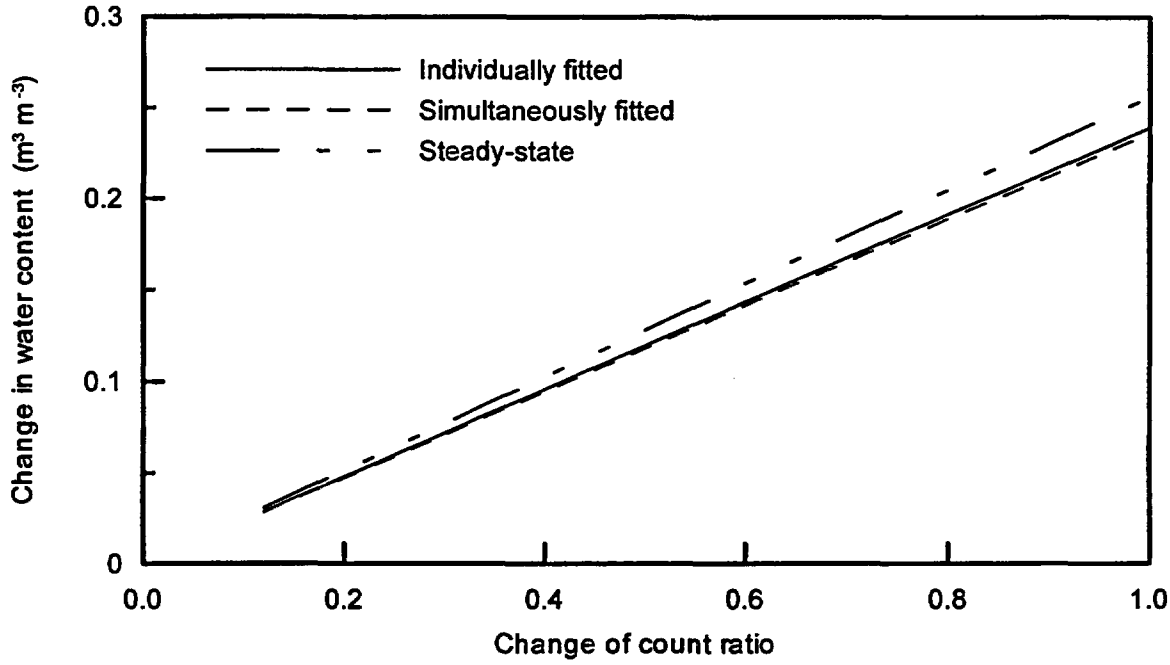

Figure 3.1-5. Differences in water storage when using the steady-state versus transient neutron probe calibration.

Table 3.1-4. Calibration results for pressure transducers used at Maricopa site.

Date	PT #	Slope	Offset	R^2	Error Est.	Location
model # - MicroSwitch 236PC15GW (Experiment 1)						
07/21/96	1	105.21	-19.13	0.999999	0.175	123
07/14/96	2	105.26	-7.18	0.999987	0.727	125
07/14/96	3	104.35	0.89	0.999988	0.689	127
07/14/96	4	104.63	5.15	0.999985	0.760	129
07/14/96	5	104.30	-11.60	0.999988	0.694	131
07/14/96	6	104.87	2.43	0.999988	0.700	133
07/21/96	7	105.85	-14.97	1.000000	0.132	141
07/14/96	8	103.40	4.13	0.999983	0.831	142
07/14/96	9	104.68	-1.11	0.999988	0.675	143
07/14/96	10	104.06	-4.38	0.999984	0.785	144
07/14/96	11	104.57	3.30	0.999988	0.683	145
07/14/96	12	105.67	-12.09	0.999992	0.559	146
07/14/96	13	104.34	-7.39	0.999989	0.649	147
07/14/96	14	104.51	5.02	0.999990	0.631	148
07/14/96	15	104.62	-3.22	0.999988	0.679	149
07/14/96	16	104.93	4.40	0.999989	0.653	150
07/14/96	17	104.75	8.03	0.999988	0.685	151
07/14/96	18	104.89	7.11	0.999989	0.666	152
07/14/96	19	104.68	10.25	0.999987	0.721	153
model # - MicroSwitch 236PC15GW (Experiments 1 and 2)						
07/14/96	20	104.46	3.44	0.999987	0.703	201
07/14/96	21	105.01	7.51	0.999988	0.696	202
07/14/96	22	104.92	4.65	0.999989	0.667	203
07/14/96	23	104.88	8.73	0.999988	0.681	204
07/14/96	24	104.80	8.12	0.999990	0.643	205
07/21/96	25	105.53	-14.22	1.000000	0.134	206
07/19/96	26	105.21	-6.40	0.999998	0.271	211
07/19/96	27	105.14	1.52	0.999998	0.281	212
07/19/96	28	105.42	3.15	0.999998	0.291	213
07/19/96	29	104.70	1.93	0.999998	0.252	214
07/19/96	30	105.61	-10.70	0.999998	0.281	215
07/21/96	31	105.64	-21.01	0.999999	0.188	216
07/19/96	32	104.95	6.08	0.999998	0.271	222
07/19/96	33	105.23	3.14	0.999998	0.280	224
07/19/96	34	105.47	4.52	0.999998	0.265	226

Date	PT #	Slope	Offset	R^2	Error Est.	Location
07/21/96	35	105.34	-16.41	0.999999	0.167	232
07/19/96	36	105.03	-9.52	0.999998	0.293	234
07/19/96	37	105.49	1.06	0.999998	0.286	236
07/19/96	38	105.44	3.35	0.999998	0.294	bad
07/19/96	39	105.26	-8.55	0.999997	0.325	242
07/21/96	40	105.85	-12.13	0.999998	0.245	243
07/21/96	41	104.81	-11.02	1.000000	0.125	242
07/21/96	42	105.11	-15.42	0.999999	0.147	243
07/21/96	43	105.52	4.91	0.999999	0.140	244
07/21/96	44	105.54	3.96	0.999999	0.143	245
07/21/96	45	105.31	0.35	0.999999	0.162	246
07/21/96	46	105.59	2.83	0.999999	0.145	253
07/21/96	47	104.68	-9.43	0.999998	0.245	254
07/21/96	48	105.09	-6.15	0.999999	0.184	255
07/21/96	49	105.33	-16.02	0.999999	0.160	256
07/21/96	50	104.36	-8.01	0.999999	0.202	241
04/09/97	51	104.81	-17.40	0.999996	0.403	241
04/09/97	52	104.74	-8.77	0.999996	0.413	251
04/09/97	53	104.42	-7.58	0.999995	0.426	252
	model # - MicroSwitch 26PCCFA1G (Experiments 1 and 2)					
07/22/96	101	144.82	98.41	0.999997	0.355	102
07/22/96	102	145.30	97.11	0.999997	0.349	103
07/22/96	103	148.90	109.23	0.999997	0.341	101
07/22/96	104	146.33	103.13	0.999997	0.329	105
07/22/96	105	147.84	114.01	0.999997	0.356	106
07/22/96	106	148.68	112.36	0.999997	0.337	104
07/22/96	107	146.63	111.65	0.999995	0.430	108
07/22/96	108	147.06	110.75	0.999997	0.364	109
07/22/96	109	146.87	110.90	0.999997	0.346	107
07/22/96	110	144.77	98.43	0.999997	0.330	111
07/22/96	111	150.69	110.46	0.999997	0.339	112
07/22/96	112	148.31	107.28	0.999997	0.332	109
07/22/96	113	149.55	114.37	0.999997	0.334	114
07/22/96	114	144.58	97.06	0.999997	0.351	115
07/22/96	115	145.87	107.60	0.999997	0.330	113
07/22/96	116	144.18	94.63	0.999997	0.363	117
07/23/96	117	144.82	102.39	0.999996	0.400	118

Date	PT #	Slope	Offset	R^2	Error Est.	Location
07/23/96	118	145.79	95.26	0.999996	0.391	116
07/23/96	119	145.04	93.81	0.999997	0.337	120
07/23/96	120	146.31	104.38	0.999996	0.406	121
07/23/96	121	146.51	107.89	0.999996	0.383	119
07/23/96	122	145.57	103.46	0.999996	0.413	123
07/23/96	123	96.69	63.40	0.999988	0.700	124
07/23/96	124	96.23	60.42	0.999992	0.580	122
07/23/96	125	95.54	56.09	0.999989	0.662	126
07/23/96	126	96.14	62.07	0.999992	0.559	127
07/23/96	127	97.89	64.47	0.999986	0.753	125

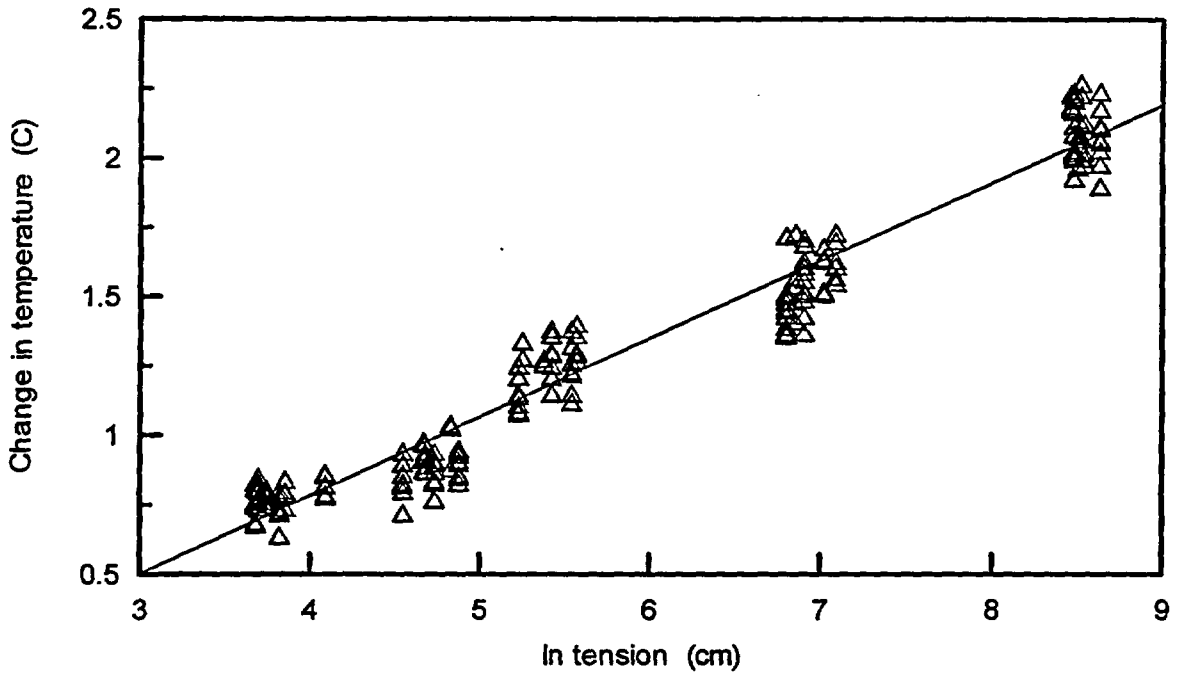

Figure 3.1-6. Scatterplot of calibration data for the 43 HDS sensors, and the general calibration curve fitted simultaneously to all data. Individual curves were used for each sensor during the field experiments.

Table 3.1-5. Results of simple linear calibration using log transformed data for heat dissipation sensors. Range in values encompasses results from 43 sensors, n = 5 per sensor.

Statistic	Lower Limit	Upper Limit	Median
y-intercept	-0.661	-0.158	-0.324
slope†	0.245	0.369	0.279
R^2	0.942	0.997	0.981
s_{yx} ‡	0.038	0.193	0.087

†Regression slope ($\Delta T/\Delta \ln \psi$) where ψ is in units of cm H_2O.
‡Standard error of estimate

complete, it was of interest to determine the number of sensors needed to obtain a similar reduction in predictive error as that obtained using data from all the sensors. Thus, HDS units were randomly chosen using sample replacement to obtain calibration data sets of 1, 6, 12, 18, 24, and 32 units corresponding to sample sizes of 5, 27, 49, 85,117, and 157. Regression parameters and standard error of estimates converged to values obtained when data sets from 12 or more HDS units were combined to form a minimum sample size of n = 49 resulting in a s_{yx} of 0.10, similar to the median value in the group of 43 calibrated sensors. Even though using a general curve would be easier with respect to data logger programming and data analysis, we found that the predictive error was greatly reduced when using individual calibration curves. Thus, individual curves were used to analyze all field data during the infiltration experiments. Calibration data are shown in Table 3.1-6.

3.1.5 Thermocouple Psychrometers

Calibration of thermocouple psychrometer units was found to be successful in terms of the linearity of the calibration curve, and standard error for estimating soil water tension. Table 3.1-7 lists the results, including the location along the buried trench in meters. We were able to achieve better than $r^2 = 0.97$ on all but five units. Standard errors were slightly higher for those units that did not calibrate to the higher correlation coefficients. Individual calibration curves were used for all field experiments.

3.2 Water Application Rates

3.2.1 Experiment 1

As stated in Section 2 above, water application rates were measured using two meters placed in series. This provided the total amount of water delivered to the 50 m by 50 m plot. During daylight hours, and whenever possible, water volumes applied to each of the six subplots were manually recorded. Totalized values are listed in Table 3.2-1. Depths of water were calculated by taking the average total volume applied in liters, and dividing by the area of application. Of the 24 days where irrigation occurred, only two days (4 and 23) experienced flow greater than 1.90 cm/day and no days experienced flow less than 1.80 cm/day. Overall, the irrigation system performed quite predictably, with a very small CV of <2%. We found that the sand filter required daily back-flushing as a way of improving overall system pressure. This discovery occurred early in the experiment and did not lead to under-pressuring of the system or low irrigation rates.

3.2.2 Experiment 2

Flow data were collected in the same manner as for Experiment 1, with totalized values recorded after the 10:00 am irrigation cycle (Table 3.2-2). The irrigation system performed more consistently during Experiment 2 than in the previous experiment. The target depth of irrigation of 2.00 cm/day was more closely met, and the CV was <1%, showing that the irrigation system was well understood.

3.3 Neutron Probe Data

3.3.1 Vertical Access Tubes

3.3.1.1 Experiment 1

Table 3.3-1 lists the frequency, depth, and identifying notes for data collection in the vertical neutron probe access tubes. At the beginning of the irrigation period, we limited data collection to the upper soil horizons, approximately 1 m deep. We then began collecting data from progressively deeper soils, as the wetting front moved downward. This reduced the time necessary for data collection, but it also limited our ability to repeatedly sample the same soil material.

With the exception of Days 5, 6, and 12, data were collected and saved without problems; we experienced power or communication problems with the probe on these three days, and data could not be saved properly. Vertical access tubes were scanned with the #66 probe only. Standard counts were taken at 2.0 m depth in the standard access tube, located approximately 20 m west of the irrigated plot, beginning on Day 6. Before this time, standard counts were taken either in the shield (Days -13 to 3) or at the 1.0 m depth in the standard access tube (Days 4 and 5). Standard counts were converted to the 2.0 m value for consistency during conversion of field counts to count ratio (CR).

The amount of data collected during Experiment 1 from the

Table 3.1-6. Calibration data for heat dissipation sensors used at Maricopa site. Calibration curve is in the form of tension (cm) = EXP ([20 sec temperature - 1 sec temperature - intercept]/slope).

Location	Sensor ID	Intercept	Slope
141	3402	-0.272	0.268
142	3403	-0.359	0.303
143	3423	-0.282	0.274
144	3400	-0.372	0.298
145	3398	-0.256	0.269
146	3396	-0.316	0.272
147	3394	-0.242	0.250
148	3261	-0.398	0.281
149	3395	-0.379	0.288
150	3397	-0.277	0.267
151	3399	-0.272	0.276
152	3401	-0.329	0.276
153	3424	-0.370	0.280
201	3437	-0.535	0.289
202	3440	-0.460	0.301
203	3441	-0.632	0.338
204	3443	-0.296	0.261
205	3421	-0.356	0.279
206	3422	-0.327	0.279
211	3426	-0.528	0.318
212	3405	-0.347	0.282
213	3429	-0.323	0.253
214	3430	-0.297	0.283
215	3434	-0.277	0.260
216	3435	-0.269	0.262
222	3404	-0.158	0.245
224	1555	-0.661	0.369
226	1556	-0.289	0.286
232	3406	-0.283	0.280
234	3407	-0.176	0.249
236	3408	-0.272	0.261
241	3409	-0.421	0.314
242	3410	-0.293	0.257
243	3411	-0.496	0.312
244	3412	-0.415	0.297
245	3413	-0.357	0.282
246	3414	-0.271	0.265
251	3415	-0.451	0.309
252	3416	-0.348	0.297
253	3417	-0.184	0.260
254	3418	-0.324	0.284
255	3419	-0.381	0.274
256	3420	-0.277	0.273

Table 3.1-7. Calibration data for thermocouple psychrometers installed in buried trench.

Y - coordinate	Slope (bar/μV)	Standard Error (bar)	r^2
0	2.650	5.724	0.968
2.5	2.587	3.470	0.988
5	2.552	3.735	0.986
10	2.674	2.952	0.991
15	2.640	4.272	0.982
20	3.229	6.856	0.954
25	2.336	6.758	0.955
30	2.599	2.279	0.995
35	2.861	2.639	0.993
40	2.934	5.800	0.967
45	2.670	7.001	0.952
50	2.789	4.459	0.981
55	2.922	7.445	0.946

Table 3.2-1. Water application during Experiment 1.

Time (days)	Daily application (cm)	Sum applied (cm)
0	1.806	1.806
1	1.837	3.643
2	1.85	5.493
3	1.818	7.311
4	1.948	9.259
5	1.865	11.124
6	1.868	12.992
7	1.864	14.856
8	1.856	16.712
9	1.849	18.561
10	1.855	20.416
11	1.817	22.233
12	1.819	24.052
13	1.837	25.889
14	1.833	27.722
15	1.831	29.553
16	1.828	31.381
17	1.852	33.233
18	1.83	35.063
19	1.838	36.901
20	1.847	38.748
21	1.857	40.605
22	1.844	42.449
23	1.96	44.409
Mean	1.85	
SD	.035	
CV (%)	1.90	

Table 3.2-2. Water application during Experiment 2.

Time (days)	Daily Application (cm)	Sum Applied (cm)	Time (days)	Daily Application (cm)	Sum Applied (cm)
0	0.718	0.718	17	1.961	33.541
1	1.325	2.043	18	1.994	35.535
2	1.962	4.006	19	1.970	37.505
3	1.965	5.971	20	1.974	39.479
4	1.971	7.943	21	1.973	41.451
5	1.989	9.931	22	n/a†	43.380
6	1.956	11.887	23	1.929	45.309
7	1.967	13.855	24	n/a	47.231
8	1.963	15.818	25	1.922	49.153
9	1.974	17.792	26	n/a	51.127
10	1.910	19.703	27	1.974	53.101
11	1.979	21.681	28	1.969	55.070
12	1.980	23.661	29	n/a	57.027
13	1.983	25.644	30	1.957	58.984
14	1.984	27.628	31	n/a	60.929
15	1.977	29.606	32	n/a	62.875
16	1.974	31.579	33	1.946	64.821
			Mean‡	1.966	
			SD	0.027	
			CV (%)	0.987	

† - Indicates that daily data were not recorded. Daily application for that day is half (or one-third) of the total for next day recorded.

‡ - Mean does not include data from Days 0 and 1

Table 3.3.1. Sampling schedule for the vertical neutron probe access tubes during Experiment 1.

Date	Time (days)	Number of Tubes	Depths (m)	Identifiers†
15-Apr-97	-13	40	3,11	
21-Apr-97	-7	40	3,11	
28-Apr-97	0	41	3	a
29-Apr-97	1	41	1	
30-Apr-97	2	41	1.5	
01-May-97	3	41	1.5	
02-May-97	4	41	2	
03-May-97	5	22	2	b
04-May-97	6	32	1.5	b
05-May-97	7	41	2	
06-May-97	8	41	2.5	
07-May-97	9	41	2.5	
08-May-97	10	41	2.5	
09-May-97	11	41	3	
10-May-97	12	20	3	b
11-May-97	13	41	3	
12-May-97	14	41	3	
13-May-97	15	41	3	
14-May-97	16	41	3,5	
15-May-97	17	10	11	d
16-May-97	18	33	3	b
18-May-97	20	10	11	d
22-May-97	24	10	11	a,d
26-May-97	28	41	3	
28-May-97	30	10	11	d
30-May-97	32	10	11	d
02-Jun-97	35	41	3,11	c
05-Jun-97	38	41	3,11	c
09-Jun-97	42	41	3,11	c
18-Jun-97	51	41	3,11	c
25-Jun-97	58	41	3,11	c
02-Jul-97	65	41	3,11	c
09-Jul-97	72	41	3,11	c

Date	Time (days)	Number of Tubes	Depths (m)	Identifiers†
16-Jul-97	79	41	3,11	c
23-Jul-97	86	41	3,11	c
30-Jul-97	93	41	3,11	c

†Explanation of identifiers
a - start/stop irrigation phase of experiment
b - problem with probe data collections - battery or communication
c - scanned total depth for all tubes
d - scanned only deep tubes

vertical access tubes was quite large. Plotting all the data in this report is not an efficient use of space; therefore, we will address water movement on a small-scale basis first using a number of representative neutron probe tubes, then discuss changes in water content at the plot scale.

Figures 3.3-1A through 3.3-1C show the change in water content for access tubes #402, #423, and #445, which are located on a line from the SW to the NE corner of the plot. Each access tube was drilled to 15 m, and the data shown were selected from Day -7 through 16. Note that shallow neutron probe tubes were no longer sampled after Day 16 (Table 3.3-1) because the wetting front had passed the bottom of the tube; deep access tubes however, continued to be sampled, though at a frequency of approximately 2-4 days. The data from these access tubes showed a pattern of increasing water content with time and depth. Variations in the water content profiles were quite similar for data collected before irrigation began and during Day 16 at depths of between 3 and 5 m, indicating some textural control. For example, Figure 3.3-1A showed significant variability in water content between 3.5 and 5.0 m depth. Soil samples collected adjacent to access tube #402 after redistribution and analyzed for texture, showed increasing clay content at 4.17 m, indicating a higher water holding capacity. Data from access tube #423 (Figure 3.3-1B) also showed similar variations with depth before and during irrigation, especially for the 3 - 5 m depth. The lack of changes in water content from 4 - 5 m depth in access tube #445 (Figure 3.3-1C) indicated that the wetting front had not reached this depth by Day 16, but that shallower soils clearly mirrored the general pattern of water content variation with depth.

Plot-wide analysis considered the wetting front velocity measured at different access tubes inside the irrigated plot for depths between 0 and 3 m.

We developed a time series of neutron probe readings for each depth and spatial location across the site, and used the readings to determine wetting front arrival (see equation 2-1). The value of the neutron probe count or water content at the maximum first derivative was approximately the midpoint between background and final steady-state readings. Relative response was used as an alternative to choosing a specific water content or count reading. By determining changes in count rate or water content, the inherent spatial variability in initial water contents and "final" (behind the wetting front) water contents were automatically taken into account. On a small number of occasions, we visually determined wetting front arrival from the data plots, instead of using the above described procedure because of either obvious noise or missing data. Because changes of water content were relatively large in this sandy soil, errors in establishing wetting front arrival were minor.

Wetting front velocities were calculated and represented as local and effective parameters. Local wetting front velocities ($v_{\Delta z}(z)$) were calculated by measuring the travel time across a depth interval, Δz, between depths z and z-1, e.g.,

$$\text{local velocity} = v_{\Delta z}(z) = \frac{(\text{depth}_z - \text{depth}_{z-1})}{(T_{a_z} - T_{a_{z-1}})} \qquad (3\text{-}2)$$

for Δz taken as low as 50 cm, and z taken to a total depth of 300 cm. Local front velocities were independent of adjacent intervals. They provide data and information about the flow processes within a restricted depth interval, but at a scale larger than could be inferred from small column samples. Local velocities were also calculated for $\Delta z = 1.0$ m and $\Delta z = 1.5$ m to evaluate the effect of measurement scale on the variability of local velocity. The velocity ($v_{eff}(z)$) was defined with ground surface as the top of the interval (i.e., depth_{z-1} and T_{az-1} from equation (2-1) equal to 0),

$$\text{effective velocity} = v_{eff}(z) = \frac{\text{depth}_z}{T_{a_z}} \qquad (3\text{-}3)$$

Note that as $\Delta z \rightarrow z$, $v_{\Delta z}(z) \rightarrow v_{eff}(z)$, and as $\Delta z \rightarrow 0$, we approach measurement scale of undisturbed column samples retrieved from the field (~ point scale), and analyzed in the laboratory for soil hydraulic properties. Thus, the local properties presented here could be thought of as intermediate scale, depending on one's perspective.

Wetting front velocities were calculated for each access tube located at least 5 m inside the irrigated plot, providing up to 26 values for each depth. The 5 m buffer zone between the access tubes and the edge of the plot added assurances that predominantly one-dimensional flow occurred in the area of interest. The range, mean, and coefficient of variation (CV) of the wetting front velocities and soil textural components were calculated, when valid, for each depth. Isovelocity plots were produced as a way of visually studying wetting front behavior across the plot. Local and effective

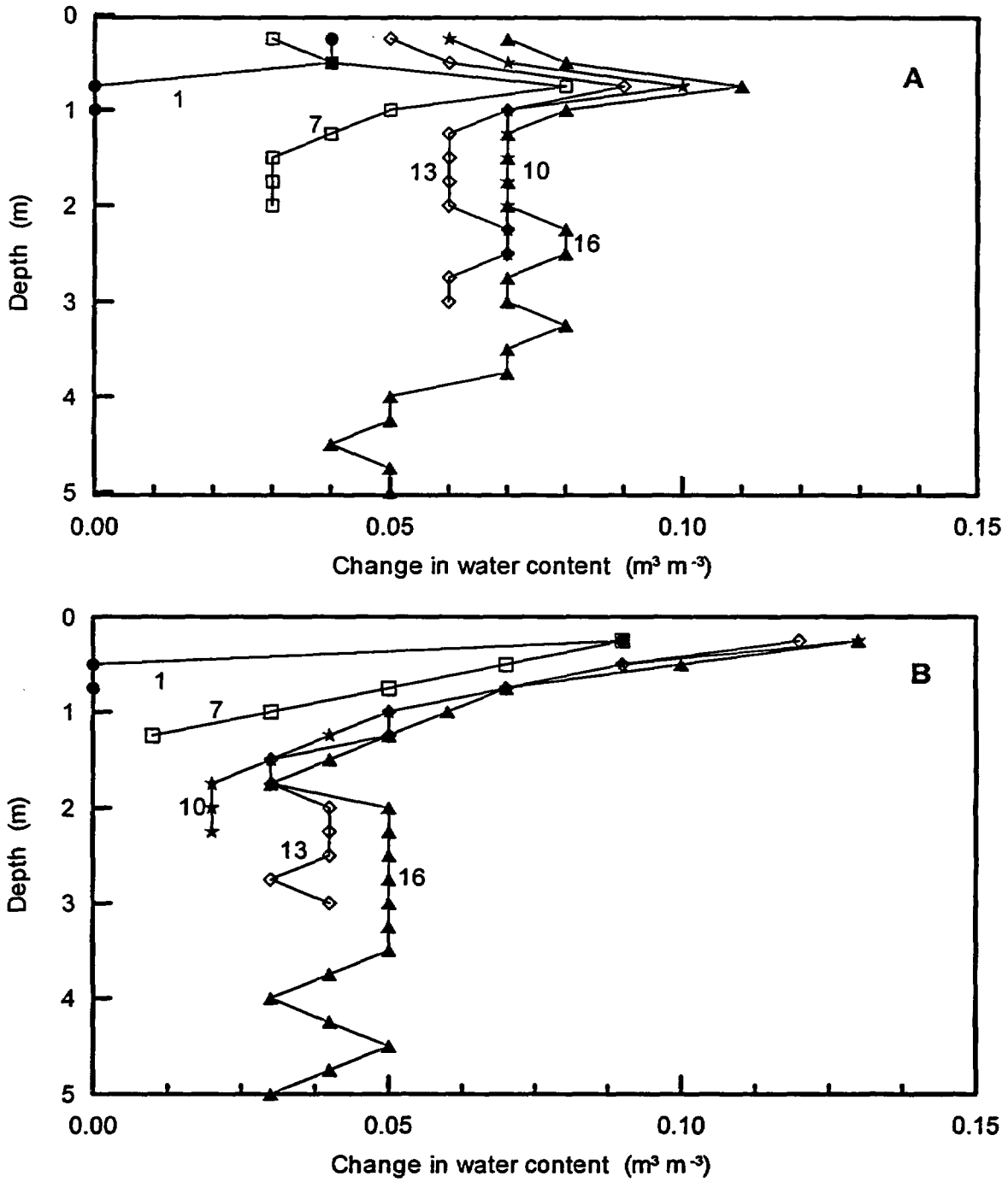

Figure 3.3-1. Change in water content for three access tubes during Experiment 1. (A) access tube #402, (B) #423 and (C) #445. Numbers on plot indicate day.

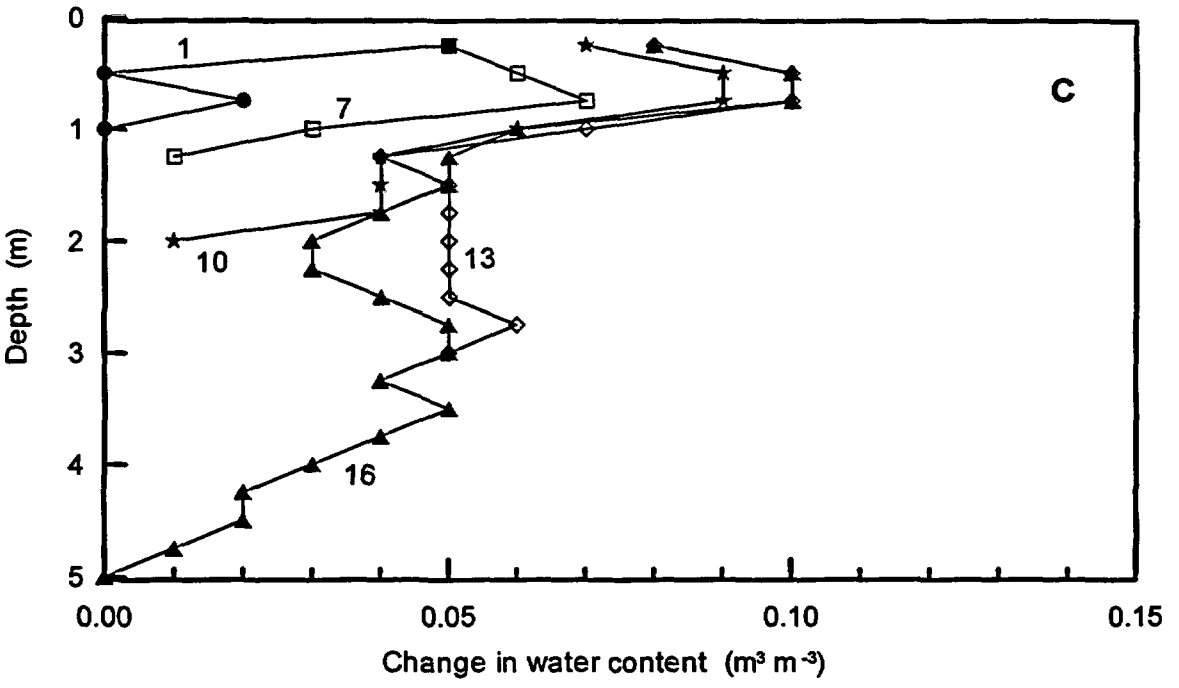

Figure 3.3-1. Change in water content for three access tubes during Experiment 1. (A) access tube #402, (B) #423 and (C) #445. Numbers on plot indicate day. (Continued)

percentages of textural components were calculated using the same methodology for averaging as for the front velocity.

Wetting front velocities and textural components were tested using a one-way analysis of variance (ANOVA). The ANOVA method analyzes multiple independent samples, and determines whether they are sampled from the same or different populations. If the local or effective front velocities, calculated for each depth interval, are statistically the same, this would provide some basis for concluding that soil heterogeneities were not large enough to significantly influence front velocities. In this analysis, we designated the different intervals as experimental treatments. Data from neutron probe access tube locations were designated as repetitions within each treatment. The null and alternative hypotheses were:

H_0: No differences in wetting front velocities or textural components exist between intervals.

H_1: Evidence suggests that wetting front velocities or textural components differed between depth intervals.

All treatments were first checked for normality. If the data were normally distributed, then a parametric ANOVA test was run. If the null hypothesis failed (e.g., data suggests that the front velocities or textural components were statistically different from one layer to the next), we then ran a Tukey Test (Montgomery, 1997), a pairwise multiple comparison procedure to determine which combination of treatment pairs were significantly different. If the treatments were found to be non-normally distributed, a Kruskal-Wallis ANOVA on ranks was performed on the medians of each treatment, not the means. The Kruskal-Wallis test does not have the same requirements of normality and/or equal variance between depths as does the ANOVA test (Huntsburger and Billingsley, 1981). If the null hypothesis failed, Dunnett's test (Montgomery, 1997) was run for pairwise comparisons, a non-parametric equivalent to the Tukey test. All statistical analyses were performed using SigmaStat (v.2, Jandel Corporation, San Rafael, CA).

Most of the depths and locations used for the analysis provided a clear arrival time, though some noise was apparent. Of the 26 neutron probe access tubes and 5 depth intervals, only seven instances occurred where data could not be used for this analysis: four instances in which instrument failure or insufficient time precluded data collection, and three in which the wetting front traveled at least 100 cm in one day (see below for further explanation). In these seven cases, wetting front arrival could not be established, so these data points were not included in the ANOVA analysis.

Figure 3.3-2 and Table 3.3-2 show the local front velocities and include descriptive statistics for each depth interval. Each contour plot in Figure 3.3-2 represents the wetting front velocity observed at the individual depth plane labeled under the plot. [Note that the plots, now 40 m by 40 m in area, represent only those access tubes found at least 5 m inside the irrigated area]. Contour levels were kept constant to make comparisons easier between depth planes. Flow through the top 1 meter of soil has the smallest range of wetting front velocities of the five depths analyzed (Table 3.3-2 and Figure 3.3-2A). The variations appear largest in the center of the plot, where higher velocities were recorded in several areas. This could possibly be from the presence of the buried trench, where the surface soil was disturbed during instrument installation. The range of velocities for the 1.5-2.0 m and 2.0-2.5 m intervals were very similar, but the mean value in the shallower interval was 54% higher.

Results of wetting front velocities found at the 2.0-2.5 m interval were very similar to the 1.5-2.0 m interval, except for a single access tube in the northeast corner of the plot where water arrived at 2.0 and 2.5 m depth on the same day. Because water content was measured in the access tubes only one time per day, the average maximum error for detecting arrival time at any particular depth is 0.5 days. On this basis, we assigned this exceptional access tube a velocity of 100 cm d^{-1} as an upper value (50 cm / 0.5 days). The unusually high velocity at this depth in the plot could have been caused by flow of water through the annular space of the access tube, or though cracks in the soil material itself.

The highest mean local front velocity in the profile was recorded for the 2.5 - 3.0 m depth interval. As for the 2.0 to 2.5 m depth, there was an outlier near the center of the plot (Figure 3.3-2E) which was also given a value of 100 cm d^{-1}. However, even without this elevated value, the recalculated mean of 41 cm d^{-1} is still much higher than those calculated for the shallower soils. This faster velocity may be related either to the higher percentage of gravel and sand (Table

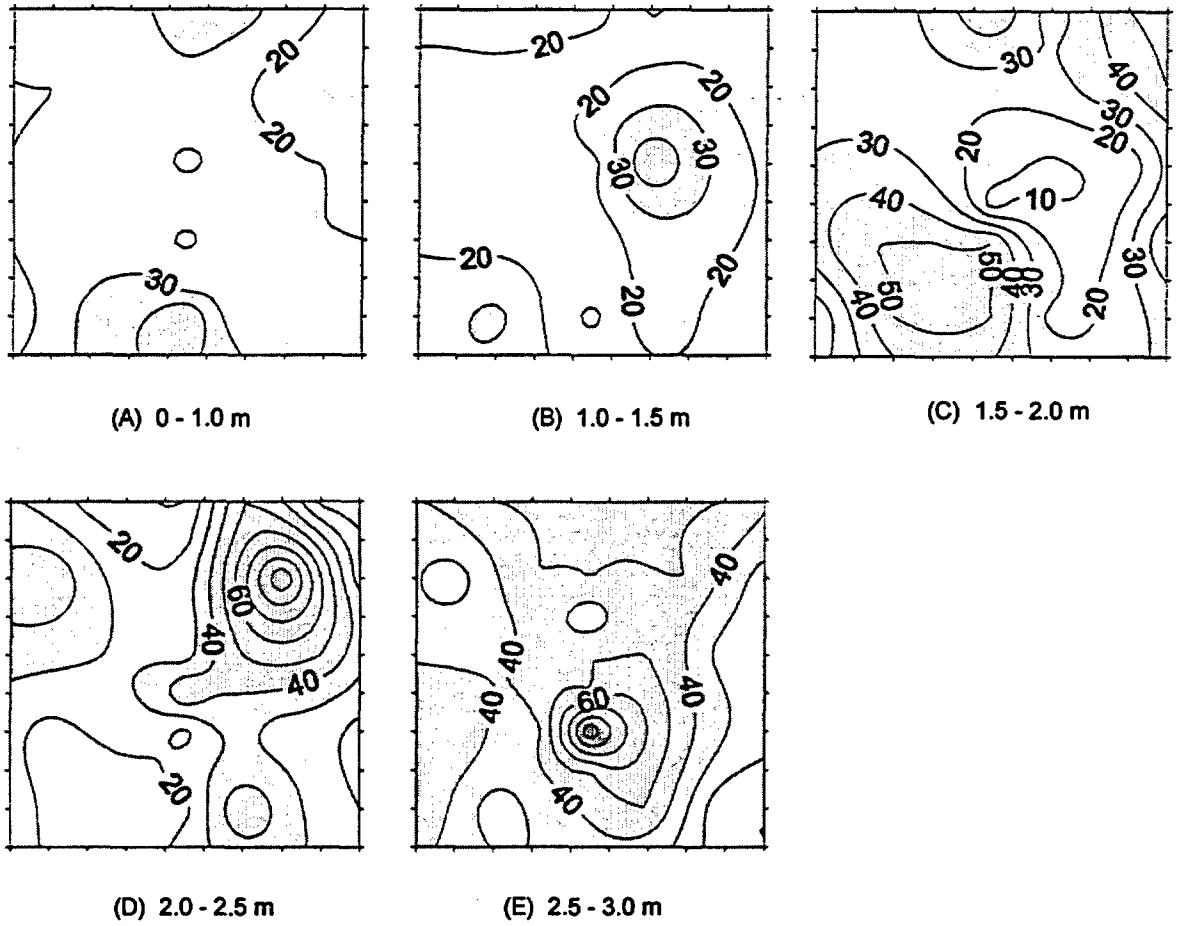

Figure 3.3-2. Local wetting front velocities (cm d^{-1}) during Experiment 1. Plots (40 m by 40 m) represent only those access tubes found at least 5 m inside the irrigated area.

Table 3.3-2. Descriptive statistics for local texture and wetting front velocity during Experiment 1.

	0 - 1.0 m	1.0 - 1.5 m	1.5 - 2.0	2.0 - 2.5 m	2.5 - 3.0 m
			Wetting Front Velocity		
range (cm d^{-1})	14-50	7-50	5-50	10-100	10-100
mean (cm d^{-1})	24.8ab	20.3b	31.3a	30.9a	43.6c
number of samples	26	25	25	26	23
CV (%)	31.3	43.0	52.6	62.4	39.6
			Gravel		
range (%)	4.5-12.9	9.9-21.9	1.0-32.6	2.2-31.4	13.7-77.4
mean (%)	8.3a†	14.9b	16.6b	19.8b	31.1b
number of samples	11	11	10	9	10
CV (%)	32.1	23.0	57.8	46.8	56.6
			Sand		
range (%)	55.1-84.5	65.1-83.3	62.9-95.1	68.7-95.8	78.6-95.6
mean (%)	68.0a	74.9ab	81.8cb	81.4c	88.1c
number of samples	11	11	10	9	10
CV (%)	14.0	8.0	12.0	11.6	5.6
			Silt		
range (%)	8.9-26.3	8.3-22.4	0.6-20.3	1.3-23.5	1.2-9.9
mean (%)	18.9a	15.1ab	9.2bc	10.6ab	4.4c
number of samples	11	11	10	9	10
CV (%)	30.6	30.6	79.7	75.3	56.4
			Clay		
range (%)	6.2-19.3	5.7-15.5	3.8-16.8	2.9-11.5	2.5-12.9
mean (%)	13.1a	9.9ab	9.0ab	8.0ab	7.5b
number of samples	11	11	10	9	10
CV (%)	31.1	29.6	39.4	36.6	45.4

† - different letters indicate significant differences at an $\alpha = 0.025$.

3.3-3) or to differences in soil structure, or both. Samples collected in this interval from access tubes contained an average percent gravel (> 2 mm fraction) of 31.1%, much higher than found closer to ground surface, though statistically the gravel contents were similar for all but the 0 to 1 m depth interval.

The contour plots of effective front velocities (Figure 3.3-3) are presented in the same way as described above (e.g., each plot has the same contour intervals and spatial scale); note that Figure 3.3-3A is identical to Figure 3.3-2A (except for contour limits) because the local and effective front velocities (and the textural components) were the same for the shallowest interval. One striking feature of the plots was a reduced spatial variability of the wetting front velocity as the wetting front reached deeper soil. This can be seen immediately by comparing plots that correspond to deeper soil, and from the information presented in Table 3.3-3. While the mean wetting front varied little with depth, the range and CV of wetting front velocity decreased as deeper soil was included in the analysis. Apparently, soil layering caused the wetting front to become more uniform across the plot as it traveled downward in the profile.

Figures 3.3-4 (A-F) show water content redistributions for the deep access tubes #402, #423, and #445. For each access tube, volumetric water contents and changes in volumetric water contents were plotted. The changes in water contents were calculated by comparing water content profiles recorded during redistribution, with the final water content profiles collected near the end of the irrigation. The water content profiles showed large variations with depth, which were due to variations in soil texture. These variations with depth were evident for all times of data collection. The general shape of each of the three profiles was maintained throughout redistribution. Note especially the significant decline in water content at depths of 8 to 10 m, and the close similarity of even small changes in water content (e.g., Figure 3.3-4A from 4 to 6.5 m). Clearly, the water content was decreasing near the surface. This decrease was almost uniform until approximately 4 m depth. Response of deeper soils was affected by continued drainage from the upper 6.5 m, which caused the wetting front to advance to greater depths and gave the appearance that deeper soils were not draining. Note how the soils at the three access tubes differed in their redistribution patterns (Figures 3.3-4 B, D, and F). Note also that the wetting front had not reached the lower end of the access tubes by the end of the irrigation phase. Therefore, below this depth, the differences in soil water content became positive with depth. The depth where this occurred varied from tube to tube. In access tubes #402 and #423, the cross-over occurred between 6 and 8 m depth, whereas in access tube #445, it occurred at approximately 4.25 m depth. The different cross-over depths are indicative of differences in soil water deficit before irrigation (thereby leading to differences in wetting front movement), and in post-irrigation water release (thereby leading to reduced internal drainage). Though it is not within the scope of this document, drainage behavior like this, along with tension data from the deep tensiometers, can be used to measure points on the hydraulic conductivity and water retention functions.

3.3.1.2 Experiment 2

Vertical access tubes were sampled during Experiment 2 according to the schedule shown in Table 3.3-4. In this section we emphasize the response from the same three access tubes as in Experiment 1 (e.g., #402, #423, and #445). These deep access tubes were located in a SW-NE transect, and represent a range in response to water application that was seen in the other access tubes. Figures 3.3-5A through 3.3-5C show the first eight days of data collection for the three access tubes. Note that full scans were not taken until Day 8, because of time and personnel constraints. This limited some of the analyses that were possible from Experiment 1 data, namely, calculation of wetting front velocities. The figures show that change in water content was extremely rapid throughout the top 3 m of soil, occurring within several days. The small changes in water contents at the 1, 2, and 3 m depth (Table 3.3-5) explain the rapid movement of the wetting front (average of 80.3 cm d^{-1}). At the beginning of Experiment 2, the soil was already relatively wet (± 0.20 m^3 m^{-3}). As a result, its hydraulic conductivity was high and water moved through the soil quickly, without much of an increase in the water content of the soil itself (± 0.025 m^3 m^{-3}). Obviously, the rapid wetting fronts virtually preclude our ability to study plot-wide wetting front arrival in depth increments of 50 cm, as done using Experiment 1 data.

Water redistribution presented for the same three access tubes are shown in Figures 3.3-6A through C. The graphs show full scans of the access tubes for Days 34, 55, 107, 176, corresponding to 1, 22, 74 and 143 days after cessation

Table 3.3-3. Descriptive statistics for effective texture and wetting front velocities during Experiment 1.

	0 - 1.0 m	0 - 1.5 m	0 - 2.0 m	0 - 2.5 m	0 - 3.0 m
			Wetting Front Velocity		
range (cm d^{-1})	14-50	13-38	14-40	16-28	18-27
mean (cm d^{-1})	24.8	21.8	22.7	22.2	23.6
number of samples	26	25	26	26	25
CV (%)	31.3	23.8	24.0	10.5	9.2
			Gravel		
range (%)	4.5-12.9	6.5-16.2	7.1-18.8	5.9-17.7	7.5-22.9
mean (%)	8.3a†	10.6ab	11.3ab	13.3bc	15.7c
number of samples	11	11	10	9	10
CV (%)	32.1	24.2	27.0	24.2	24.6
			Sand		
range (%)	55.1-84.5	61.7-84.1	64.6-84.5	69.3-87.2	70.4-88.3
mean (%)	68.0	70.6	73.1	74.2	76.9
number of samples	11	11	10	9	10
CV (%)	14.0	10.5	9.3	7.4	7.3
			Silt		
range (%)	8.9-26.3	9.4-24.6	9.4-21.2	7.8-20.1	7.0-17.2
mean (%)	18.9	17.4	15.6	14.9	12.9
number of samples	11	11	10	9	10
CV (%)	30.6	25.8	26.8	24.1	26.6
			Clay		
range (%)	6.2-19.3	6.1-16.2	5.7-14.8	5.0-13.5	4.7-13.4
mean (%)	13.1	12.0	11.4	10.9	10.1
number of samples	11	11	10	9	10
CV (%)	31.1	28.2	26.8	23.3	27.2

† - different letters indicate significant differences at an $\alpha = 0.025$.

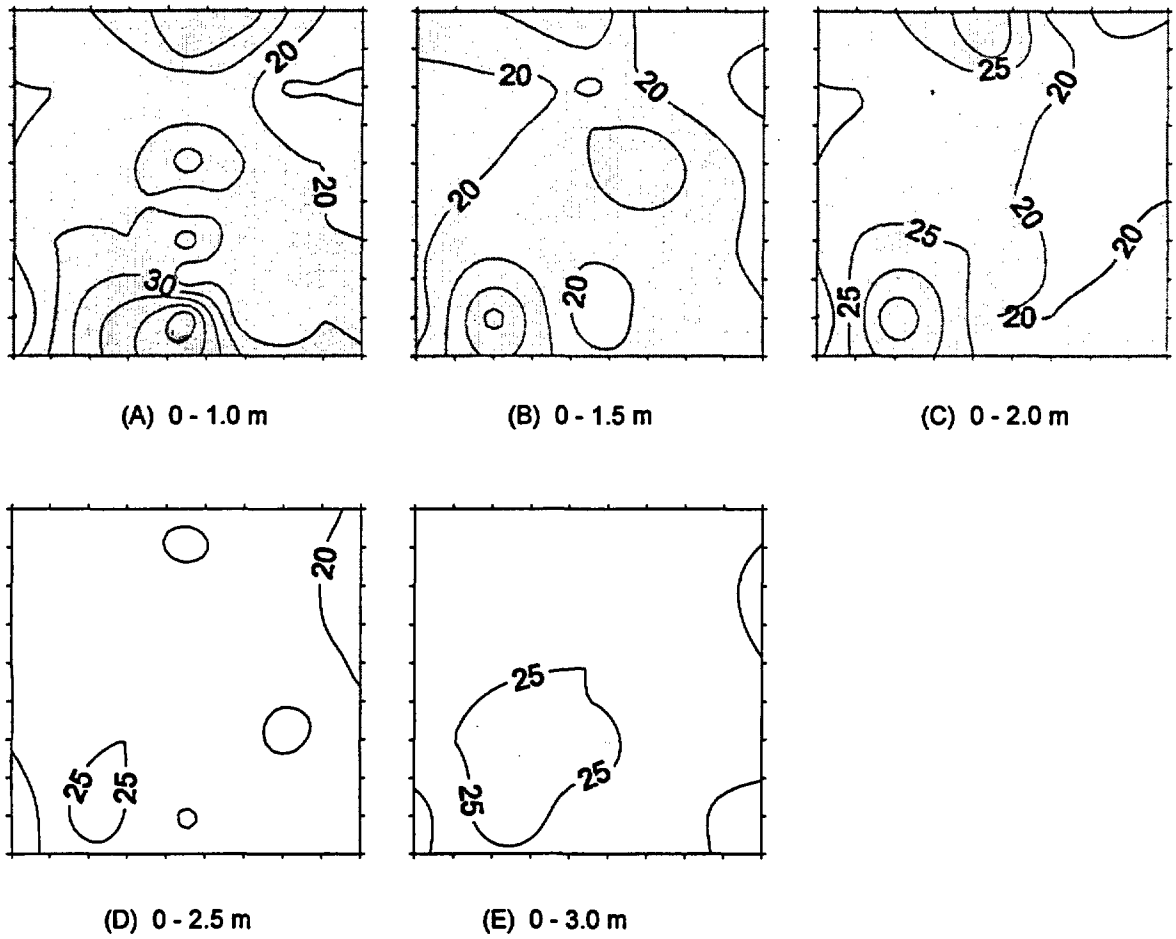

Figure 3.3-3. Effective wetting front velocities (cm d^{-1}) during Experiment 1. Plots (40 m by 40 m) represent only those access tubes found at least 5 m inside the irrigated area.

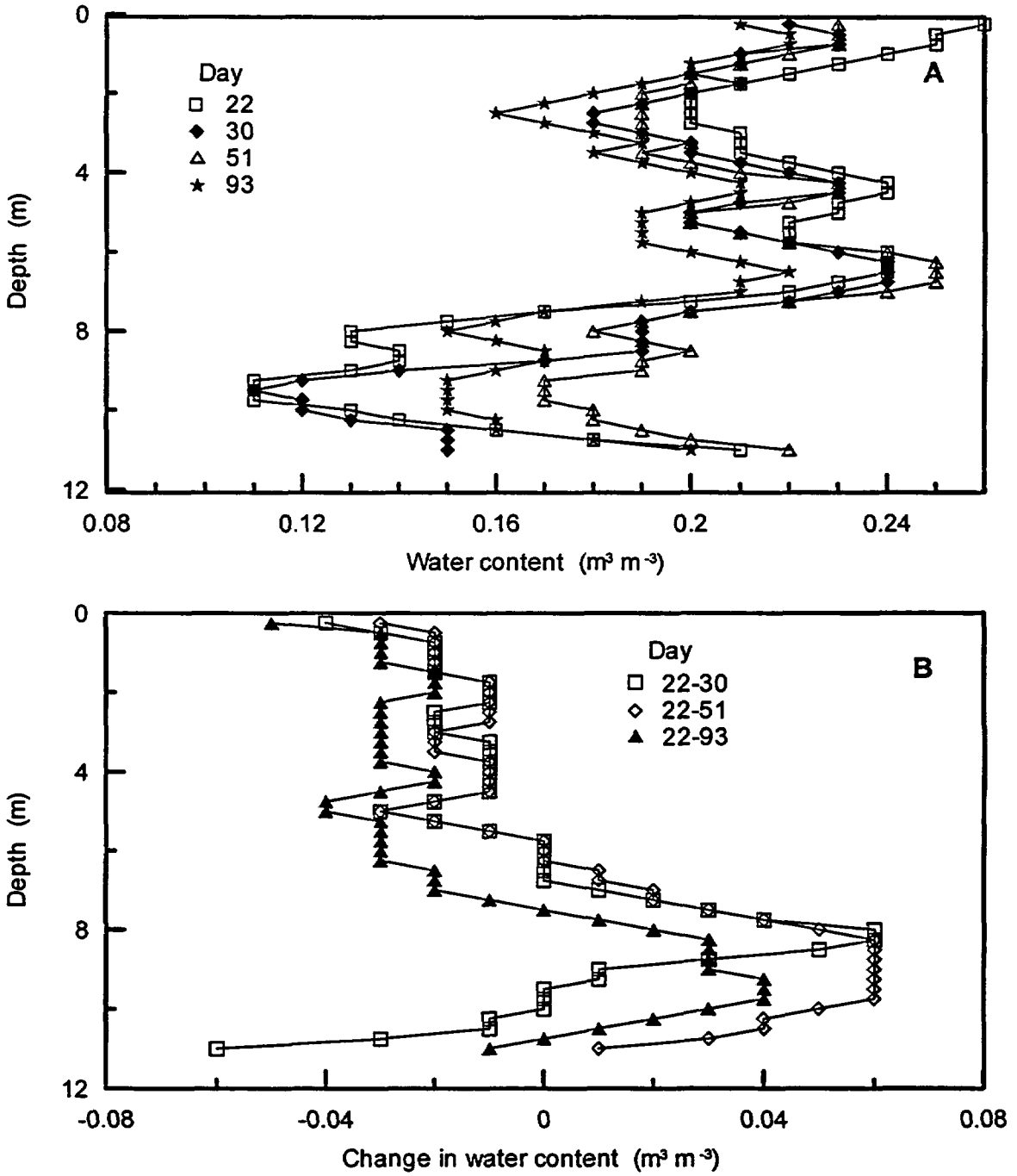

Figure 3.3-4. Water content and changes in water content for access tubes #402 (A and B), #423 (C and D), and #445 (E and F) during the water redistribution phase of Experiment 1.

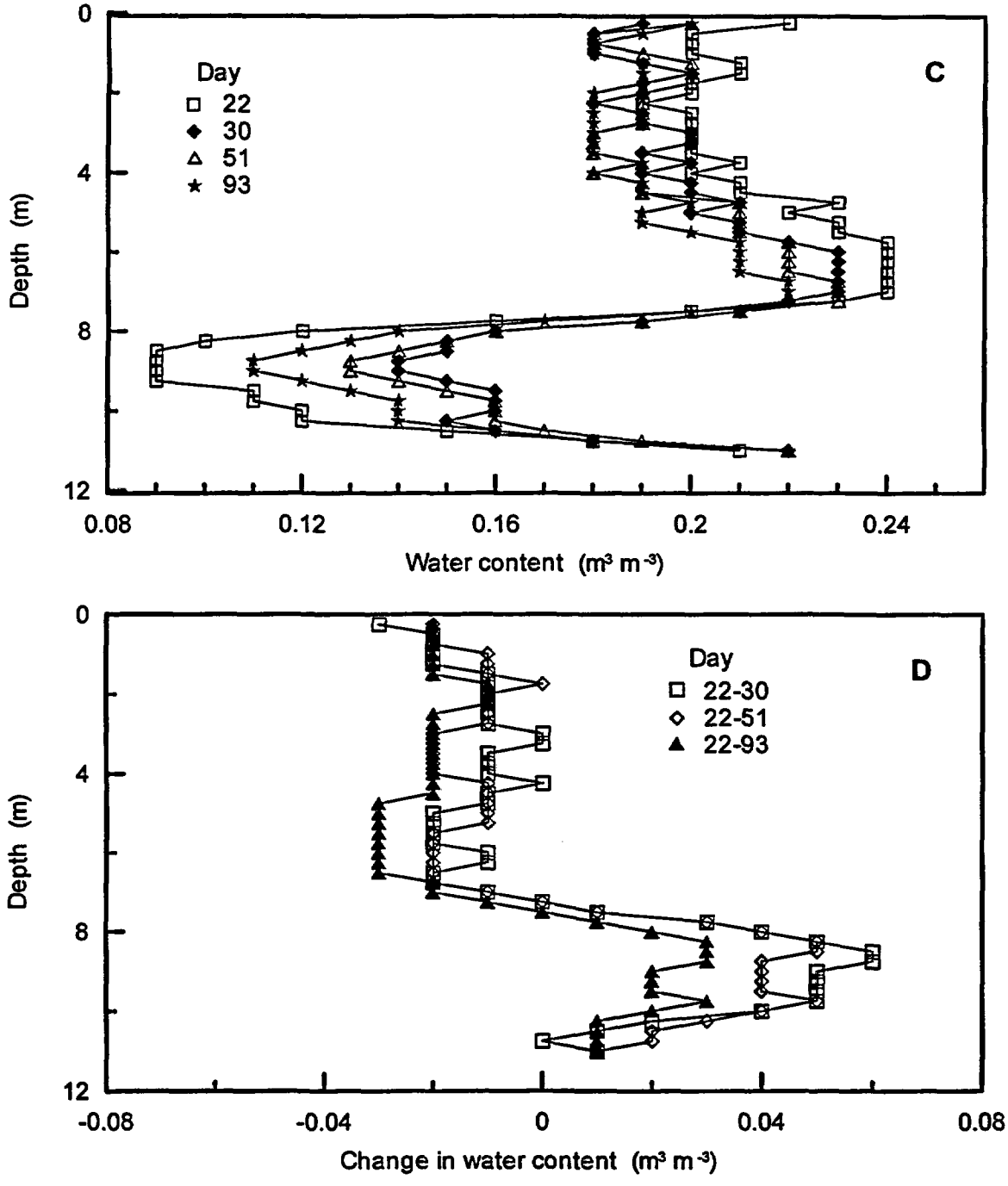

Figure 3.3-4. Water content and changes in water content for access tubes #402 (A and B), #423 (C and D), and #445 (E and F) during the water redistribution phase of Experiment 1. (Continued)

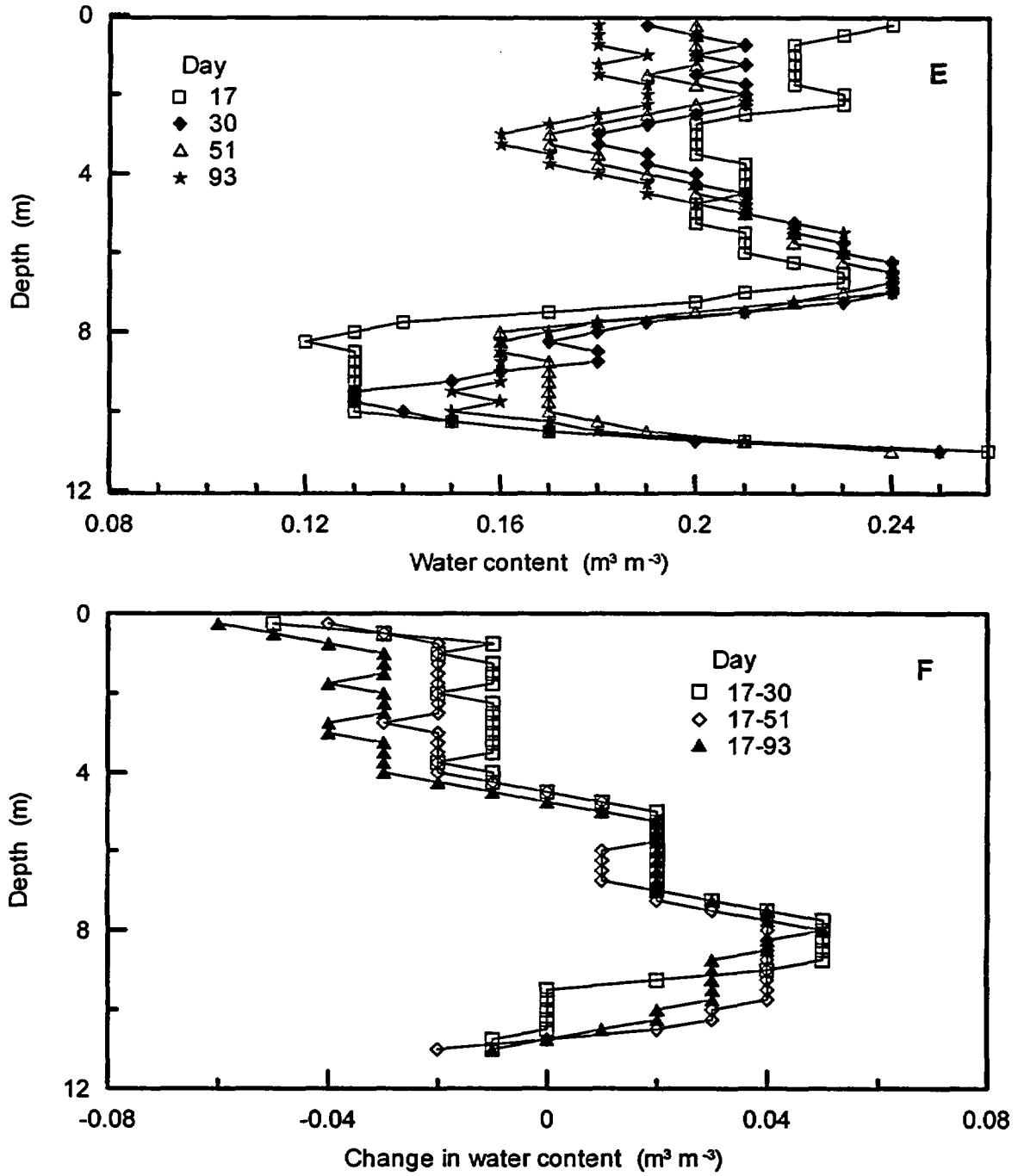

Figure 3.3-4. Water content and changes in water content for access tubes #402 (A and B), #423 (C and D), and #445 (E and F) during the water redistribution phase of Experiment 1. (Continued)

Table 3.3-4. Sampling schedule for the vertical neutron probe access tubes during Experiment 2.

Date	Time (days)	Number of Tubes	Maximum Depth (m)	Identifiers
12/03/97	0	17	3	a
12/04/97	1	41	3	
12/05/97	2	41	3	
12/06/97	3	41	3	
12/09/97	6	41	3	
12/10/97	7	40	3	
12/11/97	8	41	3,11	b
12/12/97	9	10	11	c
12/13/97	10	10	11	c
12/15/97	12	10	11	c
12/16/97	13	41	3,11	b
12/17/97	14	10	11	c
12/19/97	16	10	11	c
12/23/97	20	10	11	c
12/27/97	24	24	3,11	b
12/30/97	27	10	11	c
01/05/98	33	41	3	a
01/06/98	34	41	3,11	b
01/09/98	37	41	3,11	b
01/16/98	44	10	11	c
01/20/98	48	11	11	c
01/27/98	55	10	11	c
02/19/98	78	10	11	c
03/20/98	107	10	11	c
04/22/98	140	10	11	c
05/28/98	176	10	11	c

†Explanation of identifiers
a - start/stop irrigation phase of experiment
b - scanned total depth for all tubes
c - scanned only deep tubes

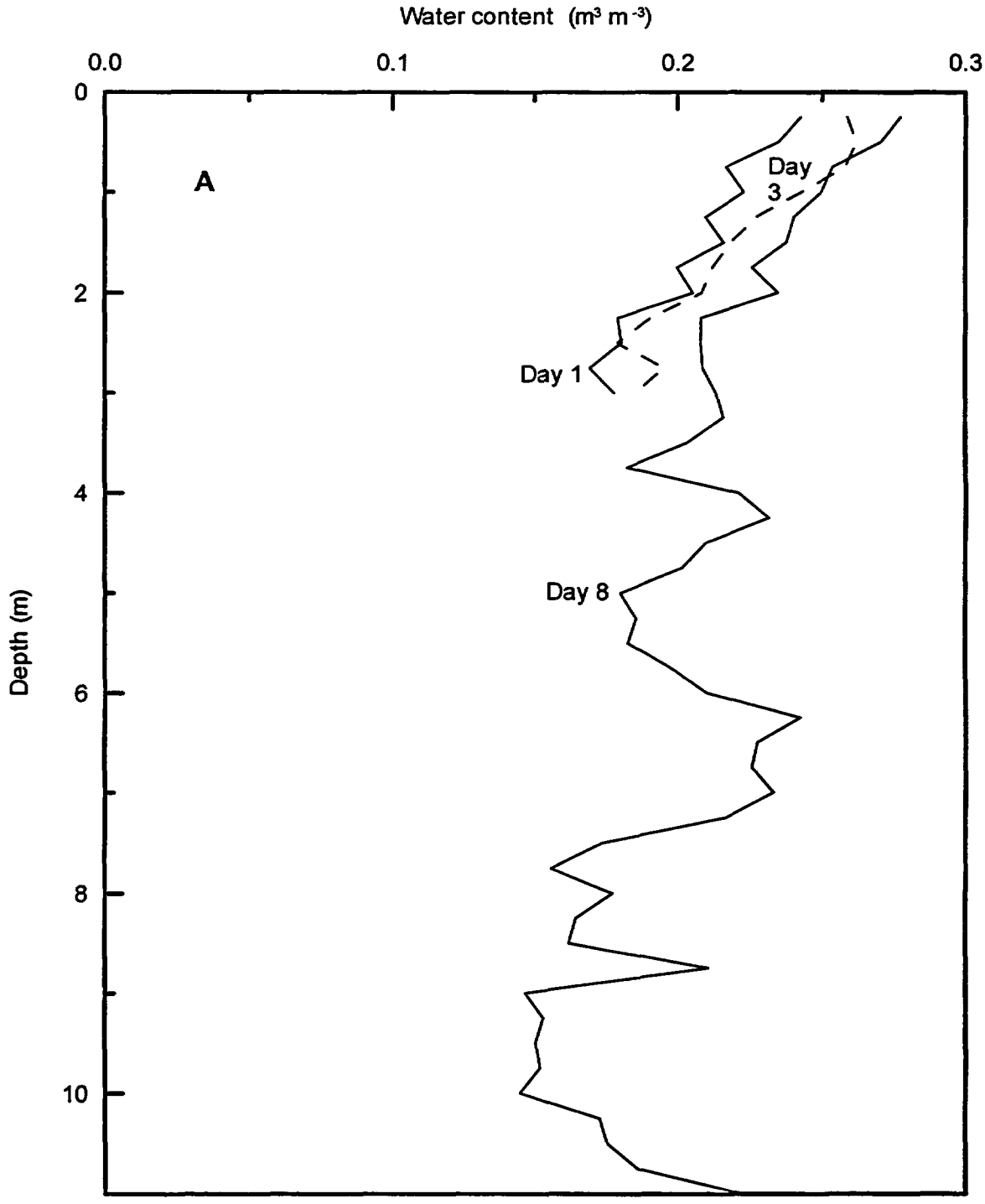

Figure 3.3-5. Vertical neutron probe water content taken from access tubes #402 (A), #423 (B), and #445 (C) during Experiment 2. Day 3 data ends at 3 m depth for all three sites.

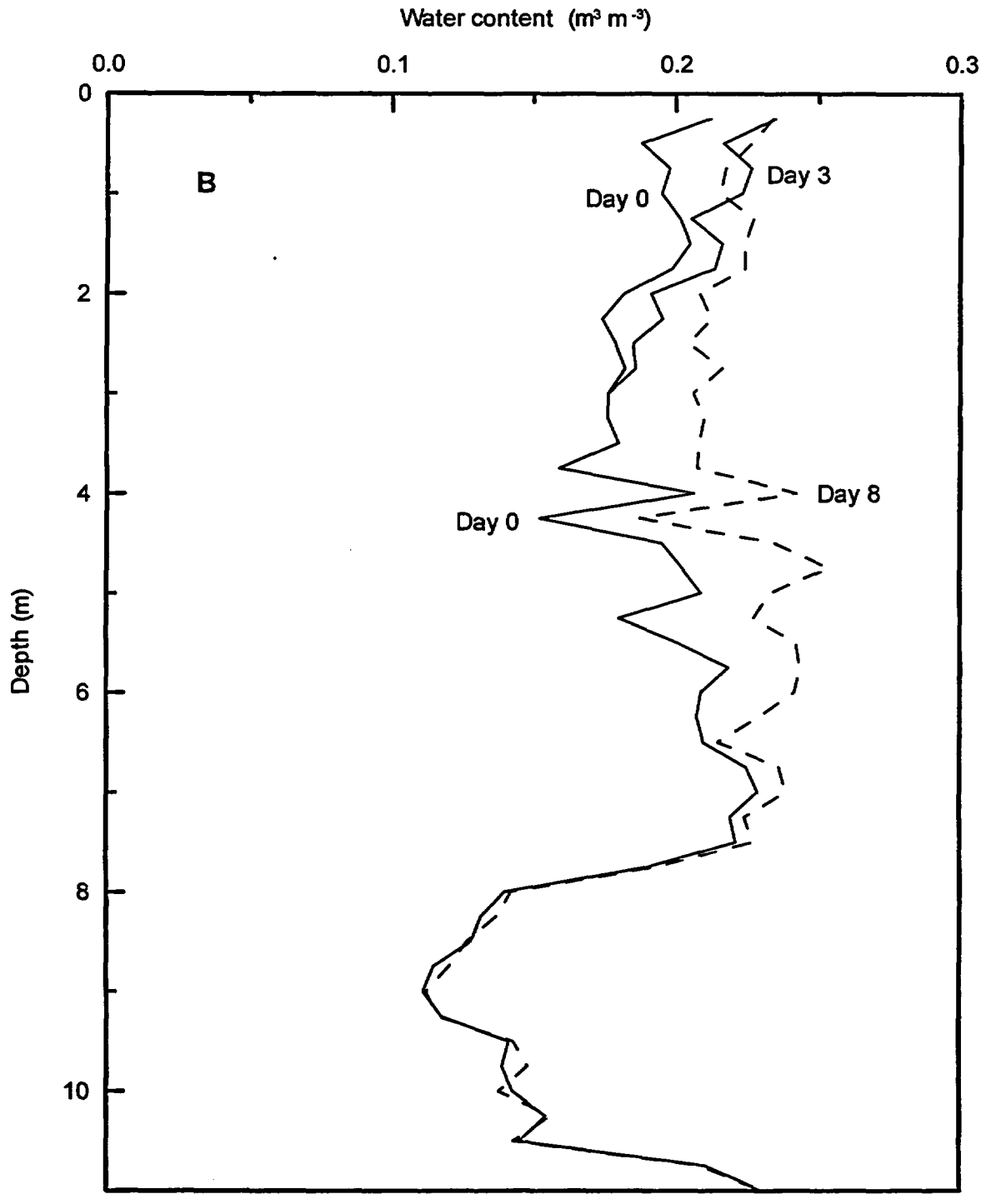

Figure 3.3-5. Vertical neutron probe water content taken from access tubes #402 (A), #423 (B), and #445 (C) during Experiment 2. Day 3 data ends at 3 m depth for all three sites. (Continued)

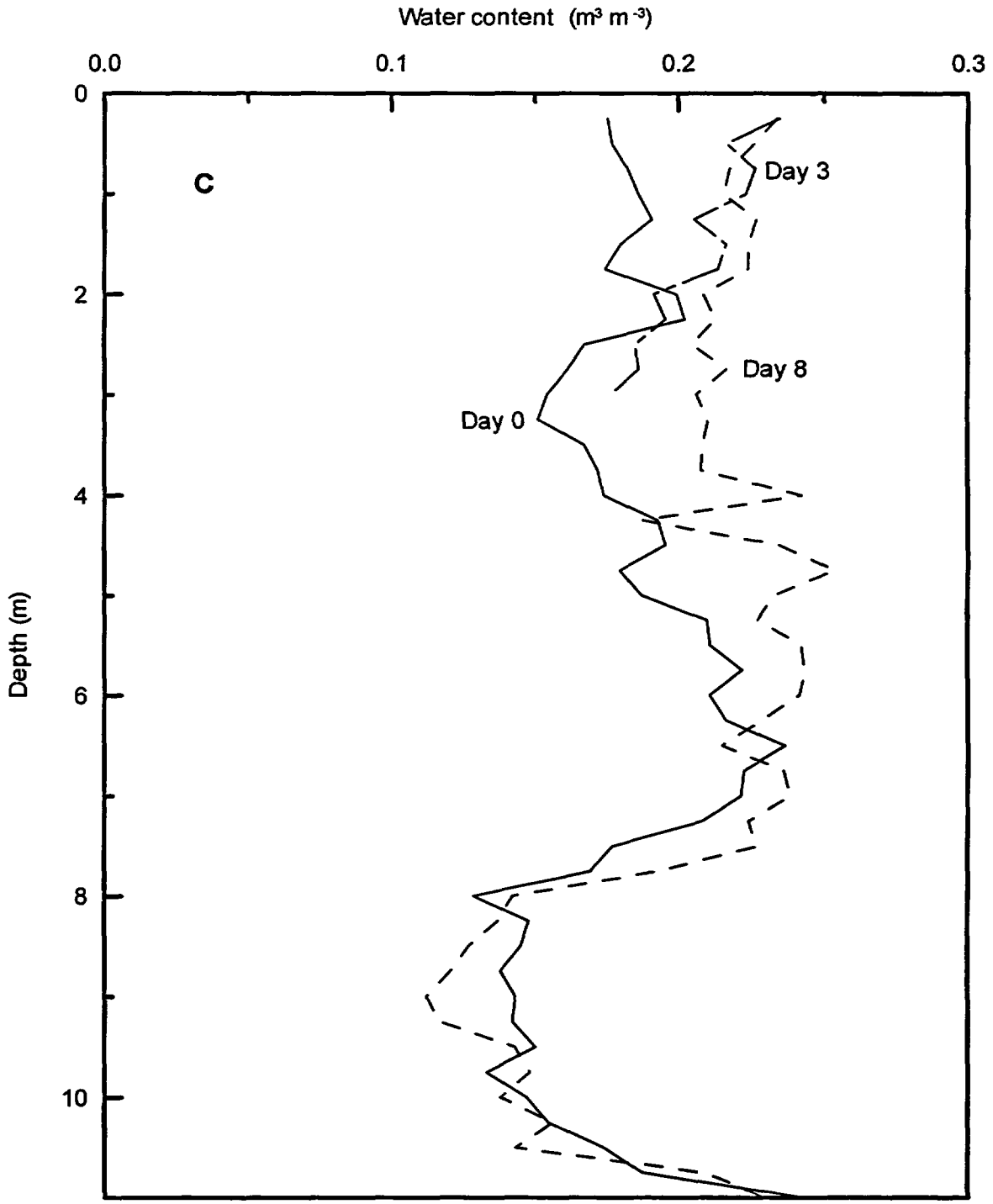

Figure 3.3-5. Vertical neutron probe water content taken from access tubes #402 (A), #423 (B), and #445 (C) during Experiment 2. Day 3 data ends at 3 m depth for all three sites. (Continued)

Table 3.3-5. Change in water content and estimated wetting front velocities measured using three representative access tubes during Experiment 2.

Depth (m)	Δθ† ($m^3\ m^{-3}$)	Wetting Front velocity‡ ($cm\ d^{-1}$)	Δθ ($m^3\ m^{-3}$)	Wetting Front velocity ($cm\ d^{-1}$)	Δθ ($m^3\ m^{-3}$)	Wetting Front velocity ($cm\ d^{-1}$)	Mean velocity ($cm\ d^{-1}$)
	#402		#423		#445		
1	0.030	65.5	0.023	85.5	0.022	89.4	80.1
2	0.025	78.6	0.020	98.3	0.026	75.6	84.2
3	0.025	78.6	0.025	78.6	0.027	72.8	76.7
					Overall Mean		80.3

† - Mean change in volumetric water content

‡ - Calculated using mean change in water content and average flux rate of 1.966 $cm\ d^{-1}$

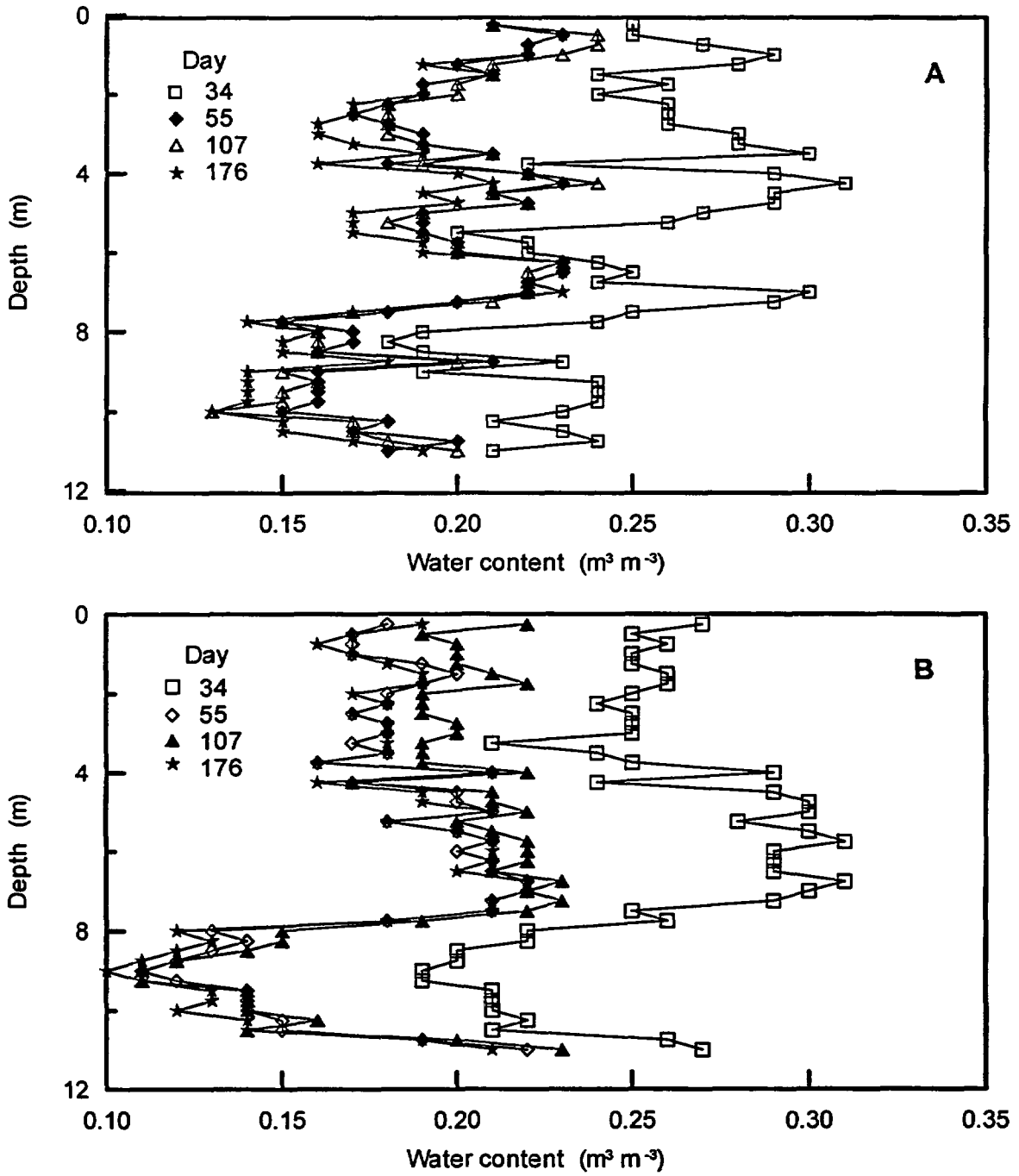

Figure 3.3-6. Redistribution of water during Experiment 2 at access tubes #402 (A), #423 (B), and #445 (C).

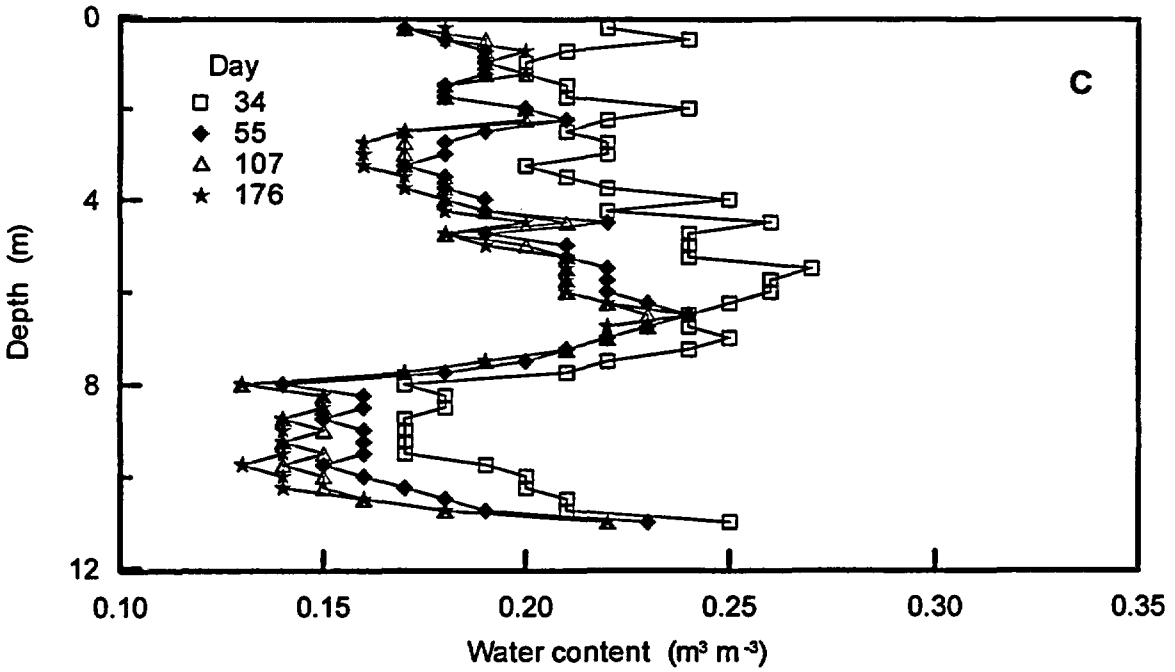

Figure 3.3-6. Redistribution of water during Experiment 2 at access tubes #402 (A), #423 (B), and #445 (C). (Continued)

of irrigation. It is apparent that most of the internal drainage occurred quickly, so that changes in water content after 22 of redistribution (Day 55) were relatively minor. For most of the depths in these example access tubes, change in water content from one measurement period to the next was probably affected by measurement variability as much as actual water drainage. This was because the standard count used for determining the ratio can vary from one day to the next, even though the standard counts were tested each day to be sure that they fall within a statistical confidence interval. No significant differences existed between water contents at the end of Experiments 1 and 2 for the three access tubes tested. Generally, water contents varied at each depth by ± 0.01 m^3 m^{-3}, and this is not enough to be significant.

3.3.2 Horizontal Access Tubes

3.3.2.1 Experiment 1

The three access tubes used for this research are called the N-S disturbed (tube #461, 7.5 cm ID HDPE, located in buried trench), N-S undisturbed (tube #462, 7.5 cm ID HDPE, located in narrow trench), and the E-W undisturbed (tube #463, 10 cm ID PVC, located in narrow trench). The sampling schedule used during Experiment 1 is found in Table 3.3-6. Water contents from four collection days are shown for each of the three access tubes in Figures 3.3-7 through 3.3-9, and labeled as listed above, respectively. Each figure shows readings from Days 0 and 4 to show repeatability of readings before significant arrival of the wetting front. Note, in Figure 3.3-7 for the N-S disturbed tube, the repeatability of water content values between these two days, with the exception of increases toward the north side of the plot. The neutron probe response to the markers was distinctive, making it relatively easy to determine the exact location of the detector in the 60 m long access tube. Four days after irrigation, arrival of the wetting front was apparent in several locations in the north side of the plot, but the wetting front has not arrived at 1.5 m at the south end of the trench. By Day 8, the wetting front had arrived throughout most of the northern section of the plot, but not in the southern 10 m, except for a peak located near $Y = 6$ m. Wetting front arrival was recorded across the entire plot by Day 13, after which daily recording of horizontal access tubes stopped.

By comparison, wetting front behavior in the N-S undisturbed trench (Figure 3.3-8) was more uniform. Note especially the distinctive lack of change in water content between Days 0 and 4. When comparing the Day 4 profile to that shown for the N-S disturbed trench (Figure 3.3-7), it appears obvious that the disturbed trench experienced significantly more variable flow, particularly in the north. The wetting front had arrived almost completely along the northern portion of the undisturbed trench by Day 8, but arrival was highly variable in the southern portion. Wetting front arrival was complete by Day 13, similar to that seen in the disturbed trench.

Readings taken in the E-W undisturbed access tube show significantly more scatter before arrival of the wetting front (Figure 3.3-9). The higher scatter could be due to the lower count of slow neutrons returning to the counter in this large-diameter, PVC pipe, with the same number of fast neutrons emitted from the source. In this case, the variability associated with the decay of americium-241 would be higher with respect to the returning neutrons, leading to poorer repeatability. Wetting front arrival, however, was still clearly observable. Note the relative dryness of the soil material in the eastern portion of the plot, when compared to the western portion on Day 8. The highly non-uniform water content in the western portion could be from textural differences in the shallow soils, or from variability in the backfilling of the narrow trench.

The dotted lines on these three graphs show the cross-over point between the N-S and E-W access tubes. Wetting front arrivals correlated fairly well (i.e., wetting fronts should have arrived at the cross-over point by the same day). In some cases, however, this did not happen. For example, the wetting front did not arrive fully on Day 8 at the E-W access tube (Figure 3.3-9), but did arrive at the access tube in the N-S disturbed trench. This can be explained by the fact that the E-W access tube is approximately 27 cm deeper than the N-S tube (see Table 2.3-3).

Similar to the analysis conducted on the vertical access tubes (especially using equation 2-1), it was possible to determine wetting front velocity from ground surface to the horizontal access tubes. Thus, the wetting front arrival was determined for each point at least 2.5 m inside the irrigated plot for each of the three access tubes. The 2.5 m buffer zone was used to reduce the effects of lateral flow of water near the edges of the irrigated plot. Figures 3.3-10 through

Table 3.3-6. Sampling schedule for the horizontal neutron probe access tubes during Experiment 1.

Date	Time	N-S disturbed	N-S undisturbed	E-W undisturbed
04/15/97	-13	✓	✓	✓
04/30/97	2	✓	✓	✓
05/02/97	4	✓	✓	✓
05/03/97	5	✓	✓	
05/04/97	6	✓	✓	
05/05/97	7	✓	✓	✓
05/06/97	8	✓	✓	✓
05/08/97	10	✓	✓	✓
05/09/97	11		✓	✓
05/10/97	12	✓	✓	✓
05/11/97	13	✓	✓	✓
05/13/97	15			✓
05/28/97	30	✓	✓	✓
06/04/97	37	✓	✓	✓
06/18/97	51	✓	✓	✓
06/25/97	58	✓	✓	✓
07/02/97	65	✓	✓	✓
07/09/97	72	✓	✓	✓
07/16/97	79	✓	✓	✓
07/23/97	86	✓	✓	✓
07/30/97	93	✓	✓	✓

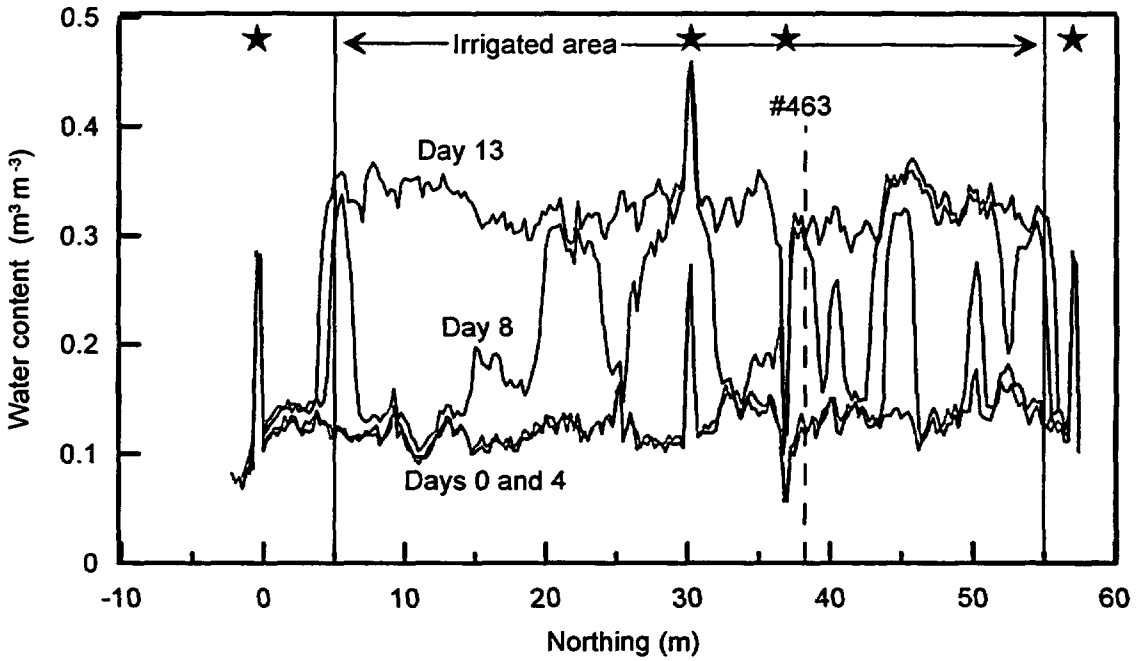

Figure 3.3-7. Water content from four collection days using the N-S disturbed horizontal access tube (#461) during Experiment 1. Stars indicate location of tubing markers or tube splice (decreasing water content) and the dashed line indicates the crossover point with the E-W tube.

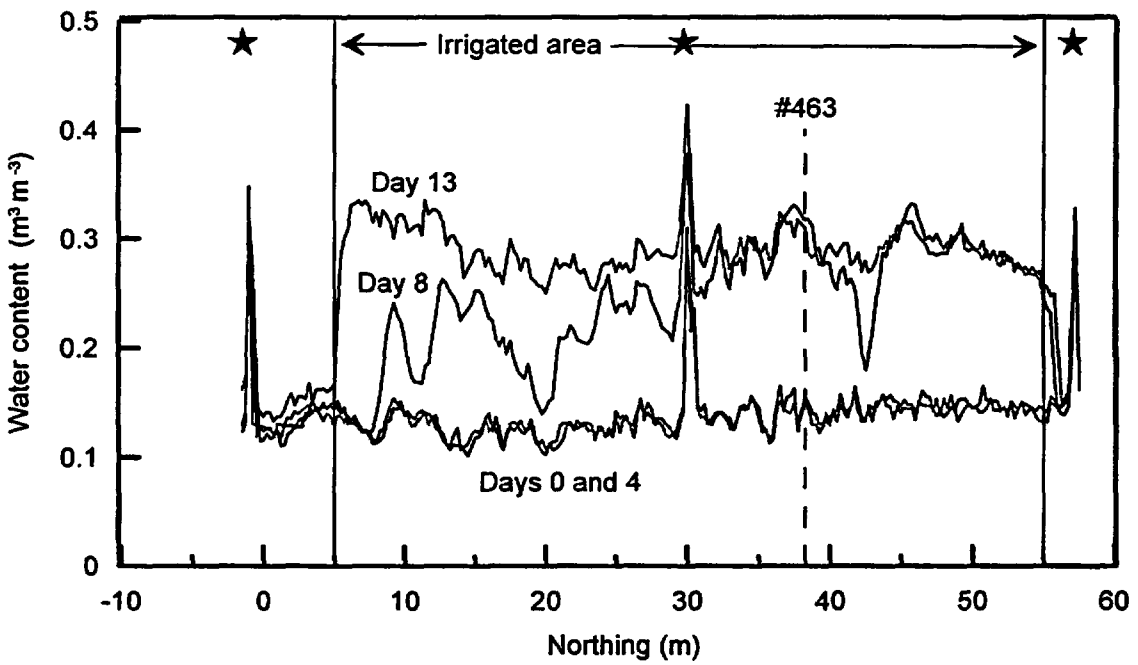

Figure 3.3-8. Water content from four collection days using the N-S undisturbed horizontal access tube (#462) during Experiment 1. Stars indicate location of tubing markers and the dashed line indicates the crossover point with the E-W tube.

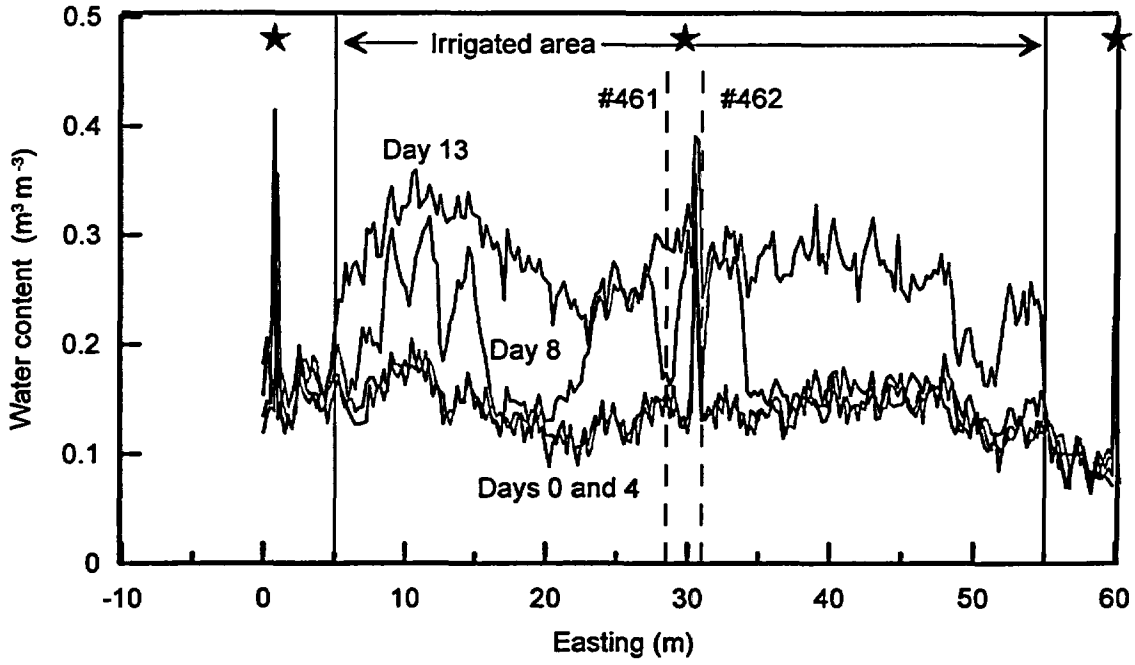

Figure 3.3-9. Water content from four collection days using the E-W undisturbed horizontal access tube (#463) during Experiment 1. Stars indicate location of tubing markers and the dashed lines indicate the crossover points with the N-S tubes.

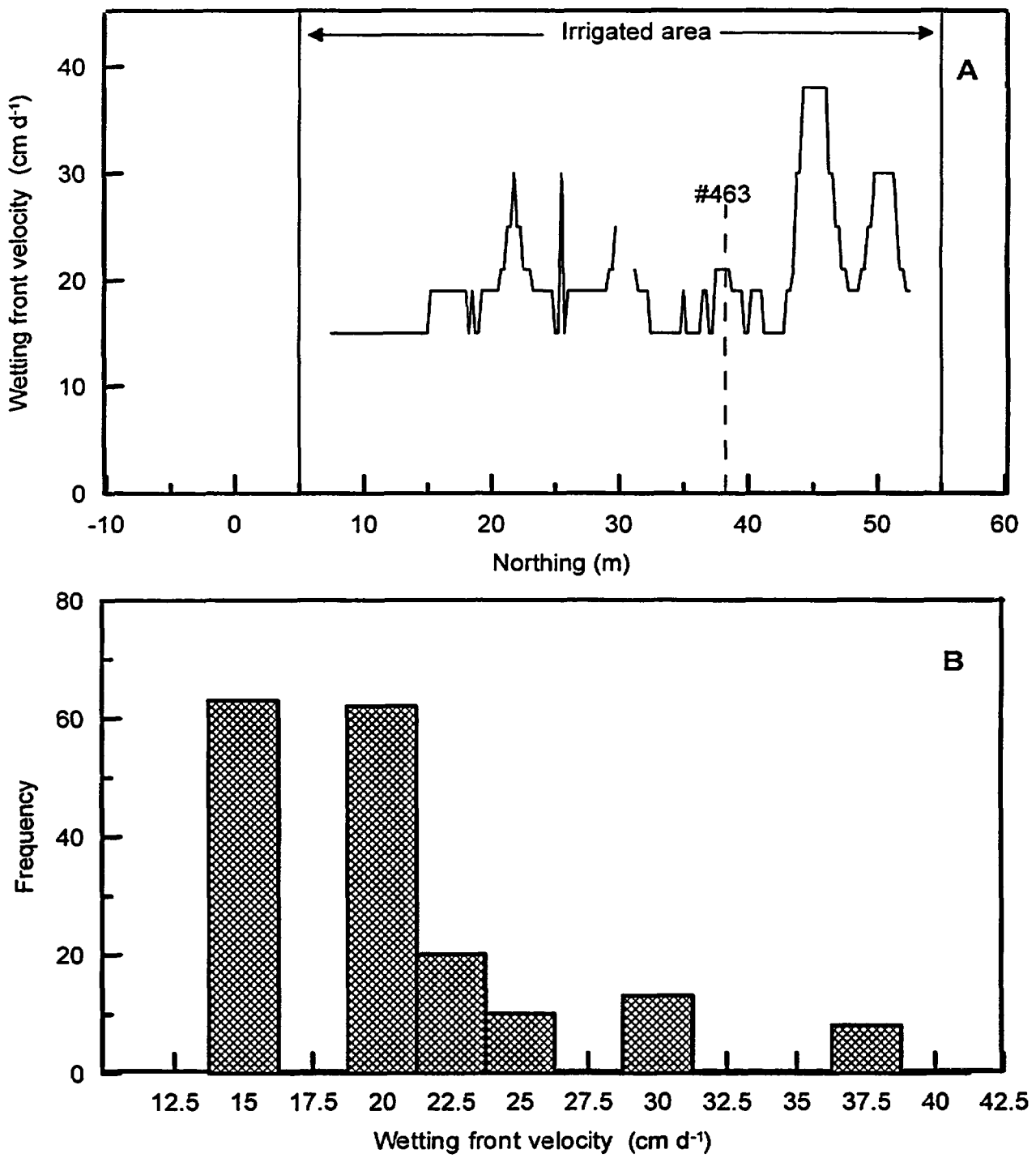

Figure 3.3-10. (A) Wetting front velocities in the N-S disturbed horizontal access tube, including (B) frequency histogram, during Experiment 1. Dashed line indicates the crossover point with the E-W tube.

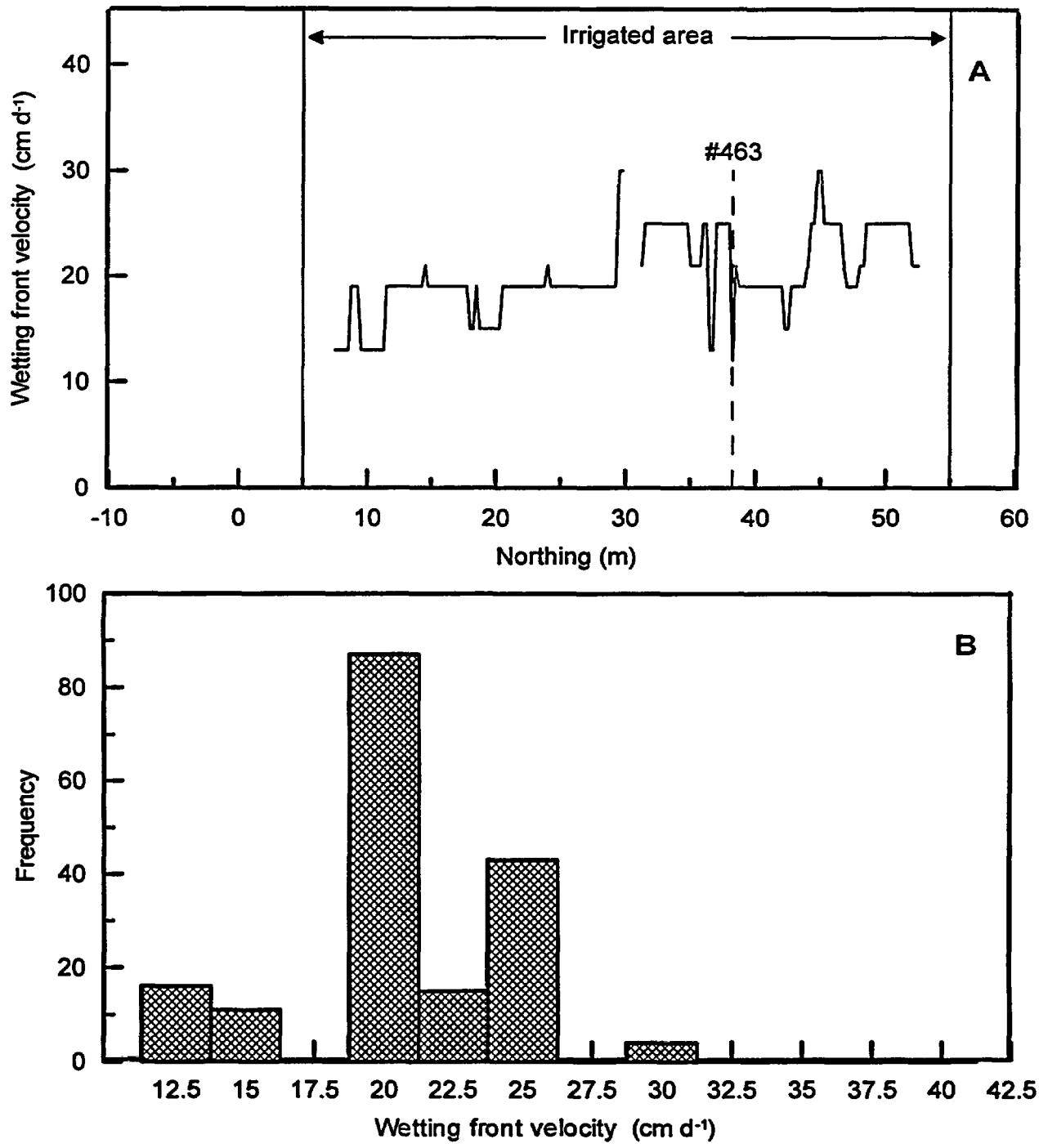

Figure 3.3-11. (A) Wetting front velocities in the N-S undisturbed horizontal access tube, including (B) frequency histogram, during Experiment 1. Dashed line indicates the crossover point with the E-W tube.

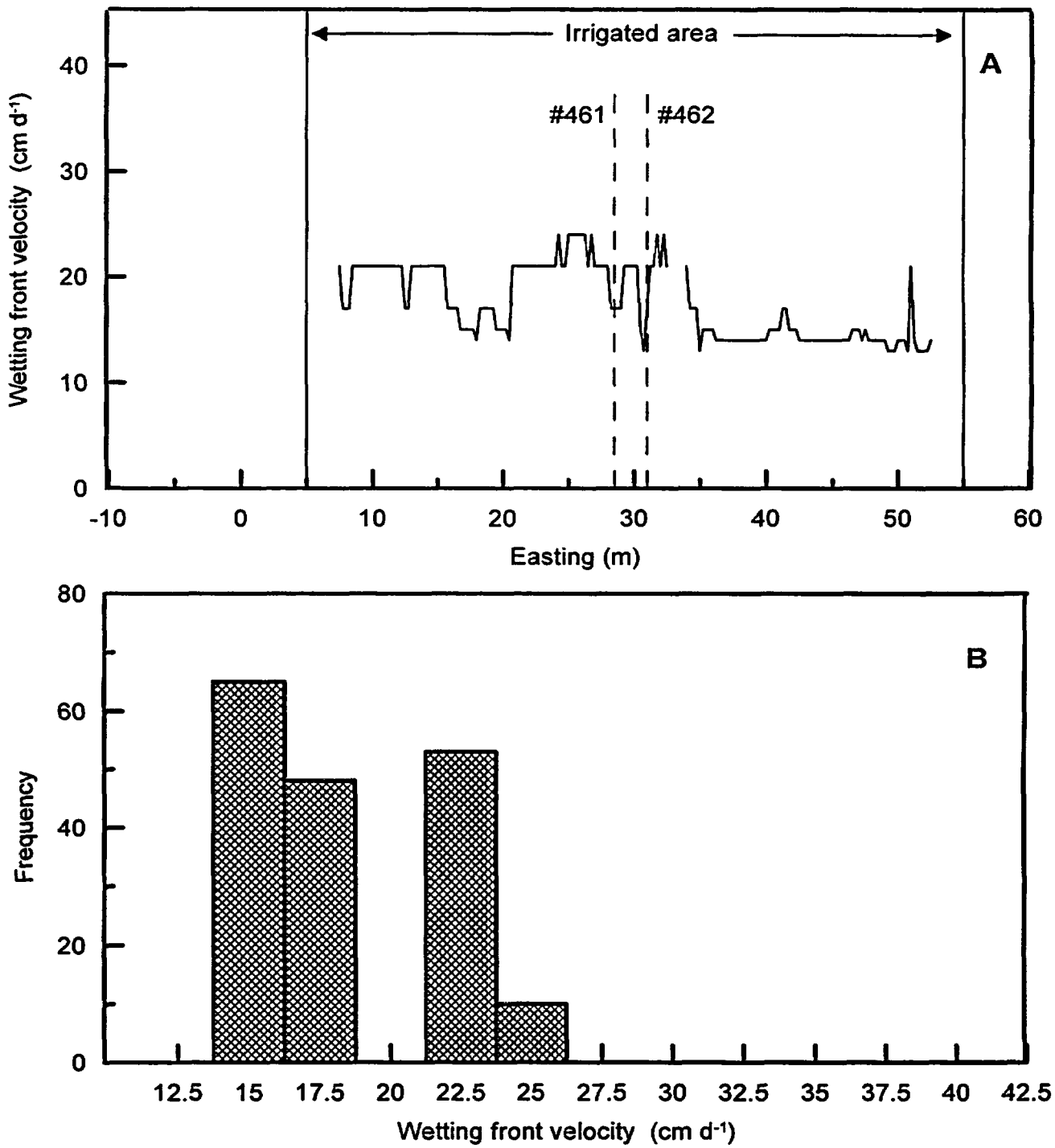

Figure 3.3-12. (A) Wetting front velocities in the E-W undisturbed horizontal access tube, including (B) frequency histogram, during Experiment 1. Dashed lines indicate the crossover points with the N-S tubes.

3.3-12 show the wetting front velocities across the irrigated plot, including a frequency histogram indicating distribution.

By comparing Figures 3.3-10 and 3.3-11 for the disturbed and undisturbed horizontal access tubes, which are offset by 3.5 m, it is possible to see certain similarities in the neutron probe response to irrigation. For example, focused flow through the backfill material may have contributed to the elevated velocities in the disturbed tube at Y = 45 and 50; however, similar responses were seen in the adjacent undisturbed tube at the same Y coordinates. This could be interpreted to mean that similarities in soil texture and/or structure in this area of the plot exerted a great influence on water movement, but that soil disturbance also contributed to some of the flow variability. Water flow toward the southern portion of the plot was less variable than in the northern portion of the undisturbed trench, but this trend was not as apparent in the disturbed trench, where several zones of high water flow were recorded. These disparate zones of high water flow in the disturbed trench also affected the frequency histogram, with a much higher positive skewness (1.66) than for the undisturbed trench (0.12).

Flow response in the E-W undisturbed trench (tube #463) shows almost no variability of wetting front velocity in the eastern portion of the plot (Figure 3.3-12). Flow velocity obviously increased toward the center and western portions of the plot, and this trend was also seen from the results using the vertical access tubes from 0 - 2 m depth (Figure 3.3-3C). The frequency histogram showed very few extreme velocities recorded across the site.

These results illustrate the benefit of having numerous monitoring points at a specific depth, using a single access tube. For water flow experiments of this type, monitoring the wetting front behavior could be achieved with relatively little site disturbance and less personnel effort, when compared to the number of vertical access tubes that would have been required to achieve the same number of data points. The paraffin and HDPE markers used with each of the horizontal tubes provided good information on the exact position of the probe as it was pulled through the tube, underneath the plot. Small variations in the readings, especially before the irrigation experiments began (e.g., Days 0 and 4), could be due to either the statistical counting nature of the neutron probe, or from small changes in the location of the probe from one day to the next day. The markers were wide enough to be easily detected by the probe, yet they were narrow enough so that errors in positioning of the probe in the tube were limited to only several centimeters.

We compared the plot-wide front velocities using the three horizontal access tubes to those calculated using the vertical access tubes. Mean velocities of 19.7, 19.9 and 17.4 cm d^{-1} were calculated for the N-S disturbed, N-S undisturbed and E-W undisturbed trenches, respectively, and Table 3.3-3 lists a mean front velocity of 21.8 cm d^{-1} at 1.5 m depth. All three velocities were comparable in terms of the coefficient of variation, which were between 21% and 27%. Though vertical access tubes appeared to record higher velocities (21.8 versus 19.0 cm d^{-1}), it is important to note that the average arrival of the wetting front differed by only a single day between the vertical and N-S horizontal access tubes. Vertical and E-W horizontal readings differed by slightly more because the horizontal access tube was installed at 1.67 m depth, instead of 1.50 m.

Redistribution of near-surface water to below 1.5 m are shown in Figures 3.3-13A through 3.3-13C for the N-S disturbed, N-S undisturbed, and E-W undisturbed trenches. Water content profiles for the four days were difficult to distinguish because their values were very close and because of random scatter in the data. However, the general similarity of the profiles on each plot indicated only a nominal change in water content at that depth and within the range of influence for the neutron probe. Lateral variations of soil texture were much less than vertical variations, in contrast to the observations made on the vertical access tubes. Therefore, if soil texture controls water holding capacity, and if the texture does not change significantly across the transect at the depth of the access tube, then water content will likely remain essential the same. Consider, for example, the transect average water content for each of the three tubes during redistribution (Table 3.3-7). During the first four weeks, average water contents decreased for each of the access tubes, then became more uniform with time. Though water was still draining from soils above these access tubes, they were not draining quickly enough to cause a significant change in the water content at ~1.5 m depth. The "increase" of average water content from Day 79 to Day 86 shows how variability of the standard counts can affect the actual water content readings. Standard counts were collected twice each day and then

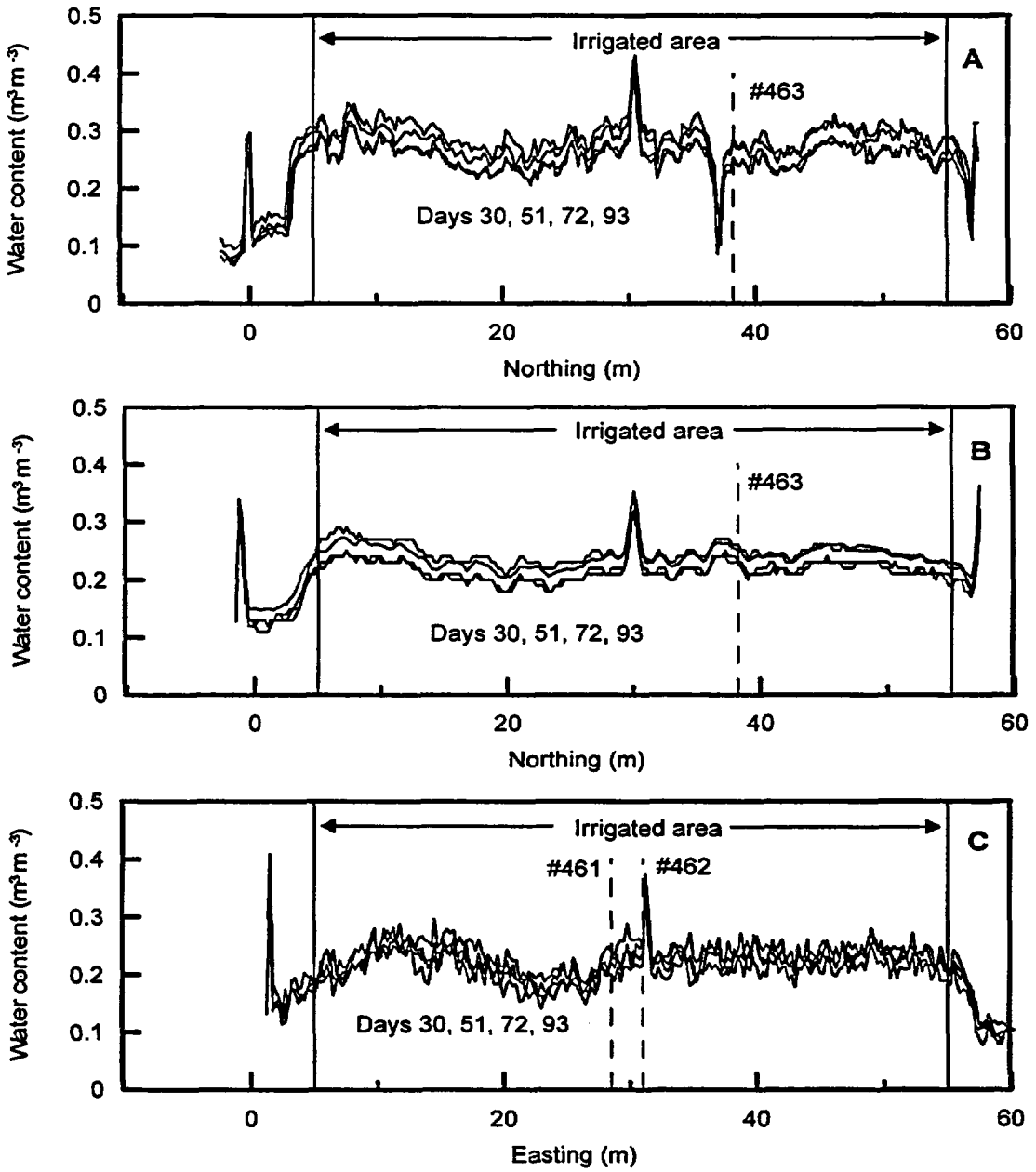

Figure 3.3-13. Water redistribution measured using horizontal neutron probe access tubes during Experiment 1. (A) N-S disturbed tube, (B) N-S undisturbed tube, and (C) E-W undisturbed tube. Dashed lines indicate crossover points with other access tubes.

Table 3.3-7. Transect average water contents measured using the horizontal neutron probe access tubes during redistribution during Experiment 1.

Experimental Time (days)	Time of redistribution (days)	Mean Volumetric Water Content N-S Disturbed ($m^3 m^{-3}$)	N-S Undisturbed ($m^3 m^{-3}$)	E-W Undisturbed ($m^3 m^{-3}$)
30	7	0.29	0.24	0.23
37	14	0.28	0.23	0.21
51	28	0.25	0.21	0.21
58	35	0.26	0.22	0.20
65	42	0.26	0.22	0.21
72	49	0.25	0.22	0.20
79	56	0.25	0.21	0.20
86	63	0.32	0.27	0.26
93	70	0.28	0.24	0.22

checked to ensure that they were not statistical outliers. The higher water contents on Day 86, corresponding to a lower average standard counts, showed that small changes in standards still can affect water contents.

3.3.2.2 Experiment 2

Table 3.3-8 shows the sampling schedule used during Experiment 2. Given the similar behavior of the three access tubes during Experiment 1, only measurements made in the undisturbed N-S access tube (access tube #462) will be described in this section. Figure 3.3-14 presents the water content profiles for four time periods. The soil material had drained additionally between the end of Experiment 1 and the beginning of Experiment 2, yielding an average change in water content of 0.023 $m^3 m^{-3}$ during this 126 day period. After irrigation began during Experiment 2, the wetting front arrived very quickly across the profile. By Day 4, most of the monitoring locations indicated wetting front arrival, and by Day 7, the soil material was at steady-state. We included in the figure the measurements made on Day 35, one day after irrigation ended, to show that the water content profiles were repeatable. The average water content increase along the entire transect was about 0.055 $m^3 m^{-3}$, excluding those values collected near the markers, much less than the average change during Experiment 1 (~0.185 $m^3 m^{-3}$). The large difference illustrates the significant soil water deficit that existed in the profile before onset of the experiments.

Figure 3.3-15 shows the redistribution of water, as recorded in access tube #462. The responses were very similar to those shown on Figure 3.3-13. Internal drainage lowered the water content along the entire transect, yielding an average decline of 0.045 $m^3 m^{-3}$, so the profile had not completely drained to pre-irrigation levels. Lateral flow was evident away from the irrigated plot, especially toward the southern end of the transect, where water contents slowly increased. With additional time, we expect the final water contents to approach those recorded immediately before the beginning of Experiment 2 irrigation.

3.4 Time Domain Reflectometry Data

3.4.1 Buried Trench

3.4.1.1 Experiment 1

We experienced significant problems with the Dynamax TDR system, associated with both ambient temperature and electrical power, causing a larger loss of data than with the other systems. During Experiment 1, ambient temperatures at the field site increased significantly and often exceeded 35°C (95°F). Temperatures inside the truck boxes, as measured using the CR7 panel thermistor, exceeded 40°C (104°F), and this likely caused operational problems with the portable computer used to interrogate the cable tester. On several occasions, data were not collected by the personal computer, even though power was available through the AC power system.

The temperature also caused the deep cell marine battery to quickly lose its charge, disabling the multiplexer. Before Experiment 1 began, when the temperatures were moderate, battery voltage was checked periodically and was found to be stable. After the experiment began, average temperatures increased significantly, and the battery charge quickly dissipated. We permanently installed a battery charger in the truck box and the multiplexer operated smoothly. Another significant problem with the field setup was an electrical feedback from the AC power system into the cable tester. This feedback caused the TDR waveform to be highly variable when low filtration (e.g., averages = 8 or lower) was chosen by the user. To smoothen out the waveform, we increased the averaging to 128. Though this greatly increased the time necessary to complete a full scan of the 13 probes, the data were more stable.

Figures 3.4-1 through 3.4-3 show the TDR response to water infiltration at the buried trench transect. The increased variability in the data after approximately Day 10 is apparent. In some cases, the data are so variable, especially toward Day 20, that water content values are highly suspect. However, it is still possible to estimate wetting front arrival by simply observing when water content increases are steady. Accepting that this method is somewhat subjective, Table 3.4-1 lists the wetting front velocities as a function of distance along the buried trench. The average wetting front velocity 17.8 cm d^{-1} is smaller

Table 3.3-8. Sampling schedule for the horizontal neutron probe access tubes during Experiment 2.

Date	Time (days)	N-S disturbed	N-S undisturbed	E-W undisturbed
12/02/97	-1	✓	✓	
12/03/97	0		✓	✓
12/07/97	4	✓	✓	✓
12/08/97	5	✓	✓	✓
12/09/97	6	✓	✓	✓
12/10/97	7	✓	✓	✓
01/07/98	35	✓	✓	✓
01/08/98	36	✓	✓	✓
01/09/98	37	✓	✓	✓
01/13/98	41	✓		
01/23/98	51	✓	✓	✓
02/19/98	78	✓	✓	✓
03/20/98	107	✓	✓	✓
04/22/98	140	✓	✓	✓

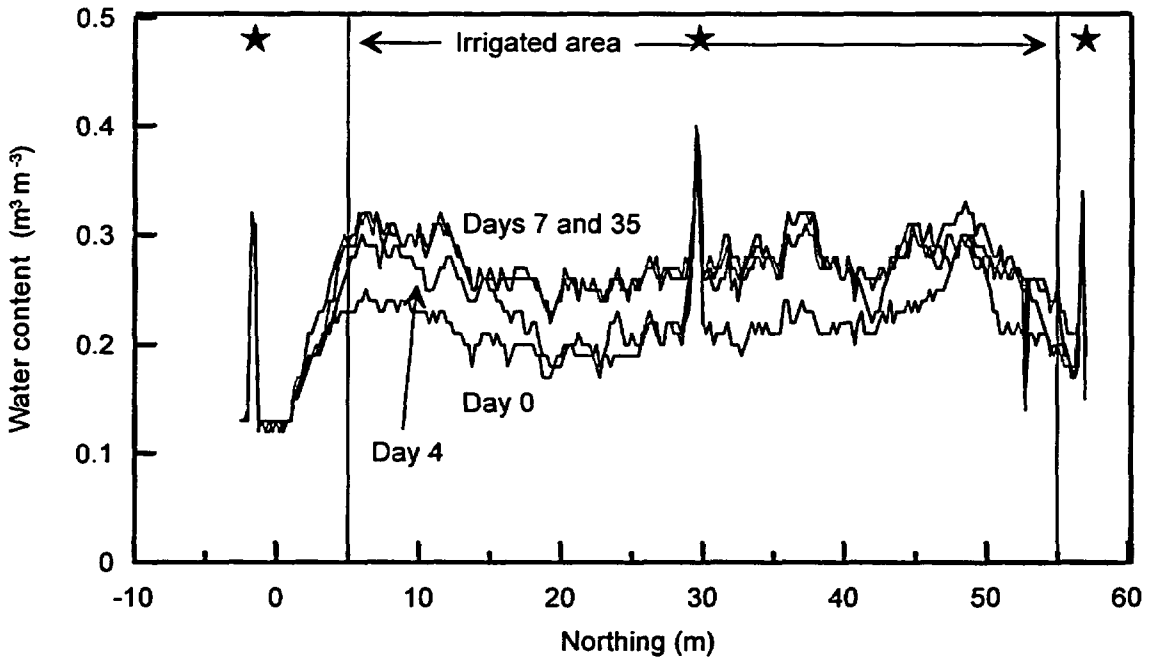

Figure 3.3-14. Water content along the N-S undisturbed horizontal access tube during Experiment 2. Stars indicate location of tubing markers.

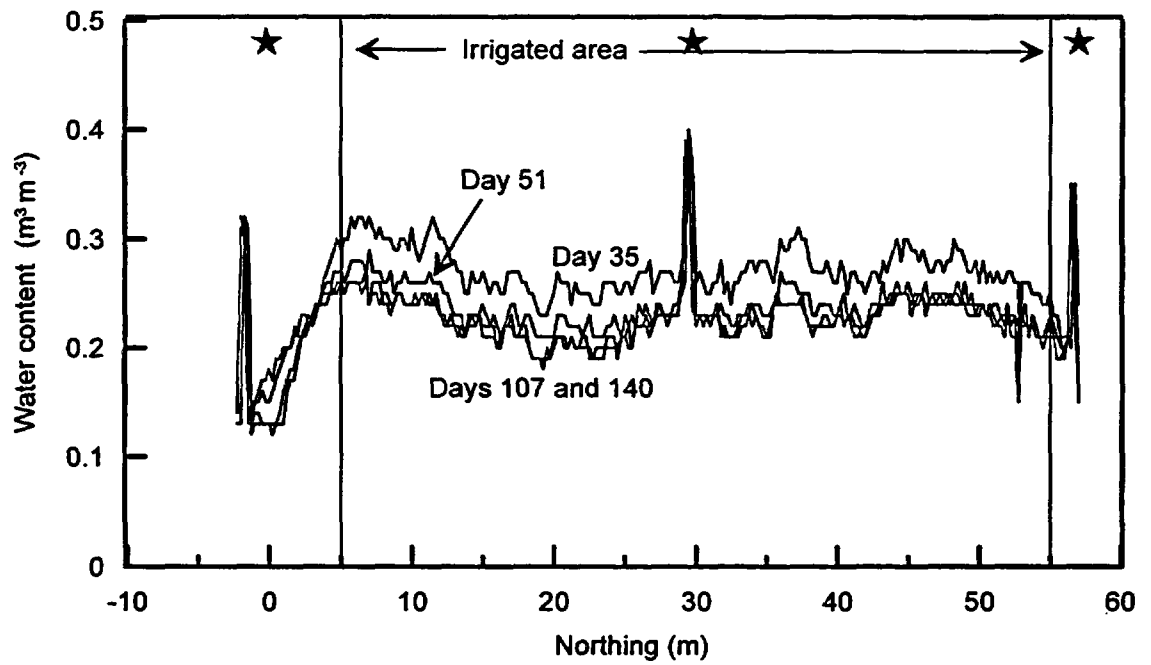

Figure 3.3-15. Redistribution of water at the N-S undisturbed horizontal access tube during Experiment 2. Stars indicate location of tubing markers.

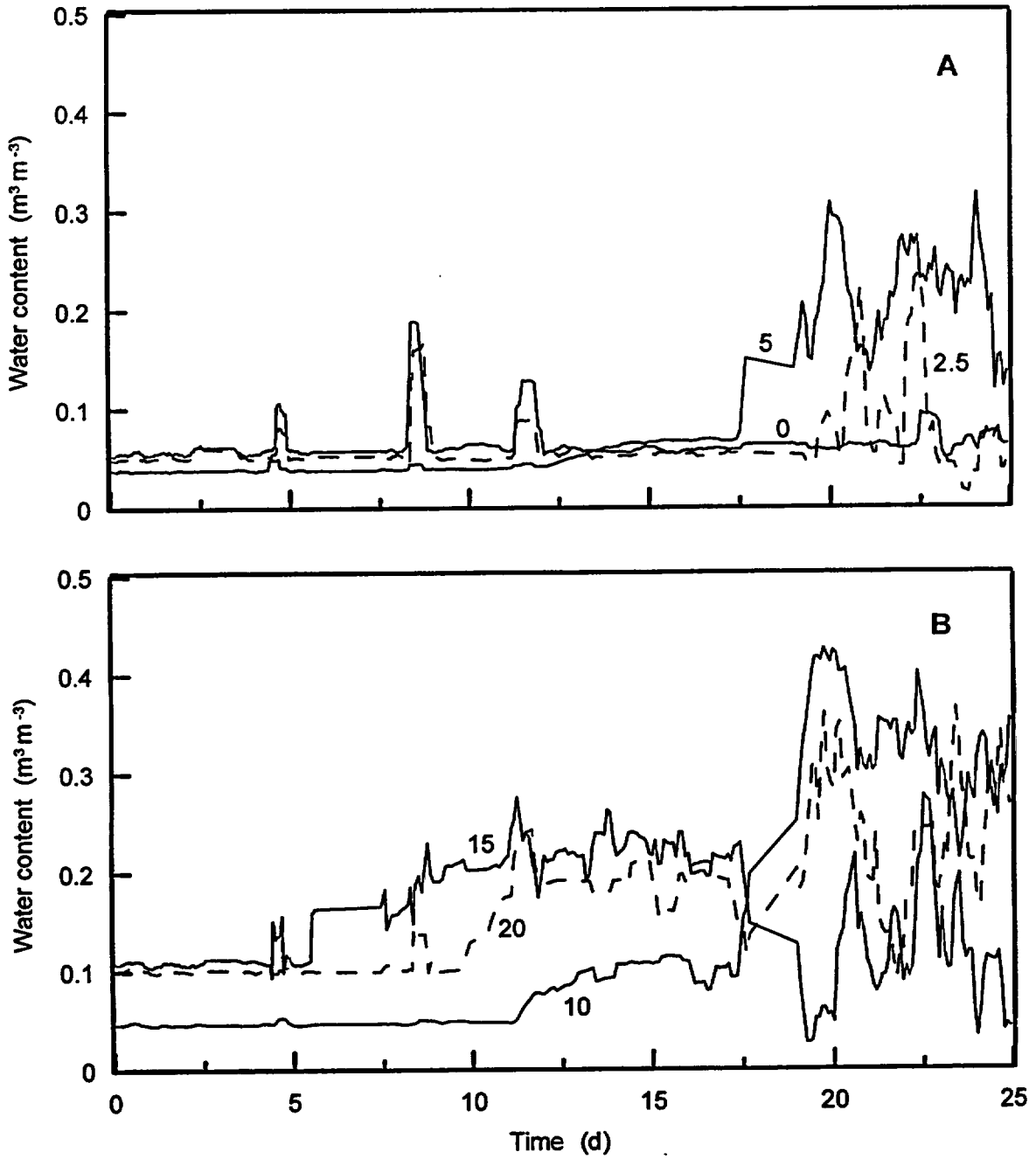

Figure 3.4-1. Response of TDR probes to water infiltration at southern end of buried trench during Experiment 1. Numbers on graph indicate y-coordinate.

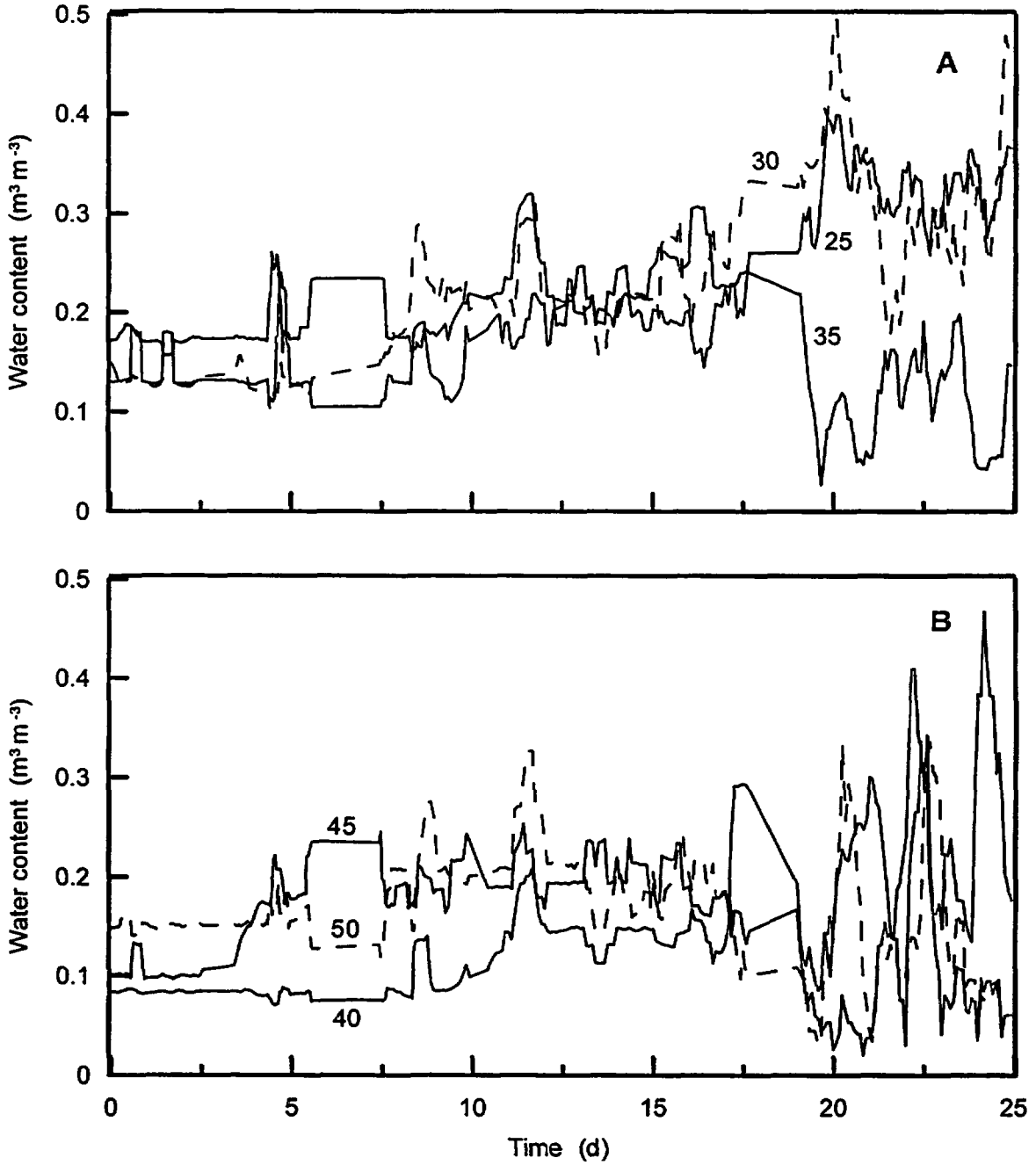

Figure 3.4-2. Response of TDR probes to water infiltration at central-northern area of buried trench during Experiment 1. Numbers on graph indicate y-coordinate.

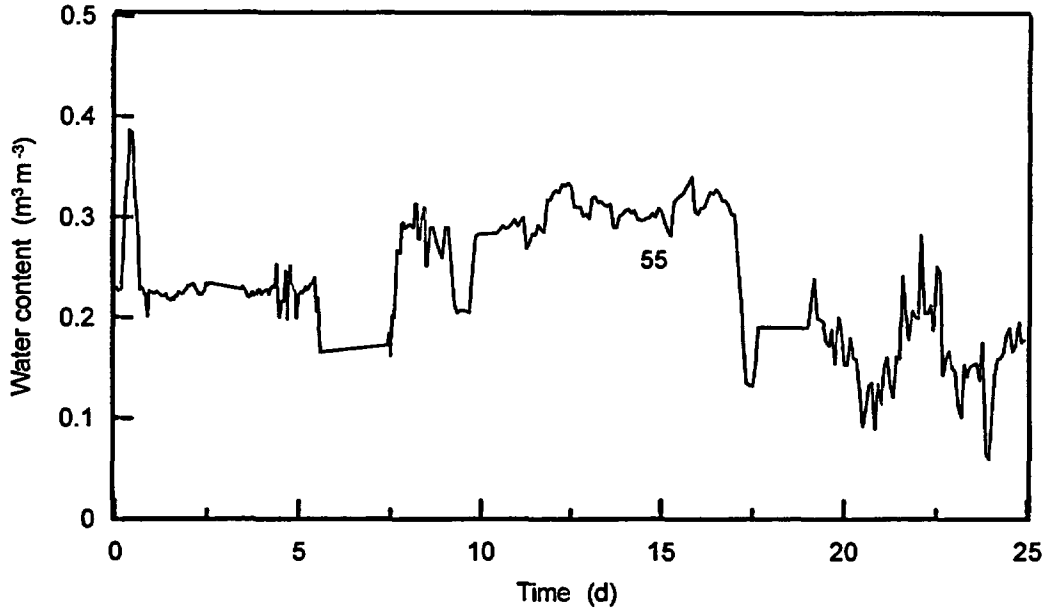

Figure 3.4-3. Response of TDR probes to water infiltration at northern end of buried trench during Experiment 1. Number on graph indicates y-coordinate.

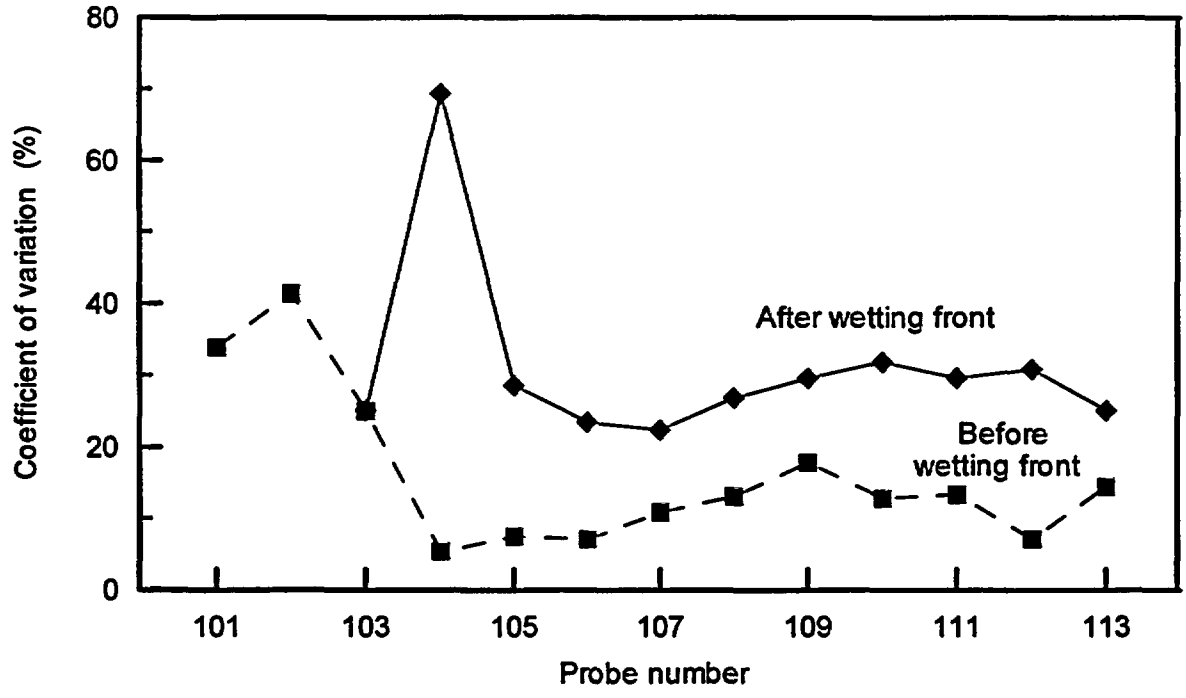

Figure 3.4-4. Coefficient of variation of TDR measurements collected before and after wetting front arrival using Dynamax TDR system during Experiment 1.

Table 3.4-1. Wetting front arrival in buried trench using Dynamax TDR system during Experiment 1.

Position	Y-coordinate (m)	Time (days)	WF velocity (cm d^{-1})
141	0	n/a	n/a
142	2.5	n/a	n/a
143	5	17.7	8.5
144	10	11.5	13.0
145	15	9.2	16.4
146	20	10.4	14.4
147	25	8.7	17.3
148	30	8.3	18.2
149	35	9.8	15.4
150	40	10.6	14.2
151	45	3.8	39.2
152	50	7.6	19.7
153	55	7.8	19.3
Mean		9.2	17.8

than that calculated from the two N-S neutron probe trenches (19.8 cm d^{-1}). The data show an overall trend of higher than average wetting front movement in the northern section of the plot, especially near Y = 45m. This was also observed in the horizontal neutron probe data using much higher resolution measurements.

After wetting front arrival, variability of measurements increased. Figure 3.4-4 shows the coefficient of variation of measurements collected along the length of the trench before and after arrival of the wetting front. The figure shows a consistently higher variation after wetting front arrival, even though the mean water content increased. Thus, either the variation of measurements is dependent on the water content, or the wetting front arrival coincided with an increase in the ambient temperature, whereby the variance is independent of water content.

Data for redistribution is not shown because the variability masked trends that would have been seen from internal drainage.

3.4.1.2 Experiment 2

The Dynamax TDR system was not operational between Days -0.5 and 6.75 during Experiment 2. At Day 6.75, the system was again placed on line and data collection began. Unfortunately, this was too late to collect information on wetting front arrival. However, several days of data collection before the irrigation phase of the experiment began allows us to evaluate variability of instrument measurements. These data are listed in Table 3.4-2, along with statistical information on the instruments after arrival of the wetting front and before the cessation of irrigation. Figure 3.4-5 shows the time series data for three probes installed at Y = 10, 20 and 35 m, where water contents increased 0.027, 0.042, and 0.035 $m^3 m^{-3}$ after the soil reached steady state. Water contents varied along the trench, increasing slightly in a northern direction. The CVs for all the probes are much lower than during Experiment 1, suggesting that the system was understood better with time.

During redistribution, the TDR system continued operating without problems until between Days 35 and 45 (January 7 - 17, 1998). After this time we detected changes in stability of the readings, and they could no longer be collected with confidence. Only those probes installed at Y = 0 and 2.5 m were operational. It is possible that coaxial connections, though sealed, began leaking after this time, explaining why the dry probes remained operational longer. Figure 3.4-5 does show almost an immediate reduction in water content after the irrigation system was turned off. Thus, even though the system is a bit "noisy," the signal of water content change was sufficient to detect water content changes of only about 0.02 $m^3 m^{-3}$.

3.4.2 Monitoring Islands

3.4.2.1 Experiment 1

We had better results using the TDR system from Campbell Scientific, Inc. over the Dynamax system installed in the trench, especially during the redistribution phase of the experiment (Figures 3.4-6 through 3.4-7). Initial difficulties with the TDR system, which caused a significant loss of data, stemmed from electrical feedback in a way almost identical to the Dynamax system. The 60 Hz AC signal was seen on the cable tester screen as a rolling sinusoidal wave, migrating toward the cable tester. Increasing the averaging to 128 improved system performance and filtered out most of the transients in the waveform. However, some variability existed (see for example, data collected before Day 40), much more than would have occurred if the system were operating solely on D/C power. For Experiment 2, the cable tester was modified so that the internal battery was used during data collection, and the AC was used to charge the internal battery during periods without data collection.

Even with data loss and AC feedback, data quality was sufficient to estimate wetting front arrival and velocities for most of the probes used in the monitoring islands (Table 3.4-3). Because wetting fronts sometimes arrived when the TDR system was off-line, it was not possible to determine exactly when the front arrived at each specific probe. For those probes that were off-line at the time of wetting front arrival, we assumed that the arrival time corresponded to the midpoint of the data gap, and the error limits were then taken as the time of data loss. The use of error limits clearly reduces the resolution of arrival times, and the ability to compare water flow behavior between the South and North islands. However, it is possible to make generalizations about possible differences between the two islands, especially when comparing water flow through deeper depths. For example, note the higher wetting front velocity

Table 3.4-2. Results of TDR measurements taken at the buried trench during Experiment 2.

Y-coordinate (m)	Mean θ before wetting front arrival ($m^3 m^{-3}$)	CV before wetting front arrival (%)	Mean θ after wetting front arrival ($m^3 m^{-3}$)	CV after wetting front arrival (%)	Change in θ ($m^3 m^{-3}$)
0	0.069	13.354	0.072	12.309	0.003
2.5	0.098	9.675	0.099	12.107	0.001
5	0.146	6.259	0.157	8.737	0.011
10	0.092	2.561	0.119	2.242	0.027
15	0.171	4.655	0.234	1.293	0.063
20	0.152	2.763	0.194	3.260	0.042
25	0.218	1.706	0.247	1.322	0.029
30	0.162	4.609	0.173	19.113	0.011
35	0.169	2.673	0.205	2.604	0.036
40	0.128	10.514	0.154	2.931	0.025
45	0.166	11.957	0.199	2.217	0.032
50	0.218	13.721	0.210	3.621	-0.008
55	0.262	2.521	0.279	3.370	0.017
Mean	0.158		0.180		0.022

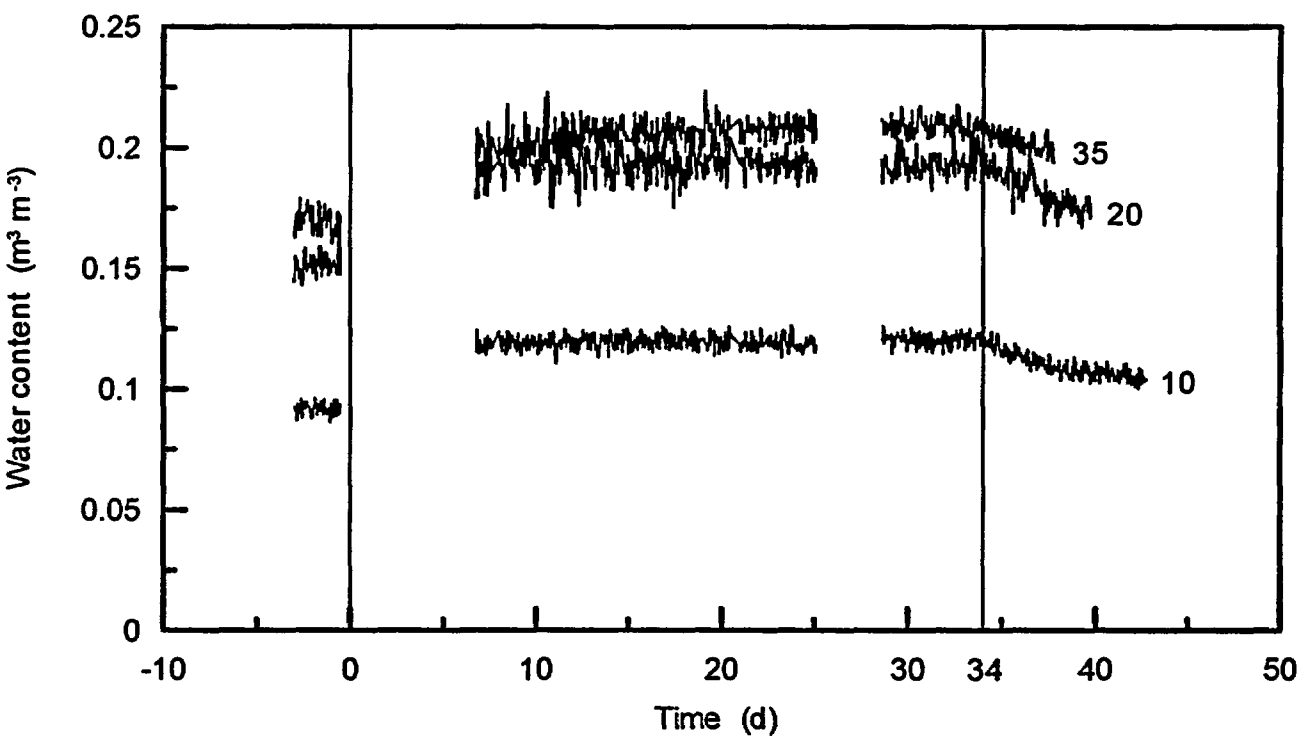

Figure 3.4-5. Water content obtained from Dynamax TDR system in buried trench during Experiment 2. Only three probes are plotted. Numbers on graph indicate y-coordinate.

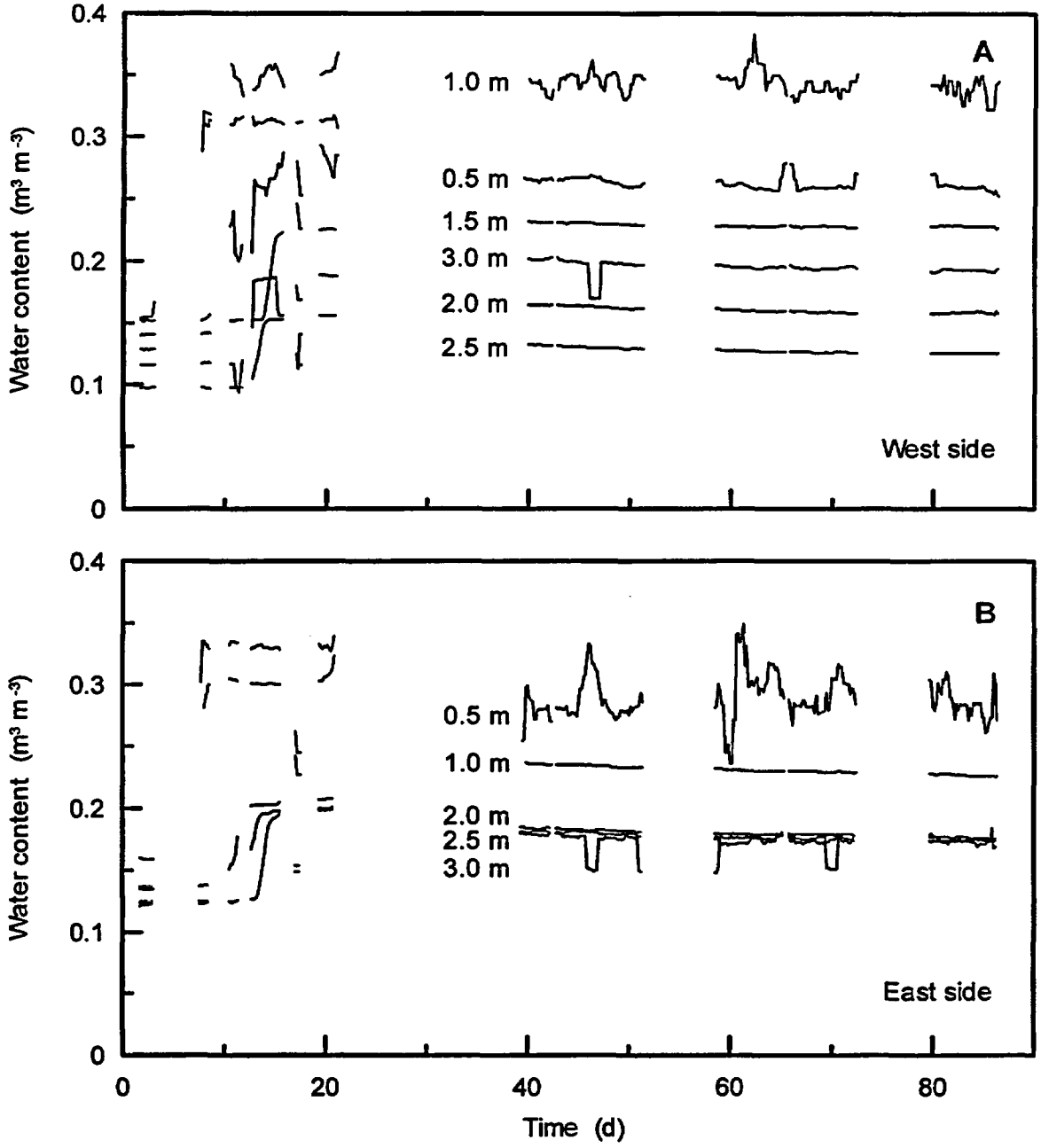

Figure 3.4-6. Response of CSI TDR system on the (A) West side and (B) East side of the South Island during Experiment 1.

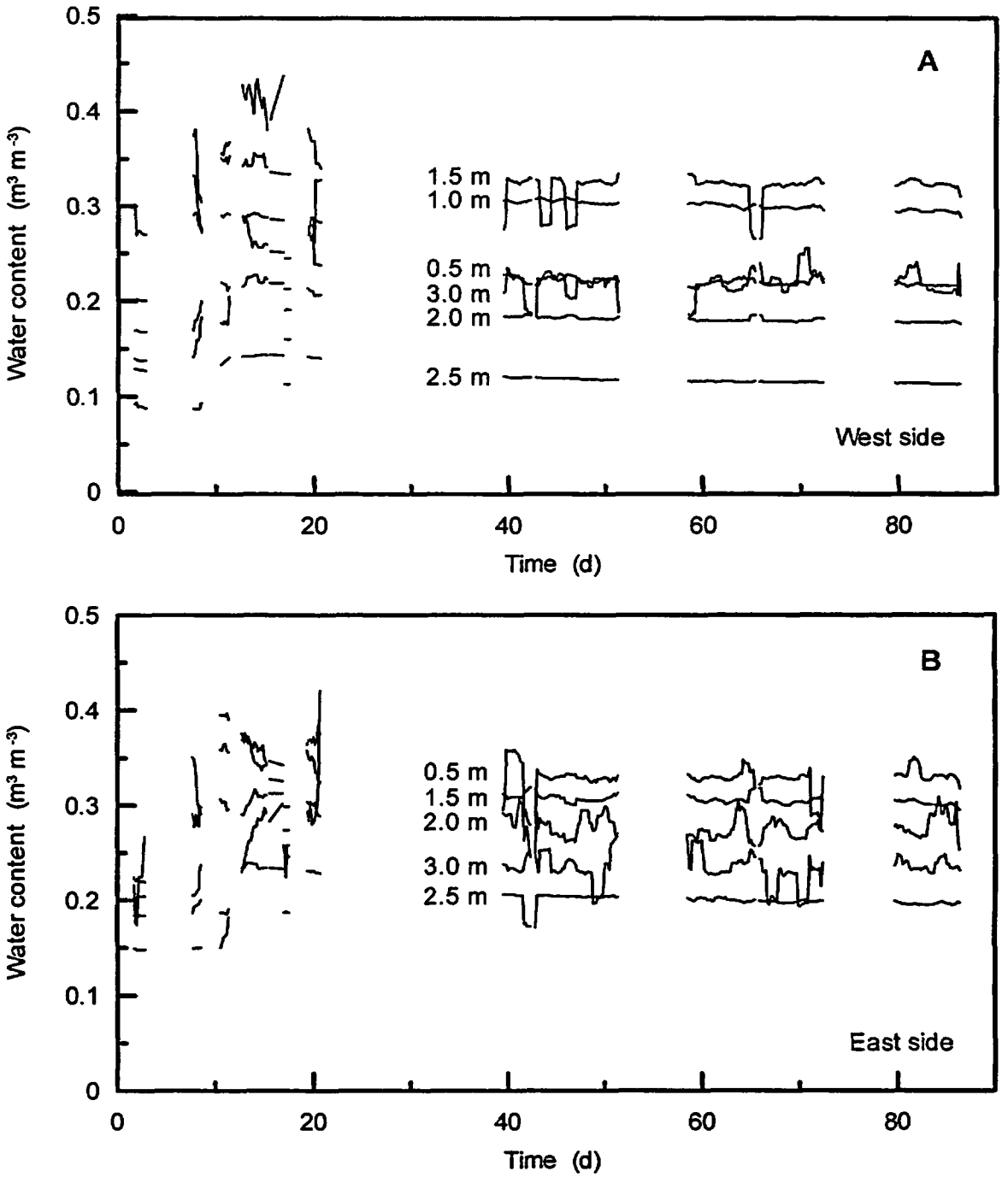

Figure 3.4-7. Response of CSI TDR system in the (A) West side and (B) East side of the North Island during Experiment 1.

Table 3.4-3. Wetting front arrival in monitoring islands using Campbell Scientific TDR system during Experiment 1.

South Island						
	West Side		East Side		Annular Space	
Depth (cm)	Time (days)	WF velocity (cm d^{-1})	Time (days)	WF velocity (cm d^{-1})	Time (days)	WF velocity (cm d^{-1})
50	5.3 ± 2.2	9.4 ± 6.4	5.3 ± 2.2	9.4 ± 6.4		
100	5.3 ± 2.2	18.8 ± 12.8	6.5†	15.4†	5.3 ± 2.2	18.8 ± 12.8
150	9.5 ± 1.0	15.8 ± 1.9	n/a	n/a		
200	11.9 ± .8	16.8 ± 1.1	11.3	17.7	11.9 ± .8	16.8 ± 1.1
250	13.3	18.8	13.2	18.9		
300	14.5	20.7	14.0	21.4	14.7	20.4
North Island						
	West Side		East Side		Annular Space	
Depth (cm)	Time (days)	WF velocity (cm d^{-1})	Time (days)	WF velocity (cm d^{-1})	Time (days)	WF velocity (cm d^{-1})
50	5.3 ± 2.2	9.4 ± 6.4	2.7	18.7		
100	5.3 ± 2.2	18.8 ± 12.8	5.3 ± 2.2	18.8 ± 12.8	5.3 ± 2.2	18.8 ± 12.8
150	n/a	n/a	5.3 ± 2.2	28.1 ± 19.2		
200	9.5 ± 1.0	21.1 ± 2.5	9.5 ± 1.0	21.1 ± 2.5	n/a	n/a
250	10.5	23.8	11.3	22.1		
300	11.9 ± .8	25.2 ± 1.7	12.8	23.4	12.7	23.6

† - Estimated

observed in deeper depths at the North island versus that measured in the South island. The wetting front arrived about two days sooner at the 200 cm deep probes, possibly as a result of the rubber skirt used in the North island.

We compared the arrival of water measured with the TDR probes to that measured using the neutron probe at access tube # 413, located between the two islands. The comparisons were somewhat qualitative, especially above 200 cm depth, because of the estimated arrival of water from the TDR probes. We found that wetting front velocities of 25, 25, and 27 cm d^{-1} were recorded using the neutron probe for depths of 200, 250, and 300 cm, respectively. They appear to be systematically higher than the TDR measured velocities listed in Table 3.4-3. Though the velocities indicate that wetting front arrival, as measured with the neutron probe, was only one or two days earlier than measured with the TDR system.

Figures 3.4-6 and 3.4-7 show a reduction of water content during redistribution. Unfortunately, a 17-day loss of data precludes accurate quantification of internal drainage from the end of active irrigation, though it is possible to account for the loss of between 0.02 - 0.04 $m^3 m^{-3}$.

3.4.2.2 Experiment 2

The data collected from the CSI TDR system appeared to be more stable than during Experiment 1 (Figure 3.4-8). Data gaps were fewer and the measurements themselves exhibited very little noise. Table 3.4-4 lists the statistics of water contents collected from the South Island, West Side, before arrival of the wetting front (this vertical transect is shown as an example). Note the extremely small Coefficients of Variation, less than 1% in all cases. The water content values themselves were consistent with the end of Experiment 1, indicating that 1) redistribution of water had essentially ceased during the hiatus between experiments, and 2) servicing of instruments and modification of datalogger programs, before Experiment 2, did not change the basic functioning of the TDR system. Figure 3.4-8A shows the time series of data collected before the start of irrigation and during wetting front arrival. Distinct changes in water content signal the arrival. Small perturbations in the data at 0.5 m depth from Day -5 to Day 0 indicate some diurnal effects in the water content readings, though they were less than 0.01 $m^3 m^{-3}$ in magnitude. The spike in water content recorded during the arrival indicated some stability problems, but the system became settled soon afterward.

Table 3.4-4 also lists the wetting front velocity calculated using two methods: direct observation using the TDR system, and from the average change in water content and measured flux rate. The velocities show a substantial increase from 0.5 to 1.5 m depth. Much of this increase can be attributed to smaller changes in water content than measured during Experiment 1. However, we noted that the observed velocities were consistently lower than calculated velocities, and that the measured change in water content was between 60% and 90% of that calculated from wetting front arrival. Also, the differences in velocities were positively correlated to the measured change in water content; thus, as the change in water content decreased, differences between measured and calculated velocities decreased. This indicates that small differences in the TDR calibration curve could exist between the soil material near the islands, versus material used specifically for probe calibration.

Figure 3.4-8B expands the time scale to show redistribution. For the most part and with the exception of values from 1.0 m depth, the readings were very stable, much more so than during Experiment 1. Substantial internal drainage near the surface was shown as the water content nearly approached pre-experimental values at all depths.

3.5 Tensiometer Data

Prior to the beginning of irrigation, tensiometer readings were taken manually with a Tensimeter (Soil Measurement Systems, Tucson, AZ) to confirm the accuracy of the pressure transducers used in both the trench and monitoring island tensiometers. Though the slope parameter of the calibration curve is stable with time, the offset can drift slightly over time. By using the Tensimeter, which can be zeroed manually, the tensiometer readings with pressure transducers can be adjusted to more accurately reflect soil tension. The Tensimeter revealed that the offsets needed to be adjusted on average by 3.49 cm (adjustments ranged from -10.63 to 18.67 cm). For the trench, the offset adjustment was 8.94 cm (ranged from -2.23 to 20.42) for Experiments 1 and 2. The offsets were adjusted by averages of 0.92 cm (range from -37.90 to 29.38 cm) and -2.90 cm (range from -43.45 to 23.61) in the monitoring

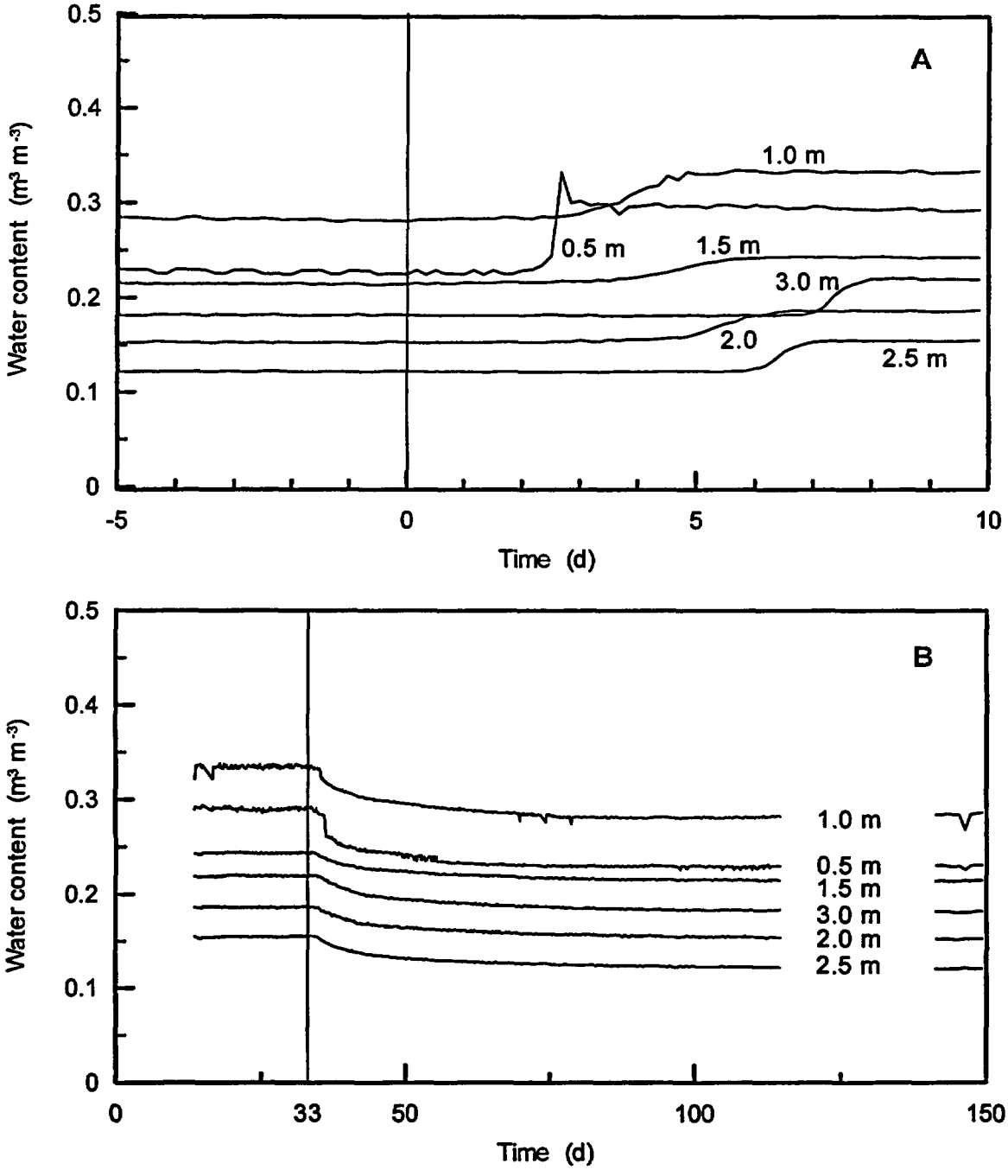

Figure 3.4-8. Water content obtained from CSI TDR system in South Island, West Side during Experiment 2 (A) irrigation and (B) redistribution.

Table 3.4-4. Results of TDR measurements using South Island, West Side during Experiment 2.

Depth (m)	0.5	1.0	1.5	2.0	2.5	3.0
Mean θ before front arrival ($m^3 m^3$)	0.228	0.283	0.215	0.153	0.122	0.182
Std. dev. before front arrival	0.002	0.001	0.000	0.000	0.000	0.001
CV	0.99%	0.44%	0.32%	0.30%	0.26%	0.28%
Mean Δθ	0.067	0.049	0.028	0.033	0.033	0.038
Front velocity recorded with TDR (cm d^{-1})	17.67	27.27	33.33	38.71	39.49	41.86
Front velocity using flux and Δθ (cm d^{-1})	29.34	33.75	40.84	44.33	46.78	47.49

islands for Experiments 1 and 2, respectively. Tensimeter readings were also taken routinely during the experiment to study the stability of the offset parameters in each of the pressure transducers. These modifications were then made to the output data set after downloading from the CR7 datalogger.

3.5.1 Buried Trench

3.5.1.1 Experiment 1

Tensiometers located in the trench were problematic due to several reasons. The main cause is believed to be due to exposure of the transducer wiring to moisture which would cause sudden interruptions of data collection and slow corrosion of the exposed wiring. This at times led to highly erroneous values of soil water tension. Figure 3.5-1 shows the arrival of the wetting front for the tensiometers located in the southern section (Y = 0 to 25 m) and the northern section (Y > 25 m) of the plot. Transducers located at Y = 5 m in the southern section of the trench and Y = 35 and 45 m in the northern section failed to provide reliable data due to corrosion of the wiring due to moisture. Of the six tensiometers located at a depth of 1.0 m, only two (e.g., Y = 15 and 25 m) provided reasonable tension values and responses from the pressure transducers affixed to the tensiometer. The transducer located at Y = 55 m provided an arrival response to the wetting front but soon thereafter failed due to electrical shorting of the wires.

The wetting front arrival times and velocities are shown in Table 3.5-1. They compared well with the values determined from the 1.0 m deep TDR probes and HDS located in the monitoring islands, which are discussed elsewhere in the report.

Electrical problems were also experienced with the tensiometers installed at 1.5 m depth. Of the 13 tensiometers, 11 were located under the irrigated area of the plot. Eight provided reliable data for estimating wetting front arrival times with two providing reliable tension values during redistribution (Figure 3.5-2: Y = 10 and 25 m). The remaining 6 transducers failed due to electrical shorting. One additional transducer (Y = 5 m) failed prior to irrigation due to moisture effects on wiring and/or blockage of the gage transducers. Two tensiometers (Y = 15 and 25 m) appeared to have problems with water flow through the porous cup. Two of the 13 trench tensiometers (Y = 0 and 2.5 m) were located outside of the irrigated area and did not appear to encounter any of the problems associated with most of the other tensiometers.

Arrival times and wetting front velocities were determined for 8 of the possible 11 tensiometers located in the irrigated area (Table 3.5-1). Wetting front velocities ranged from 12.0 cm d^{-1} at Y = 10 m to 32.1 cm d^{-1} at Y = 45 m, though no spatial pattern was evident. Similar velocities were determined by the neighboring TDR and HDS instruments (to be discussed below).

To check the reliability of the tensiometers and pressure transducers, direct tension values were periodically determined with a Tensimeter (Soil Measurement Systems, Tucson, AZ), a hand-held pressure transducer. The Tensimeter provided reasonable values of tension for all the 1.0 m deep tensiometers except at Y = 45 m (Table 3.5-2), which had a faulty seal. For the 1.5 m deep tensiometers, the Tensimeter provided reasonable values for all but two of the tensiometers (Y = 15 and 25 m). Table 3.5-2 shows realistic soil water tensions and expected redistribution patterns. On Day 9 the average soil water tension was relatively high along with the standard deviation because the wetting front had not arrived at all the tensiometer locations by this day.

3.5.1.2 Experiment 2

Figure 3.5-3 shows the arrival of the wetting front for both the southern (Y = 0 to 25 m) and northern (Y = 30 to 55 m) sections of the plot. Table 3.5-3 provides the wetting front velocities for the trench tensiometers, which compared favorably with the values determined from the HDS instruments. The average wetting front velocity was twice as high as observed during Experiment 1. This was primarily due to the initial conditions of the soil, which were much wetter than before Experiment 1. Irrigation during Experiment 1 caused an average decrease in the soil water tension of 132.9 cm of water, with range of 102 (Y = 10 m) to 187 cm of water (Y = 55 m, depth of 1.0 m).

Of the tensiometers installed at 1.0 m depth, only the instruments located at Y = 25 and 55 m provided usable data. Tensiometers located at Y = 5, 15, 35, and 45 m failed to provide any realistic data due to either leaks within the tensiometer (Y = 35 and 45 m) or to transducer malfunction

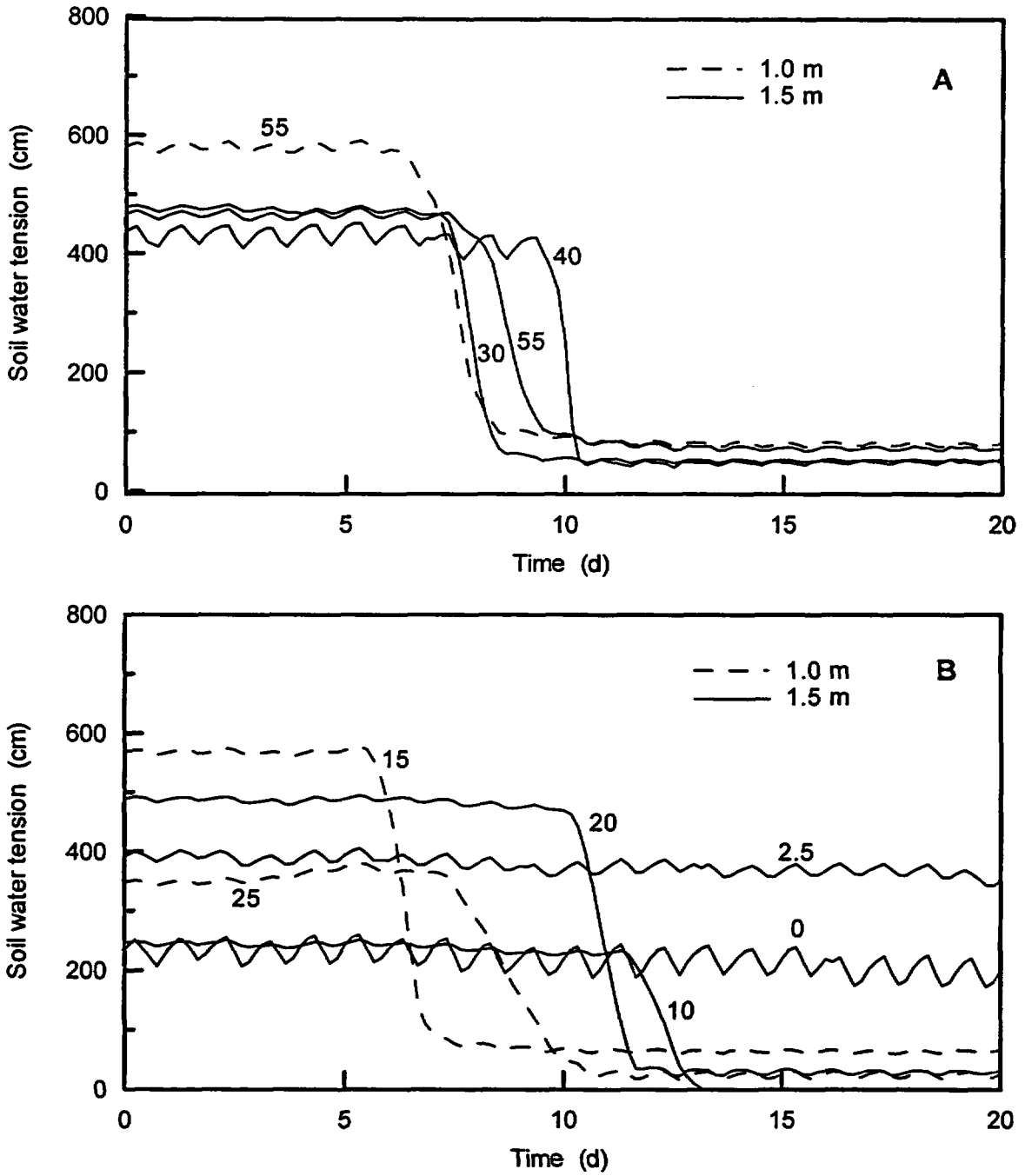

Figure 3.5-1. Response of tensiometers in the buried trench to water infiltration during Experiment 1. Figure shows the arrival of the wetting front for the (A) northern and (B) southern ends of the trench. Data for Y = 35, 45 and 50 m are not plotted because we have low confidence in the data values even though the wetting front arrival is clear.

Table 3.5-1. Wetting front arrival in buried trench using tensiometers during Experiment 1.

Y-coordinate (m)	Time (days)	WF velocity (cm d^{-1})
---------- Depth = 1.0 m ----------		
5	unavailable	n/a
15	6.50	15.38
25	8.66	11.55
35	unavailable	n/a
45	unavailable	n/a
55	7.66	13.05
---------- Depth = 1.5 m ----------		
0	no arrival	n/a
2.5	no arrival	n/a
5	unavailable	n/a
10	12.50	12.0
15	unavailable	n/a
20	11.33	13.2
25	unavailable	n/a
30	8.00	18.8
35	10.50	14.3
40	10.00	15.0
45	4.67	32.1
50	5.33	28.1
55	8.5	17.7

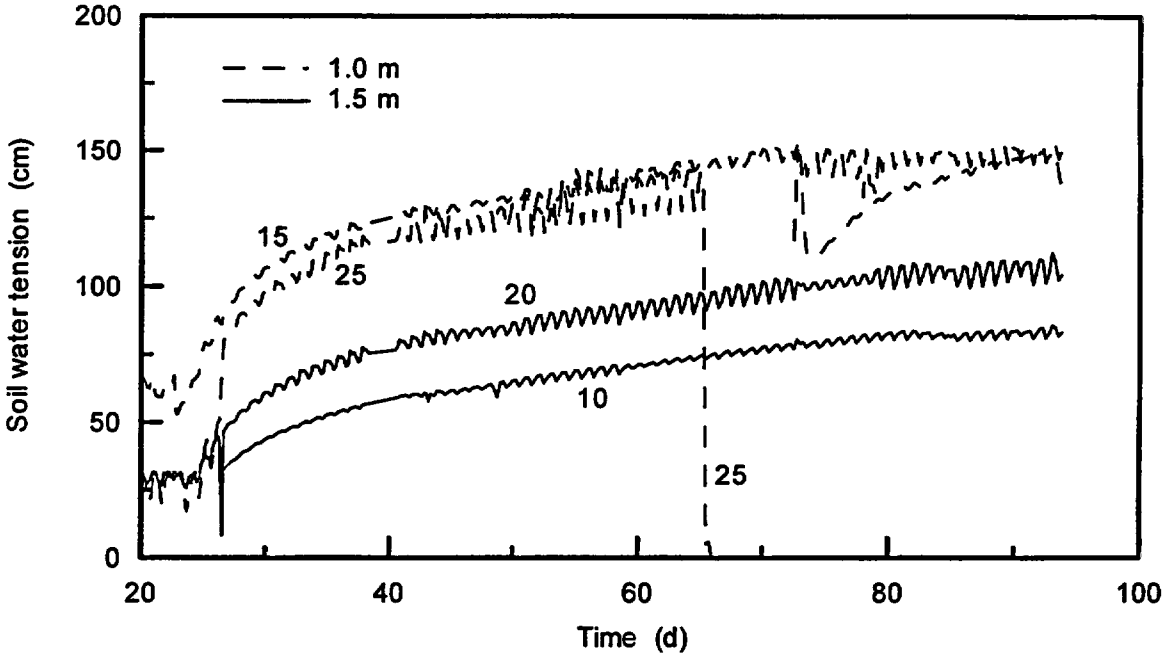

Figure 3.5-2. Response of tensiometers in the buried trench during Experiment 1 redistribution.

Table 3.5-2. Tensimeter data (cm of water) for buried trench during Experiment 1.

Depth (m)	Y-coordinate (m)	Experiment Day 9 ‡	26	44	65	79	93
1.0	5	550.2	51.3	107.1	126.9	142.0	137.9
	15	68.5	89.9	134.5	157.1	141.1	158.5
	25	109.1	63.5	115.7	134.6	149.1	140.6
	35	-33.2 †	-56.4 †	107.1	142.1	144.8	142.4
	45		problem with tensiometer				
	55	-87.0 †	78.7	126.4	145.5	121.1	155.60
	Mean	n/a	n/a	118.2	141.25	139.6	147.0
	Std. Dev.	n/a	n/a	10.8	10.2	9.7	8.4
1.5	0 *	231.9	242.2	257.3	275.7	274.6	281.2
	2.5 *	366.1	358.1	322.5	73.5	232.9	268.5
	5	158.8	-51.5 †	70.3	84.2	77.2	93.4
	10	249.2	10.4	77.9	94.5	104.5	107.4
	15		tensiometer not operational				
	20	491.2	46.1	87.6	107.3	117.1	119.6
	25		tensiometer not operational				
	30	33.8	50.1	80.5	100.9	83.8	92.0
	35	94.7	-65.7 †	92.7	109.3	-66.5 †	106.7
	40	402.7	51.1	85.6	98.2	73.1	NM
	45	24.6	47.1	75.9	93.7	97.7	102.6
	50	26.6	46.0	76.4	93.7	55.5	66.7
	55	78.5	54.2	NM	114.0	104.2	121.6
	Mean	n/a	43.6	80.9	99.5	89.1	101.3
	Std. Dev.	n/a	13.8	6.8	8.8	19.0	16.4

† Not used in calculation of average and standard deviation

‡ By Day 9 the wetting front had not arrived at all tensiometer locations and therefore an average and standard deviation was not determined. Note: Negative values denote a positive pressure. This of course is not possible and indicates that the amounts of water used to refill the tensiometer were not recorded or recorded improperly.

* located beneath linear but not in irrigated area

** excluding tensiometers located at Y = 0 and 2.5 m

NM = not measured

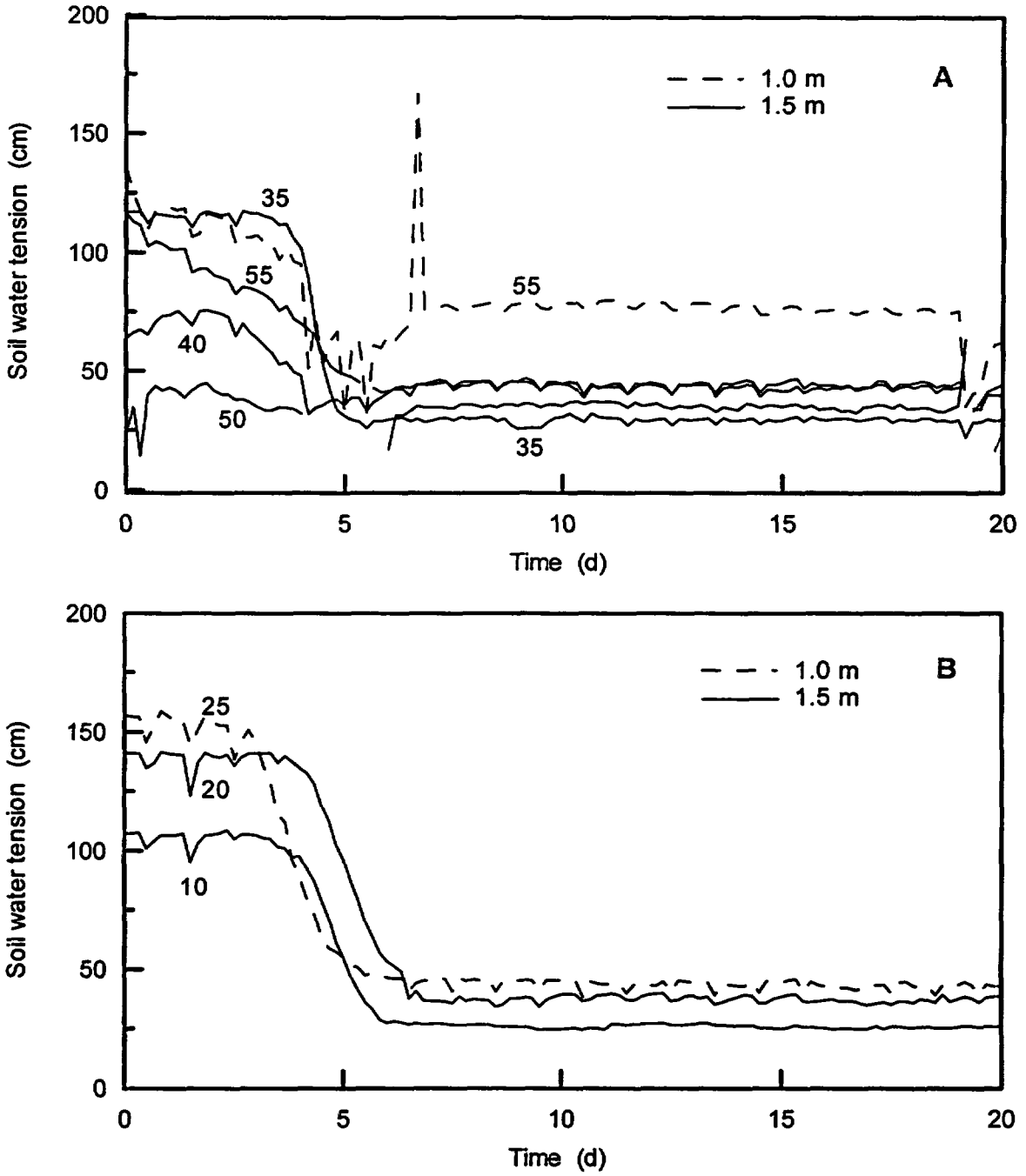

Figure 3.5-3. Response of tensiometers in the buried trench to water infiltration during Experiment 2. Figure shows the arrival of the wetting front for (A) the northern and (B) southern ends of the trench. Numbers indicate the y-coordinate.

Table 3.5-3. Wetting front arrival for the buried trench using tensiometers during Experiment 2.

Y-coordinate (m)	Time (days)	WF velocity (cm d^{-1})
---------- Depth = 1.0 m ----------		
5	unavailable	n/a
15	unavailable	n/a
25	3.8	26.1
35	unavailable	n/a
45	unavailable	n/a
55	4.0	25.0
---------- Depth = 1.5 m ----------		
0	unavailable	n/a
2.5	unavailable	n/a
5	unavailable	n/a
10	4.7	32.1
15	unavailable	n/a
20	4.7	32.1
25	unavailable	n/a
30	unavailable	n/a
35	4.2	36.0
40	4.0	37.5
45	unavailable	n/a
50	2.3	64.4
55	4.3	34.6

(Y = 5 and 15 m). Of the tensiometers installed at 1.5 m depth, 6 of the 13 were operational (Y = 10, 20, 35, 40, 50, and 55 m). Failure of the other tensiometers were due either to leaks in the tensiometer (Y = 25 m) or a combination of moisture effects of the transducer and wiring. Rainfall events prior to Days -2 to -1 and during Days 4 and 19 the appeared to temporarily affect the operation of certain transducers (Y = 55 for both 1.0 and 1.5 m, 40, 50 and 35 at 1.5 m depth). After the rainfall event, a period of 1 to 2 days were required until the transducers began to perform normally.

Figure 3.5-4 shows the redistribution of the soil water after irrigation (e.g., Day 33) for the northern and southern sections of the plot. Of the transducers which had operated properly for the first 25 days, only one (Y = 50 m) failed to provide any reliable redistribution data. As was the case for the first 25 days of Experiment 2, transducers (Y = 55 for both 1.0 and 1.5 m, 40, and 35 at 1.5 m depth) were affected by periodic rainfall events on Days 63, 67, 74, 76, 83, 101, 113, 115, 116, and 119. Each rainfall event was immediately followed by 1 to 2 days after which the transducers returned to normal operation. This is believed to be due to the transducers and wiring becoming extremely damp followed by a "drying out" period. Three tensiometers (Y = 10, 20 at 1.5 m, and 25 at 1.0 m depth) provided similar tension responses after irrigation had ended for Experiment 1 and Experiment 2 indicating a redistribution pattern that was consistent between experiments.

The Tensimeter data obtained during Experiment 2 are presented in Table 3.5-4. These data showed slowly increasing tensions with time, indicative of a slowly draining profile. For example, the mean transect tension at 1.5 m increased from about 37 cm during irrigation to about 105 cm five months after irrigation was terminated.

As indicated above, the tension data were corrected using the Tensimeter readings and adjusting the calibration offset. Figure 3.5-5 shows an example of how this correction changed the value of the tensiometer reading. The uncorrected and corrected tension readings are identical except for the offset, which was adjusted downward by 10.6 cm after comparing the readings to those collected with the Tensimeter. Using the uncorrected data for determining the wetting front arrival would have been appropriate in this case because only changes in tension were used in the calculations (offset is subtracted out). However, if the true "value" was needed, then the corrected tension would be needed. The figure shows the level of error that could be present in uncorrected tension.

3.5.2 Monitoring Islands

3.5.2.1 Experiment 1

Figure 3.5-6 shows the response of tensiometers to water infiltration using both the West and East sides of the South Island. All data were corrected for the hanging water column, calculated to be 16.9 cm. Arrival times and wetting front velocity were very similar at both sides of the monitoring island. The largest differences occurred at 100 cm depth, where the tensiometer on the East side detected water arrival 1.3 days before the West side (Table 3.5.5). As described above using the neutron probe data, differences in wetting front movement tended to average out with depth. As water moved through progressively deeper soil, differences in wetting front velocity became smaller. Toward the bottom of the vertical transects, water arrived at the different locations within one or two measurement events, each event being 4 hours.

Flow response at the North Island (Figure 3.5-7) indicated that the rubber skirt affected water flow, at least toward the top of the soil profile. Note the response on the East Side of the monitoring island, where the wetting front arrived at the 100 cm depth prior to the 50 cm depth. The wetting front velocity observed here was 37.45 cm d^{-1}, faster than other tensiometers at that or any other depths in the islands. This rapid response could have been caused by funneled water movement around the rubber skirt, though the possibility of preferential flow toward the tensiometer can not be ruled out. A plot of wetting front velocity with depth shows that the North Island experienced faster flow throughout the entire profile (Figure 3.5-8).

This trend of faster flow with depth, however, was not observed from the neutron probe data collected from the access tube located adjacent to the islands (tube #413). Wetting front velocities from access tube #413 were determined to be 25, 21, 25, 25, and 26 cm d^{-1} for depths of 1, 1.5, 2, 2.5, and 3 m, respectively. No trend was apparent from these data, although these velocities were higher than the average velocities calculated for the entire plot. Other

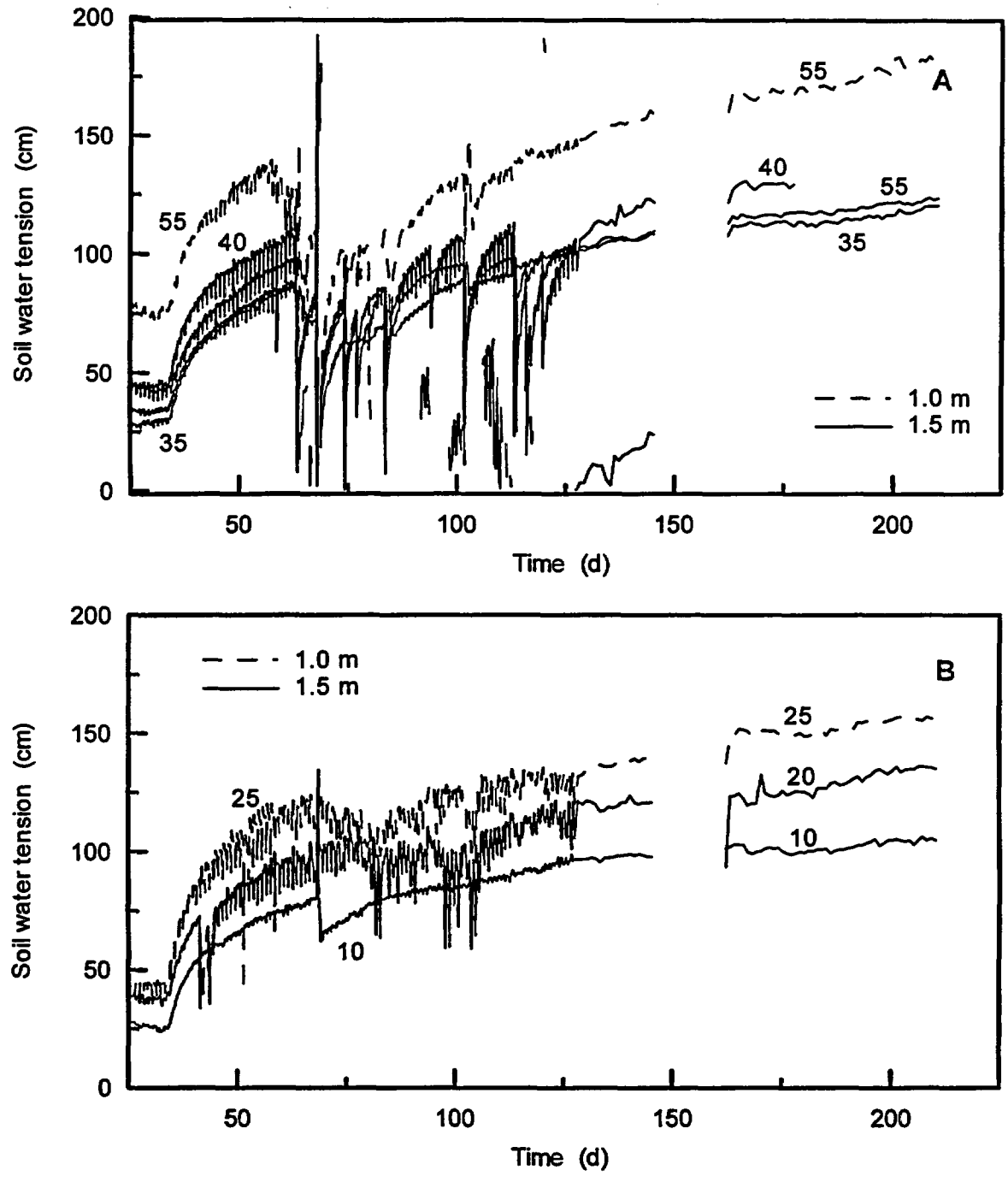

Figure 3.5-4. Response of tensiometers in the buried trench during Experiment 2 redistribution for the (A) northern and (B) southern ends of the trench. Numbers indicate the y-coordinate.

Table 3.5-4 Tensimeter data (cm of water) for buried trench during Experiment 2.

Y-coordinate (m)	Experiment Day 1 ‡	14	35	51	65	105	169
	Depth = 1.0 m						
5	85.2	52.1	67.9	104.1	100.2	105.8	133.9
15	86.1	70.8	43.6	137.3	92.4	116.5	162.4
25	164.8	51.4	57.3	121.1	126.1	166.3	140.1
35			tensiometer not operational				
45			tensiometer not operational				
55	117.1	63.1	67.9	117.5	86.1	111.3	141.70
Mean	113.3	59.4	59.2	120.0	101.2	125.0	144.5
SD	37.3	9.0	10.0	13.6	14.4	26.4	12.2
	Depth = 1.5 m						
0 *	173.2	136.5	136.1	140.3	70.3	54.4	144.6
2.5 *	48.3	66.5	66.4	82.8	50.2	74.2	102.2
5	59.6	27.4	39.5	70.0	65.4	-62.4 †	92.2
10	114.5	18.0	43.3	74.8	84.8	98.0	112.3
15	-3.2 †	39.4	54.5	NM	-96.1 †	NM	NM
20	138.2	43.7	44.7	88.7	95.0	114.9	129.9
25			tensiometer not operational				
30	46.5	32.9	34.0	87.4	50.2	78.7	112.8
35	123.3	39.8	31.4	83.5	67.0	97.3	111.7
40	67.4	38.2	44.2	86.6	61.4	85.0	94.2
45	47.5	33.9	36.1	90.0	49.7	67.4	78.3
50	38.8	35.1	32.4	71.8	40.6	69.7	-58.5 †
55	103.6	46.3	43.6	90.9	72.6	84.6	106.6
Mean	n/a	34.5	40.4	82.6	65.2	87.0	104.8
SD	n/a	7.8	6.8	7.7	16.4	14.9	14.9

† Not used in calculation of average and standard deviation. Note: Negative values denote a positive pressure. This is not possible and indicates that the amounts of water used to refill the tensiometer were not recorded or recorded improperly.
‡ By Day 1 the wetting front had not arrived at all tensiometer locations and therefore an average and standard deviation was not determined.
* located beneath linear but not in irrigated area
** excluding tensiometers located at Y = 0 and 2.5 m
NM = not measured

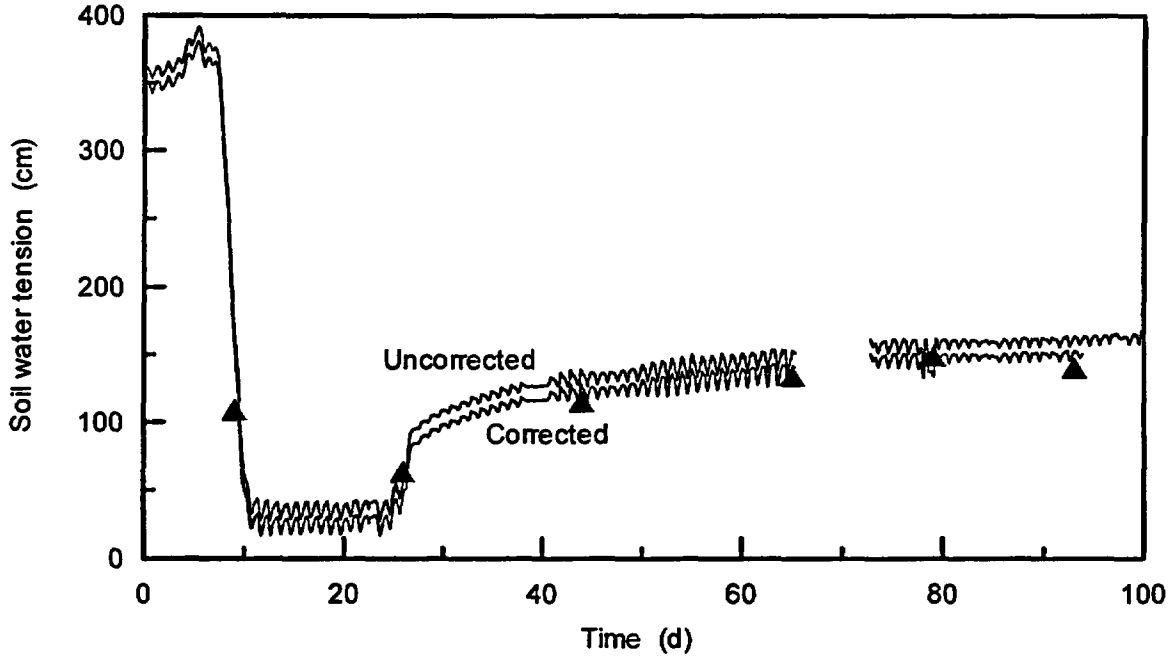

Figure 3.5-5. Example of corrected and uncorrected tension readings using a tensiometer located at 1 m depth, Y = 25 m. Solid lines are from the pressure transducer, and triangles are from the Tensimeter.

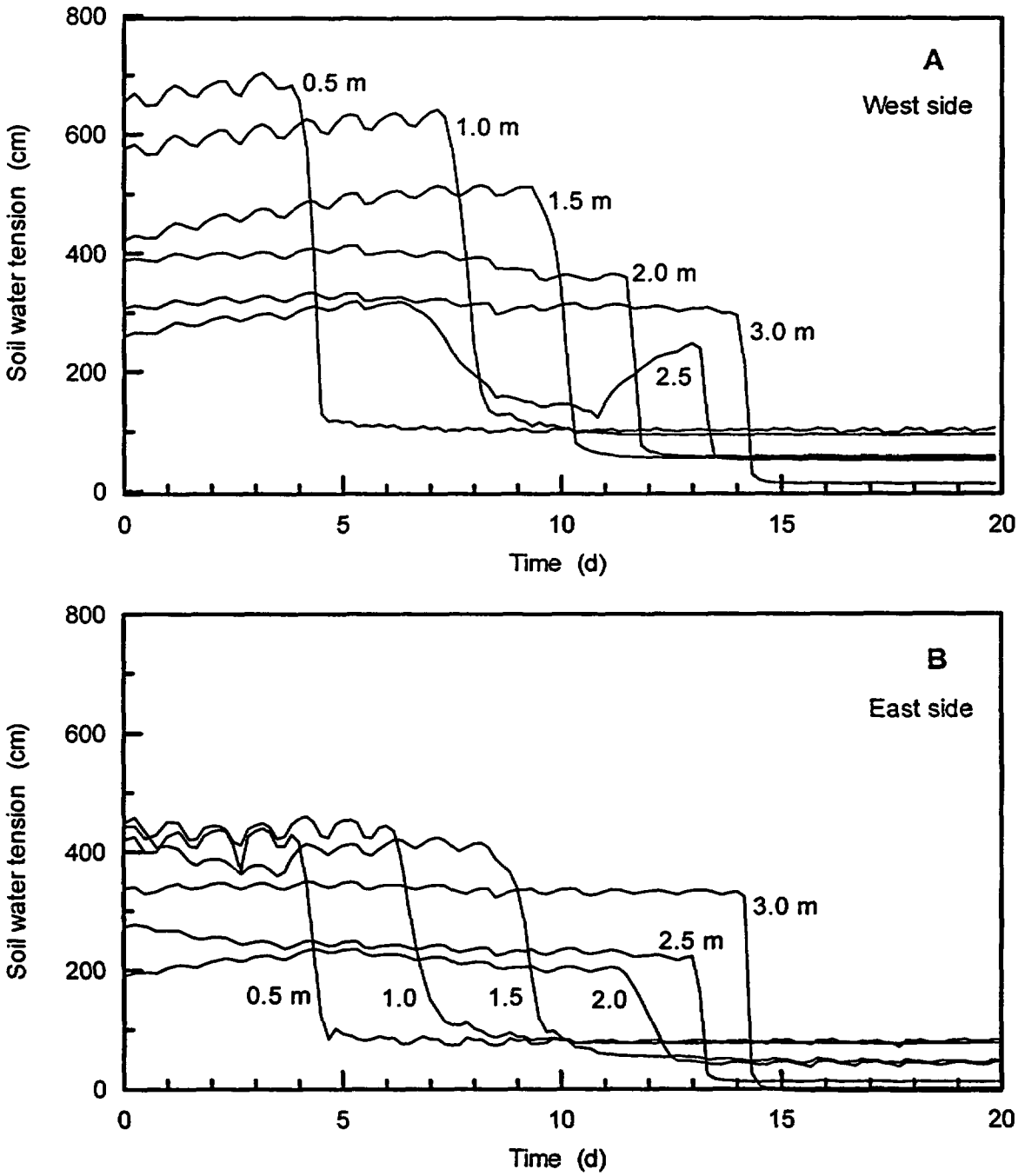

Figure 3.5-6. Response of tensiometers to water infiltration using both the (A) West and (B) East sides of the South Island during Experiment 1.

Table 3.5-5. Wetting front arrival and velocities using tensiometers installed in monitoring islands during Experiment 1.

Depth (cm)	Time (days)	WF velocity (cm d^{-1})	Time (days)	WF velocity (cm d^{-1})	Time (days)	WF velocity (cm d^{-1})	Time (days)	WF velocity (cm d^{-1})	Mean vel. (cm d^{-1})
	S. Island - West		S. Island - East		N. Island - West		N. Island - East		
50	4.33	11.6	4.33	11.6	4.17	12.0	3.83	13.1	12.1
100	8.00	12.5	6.67	15.0	5.50	18.2	2.67	37.5	20.8
150	10.00	15.0	9.33	16.1	6.50	23.1	8.17	18.4	18.2
200	11.67	17.1	12.00	16.7	8.50	23.5	9.33	21.4	19.7
250	13.33	18.8	13.17	19.0	9.83	25.4	11.33	22.1	21.3
300	14.17	21.2	14.33	20.9	11.00	27.3	12.67	23.7	23.3

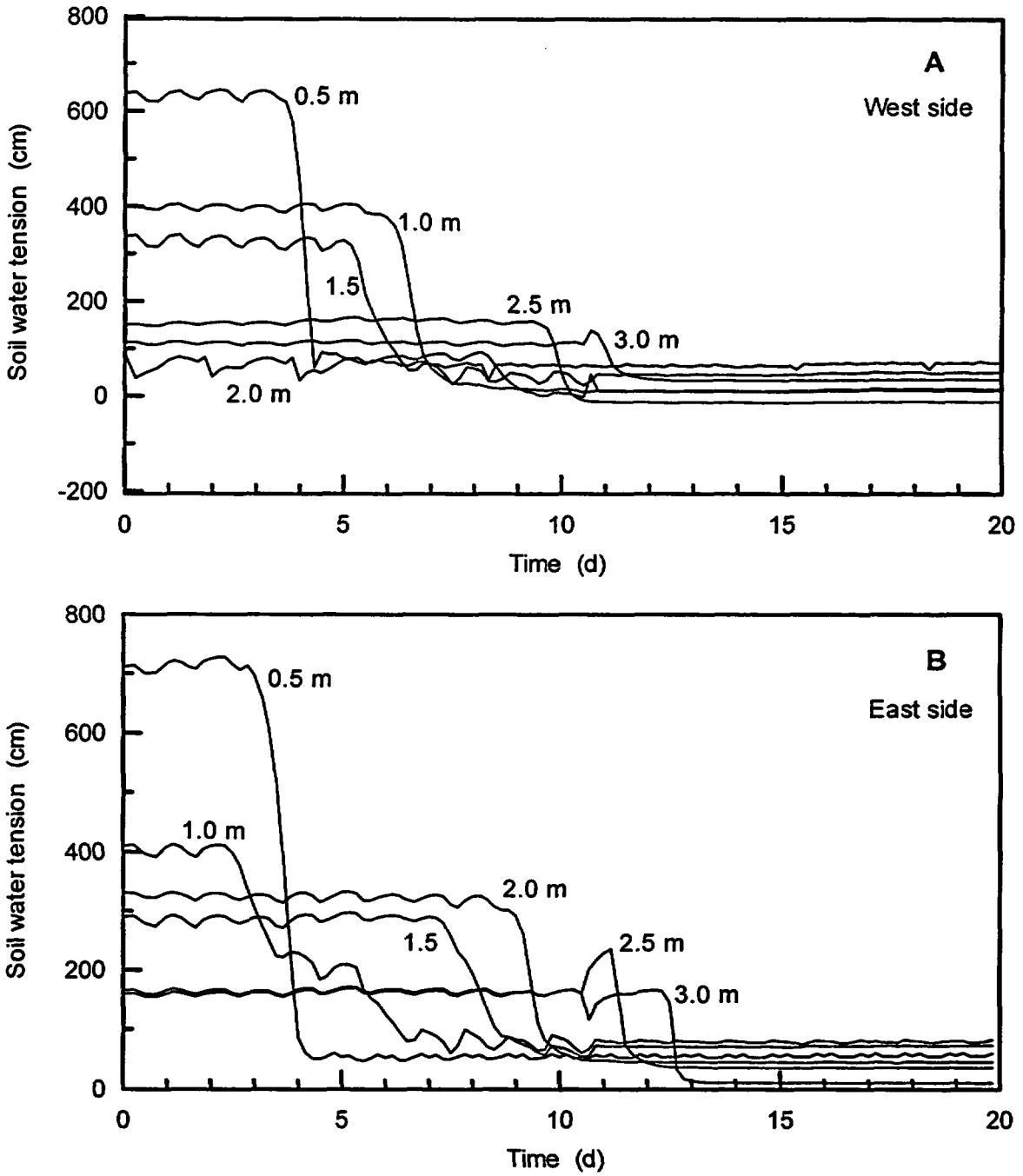

Figure 3.5-7. Response of tensiometers to water infiltration using both the (A) West and (B) East sides of the North Island during Experiment 1.

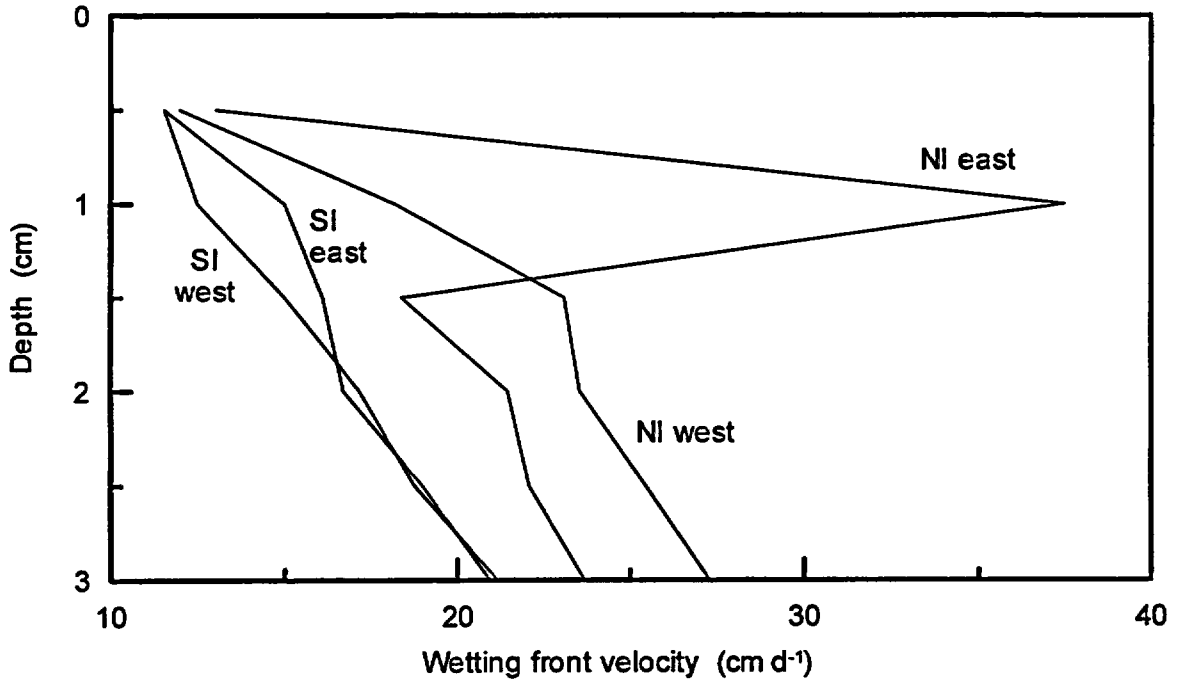

Figure 3.5-8. Wetting front velocities for the South and North Islands, measured using tensiometers during Experiment 1.

access tubes nearby show velocities similar to that of access tube #413. At the base of the monitoring islands, where velocities determined from the tensiometers reached their maximum, we found that tensiometer-calculated velocities ranged from 5 cm d^{-1} slower to 1.3 cm d^{-1} faster than those calculated from the neutron probe. Variability of hydraulic properties from the South Island to the North Island, with the neutron probe located in between, could explain these differences.

During redistribution, shallower tensiometers indicated a significantly higher level of soil draining than did the deeper tensiometers (Figures 3.5-9 and 3.5-10). During the redistribution process, especially with the soil surface covered to prevent evaporation, soil water from shallow depths drains downward (soil water throughout the profile drains downward due to gravitational forces). This soil water supplies fluid to the deeper soils, thereby giving the appearance that deeper soils are not draining. As the shallow soils lose water, intermediate soils will begin to show signs of losing water, and then ultimately, so will the deeper soils. The changes in water tension in Figures 3.5-9 and 3.5-10 illustrate this process. In the South Island, East side, tension changes recorded at depths of 50, 100, and 150 cm were 86, 74 and 58 cm of water after 20 days of redistribution (e.g., after Day 43), respectively.

3.5.2.2 Experiment 2

Only the tensiometers installed in the South Island, West Side will be discussed in this section. This will provide information on performance of the instrument with minimal repetition from above. Figure 3.5-11 shows a 15-day time series of readings taken before irrigation began and then during water breakthrough. The tensiometers were not affected significantly by diurnal temperature cycles, as seen both by the figure and the statistical results on Table 3.5-6. Coefficients of variation in the readings were very low for all six tensiometers. Tension values were consistent with the end of redistribution from Experiment 1, indicating that the instruments continued to function properly.

Water arrival was distinct throughout the profile and very consistent with those found using the TDR system (see Section 3.4.2.2). Small differences in front velocity could easily be attributed to soil variability or range of influence of the different instruments. The velocities were found to be approximately twice those calculated for Experiment 1, indicating that the soil water deficit before Experiment 2 was approximately one-half of the deficit before Experiment 1.

Redistribution (Figure 3.5-12) was almost identical in shape and relative magnitude to that recorded during Experiment 1 (see Figure 3.5-9). With the exception of the tensiometer at 100 cm depth, which obviously experienced a problem with leaking, all the tensiometers provided stable and reliable tensions. Small dips in the tensions, especially at Day 58, most likely occurred when manual readings were taken with the Tensimeter. The data from Figure 3.5-12, when compared to results from Experiment 1, show excellent repeatability and illustrate that the tensiometers can provide stable readings in the field, given appropriate maintenance requirements and installation.

3.5.3 Deep Tensiometers

3.5.3.1 Experiment 1

Overall, the deep tensiometers provided excellent data, both from the standpoint of response to wetting front arrival (Figures 3.5-13A through C) and measurement stability. Note the relatively small diurnal fluctuations on these unsmoothed data, reflecting the lack of temperature changes at depth. Also, the lack of a hanging water column at the tensiometer cup means that data correction for column length was not necessary. Figure 3.5-13A, plotted using tensiometer data from the 3 m depth, showed that spatial variability of water arrival did exist on the plot. Velocities varied from 19.6 to 27.7 cm d^{-1}, with an average velocity of 23.3 cm d^{-1} (Table 3.5-7), almost identical to the average velocity observed from the neutron probe (e.g., 23.4 cm d^{-1}). Given the difference in ranges of influence between the tensiometer and neutron probe, the differences in observed wetting front velocity are negligible.

The tensiometer labeled CE in Figure 3.5-13A detected wetting front arrival earlier than any other unit; however, the slow decrease in tension, markedly different from other tensiometer responses, indicated that either the tensiometer seal was slowly degrading, or that water preferentially moved through the backfill material in the annular space. The CE tensiometer then detected a second distinct reduction in tension during Day 15, indicating either a

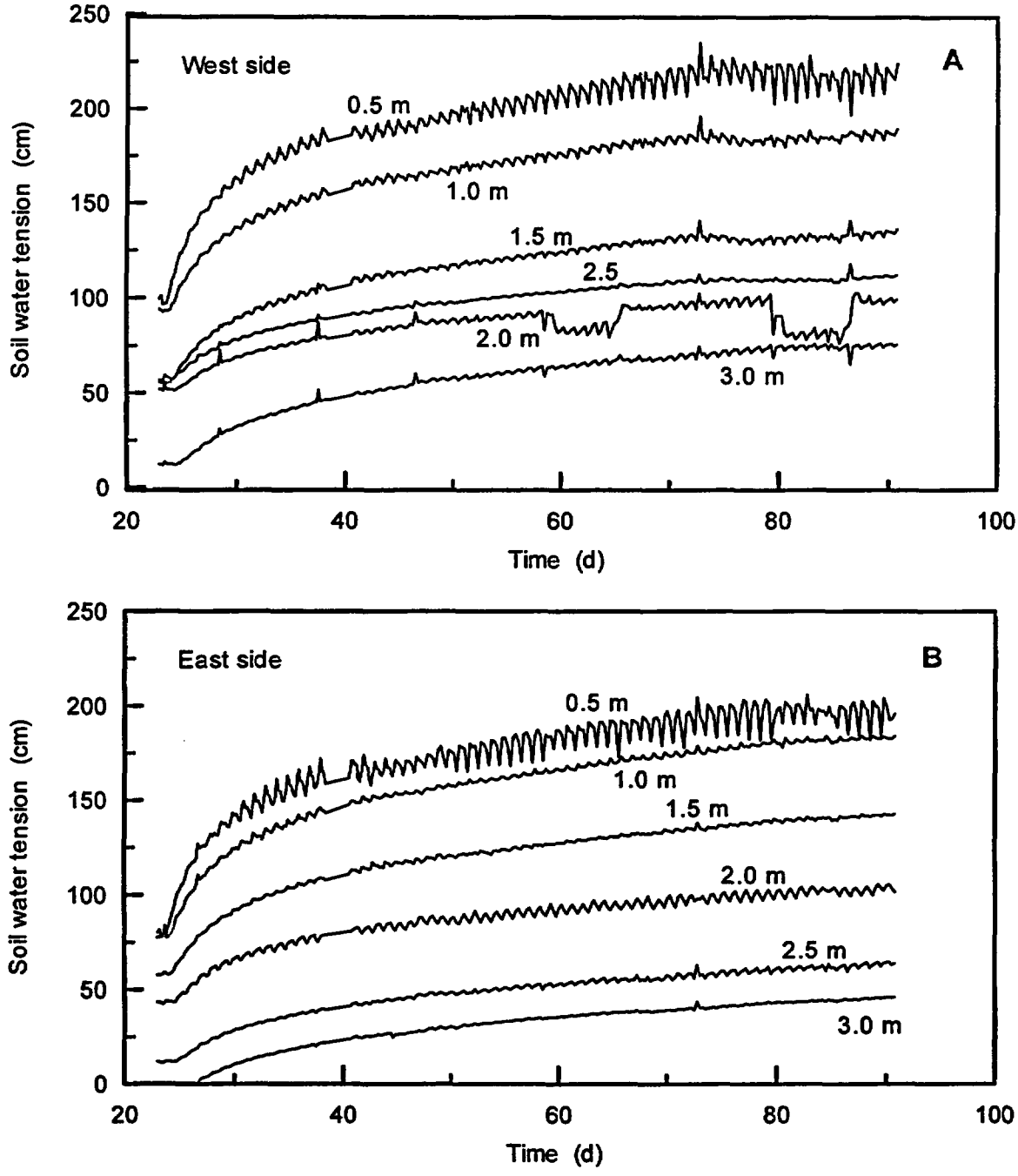

Figure 3.5-9. Response of tensiometers to redistribution at the (A) West side and (B) East side of the South Island during Experiment 1.

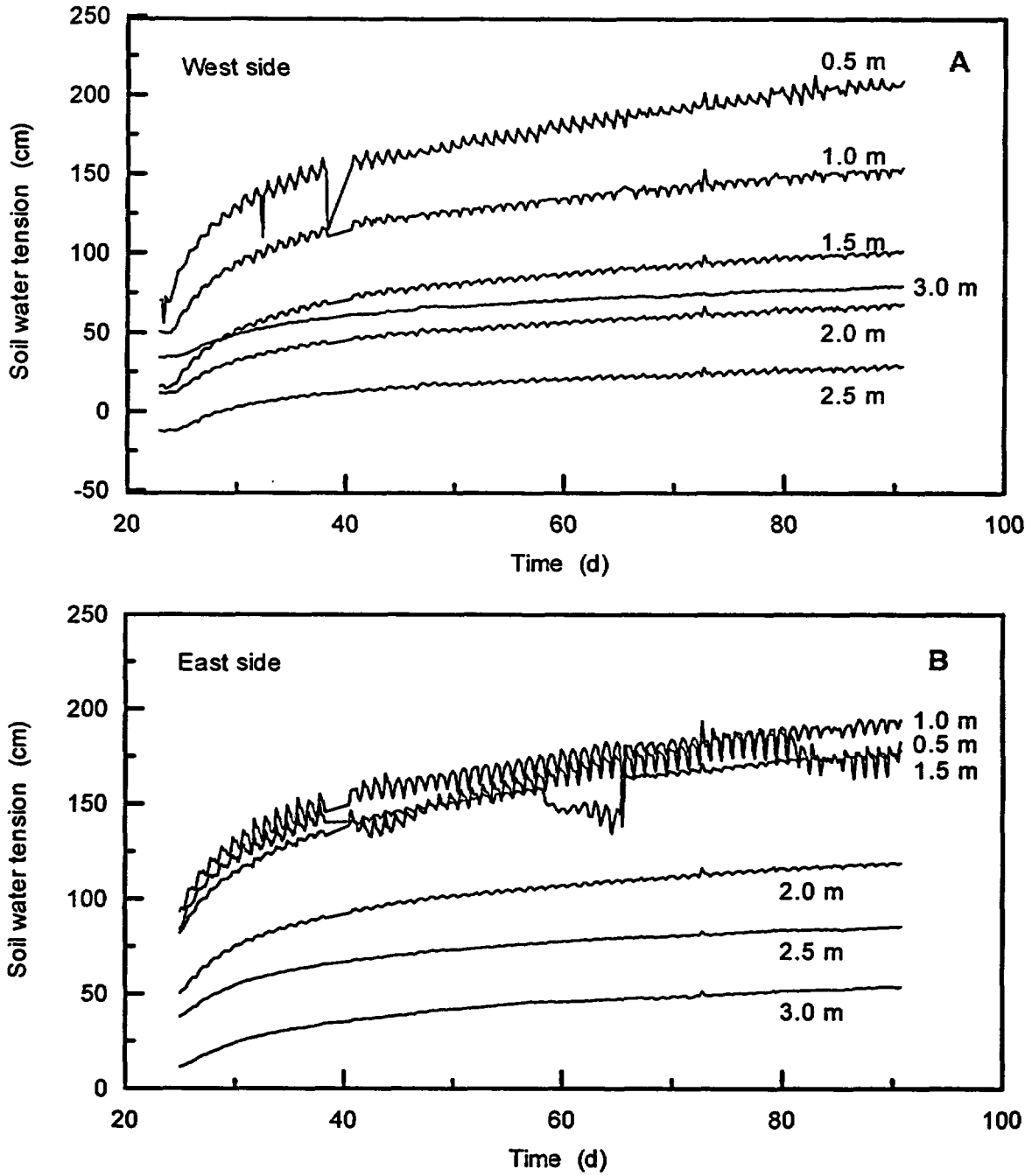

Figure 3.5-10. Response of tensiometers to redistribution at the (A) West side and (B) East side of the North Island during Experiment 1.

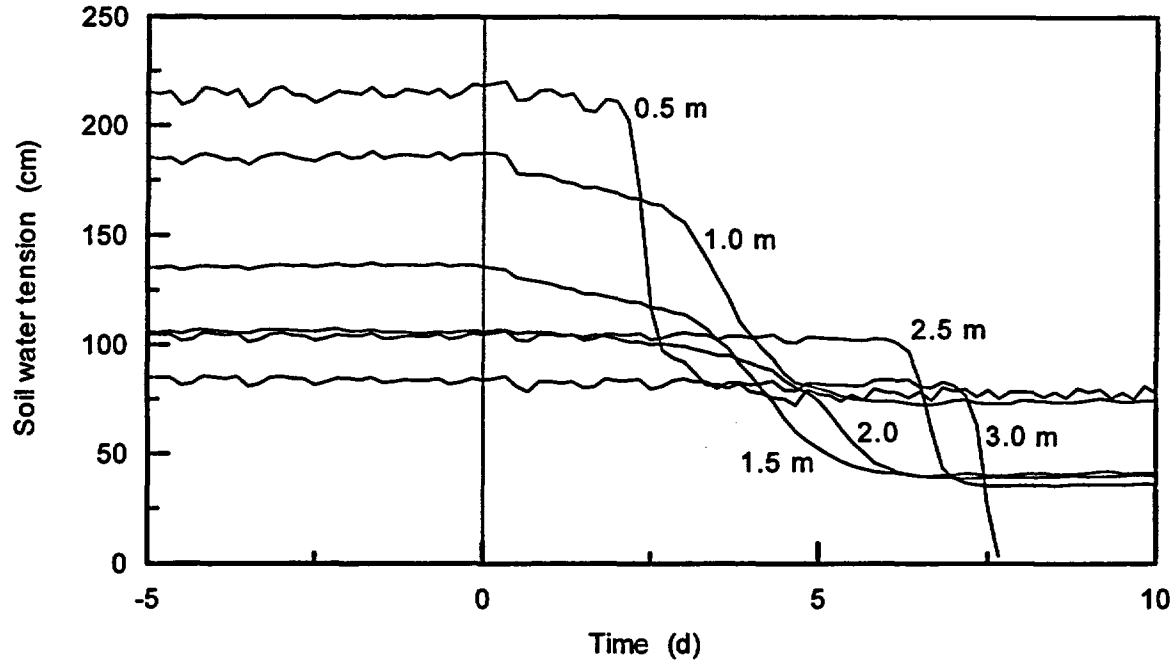

Figure 3.5-11. Tensiometer data from South Island, West Side collected during irrigation phase of Experiment 2.

Table 3.5-6. Results of tensiometer measurements for the South Island, West Side during Experiment 2.

Depth (m)	0.5	1.0	1.5	2.0	2.5	3.0
Mean tension before front arrival (cm)	207.00	161.53	119.05	88.12	81.92	110.29
Std. dev. before front arrival	2.61	1.53	0.95	0.65	1.14	1.33
CV (%)	1.26	0.95	0.80	0.74	1.39	1.20
Change in tension (cm) †	137.04	106.95	95.40	62.79	62.68	60.11
Front velocity (cm d^{-1})	21.43	27.27	34.64	38.71	37.50	40.91

† - Calculated using steady-state readings before and after arrival of wetting front.

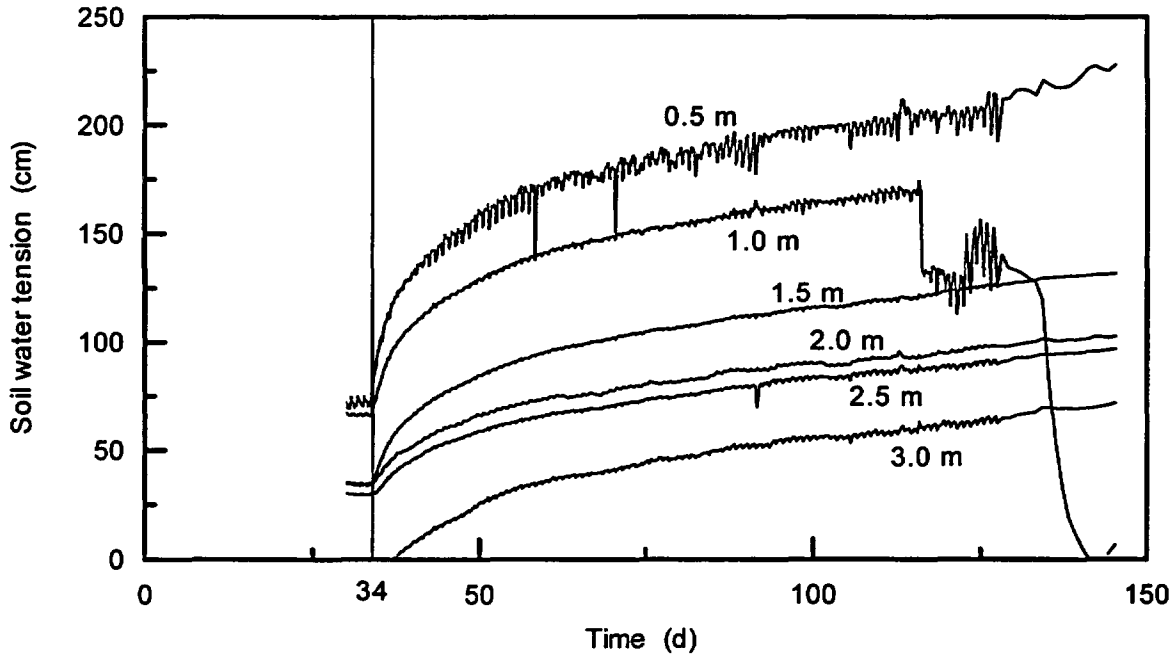

Figure 3.5-12. Response of tensiometers at South Island, West side during redistribution phase of Experiment 2.

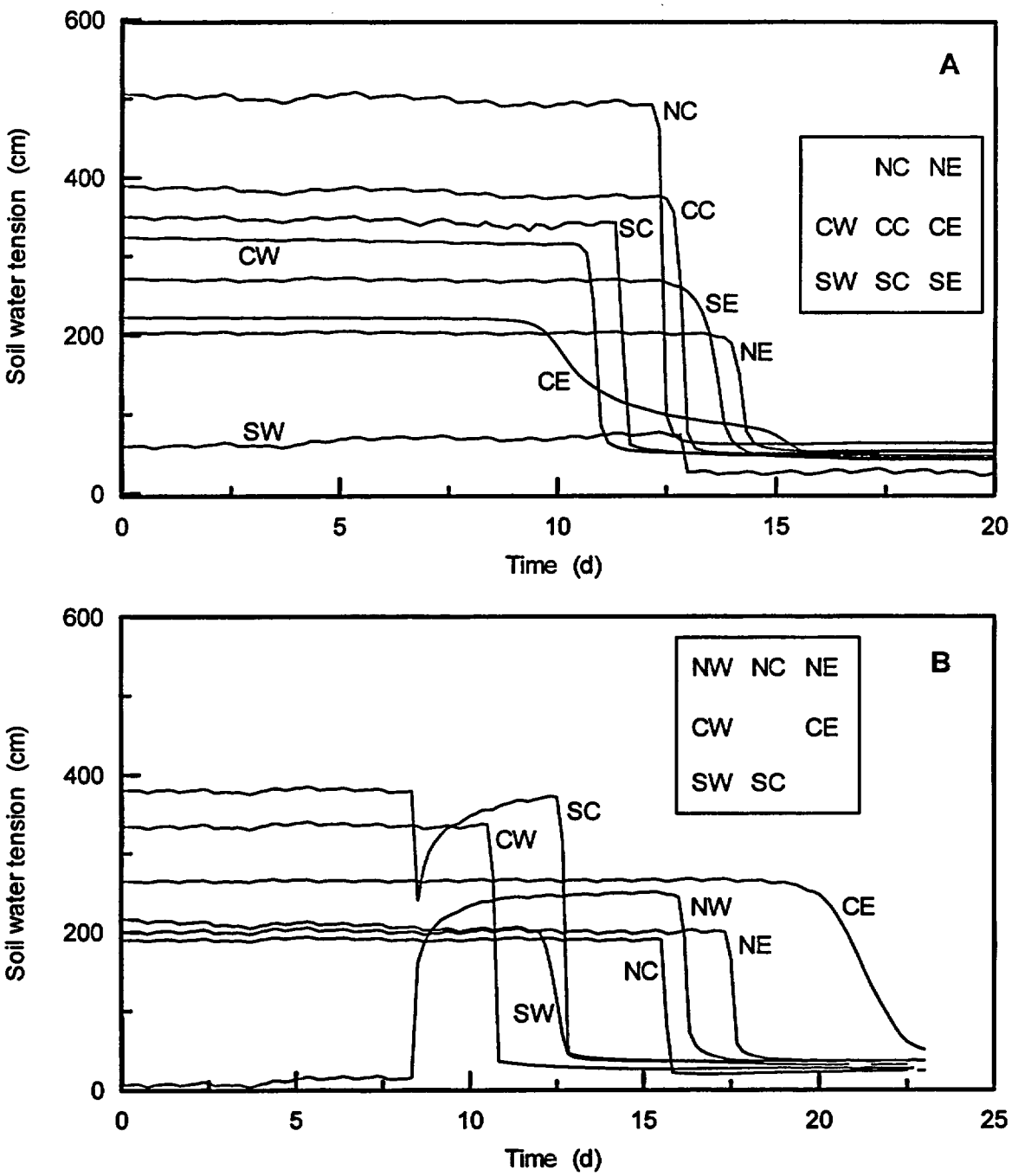

Figure 3.5-13. Response of deep tensiometers completed at (A) 3, (B) 5 and (C) 10 m depth during water infiltration for Experiment 1. Letters on graph indicate location. Note different scales on X and Y axes.

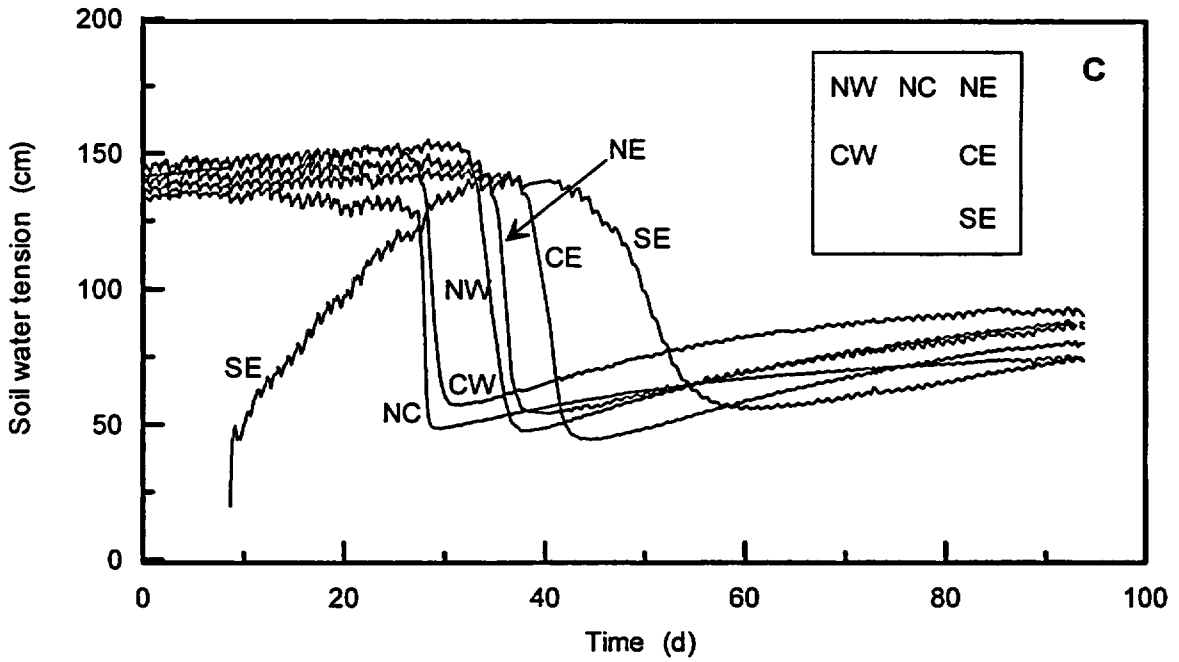

Figure 3.5-13. Response of deep tensiometers completed at (A) 3, (B) 5 and (C) 10 m depth during water infiltration for Experiment 1. Letters on graph indicate location. Note different scales on X and Y axes. (Continued)

Table 3.5-7. Wetting front arrival using deep tensiometers during Experiment 1.

Position	Time (days)	WF velocity (cm d^{-1})	Time (days)	WF velocity (cm d^{-1})	Time (days)	WF velocity (cm d^{-1})
	3 m depth		5 m depth		10 m depth	
SW	13.00	23.1	12.50†	40.0†	n/a	n/a
SC	11.50	26.1	12.67	39.5	n/a	n/a
SE	13.67	22.0	n/a	n/a	49.75	20.1
CW	10.85	27.7	10.67	46.9	28.50	35.1
CC	13.00	23.1	n/a	n/a	n/a	n/a
CE	15.33	19.6	21.83	22.9	40.50	24.7
NW	n/a	n/a	16.17	30.9	34.17	29.3
NC	12.50	24.0	15.67	31.9	28.00	35.7
NE	14.17	21.2	17.50	28.6	36.17	27.7
Mean	13.00	23.3	15.29	34.4	36.18	28.8
CV	10.31%	10.45%	22.74%	21.90%	20.58%	19.13%

† - Results are suspect because of potentially faulty tensiometer seal.

complete failure of the seal, or the true wetting front arrival. Because the tension readings after Day 15 closely approximated those of the other tensiometers, the latter explanation appears more plausible. Another interesting aspect of Figure 3.5-13A is that the three slowest wetting fronts were detected by tensiometers on the eastern side of the plot. Tensiometers toward the western side of the plot indicated faster water movement, and tensiometers installed in the center of the plot were in between. The tensiometer labeled SW was probably not functioning properly, as can be seen by the very low initial tension.

Figure 3.5-13B shows the response for the 5 m deep tensiometers. Similar to the results from the 3 m deep units, the slowest wetting front movement was recorded toward the eastern side of the plot, and the fastest movement was recorded toward the west. We determined the local velocity between 3 and 5 m depth by measuring the wetting front travel time between these two depths. One of the tensiometers recorded wetting front arrival before their corresponding unit at 3 m depth. At the CW location, the difference between wetting front arrival was only 4 hours, or one data collection event; thus, these could have arrived nearly simultaneously. Local velocities ranged from 30.8 to 178.9 cm d^{-1} for those tensiometers where both 3 and 5 m readings were reliable. Obviously, the very rapid flow to the deeper tensiometer units could have been caused by annular flow. The 3 and 5 m deep units were located laterally two meters apart from one another, or a true offset of 2.83 m. Differences in soil texture may explain some of the differences, especially when considering that the 0-5 m velocity is 45% faster than the velocity from 0-3 m. A coarser textured soil has a lower water content, and a resultant higher velocity for the same downward flux.

Water front arrivals were measured with six of the nine 10 m deep tensiometers (Figure 3.5-13C). Electrical shorting or the lack of adequate sealing between the stopper and the tensiometer cup rendered three units unreliable. Wetting fronts arrived after irrigation ended, showing significant internal drainage in the vicinity of the wetting front (Table 3.5-6 lists the values). Velocities decreased from those measured at 5 m depth, though this result was influenced by the fact that irrigation was no longer occurring. The variability of arrivals, as seen from the CV, was surprisingly low (< 20%), and could be the result of the strong layering in the field, the depth of the profile (i.e., providing more time smooth out the flow), and the change in boundary conditions. The results show how layering damps differences in wetting front movement in deep soil profiles. This was also observed from the velocities calculated from the neutron probe data.

Tensions after redistribution for the 3 m deep units (Figure 3.5-14) were clustered around 100 cm, with the NC and SW units exhibiting significantly higher and lower tensions, respectively. Only the SW unit appeared to be affected by diurnal temperature changes; the other units showed very smooth responses with time. The similarity of final tensions could be due to similarities of texture at those depths. Tensions at 3 m depth approached steady-state more quickly than those found at 5 and 10 m depths, where steady-state was not observed because of internal drainage from 3 to 5 and 10 m.

3.5.3.2 Experiment 2

The deep tensiometers did not perform as well as expected during Experiment 2. In most cases, for most of the depths monitored, very small responses were recorded with the datalogger. In some cases, the responses could be not correlated with water application or redistribution, leading us to believe that we were recording random variations of the calibration offset. However, some of the units provided what appeared to be significant changes of tension with time. For example, Figure 3.5-15A and B shows the response to water addition and redistribution for all tensiometers that operated reliably. Several gaps are apparent in almost each of the datasets represented on the figures. Gaps occurred when obviously erroneous data were collected and were subjectively removed. Most of the time periods removed correspond to precipitation events, though it is not clear exactly why large reductions in tension occurred during and immediately following rainfall. It is possible that increased humidity or direct water contact on the electrical connections at the soil surface could have shorted the wiring, causing a reduction in the excitation at the pressure transducer. After the precipitation ended, in many cases, tensions rebounded to original levels.

Most of the units which produced reliable data were completed at 10 m depth (Figure 3.5-15B). Of the five units available, four showed water breakthrough between Days 10.3 and 11.7 (front velocities between 85.7 and 96.8 cm d^{-1}), and the fifth tensiometer showed water breakthrough shortly thereafter. The range of time for arrival at these five

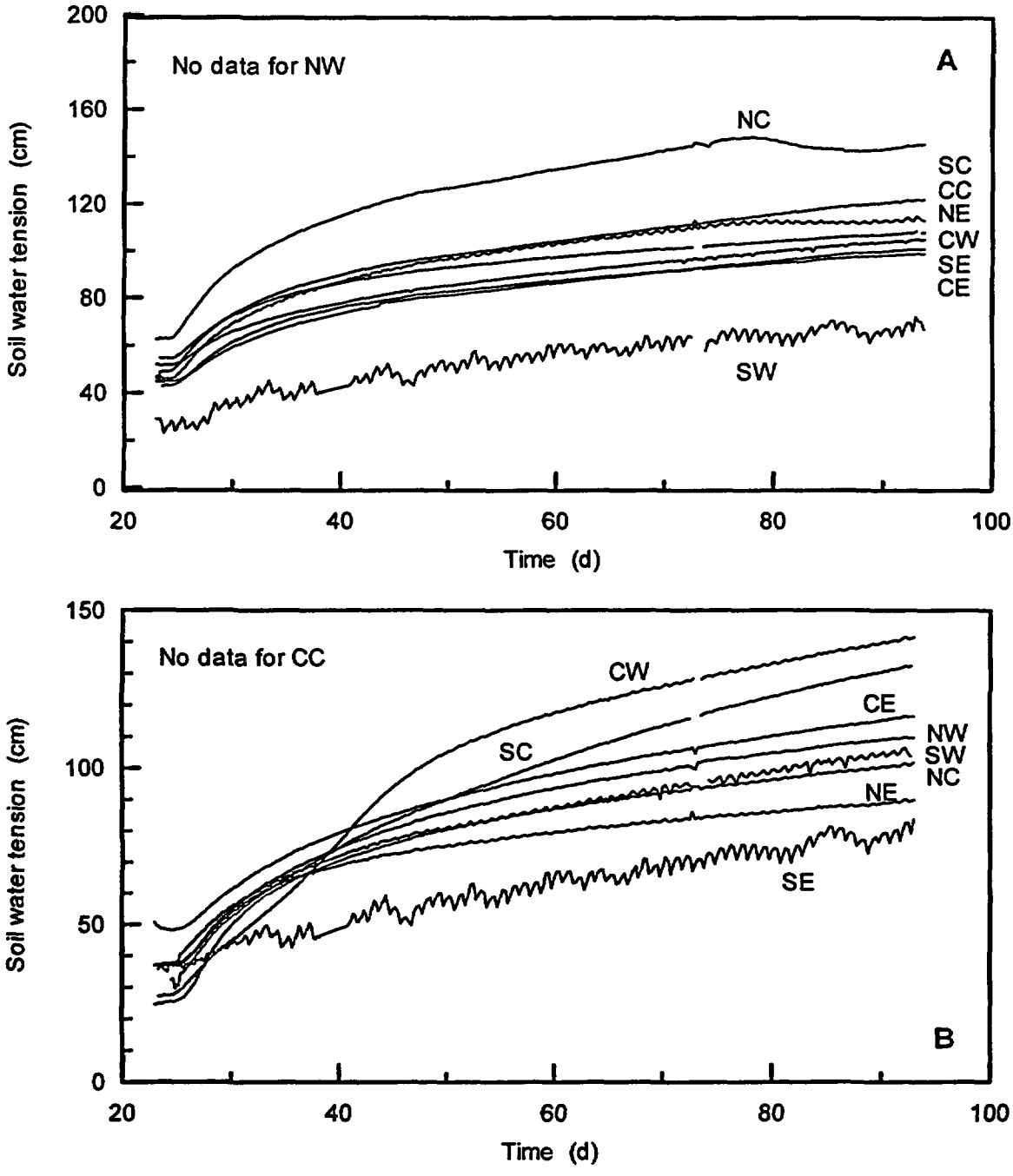

Figure 3.5-14. Response of deep tensiometers at (A) 3 m and (B) 5 m depths during redistribution phase of Experiment 1.

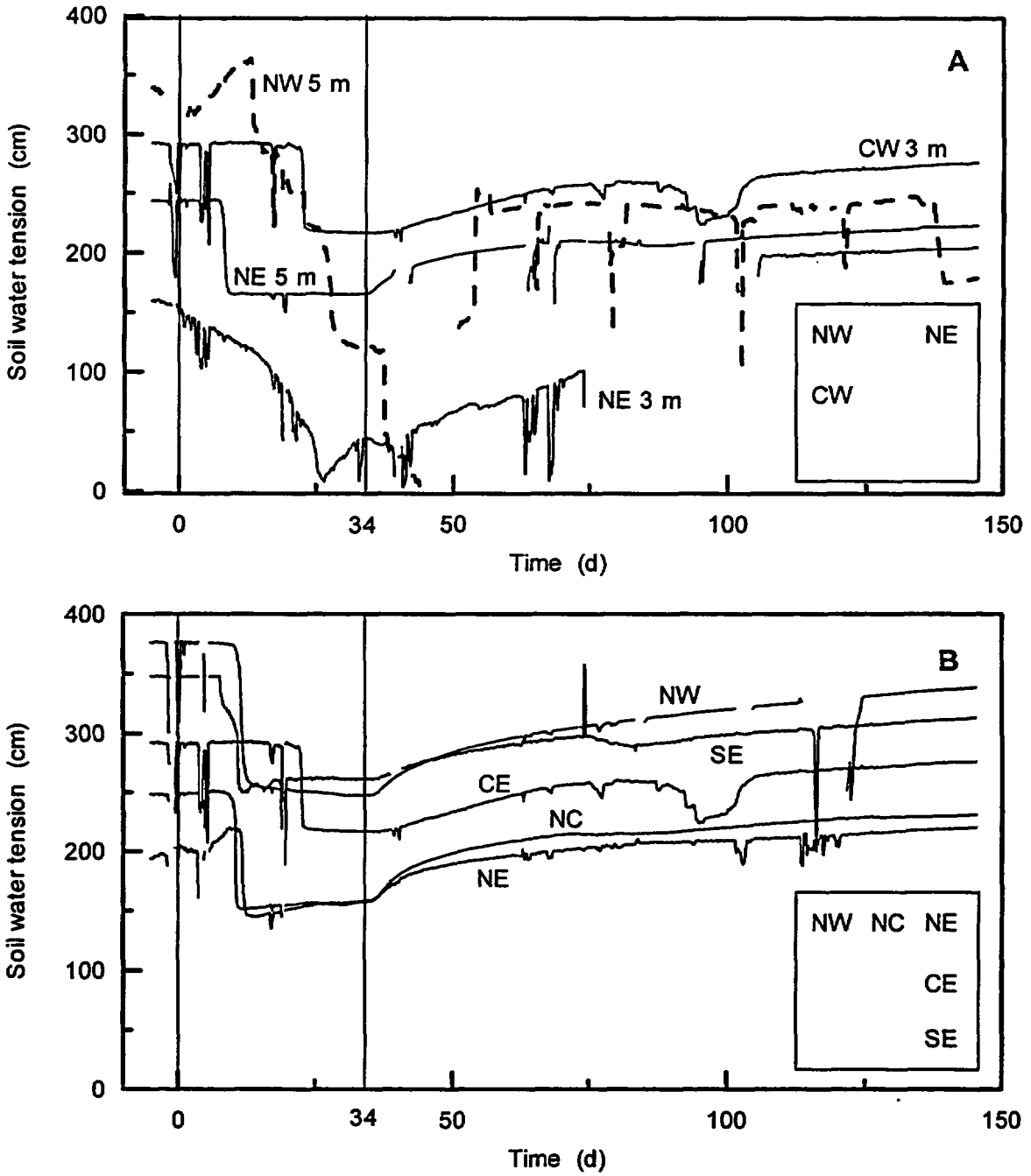

Figure 3.5-15. Response of deep tensiometers during Experiment 2. (A) combines the available tensiometers completed at 3 and 5 m depths. (B) includes the functional tensiometers completed at 10 m depth.

tensiometers (1.3 days) is small compared to water arrival at much shallower depths during Experiment 1 (4.5 days), showing that water flow through this pre-wetted soil was more uniform. Also note that the difference between water breakthrough at 5 m and 10 m depths located at the NE corner of the plot, was only 3.7 days. This difference would correspond to water flow at more than 135 cm d^{-1}, which is not reasonable given the boundary conditions and soils.

3.6 Heat Dissipation Sensor Data

3.6.1 Buried Trench

3.6.1.1 Experiment 1

Figures 3.6-1A and B shows the HDS responses prior to and after arrival of the wetting front along the buried trench. Note the significant diurnal fluctuation in the HDS response, which was seen in all the HDS units. Maximas and minimas occurred at 20:00 and 08:00, respectively, indicating a temperature effect. Technical representatives at Campbell Scientific, Inc. suggested that the cause of the fluctuations was, in part, temperature dependence of the constant current source used for the HDS units. Apparently, some of the constant current interface units were affected by this dependency, which can cause different temperature increases in the HDS units themselves. If the level of heating in the ceramic cup changes over time, then the resulting ΔT would also change.

Research work at Campbell Scientific, Inc. has shown that fluctuations of tension can be as high as ±10% or more in dry soils. When the soil becomes wetter and the thermal conductivity increases (Wierenga et al., 1970), the diurnal fluctuations decrease. Before the wetting front arrived, soil tensions at, for example Y = 40 m, were being measured at approximately 305 cm ± ~12 cm. After the wetting front arrived, tension at the same location reduced to 45 cm ± 3 cm, following the same trend as found by Campbell Scientific, Inc. Though it is too late to repair the interfaces, knowing that much of the fluctuations was due to the instrumentation allows us to either filter or average out the fluctuations, without filtering out true soil water phenomena.

Each of the HDS units responded to the wetting front, except for the unit at Y = 2.5 m, which indicated no wetting front arrival (Figure 3.6-1A). The unit at Y = 0 m was not plotted. Both Y = 0 and 2.5 m were outside the irrigated area. Several comments can be made about the HDS responses to water application. First, distinct and visible reductions in the tensions signaled the arrival of the wetting front at each of the units. For example even subtle wetting front arrivals at Y = 5 and Y = 50, can be easily seen. The rapid drop of tensions indicate: 1) a sharp wetting front, 2) good contact between the ceramic cup and the native soil, and 3) excellent response time for the HDS units.

We evaluated wetting front arrival times and velocities for each of the HDS units, using the same method as applied to the neutron probe data (equation 3-2). The results show widely scattered arrival times, especially on both the northern and southern edges of the irrigated plot, reflecting differences in soil hydraulic properties. The velocities calculated for the trench ranged from 13.43 to 42.86 cm d^{-1}, for those units located at least 5 m inside the irrigated plot (Table 3.6-1) [The HDS unit at Y = 5 m, at the southern edge of the irrigated plot, recorded the slowest wetting front velocity in the trench.] Note also the extremely rapid wetting front movement at Y = 45 (velocity = ~43 cm d^{-1}). At this location, we observed the same phenomenon with the horizontal neutron probe in both the N-S undisturbed and disturbed trenches. It is also clear that the wetting front migrated slower in the southern portion of the plot than in the northern portion of the plot; average velocities south and north of Y = 30 m (the plot center) were 15.1 and 24.6 cm d^{-1}, respectively, with an overall mean velocity of 19.9 ± 8.3 cm d^{-1}. These results, compare favorably with data from the two N-S neutron probe access tubes, and provide good confirmation that flow behavior was due more to the soil texture and structure in that vicinity, than to the backfilling method used for the different instruments.

After the end of irrigation on Day 23, water was allowed to redistribute for 60 days, resulting in lower soil water contents and increased tensions. Figures 3.6-2A and B show these 60 days of data collection for each of the HDS units that experienced wetting front arrival (e.g., from Y = 5 to Y = 55 m). The figure shows that the diurnal fluctuations of HDS response are similar but less pronounced than the fluctuations occurring before the soil became moist. This is most likely due to the increased thermal conductivity of the ceramic cup from the higher water content, leading to a smaller error from oscillations of the supply current (J. Bilskie, 1998, personal

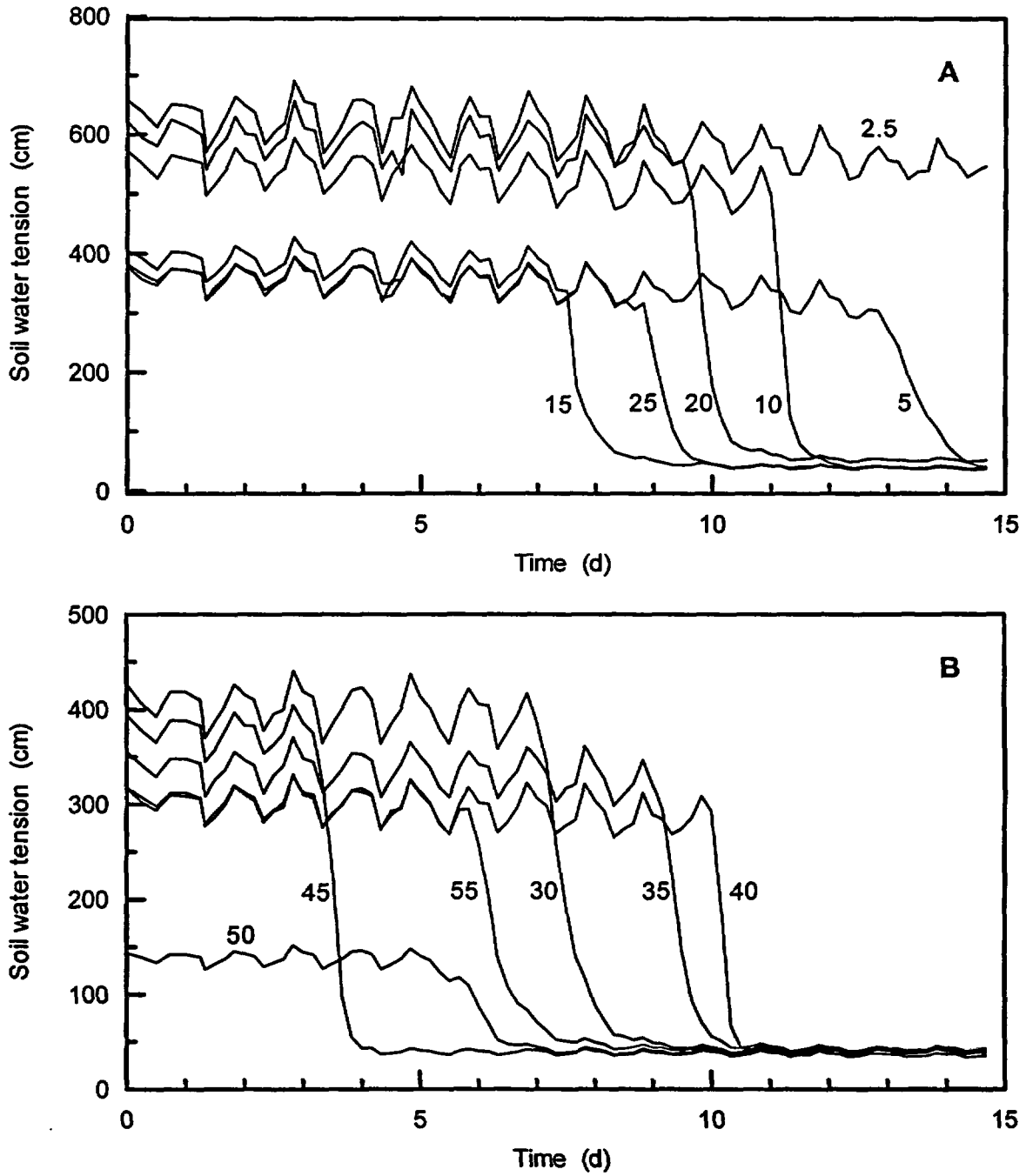

Figure 3.6-1. Response of HDS units in buried trench transect to water infiltration during Experiment 1. Numbers on graph indicate y-coordinate. Note different y-scales for (A) southern and (B) northern portions of the trench.

Table 3.6-1. Wetting front arrival in buried trench using HDS units during Experiment 1.

Position	Y-coordinate (m)	Time (days)	WF velocity (cm d^{-1})
141	0	no arrival	n/a
142	2.5	no arrival	n/a
143	5	13.33	11.3
144	10	11.17	13.4
145	15	7.83	19.2
146	20	9.83	15.3
147	25	9.17	16.4
148	30	7.17	20.9
149	35	9.33	16.1
150	40	10.17	14.7
151	45	3.50	42.9
152	50	6.00	25.0
153	55	6.17	24.3
Mean		8.52	20.0
CV (%)		30.7	41.8

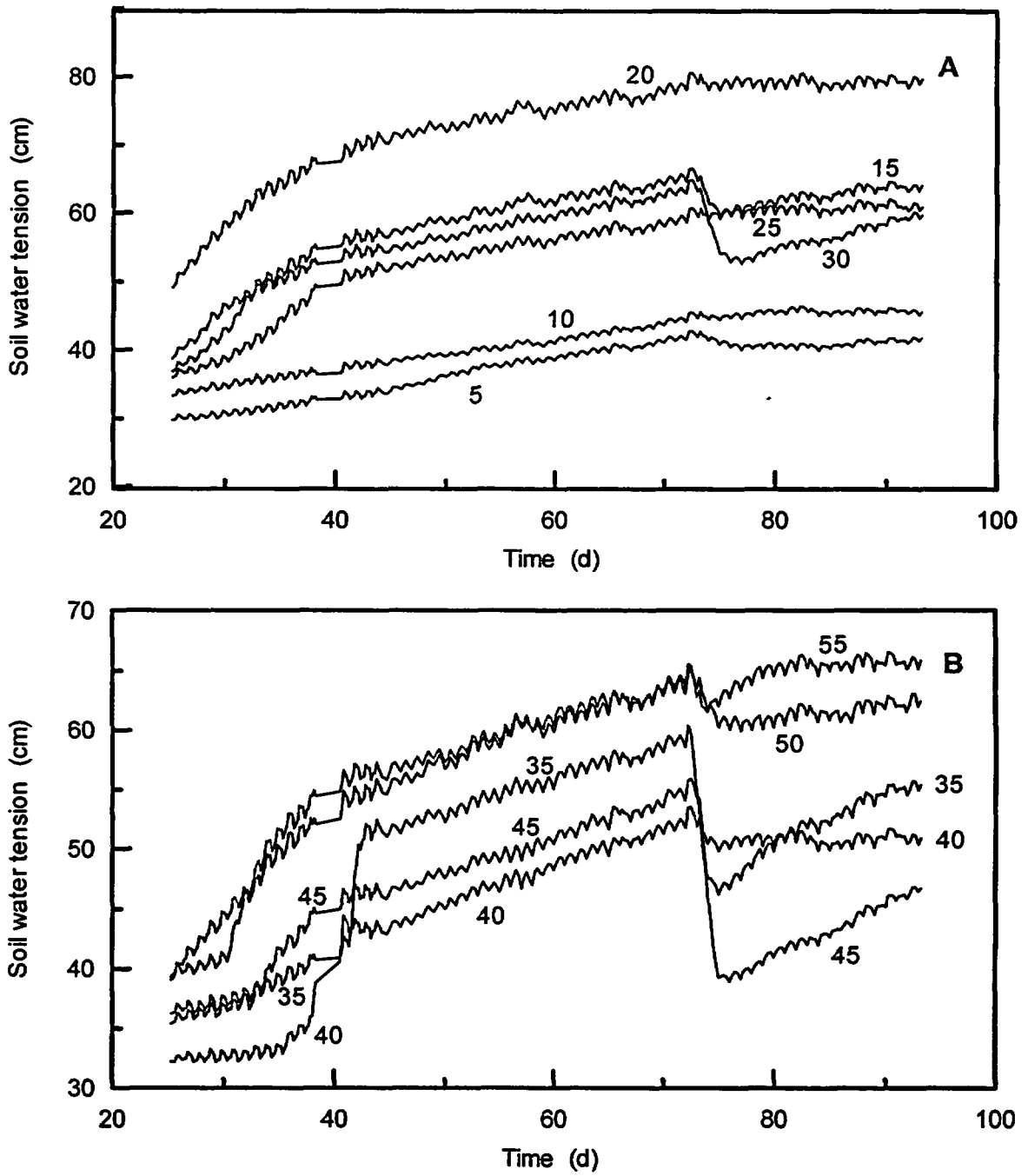

Figure 3.6-2. Five-point moving averages of HDS response to redistribution in the buried trench during Experiment 1. Numbers on graph indicate y-coordinate. Note different scales for (A) southern and (B) northern portions of the trench.

communication). Ignoring the diurnal fluctuations, it is clear that the soil did not return to the original water content at the end of redistribution.

The spread of tension values during redistribution was quite high along the trench, ranging from 39 to ~75 cm on Day 60. By contrast, Tensimeter readings of the trench tensiometers taken near that same time showed a range from 84 to 114 cm tension. It is not clear why the HDS readings were more variable along the length of the trench, or why they were much lower in value. It is possible that soil texture can explain some of the variability, but it is unlikely to explain the much lower tension values, leading us to suspect that 1) the HDS calibration curves drifted with time, or 2) that the units were exhibiting hysteretic behavior, such that they were more sensitive during sorption than during desorption. Without removing the instruments, checking the calibration curves was not possible; thus, we are unable to fully explain the differences.

On Day 72.5, we experienced a large decline in tension for many of the HDS units. Figure 3.6-2 shows a decline of almost 15 cm for units at Y = 35 and 45 m. Most of the other units responded similarly but to a lesser extent. On Day 72, field personnel were at the site, collecting data and servicing monitoring instruments. Though most tensiometers were not fully operational during redistribution, tensiometers were serviced on that day, explaining the decline in tension recorded at Y = 40 m. This, of course, would not explain the decline in HDS values. Environmentally, a total of 6 mm precipitation was recorded at the AZMET station, 100 m SE of the site, during the evening between Day 72 at 21:00 hours and Day 73 at 08:00 hours. This small amount of precipitation also could not explain the decline. It is possible that flood irrigation occurred at the alfalfa field immediately north of the plot, during the evening of Day 72, causing a decline in tension at the northern HDS units, but not at the southern units. EM-31 data collected on Days 72 and 79 would have shown an increase in electrical conductivity in the northern (and central) areas of the plot, but changes were small in magnitude and random (see Section 3.8 below). We have no other plausible explanation for this large change and must therefore assume that a mechanical malfunction occurred with the datalogger or constant current interfaces used to operate the trench HDS units.

3.6.1.2 Experiment 2

The HDS measurements indicated a substantial reduction in the variability of flow along the buried trench. Table 3.6-2 lists the arrival times and wetting front velocities for each of the units. The average front velocity was higher than recorded during Experiment 1 (32.2 versus 19.9 cm d^{-1}), and the coefficient of variation was much lower (4.67% versus 41.84%). It is apparent that the hydraulic conductivity of the soil quickly approached the flux rate imposed at the upper soil surface, such that the pore water velocity was virtually the same along the trench. Figure 3.6-3A shows the time series of readings for 15 days. Some diurnal fluctuation was apparent both before and after wetting front arrival, but the change in tension from wetting front arrival was distinguishable. Differences in arrival time were difficult to detect.

The HDS unit, which was installed 5 m south of the edge of the irrigated plot (# 141) still indicated no breakthrough of water, showing that lateral flow was restricted to within a few meters. We found that several other units, listed as NR in Table 3.6-2, were affected by some other environmental factor that caused water breakthrough to occur between Days -1.0 and 0.5. Approximately 15 mm of precipitation occurred on Day -2, but it is doubtful that this relatively small amount of rain could have caused significant tension changes at 1.5 m depth. It is possible that flood irrigation of an alfalfa field immediately north of our plot could have caused significant lateral flow, but neutron probe data readings (especially in the E-W horizontal access tube) did not detect water content changes. No other explanation is forwarded for early water breakthrough.

Water redistribution for the first 120 days is shown in Figure 3.6-3B. Soil water tensions returned to their original values prior to Experiment 2 irrigation. Internal drainage for the HDS unit at Y = 10 m was much less than the other two shown on the graph, indicating a higher water holding capacity of the soil. Large levels of noise were recorded from the HDS unit at Y = 35 m, especially on Days 63, 69, 74 and 84, but not from the other unit shown on the figure. Though it may be coincidental, rainfall was recorded on each of these days immediately prior to the reduction in tension. Respectively, 11, 12, 12 and 8 mm of precipitation were recorded from the nearby AZMET station on these days, indicating some hydraulic connection between the HDS units and ambient meteorological conditions. It is

Table 3.6-2. Wetting front arrival in buried trench using HDS units during Experiment 2.

Position	Y-coordinate (m)	Time (days)	WF velocity (cm d^{-1})
141	0	no arrival	n/a
142	2.5	NR†	NR
143	5	NR	NR
144	10	4.5	33.3
145	15	4.33	34.6
146	20	4.33	34.6
147	25	4.5	33.3
148	30	NR	NR
149	35	4.5	33.3
150	40	NR	NR
151	45	NR	NR
152	50	NR	NR
153	55	5	30.0
Mean		4.53	32.2
CV (%)		4.97	4.7

† NR - indicates that water arrival was affected by external changes in water content, which occurred on Day -1.5.

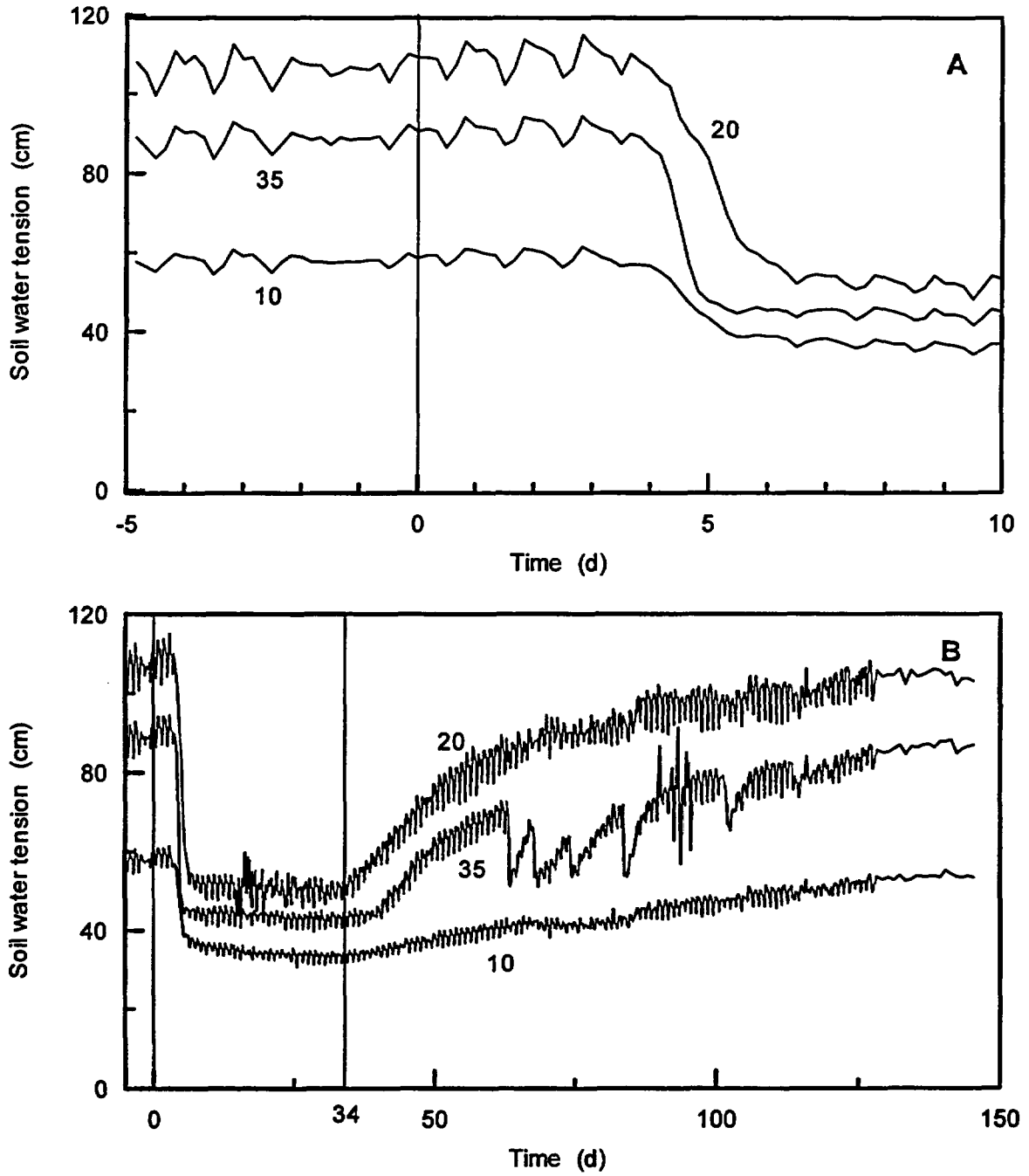

Figure 3.6-3. Soil water tension obtained from selected HDS units, installed in buried trench, during (A) irrigation and (B) redistribution phases of Experiment 2. Numbers on graph indicate y-coordinate.

possible that the cover material could have small leaks in the vicinity, leading to small inputs of water above the HDS unit, or that the increase in humidity somehow affected the operation of the constant current interface. It is not clear which of these explanations are valid.

3.6.2 Monitoring Islands

3.6.2.1 Experiment 1

Figures 3.6-4 and 3.6-5 show the HDS response from water infiltration in the South and North Islands, respectively. Both plots show very distinct wetting front arrivals. Table 3.6-3 lists the arrival time and associated velocities. Changes in soil water tension, due to the arrival of the wetting front, greatly exceeded the diurnal fluctuations that were apparent in the data. Both vertical transects in the South Island showed similar wetting front arrivals, though the velocity was slightly faster on the West Side. Wetting front velocities increased with depth (Figure 3.6-6). Of particular notice was the velocity measured at 1.5 m depth; both vertical transects experienced velocities close to 16.5 cm d^{-1}, which was almost identical to the wetting front velocity measured using the HDS in the buried trench at the same Y-coordinate (e.g., Y = 20 m). Recalling that the South Island was not equipped with a rubber skirt, as was the North Island, we can say that the water flowed unimpeded and unchanneled through the soil, allowing us to directly compare instruments from different monitoring strategies.

Measurement of soil water tension in the North Island indicated faster wetting front velocities than in the South Island (Figure 3.6-6). This was due, in part, to the presence of the rubber skirt that was intended to prevent water from traveling preferentially through the backfill material in the annular space. The impermeable rubber material, diverted water away from the annular space, but concentrated water directly above the vertical transect of the monitoring instruments. This increased "flux" led to water flow that was faster than the native soil surrounding the monitoring island. Thus, the rubber skirt seems to have the unintended result of advancing the velocity of water around the North Island. Numerical simulations of this phenomenon should be able to explain some of the questions concerning the rubber skirt.

Similar to that observed for the trench units, tension readings never increased to pre-irrigation levels (Figures 3.6-7 and 3.6-8). Redistribution did lead to some tension increases, but they were very slight and the soil reached apparent steady levels after only 30 days.

3.6.2.2 Experiment 2

We chose to follow the convention used above and focus only on the HDS units installed in the South Island, West Side. Table 3.6-4 shows associated statistics of HDS measurements before the wetting front arrived, and the wetting front velocity, as measured using the instruments. The average tensions were much higher in the surface soils and decreased with depth, especially at 2.0 and 2.5 m depths. Standard deviations were also higher, correlating positively with the readings in almost every case. Coefficients of variation were higher than the CSI TDR system, likely because of 1) diurnal fluctuations of the current excitation of the units, or 2) true changes in surface tension due to heating and cooling of the soil surface, or a combination of both.

Figure 3.6-9A shows the data for HDS units installed at the South Island, West Side. Distinct changes in tension were recorded at several depths, such as 0.5 and 1.0 m, but they were less distinct at 2.0 and 2.5 m. In all cases, however, the wetting front arrival could be determined with little trouble. The associated velocities are listed in Table 3.6-4. The increase in velocities with depth was apparent, as were the similarities in values when compared to tensiometers and TDR units. The results also mirrored the general trends recorded during Experiment 1, with a higher soil water deficit in the surface 1 m of soil, and a lower deficit in soils between 2.0 and 2.5 m, leading to a more rapid movement of soil water. The results also showed good repeatability of the HDS instruments installed in the monitoring islands during both experiments.

Redistribution of water is shown in Figure 3.6-9B. Note the significant internal drainage in the shallower soils that have higher water holding capacity. Tension at 0.5 m depth increased from about 90 cm to over 200 cm during the first 115 days of redistribution. Increases were less for the deeper soils, reflecting the supply of water from above and the different texture of the soil. Note that tensions on Day 150 were very close in value to tensions recorded before irrigation began, indicating that soil water conditions were

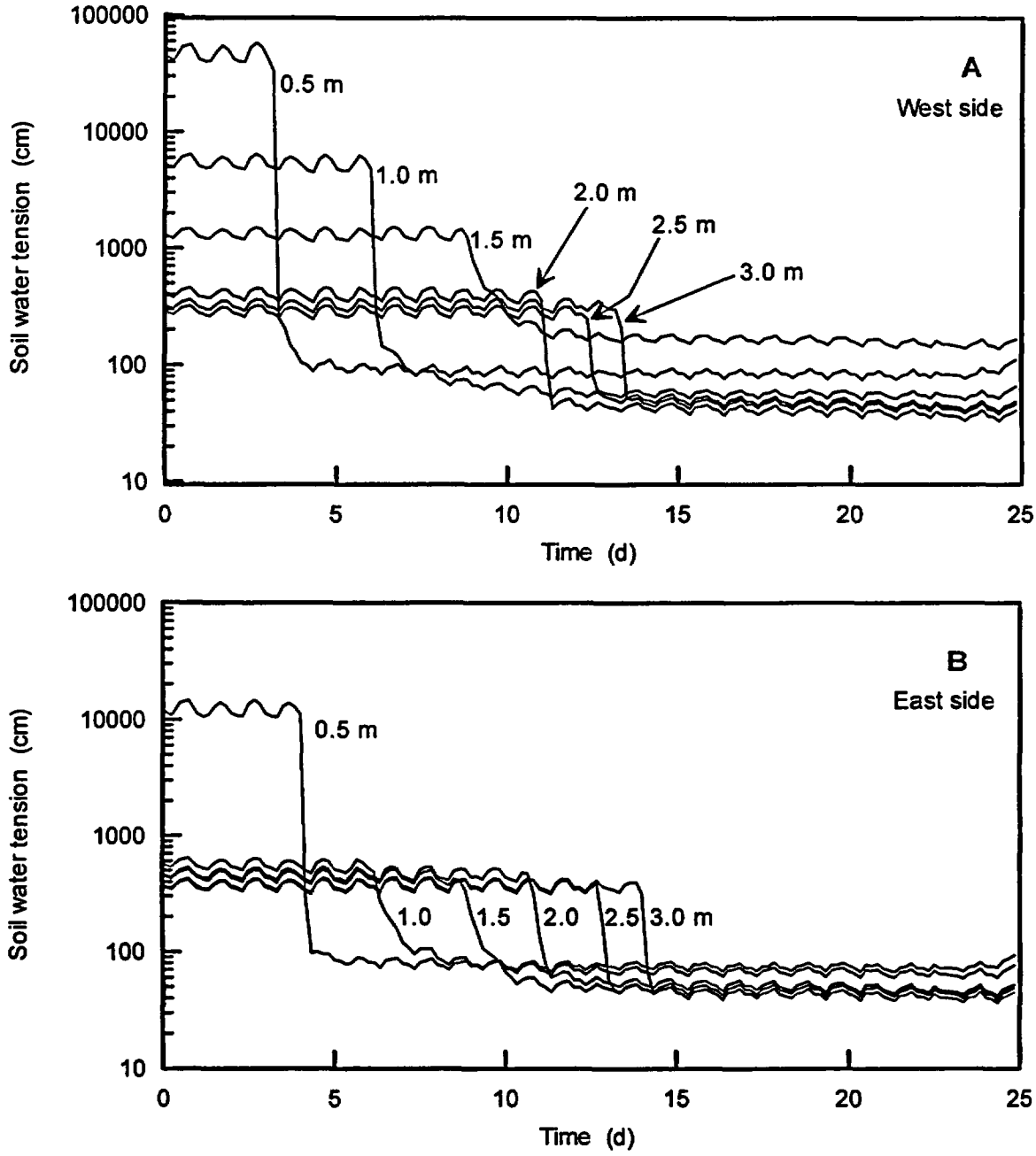

Figure 3.6-4. Response of HDS units on the South Island (A) West side and (B) East side to water infiltration during Experiment 1.

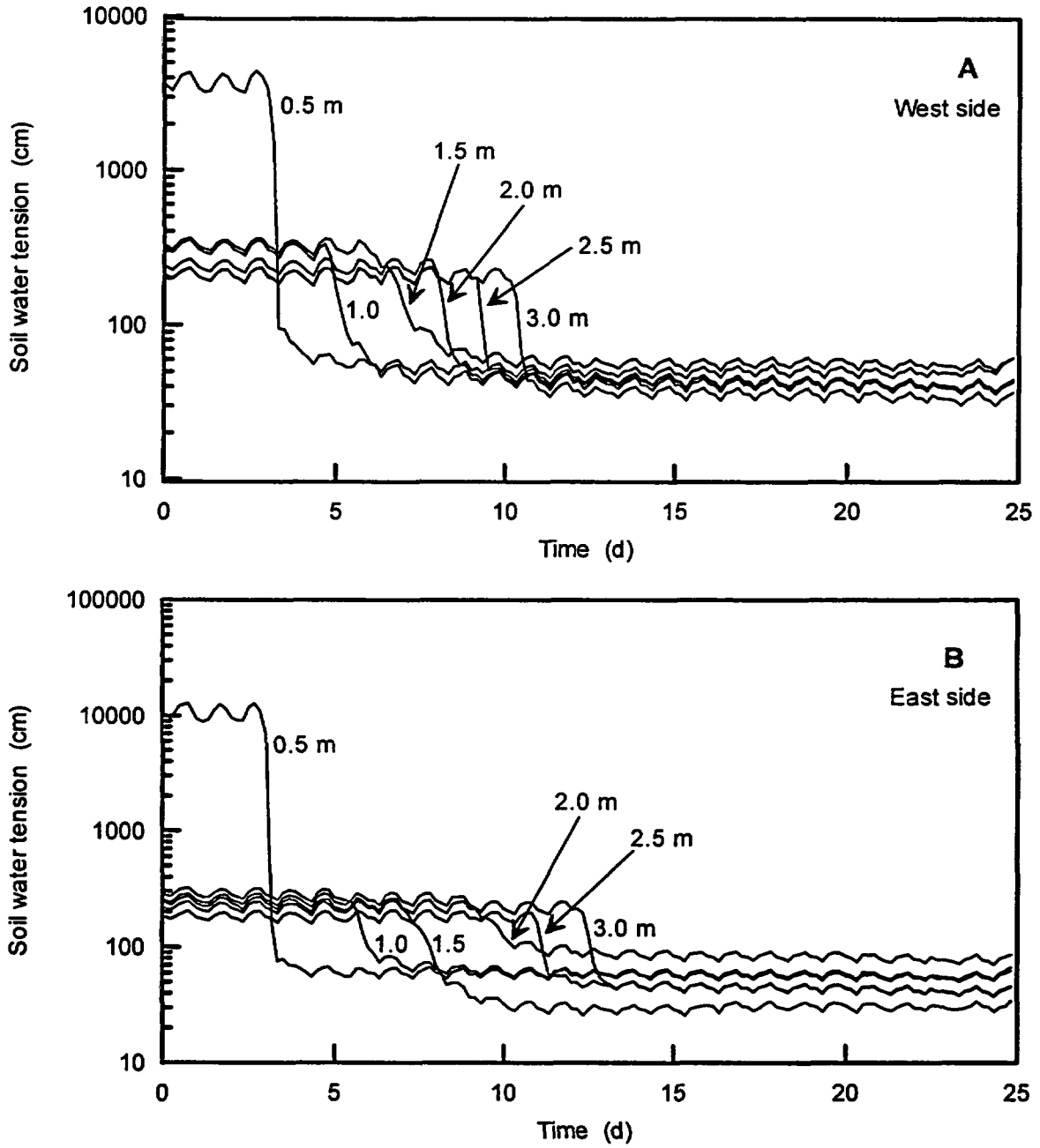

Figure 3.6-5. Response of HDS units on the North Island (A) West side and (B) East side to water infiltration during Experiment 1.

Table 3.6-3. Wetting front arrival using HDS installed in monitoring islands during Experiment 1.

Depth (cm)	Time (days)	WF velocity (cm d^{-1})	Time (days)	WF velocity (cm d^{-1})	Time (days)	WF velocity (cm d^{-1})	Time (days)	WF velocity (cm d^{-1})	Mean velocity (cm d^{-1})
	S. Island - West		S. Island - East		N. Island - West		N. Island - East		
50	3.17	15.8	4.17	12.0	3.33	15.0	3.17	15.8	14.7
100	6.00	16.7	6.33	15.8	4.83	20.7	5.83	17.2	17.6
150	9.17	16.4	9.00	16.9	6.83	22.0	7.33	20.5	18.9
200	11.17	17.9	10.83	18.5	8.17	24.5	9.17	21.8	20.7
250	12.33	20.3	12.83	19.5	9.33	26.8	11.00	22.7	22.3
300	13.33	22.5	14.17	21.2	10.33	29.0	12.67	23.7	24.1

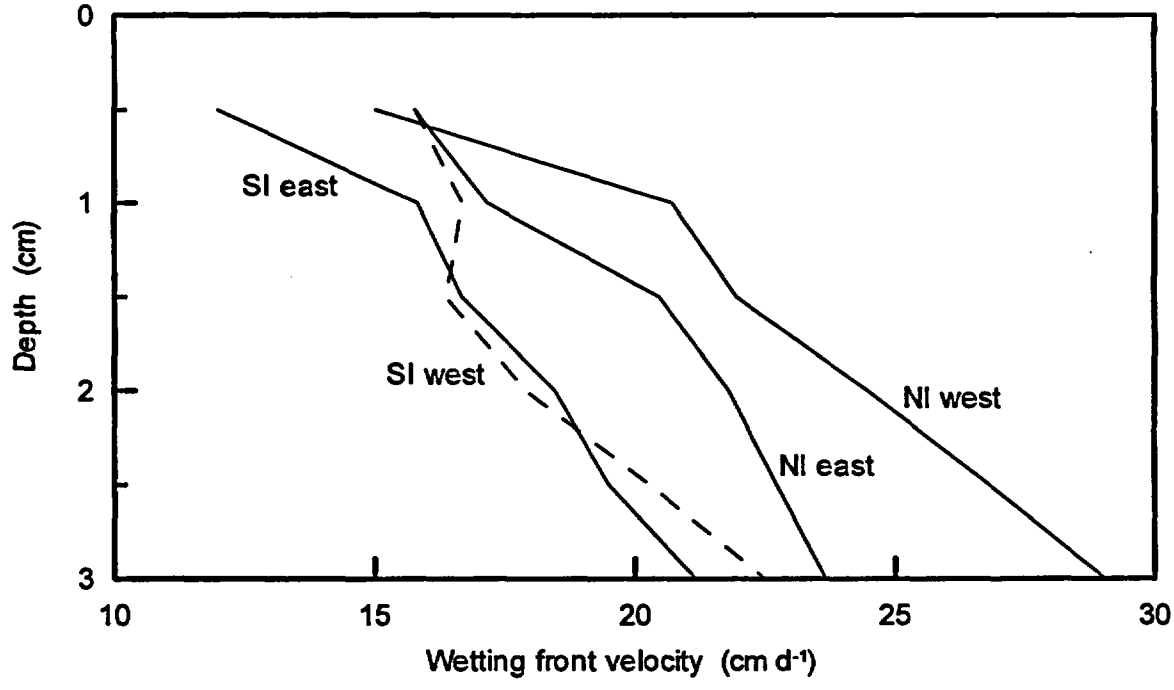

Figure 3.6-6. Wetting front velocities around the monitoring islands measured using HDS units during Experiment 1.

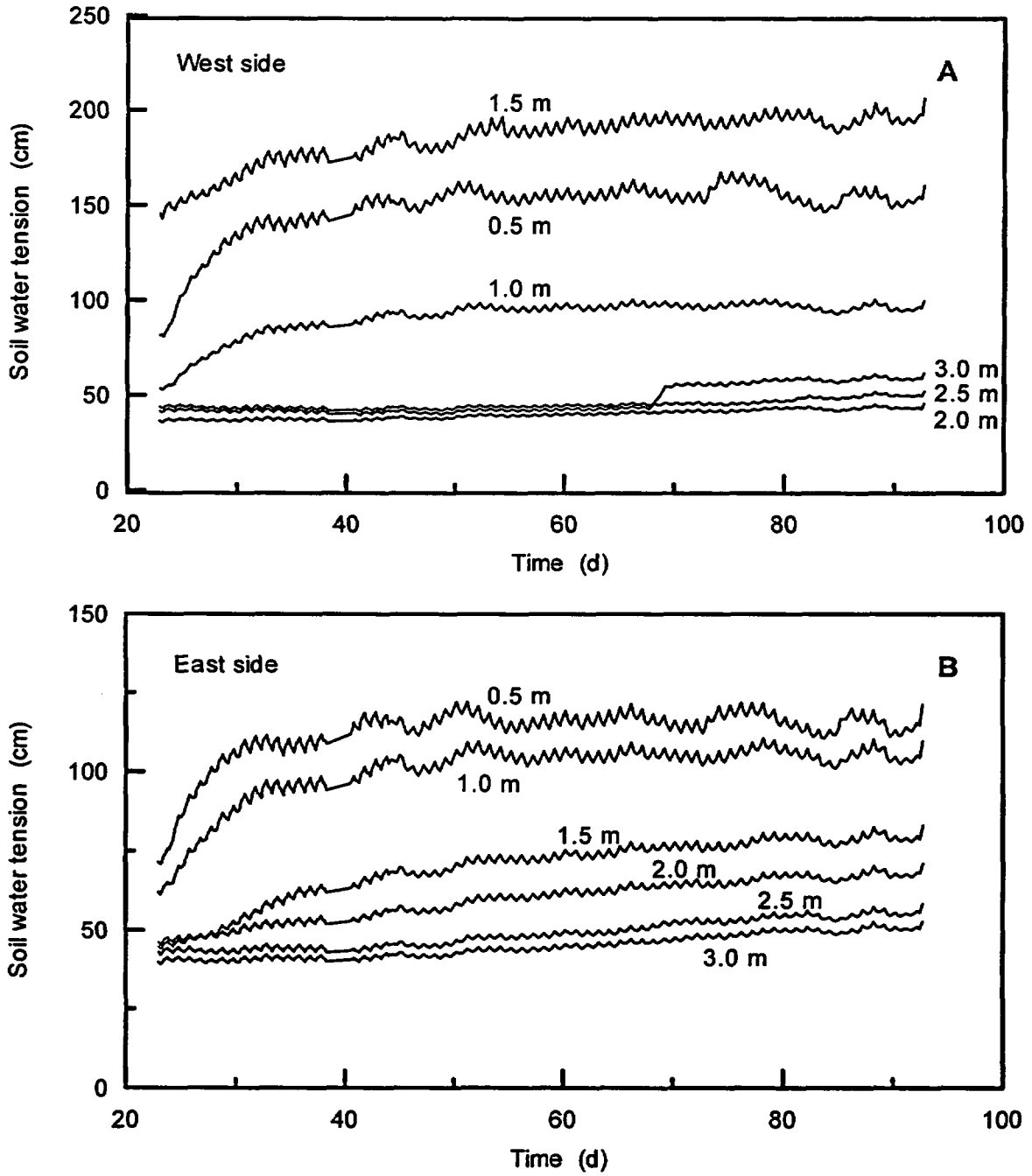

Figure 3.6-7. Response of HDS units on the South Island (A) West side and (B) East side during redistribution phase of Experiment 1. Note that some of the lines may not be distinguishable because they overlap.

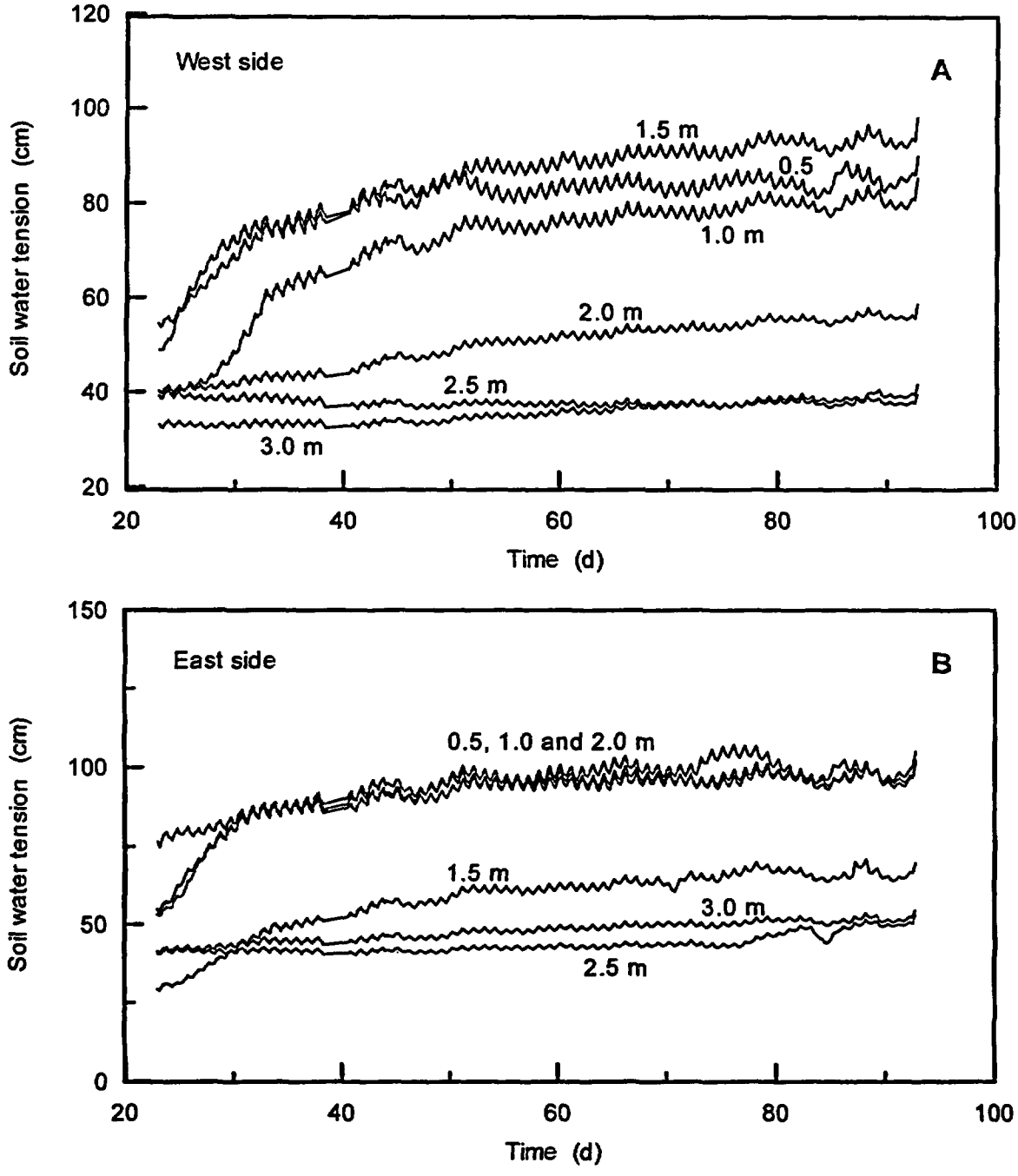

Figure 3.6-8. Response of HDS units on the North Island (A) West side and (B) East side during redistribution phase of Experiment 1. Note that some of the lines may not be distinguishable because they overlap.

Table 3.6-4. Results of HDS measurements for South Island, West Side during Experiment 2.

Depth (m)	0.5	1.0	1.5	2.0	2.5	3.0
Mean tension before front arrival (cm)	273.76	142.37	239.26	54.38	60.96	75.04
Std. dev. before front arrival	9.12	3.64	5.82	1.30	1.27	1.69
CV	3.33%	2.56%	2.43%	2.39%	2.08%	2.26%
Change in tension (cm)	185.9	85.3	79.1	14.7	12.7	31.5
Front velocity (cm d^{-1})	23.07	27.27	33.33	37.50	37.50	40.91

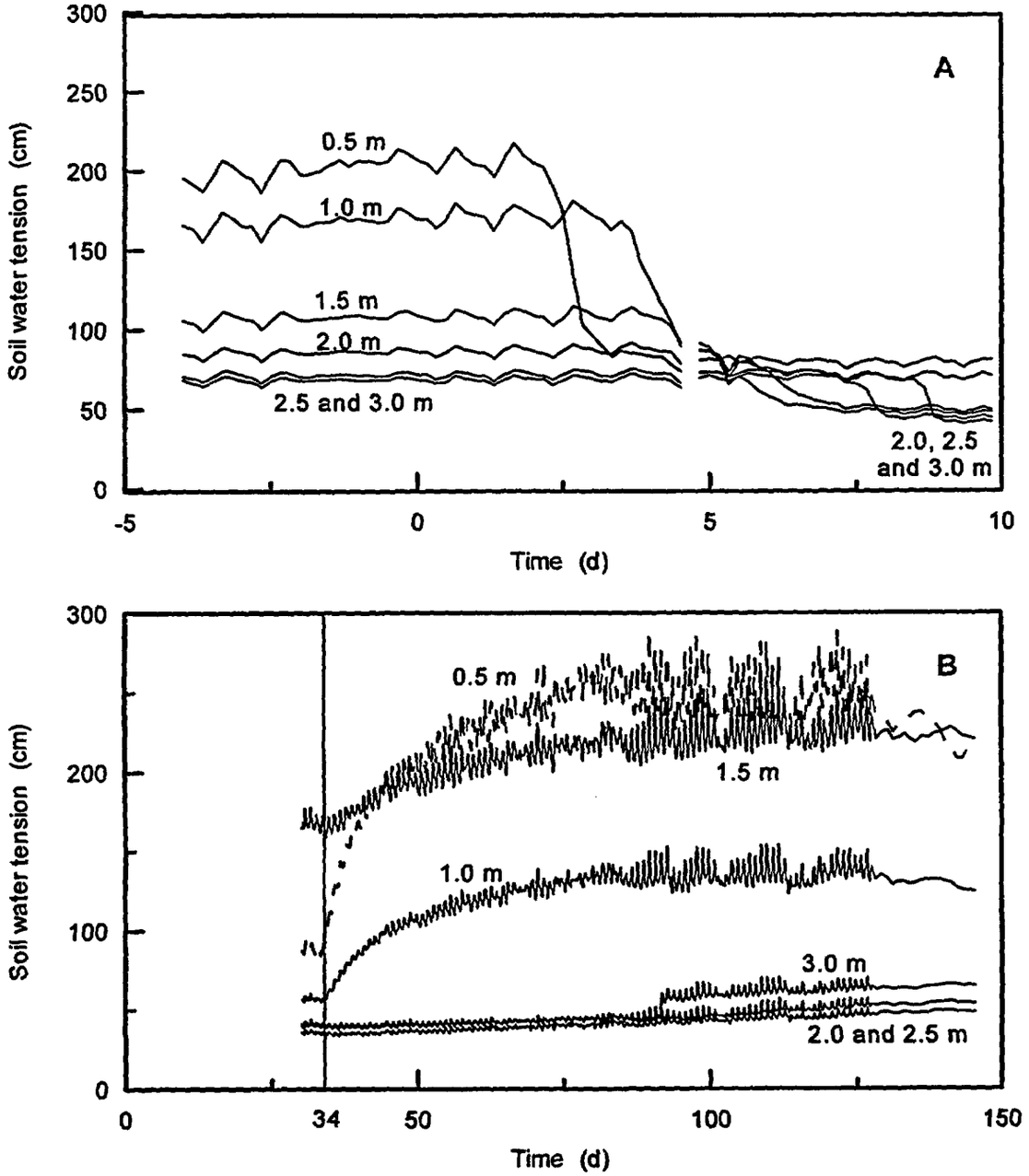

Figure 3.6-9. Soil water tension data obtained from HDS units installed in South Island, West side during (A) irrigation and (B) redistribution phases of Experiment 2.

approaching steady-state. Note also the increase in diurnal amplitude beginning on Day 90. The increase cannot be readily explained either by field or ambient meteorological occurrences, since daily field activities had essentially ceased by this time and no significant amounts of rainfall or temperature extremes were recorded. The reduced diurnal amplitude beginning on Day 187 was caused by a change of data collection frequency from 0.25 to 1.00 days.

3.7 Thermocouple Psychrometer Data

3.7.1 Experiment 1

Most of the information shows that little to no usable information can be taken from these units. However, it may be possible to use just the time when the wetting front arrived at each of the units, by recording when the TCP units began to fail (due to wetness of the soil).

3.7.2 Experiment 2

Because of the high level of soil wetness prior to the beginning of Experiment 2, and the poor performance of these instruments during Experiment 1, data were not collected from the psychrometers. Thus, they will not be discussed further.

3.8 Surface Electromagnetic Induction Data

The measured EC_a for EM-38 and EM-31 varied in the plot before the water application. Average of EM-38 horizontal measurements was 16.9 mS/m (standard deviation = 3.9 mS/m); EM-38 vertical measurements was 19 mS/m (standard deviation = 3.8 mS/m). For EM-31, the average of horizontal measurements was 30.8 mS/m (standard deviation = 3.9 mS/m), and the average of vertical measurements was 40 mS/m (standard deviation = 5 mS/m). The average EC_a values increased with the penetration depth of EM instruments and their associated modes. This is because the water content was higher at deeper depths. The lateral variability was not significant for any single mode.

3.8.1 Experiment 1

The irrigation water applied to the plot had an average EC = 9.2 mmho/cm (standard deviation = 0.04 mmho/cm). Figures 3.8-1 to 3.8-4 show the daily contours of the EM readings of EM-38 and EM-31 under two modes for Days 0, 1, 4, and 7. These contours show the increase of EC_a values in the irrigated area, demonstrating the capability of using EM to monitor the soil water/storage increase inside the irrigated area. The boundary of water application can be clearly defined using these EC_a contour maps. The EC_a values using EM-38 increased by 20 to 50 mS/m inside the irrigated area, but were constant outside the irrigated area. After Day 8, almost no changes were found for EM-38 readings. This observation supports the basic observation, from other instruments, that steady-state infiltration conditions had been established in the top 1.5 m of soil. No change in soil water content or water storage was expected after Day 12, so no EM-38 measurements were taken after this day (Table 3.8-1). The EM-31 instrument, with a greater penetration depth, was used for taking measurements until the end of the experiment. The EC_a values obtained with EM-31 increased by 20 to 40 mS/m above background readings inside the irrigation area, and were constant outside the irrigation area, similar to the EM-38 instrument.

Only EM-31 measurements were taken during Experiment 1 redistribution. Measurements indicated a slow reduction in the EC_a readings. For example, as shown in Figure 3.8-5, EM-31 horizontal readings reached its highest reading at the Y = 10.3 m transect around Day 15 and started decreasing after Day 20. Figure 3.8-6 shows that EM-31 vertical readings were also highest at the Y = 10.3 m transect around Day 20, decreasing slightly after during redistribution. The magnitude of the decrease of EC_a was relatively small in comparison to the increased magnitude during the infiltration phase of Experiment 1 (EC_a reduced by only 10 mS/m during the full redistribution period).

3.8.2 Experiment 2

The EC_a values measured, using EM-38 and EM-31, varied in the plot before water application, but were higher in value than before Experiment 1, caused by the higher initial water content. The average of the EM-38 horizontal measurements was 33.3 mS/m (standard deviation = 4.9

Table 3.8-1. Sampling schedule for the electromagnetic induction measurements during Experiment 1.

Date	Time (days)	EM-31		EM-38	
		Vertical	Horizontal	Vertical	Horizontal
4/07/97	-21	✓	✓	✓	✓
4/29/97	1	✓	✓	✓	✓
4/30/97	2			✓	✓
5/01/97	3			✓	✓
5/02/97	4	✓	✓	✓	✓
5/03/97	5			✓	✓
5/04/97	6			✓	✓
5/05/97	7	✓	✓	✓	✓
5/06/97	8			✓	✓
5/07/97	9			✓	
5/08/97	10			✓	
5/09/97	11			✓	
5/10/97	12			✓	
5/12/97	14	✓	✓		
5/14/97	17	✓			
5/17/97	19	✓	✓		
5/19/97	21	✓	✓		
6/04/97	37	✓	✓		
6/11/97	44	✓	✓		
6/18/97	51	✓	✓		
6/25/97	58	✓	✓		
7/09/97	72	✓	✓		
7/16/97	79	✓	✓		
7/23/97	86	✓	✓		
7/30/97	93	✓	✓		

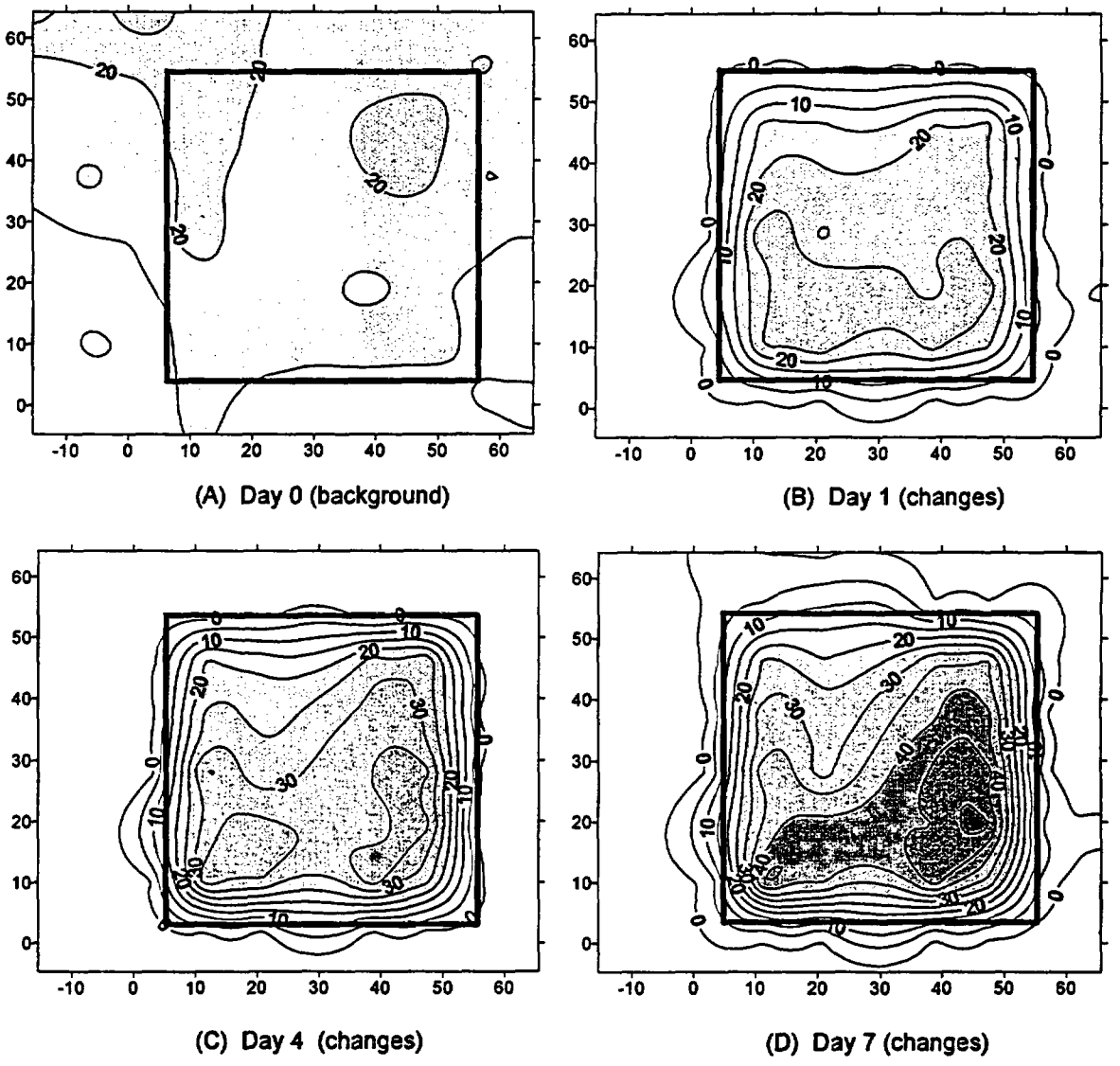

Figure 3.8-1. EM-38 horizontal measurement contours on background and changes in EC_a during Experiment 1. Changes indicate day's reading minus background value.

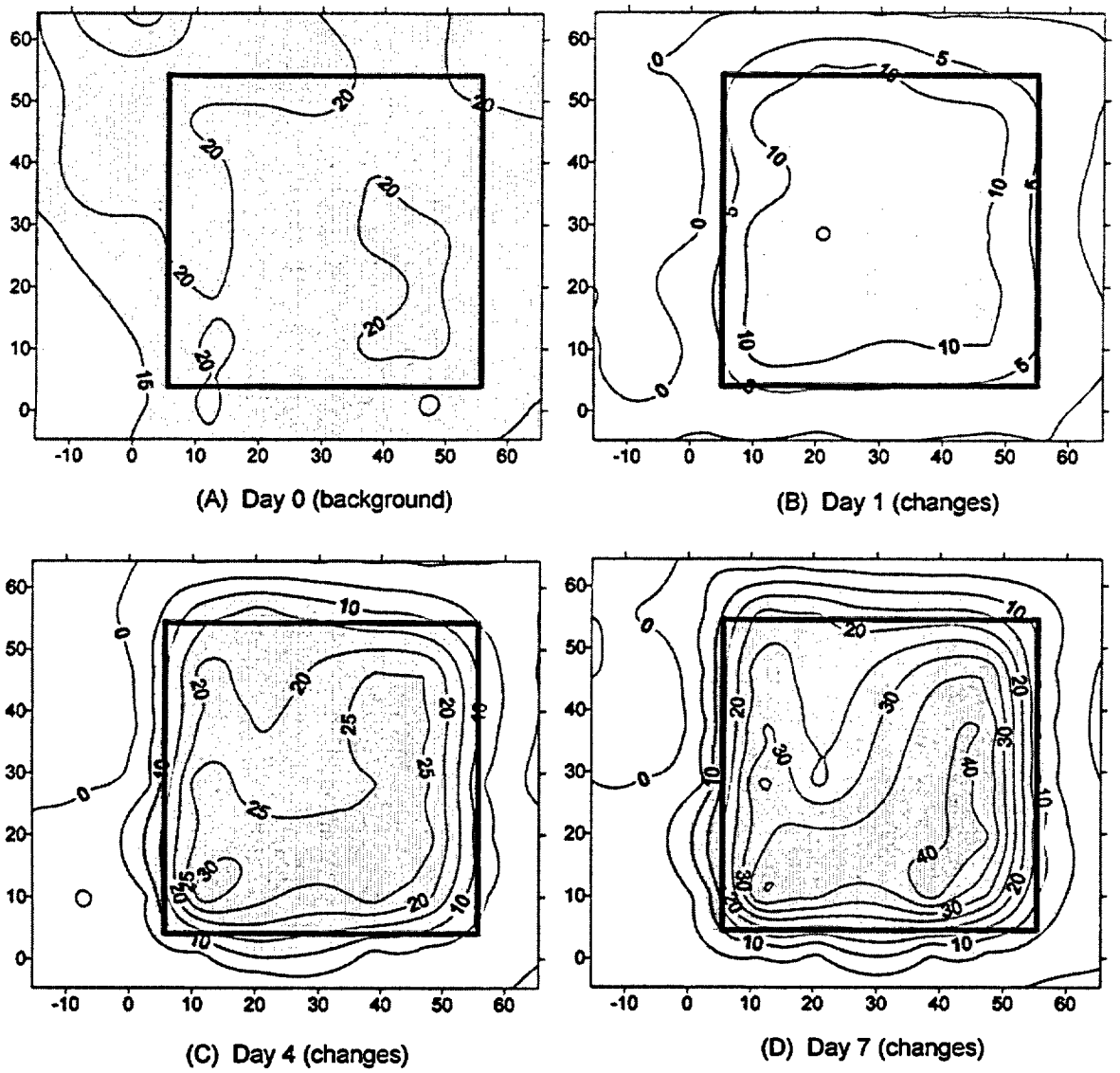

Figure 3.8-2. EM-38 vertical measurement contours on background and changes in EC_a during Experiment 1. Changes indicate day's reading minus background value.

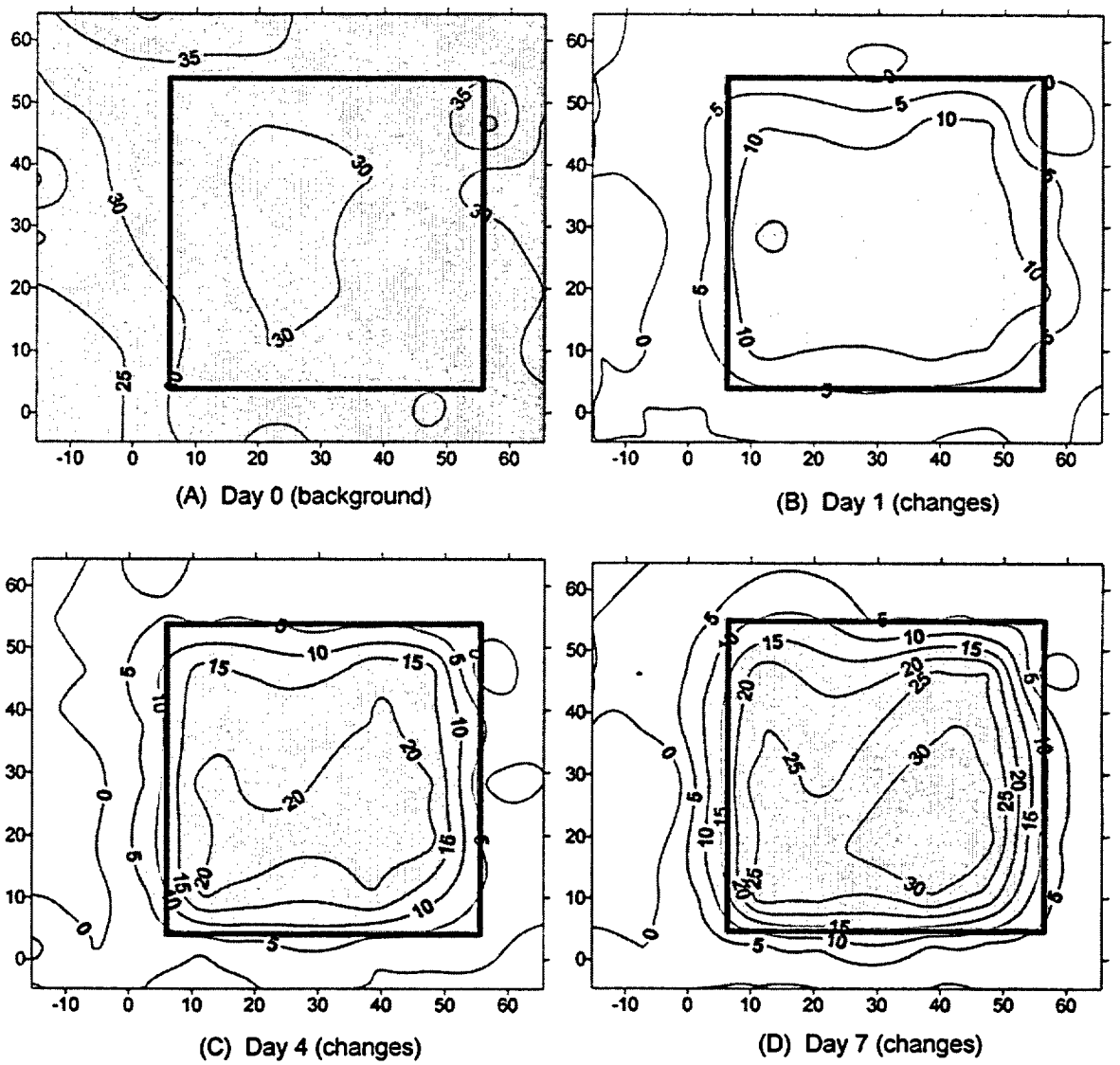

Figure 3.8-3. EM-31 horizontal measurement contours on background and changes in EC_a during Experiment 1. Changes indicate day's reading minus background value.

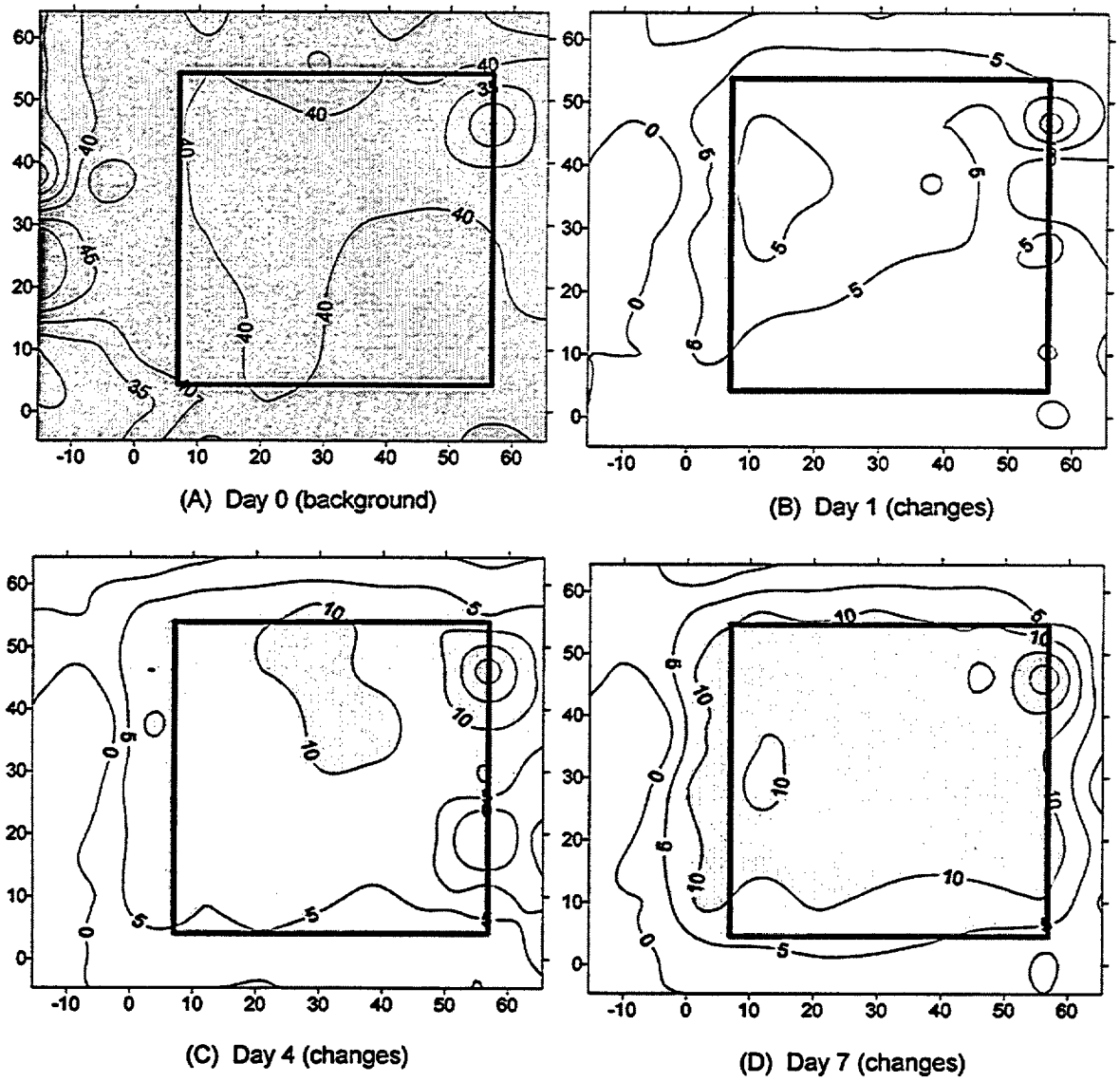

Figure 3.8-4. EM-31 vertical measurement contours on background and changes in EC_a during Experiment 1. Changes indicate day's reading minus background value.

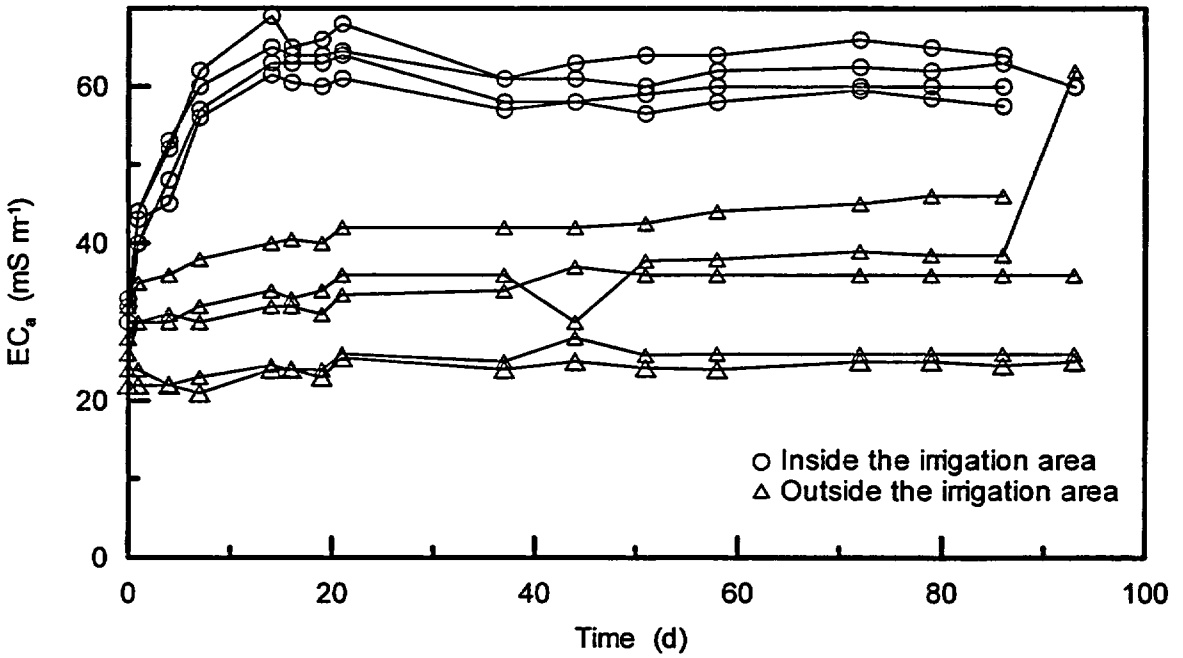

Figure 3.8-5. EM-31 horizontal measurements on Y = 10.3 m transect during Experiment 1.

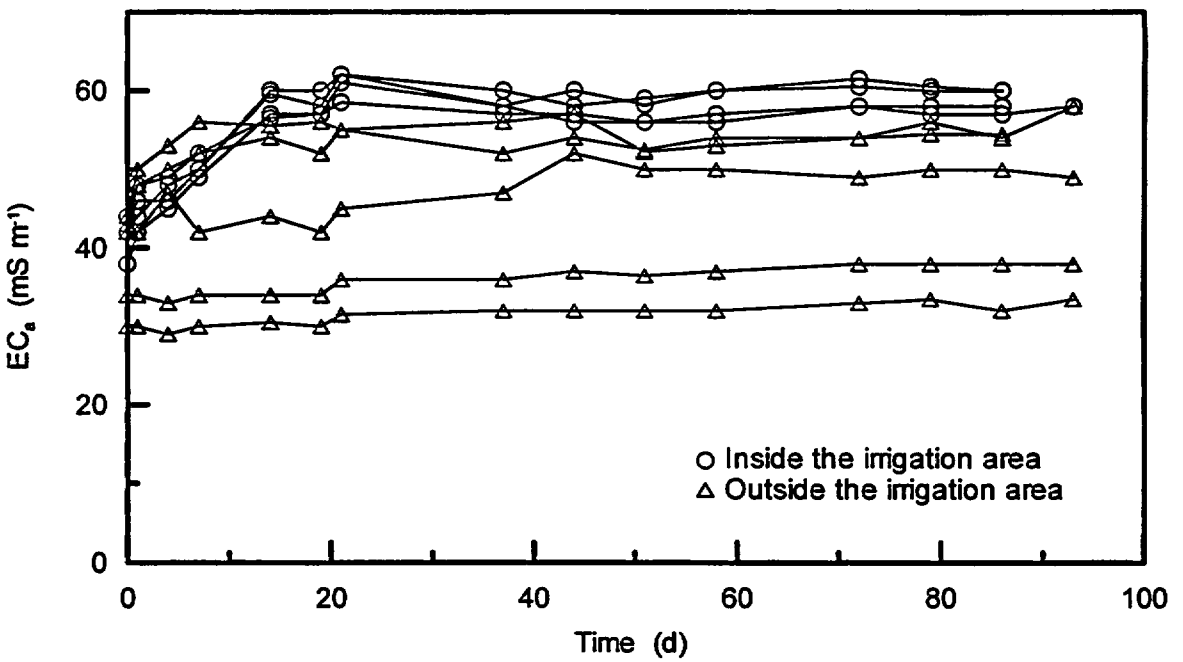

Figure 3.8-6. EM-31 vertical measurements on Y = 10.3 m transect during Experiment 1.

mS/m); the average of the EM-38 vertical measurements was 35.7 mS/m (standard deviation = 5.9 mS/m). The average readings from the EM-31, in horizontal and vertical modes, were 47.6 mS/m (standard deviation = 4.9 mS/m) and 51.6 mS/m (standard deviation = 2.9 mS/m), respectively. The lateral variability was still not significant for any mode of two EM instruments. However, the EC contours for EM-38 (Figures 3.8-7 to 3.8-10) show a low EC zone in the northern part of the plot on Day 0, which was also found in a pre-survey conducted in December 1995. Table 3.8-2 lists the dates for measurements.

Saline water with EC = 2 mmho/cm was applied to the plot for 7 days, and lower salinity irrigation water (EC = 1 mmho/cm) applied thereafter. Daily EM response contours are shown in Figures 3.8-7 to 3.8-10. Values of EC_a increased by a range of 10-20 mS/m, and were less than those shown for Experiment 1, because the increase of solution EC was not as great as the water content increase for Experiment 1. However, the EM response did increase inside the plot during the saline water application and the water application boundary can be clearly observed from the contour plots. After flushing the saline water downward through the soil profile, EC_a values slowly decreased. This was a result of the decrease in soil water salinity, as the soil water content was unchanged.

During Experiment 2 redistribution, EC_a values from EM-31 horizontal and vertical modes at transect Y = 10.3 m decreased slowly as the soil water drained slowly downward (Figure 3.8-11 and 12). This change in EC_a was always within the 10 mS/m range.

3.8.3 Use of EM to Monitor Soil Water Conditions

Quantitatively, it is difficult to use the EM response to determine the absolute soil water content or storage in the soil profile. However, a general trend can be observed from Figures 3.8-1 to 3.8-4. In the northern central part of the plot, low EC_a values were observed at all times. Since EC_a change during Experiment 1 was primarily a response of change in soil water content and storage in the soil profile, the low EC_a area indicated the presence of soil material with low soil water storage. Distinct soil texture and soil hydraulic properties should be expected in this region. To evaluate the potential of using EM measurements to monitor soil water content and storage changes, the correlation between EM and neutron probe water content or counts was studied. Figures 3.8-13 to 3.8-15 show the relationship between soil water storage using the neutron probe at three access tubes (#402, #425, #442), versus the change in EC_a measured using the EM-38 instrument. The correlation coefficient shown on each plot demonstrates a strong relationship between EM response and water storage measured with the neutron probe.

As stated above, the dominating factor for the increase of EC_a during Experiment 1, was the increase in soil water content and storage in the soil profile. Volumetric water contents, measured using neutron probe, increased from 10-12% to 20-25 % during the water application. If we assume that other conditions in the soil profile remained constant, for example clay content and cation exchange capacity, then the change in EC_a would be caused primarily by the water content increase. There were variable responses inside the irrigation area, indicating that changes in water content were variable. Thus, we selected three EM monitoring points according to the EM response contour plots. The nearest vertical neutron probe access tubes were chosen to represent EM monitoring points (#425, #432, #442 represent the high, intermediate, and low EC_a regions, respectively).

After Day 1 of water irrigation, EC_a values responded to the increased soil water content. Water content and storage in the soil profile increased until steady state was reached, signaling that EM readings should also be constant in time. The EM-38 in horizontal mode, with the shallowest penetration or response depth, thus reached steady state first, and had the largest increase in EC_a with time as compared to the EM-31 in either mode. Figures 3.8-16 to 3.8-18 showed that the EM-38 horizontal mode reached its highest value quickly, and remained relatively unchanged thereafter. The EM-38 vertical reading reached its greatest value next, followed by the EM-31 horizontal, which responded less for the early period of water application. The EM-31 vertical had the most gentle slope and increased for the longest time period during water application. The wetting front depth may be approximated by monitoring the stabilizing time for each mode of EM-31 and EM-38. Using this approach, we approximated the depth of the wetting front in the immediate vicinity of access tubes #425, #432, and #442 (Table 3.8-3). The approximation clearly demonstrated that the location near access tube #442 had the lowest EC_a readings and the fastest wetting front velocity, while tube #425 had the highest EC_a readings and

Table 3.8-2. Sampling schedule for the electromagnetic induction measurements during Experiment 2.

Date	Time (days)	EM-31 Vertical	EM-31 Horizontal	EM-31 Sounding†	EM-38 Vertical	EM-38 Horizontal	EM-38 Sounding
12/02/97	-1	✓	✓	✓	✓	✓	✓
12/04/97	1	✓	✓	✓	✓	✓	✓
12/05/97	2	✓	✓	✓	✓	✓	✓
12/06/97	3	✓	✓	✓	✓	✓	✓
12/07/97	4	✓	✓	✓	✓	✓	✓
12/08/97	5				✓	✓	✓
12/09/97	6	✓	✓	✓	✓	✓	✓
12/10/97	7	✓	✓	✓	✓	✓	✓
12/11/97	8	✓	✓	✓	✓	✓	✓
12/15/97	12	✓	✓	✓	✓	✓	✓
12/16/97	13				✓	✓	✓
12/17/97	14				✓	✓	✓
12/18/97	15	✓	✓	✓	✓	✓	✓
12/21/97	18	✓	✓	✓			
1/05/98	33				✓	✓	✓
1/06/98	34	✓	✓	✓	✓	✓	✓
1/07/98	35				✓	✓	✓
1/08/98	36	✓	✓	✓	✓	✓	✓
1/09/98	37				✓	✓	✓
1/12/98	40	✓	✓	✓			
1/13/98	41				✓	✓	✓

† - refers to vertical profiling measurements taken at five locations on the irrigated plot.

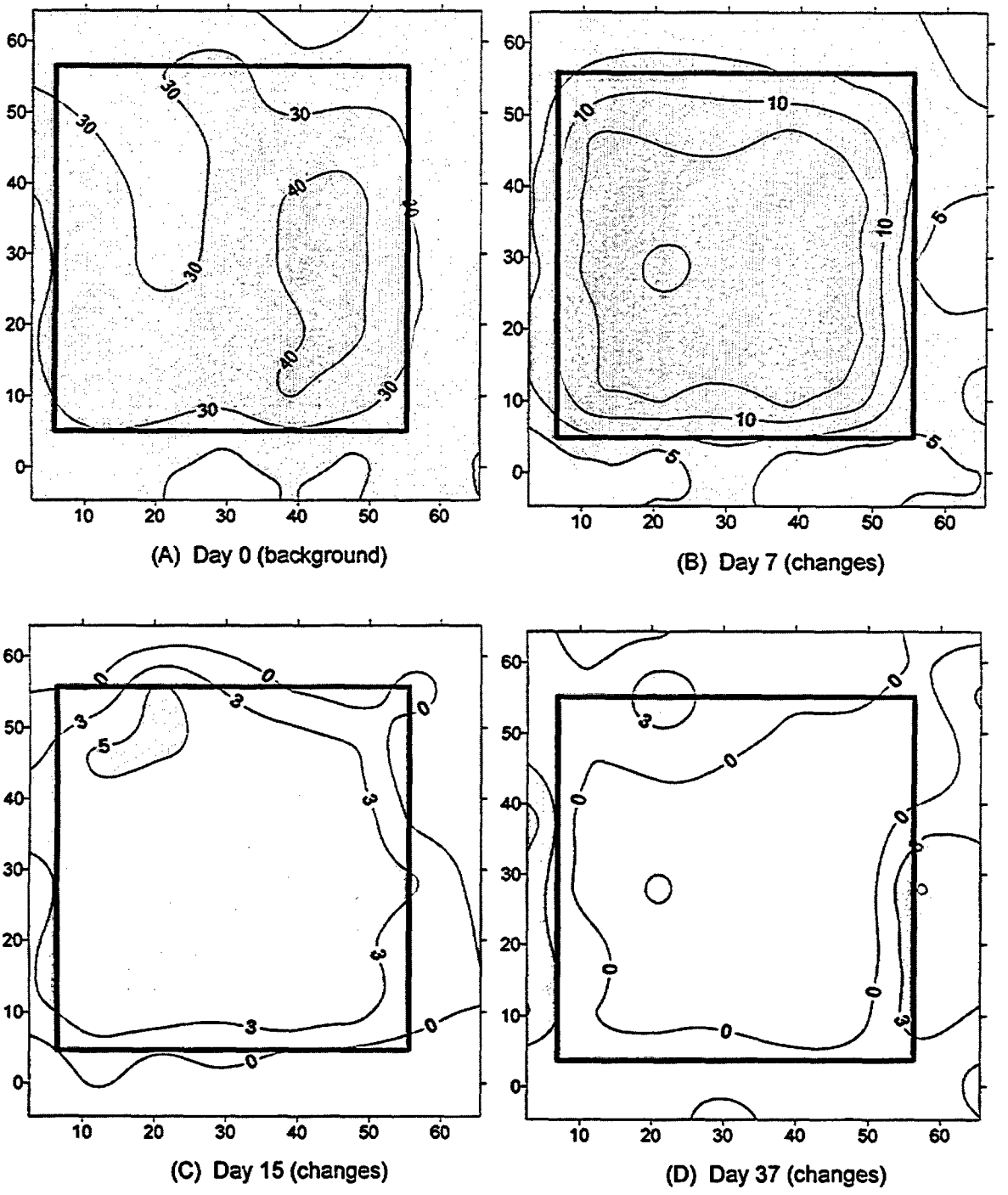

Figure 3.8-7. EM-38 horizontal measurement contours on background and changes in EC_a during Experiment 2. Note that contour levels for (A) are different than for (B) through (D). Changes indicate day's reading minus background value.

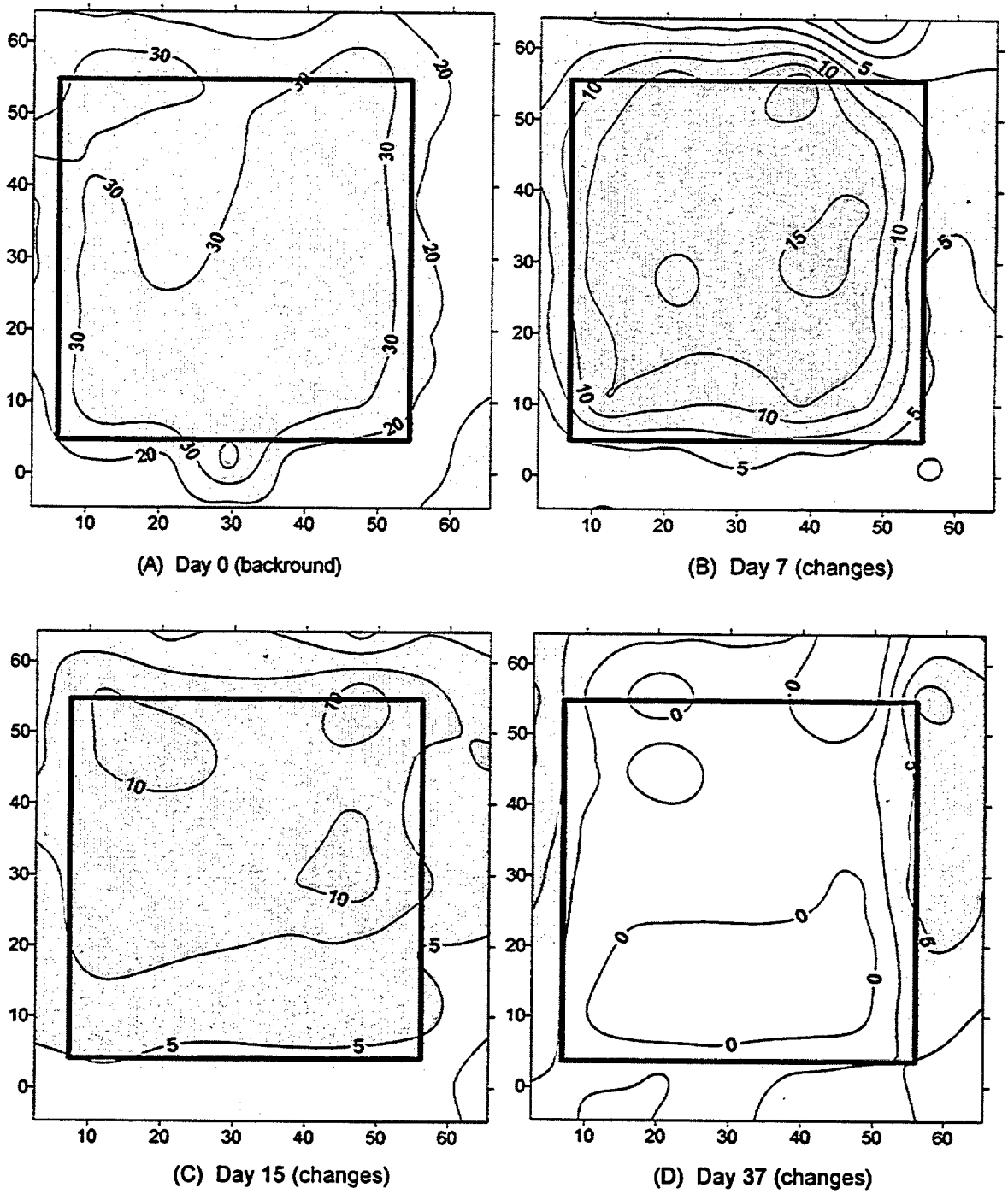

Figure 3.8-8. EM-38 vertical measurement contours on background and changes in EC_a during Experiment 2. Note that contour levels for (A) are different than for (B) through (D). Changes indicate day's reading minus background value.

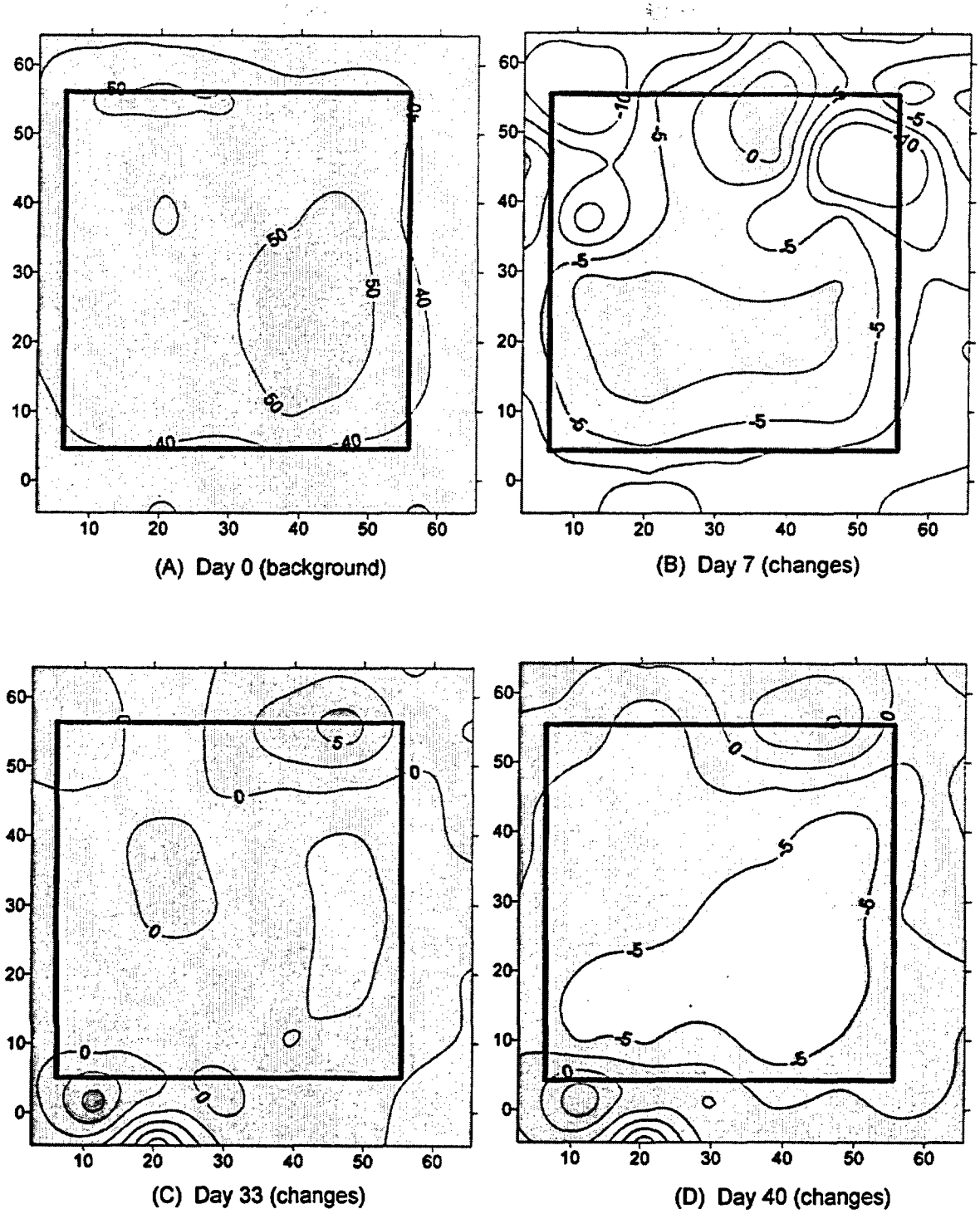

Figure 3.8-9. EM-31 horizontal measurement contours on background and changes in EC_a during Experiment 2. Note that contour levels for (A) are different than for (B) through (D). Changes indicate day's reading minus background value.

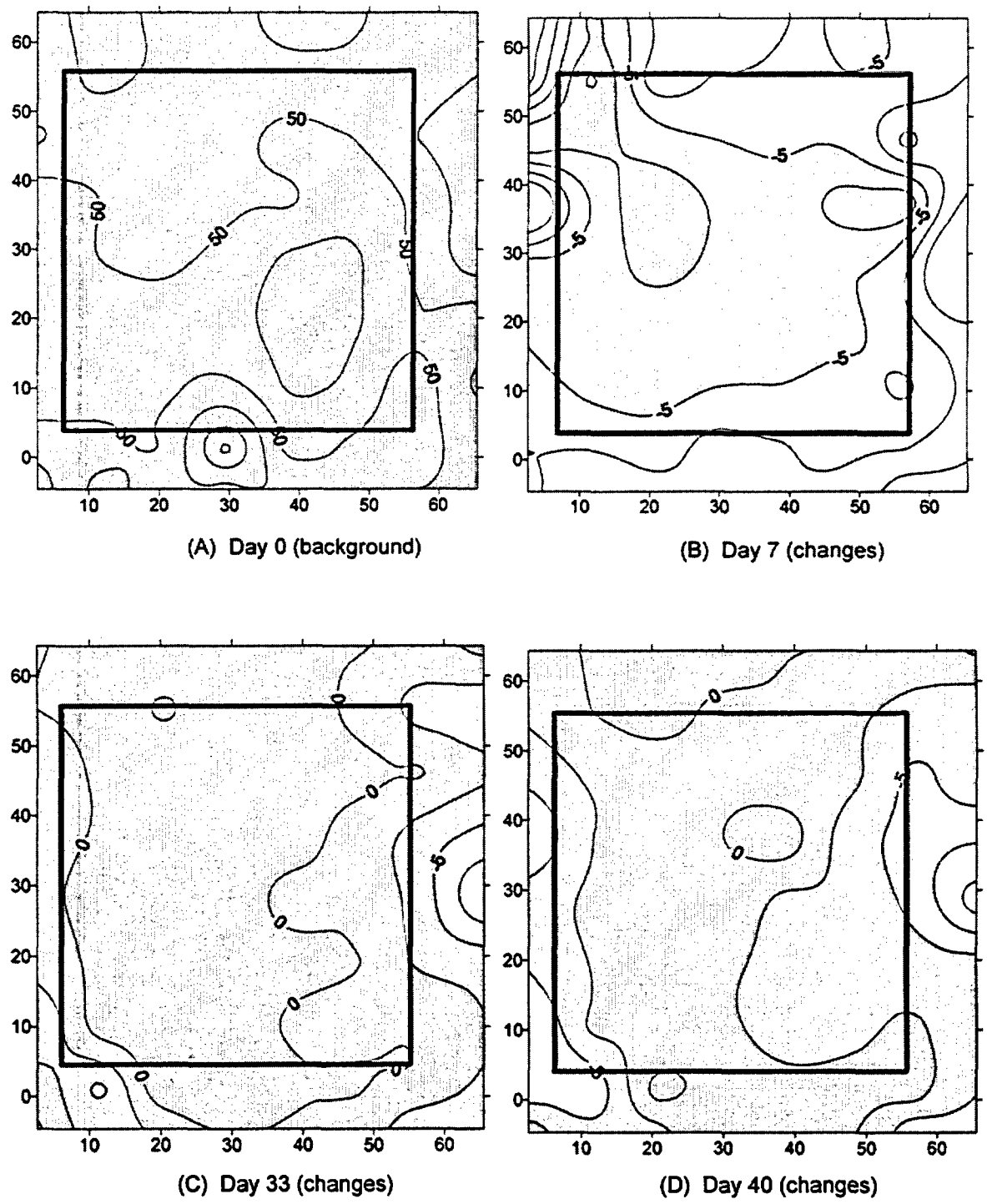

Figure 3.8-10. EM-31 vertical measurement contours on background and changes in EC_a during Experiment 2. Note that contour levels for (A) are different than for (B) through (D). Changes indicate day's reading minus background value.

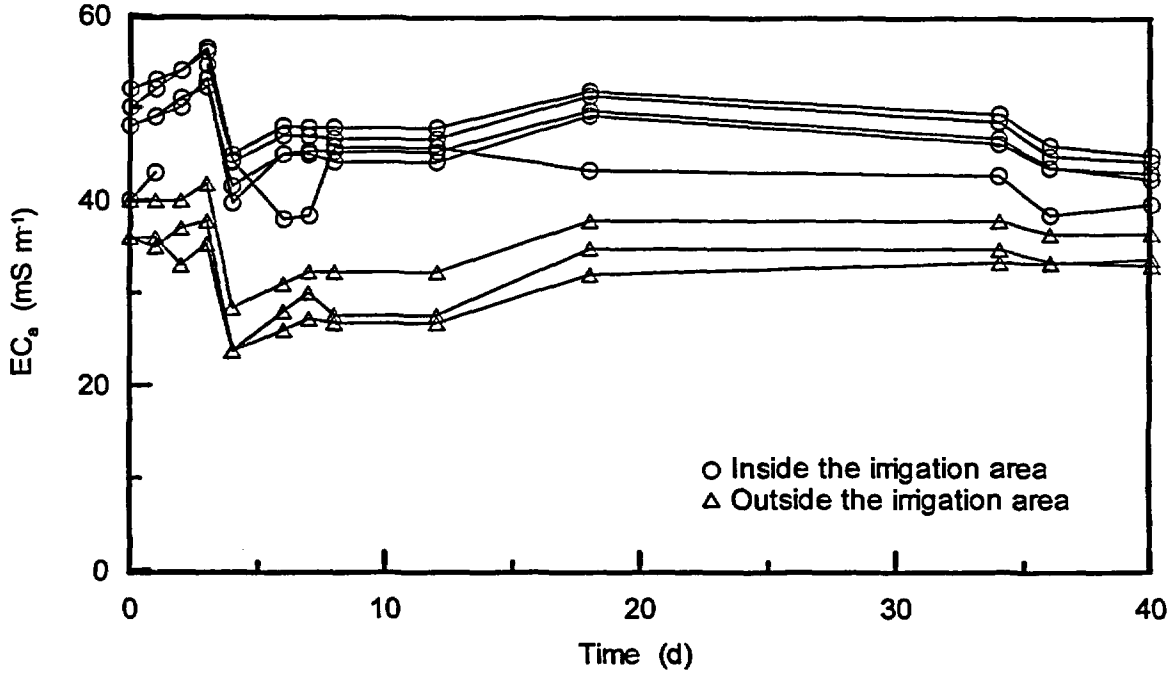

Figure 3.8-11. EM-31 horizontal measurements on Y = 10.3 m transect during Experiment 2.

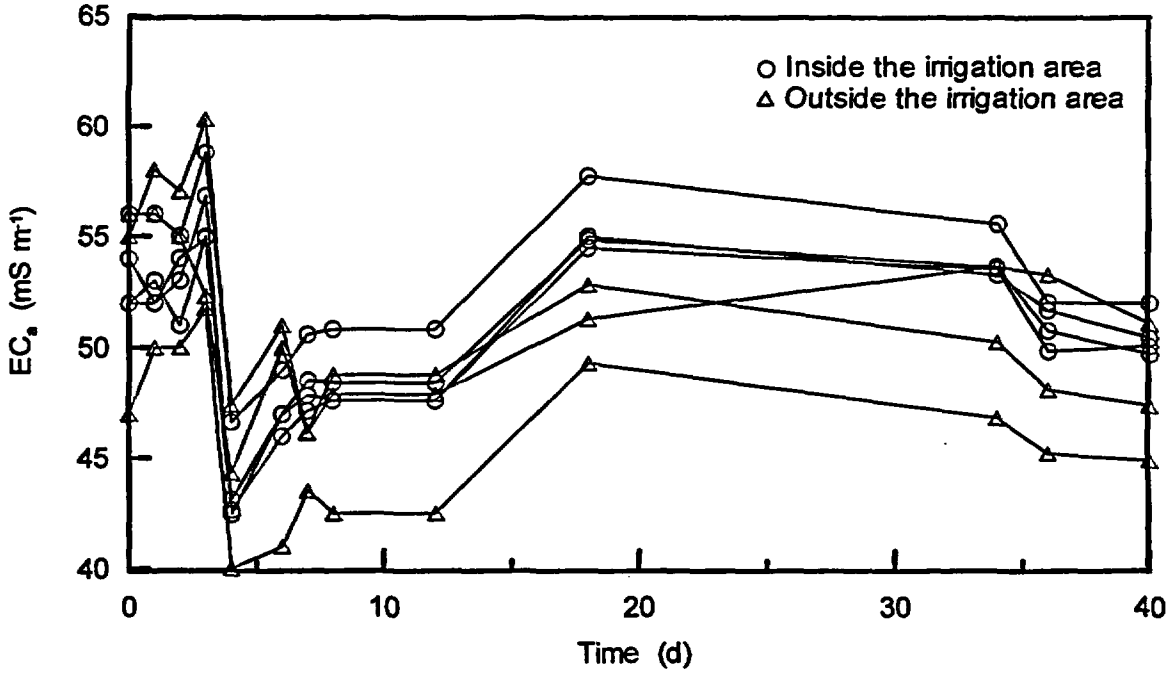

Figure 3.8-12. EM-31 vertical measurements on Y = 10.3 m transect during Experiment 2.

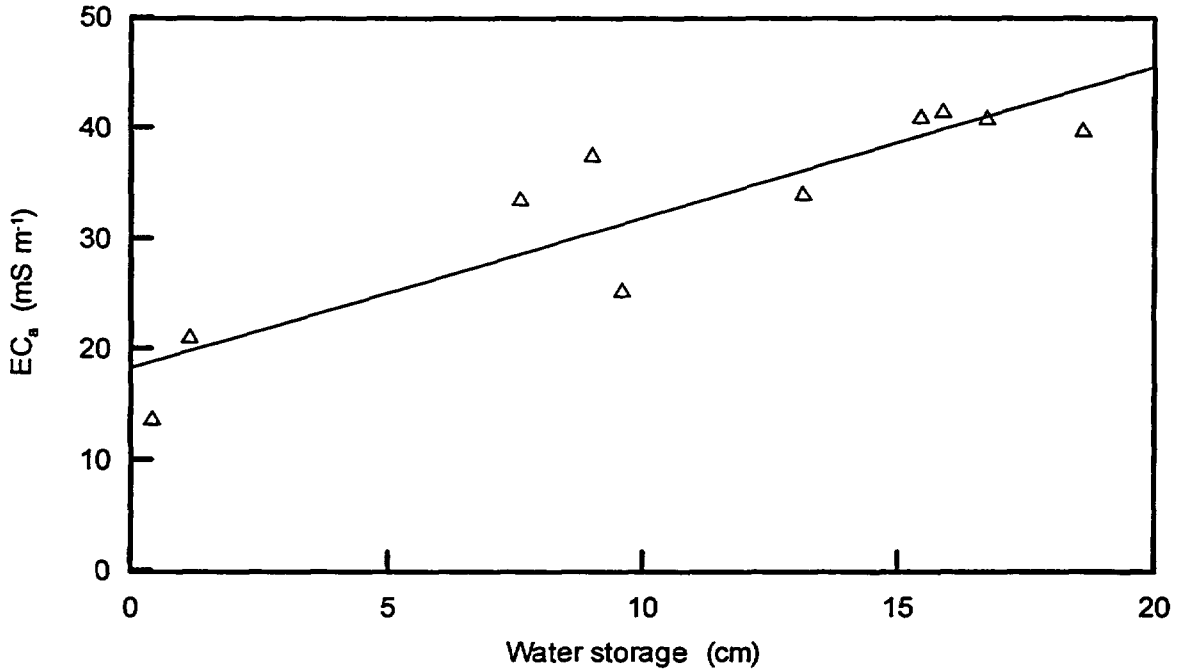

Figure 3.8-13. Correlation between EM-38 horizontal measurements and soil water storage (from neutron probe) at vertical neutron probe access tube #402 of Experiment 1.

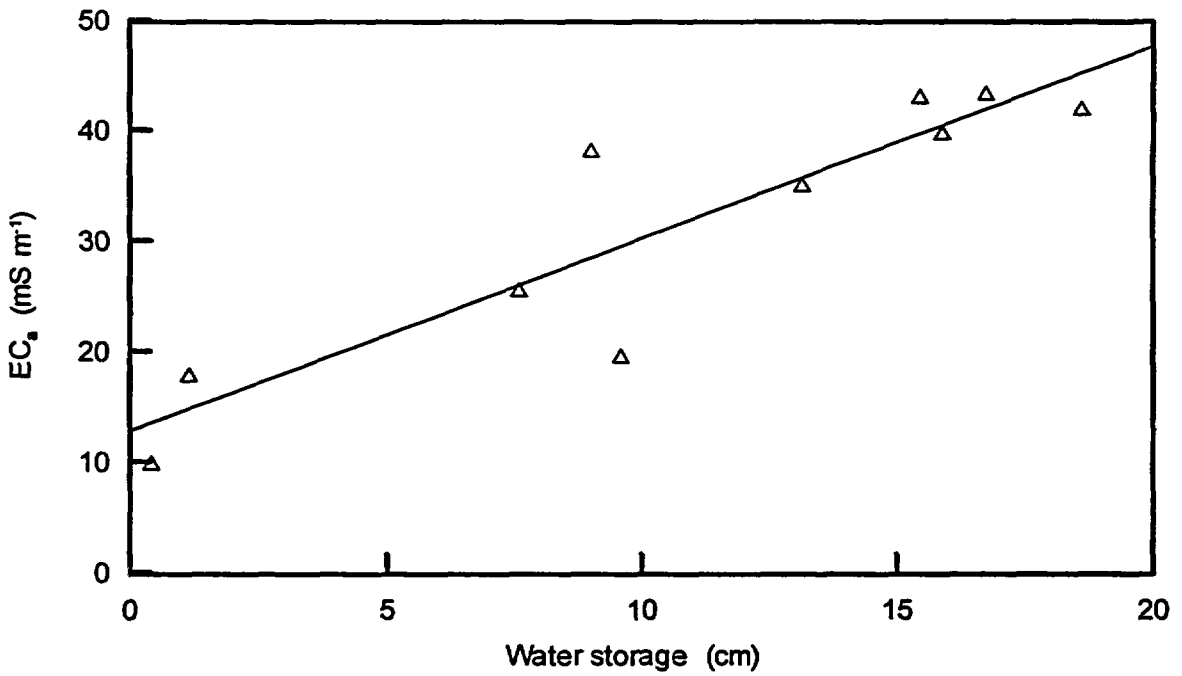

Figure 3.8-14. Correlation between EM-38 horizontal measurements and soil water storage (from neutron probe) at vertical neutron probe access tube #425 of Experiment 1.

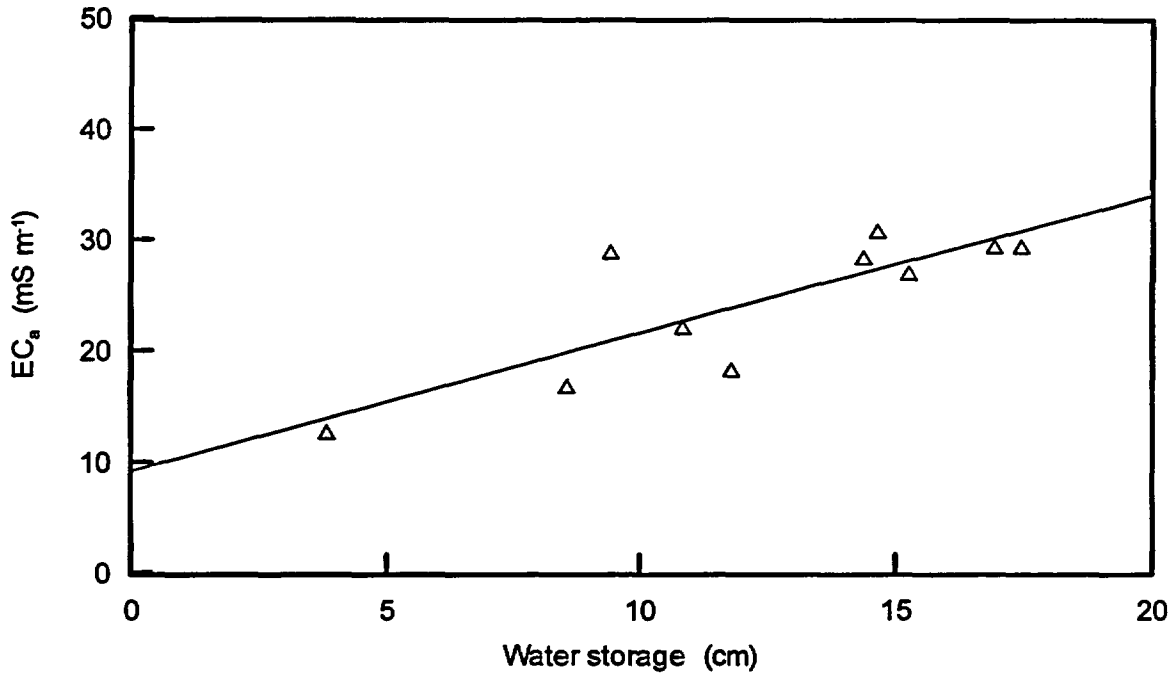

Figure 3.8-15. Correlation between EM-38 horizontal measurements and soil water storage (from neutron probe) at vertical neutron probe access tube #442 of Experiment 1.

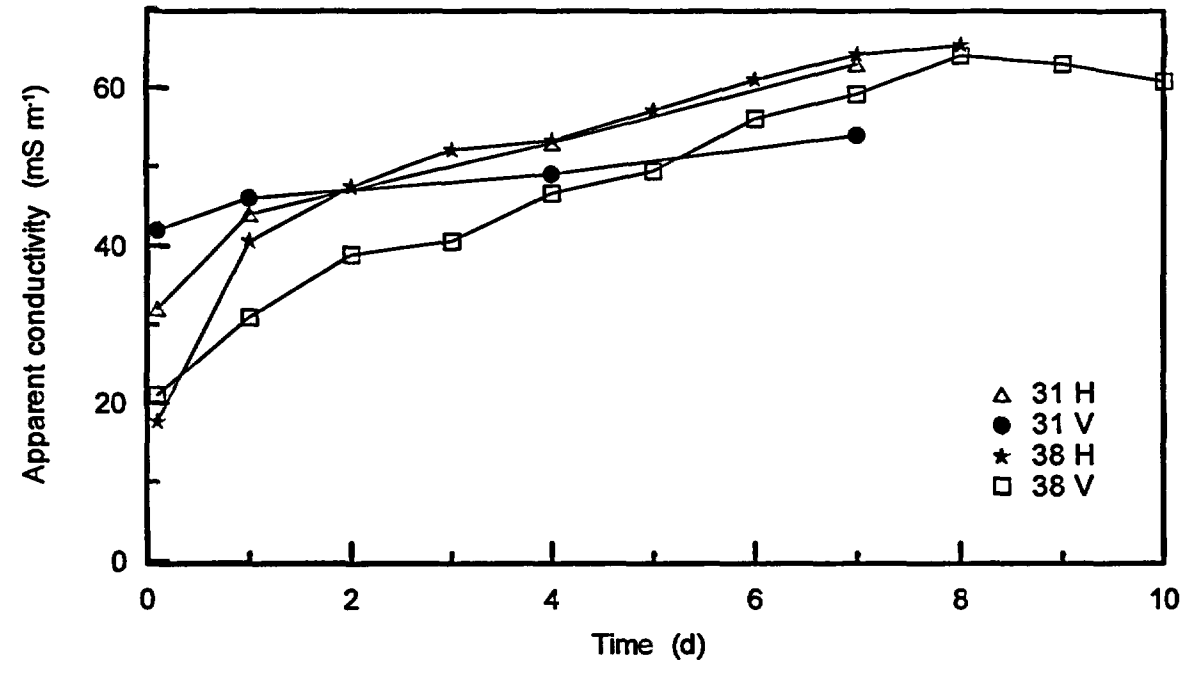

Figure 3.8-16. EM measurements at vertical neutron probe access tube #425 during Experiment 1.

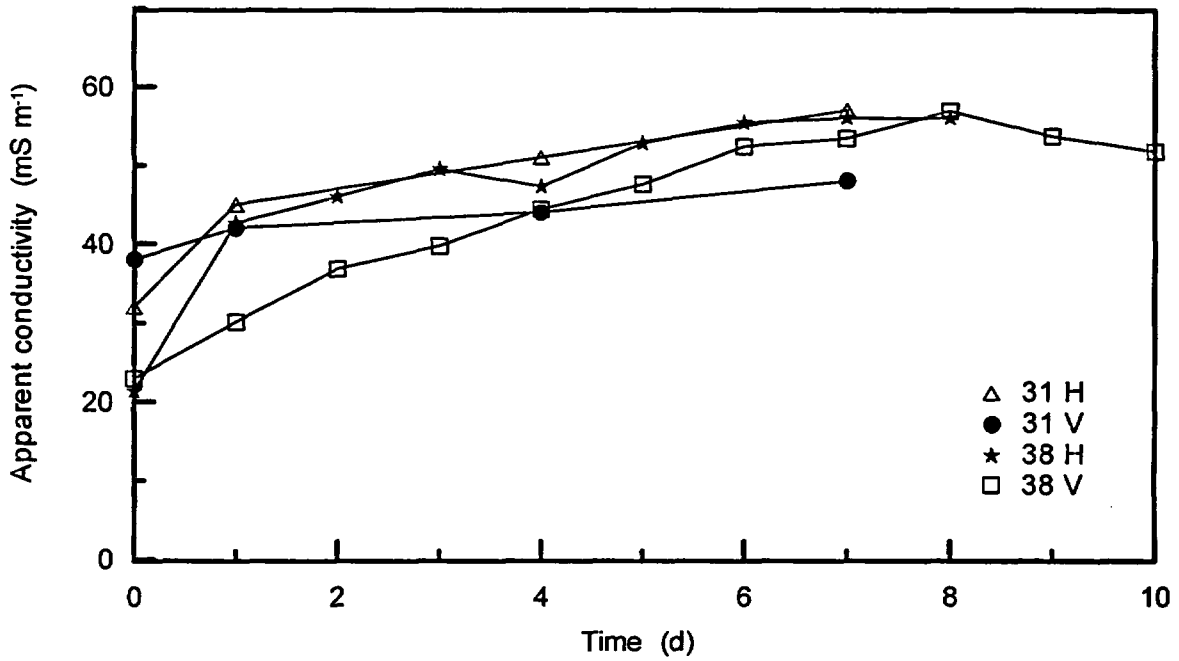

Figure 3.8-17. EM measurements at vertical neutron probe access tube #432 of Experiment 1.

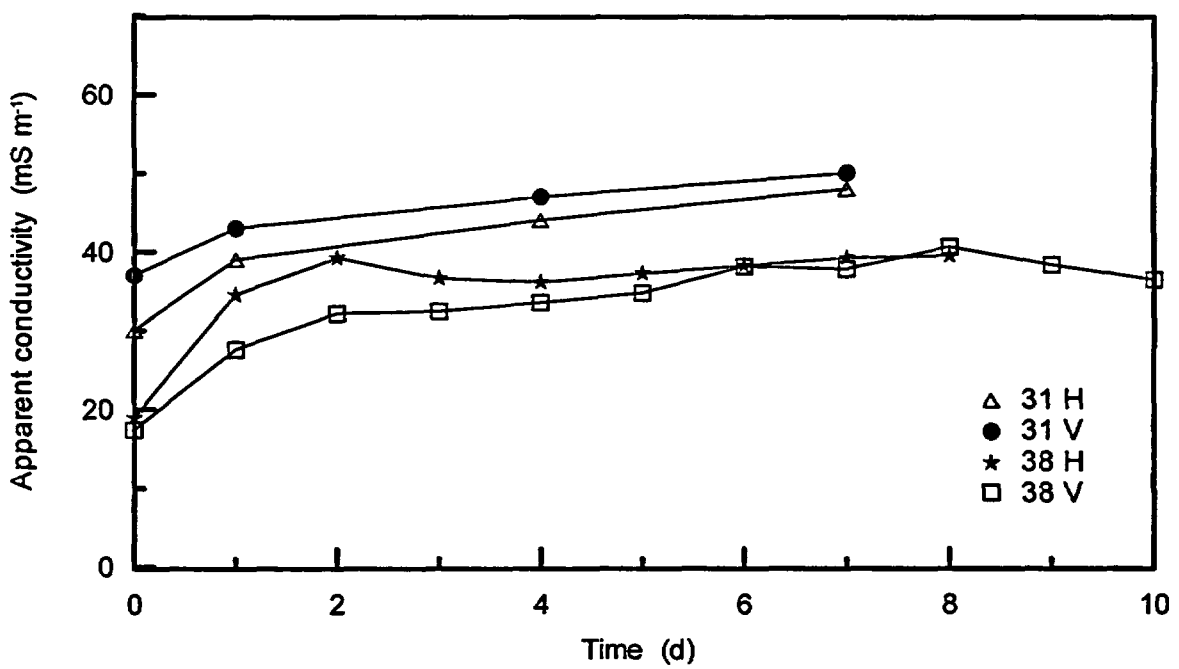

Figure 3.8-18. EM measurements at vertical neutron probe access tube #442 during Experiment 1.

Table 3.8.3. Approximate arrival times of wetting front at different depths.

Depth (m)	0.75	1.5	3	6
VNP-425	NA	8 days	14 days	>20 days
VNP-432	6 days	8 days	7-14 days	>14 days
VNP-442	2 days	6 days	14 >> but >7 days	14> but >> 7 days

the lowest wetting front velocity. The ability to approximate the wetting front depth using a non-invasive monitoring technique could be beneficial when evaluating water content changes in near-surface soil material.

The results from Experiment 2 showed that the use of saline irrigation water, with high EC, did cause higher EC_a readings. The response was relatively small (from 1 to 2 mmho/cm), and was masked somewhat by the increase in EC_a from changes in water content. However, if the soil water content was constant in time, then changes to EC_a could be attributed solely to change in salinity. It would be difficult, in this case, to track the saline water front using this method. Because the water content and soil water EC were changing simultaneously, we cannot isolate either factor using the EM response. However, the change in soil water EC played a less important role in Experiment 2, than during Experiment 1, given that the soil water content increased by only 0.03-0.05 $m^3 m^{-3}$ versus 0.10-0.12 $m^3 m^{-3}$ for Experiment 1.

3.9 Crosshole ERT Data

3.9.1 Experiment 1

An initial background data set was collected on April 11, 1997, before application of water to the soil. This background data set was used for determining the change in electrical resistance during the experiment. Figure 3.9-1 shows the inverted data set for 5 2-D planes, each oriented E-W at Y = 30 m. The inverted ERT images corresponded well with the EM-39 data collected from the deep neutron probe access tubes adjacent to the ERT boreholes (Stubben and LaBreque, 1997; data not shown). The images also correspond well with the known geology at the site. The water table, located approximately 11.5 m below ground surface, was visible in the ERT images as a low resistivity layer of about 10 Ohm m, starting at between 11 and 12 m depth, the deeper gravel layer is shown clearly in the ERT images as a high resistivity layer of approximately 100 Ohm m. This layer is fairly continuous electrically and appears to be dipping slightly toward the east. The sand lens, known to exist from 3 - 5 m depth, is visible as a strongly conductive layer of approximately 10 Ohm m. The upper gravel layer, which is lithologically continuous from about 3 - 4 m depth, is seen as a faint and not very continuous layer of over 30 Ohm m between 3 and 4 m depth. This layer is less continuous electrically, probably due to a higher clay content.

Data sets were collected during Experiment 1 on Days 4, 8, 11, 18, 25, and 32. Full inversion of all the time periods was not completed at the time of this writing, owing to the very complicated computer work and the lack of personnel. However, two data sets should provide representative responses of the ERT system to water application and subsequent infiltration into the soil, and are shown in Figures 3.9-2 and 3.9-3 for Days 8 and 18, respectively. Both figures plot the change in electrical conductivity with depth, as a percent of the background values; thus, increases in conductivity, from those measured before water infiltration, are plotted as positive values and vice versa. According to Stubben and LaBreque (1997), the wetting front should be in the immediate vicinity of the contour line corresponding to 30% increase in conductivity. The lateral offsets between the ERT boreholes and neutron probe tubes were 3.5 m for pairs ERT-4 and access tube #423 and 1 m for the other pairs.

Table 3.9-1 lists the wetting front depths estimated from the ERT inversion data and the neutron probe data. The data suggest that the ERT method was very effective at determining the estimated depth of the wetting front. In most cases, the ERT method was within 0.5 m of the depth measured with the neutron probe. However, we also noted that the wetting front depth was underestimated in all but one case. In the case of ERT-5 and ERT-4 on Day 18, it appears that the wetting front depth was significantly underestimated. Using the neutron probe method, we found that the water content change was less than 0.05 $m^3 m^{-3}$, and usually less than 0.025 $m^3 m^{-3}$, suggesting that a lower limit exists for detecting change in soil water content. In the eastern portion of the plot, where slower wetting fronts corresponded to higher soil water deficits, the ERT method was quite accurate in the determination of wetting front depth. However, toward the western portion of the plot, where we observed very rapid movement of water and correspondingly smaller changes in water content, the ERT method did not appear to be as robust.

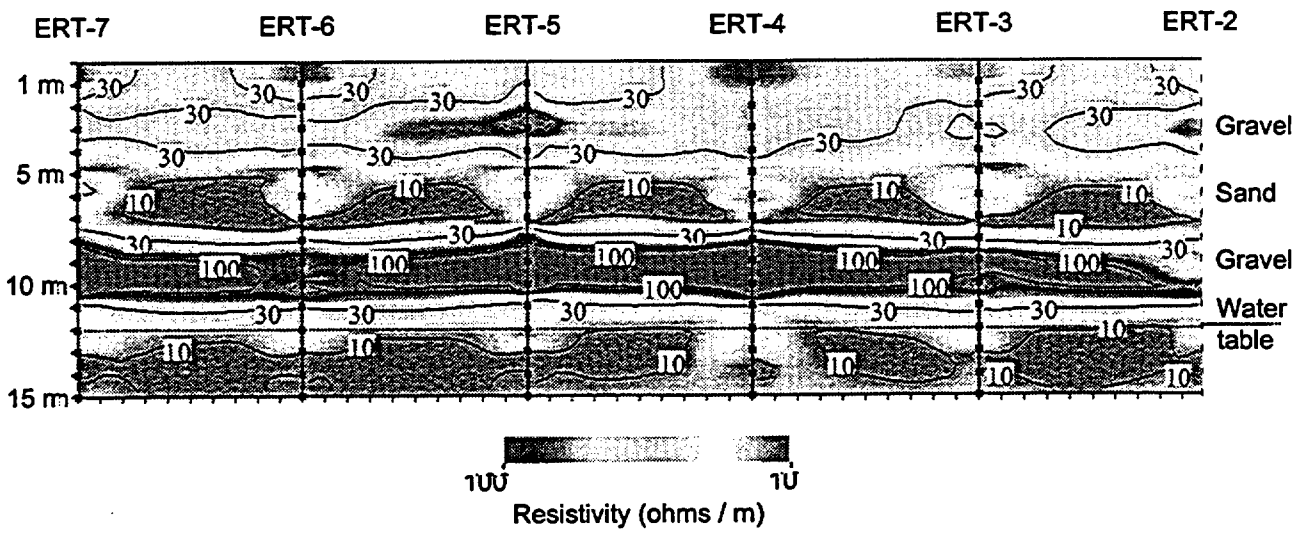

Figure 3.9-1. Inversion results for the background data set. Numbers on plot are in units of Ohm-m.

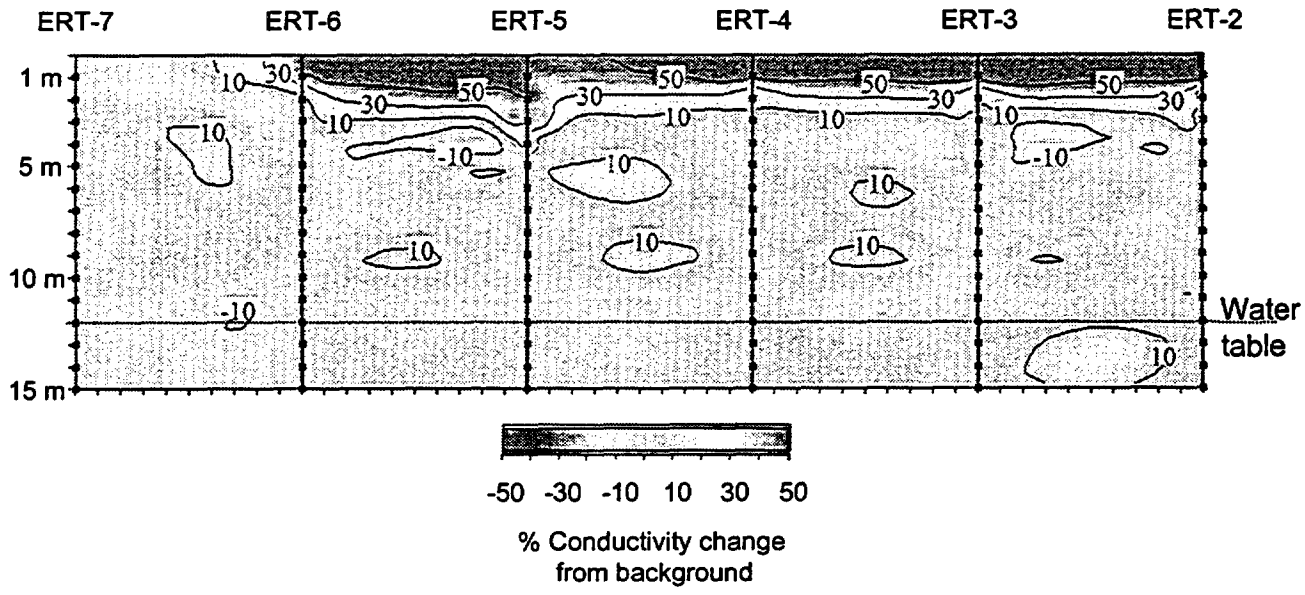

Figure 3.9-2. Inversion results for Day 8 during Experiment 1, and are shown as percent difference in conductivity from the background data set.

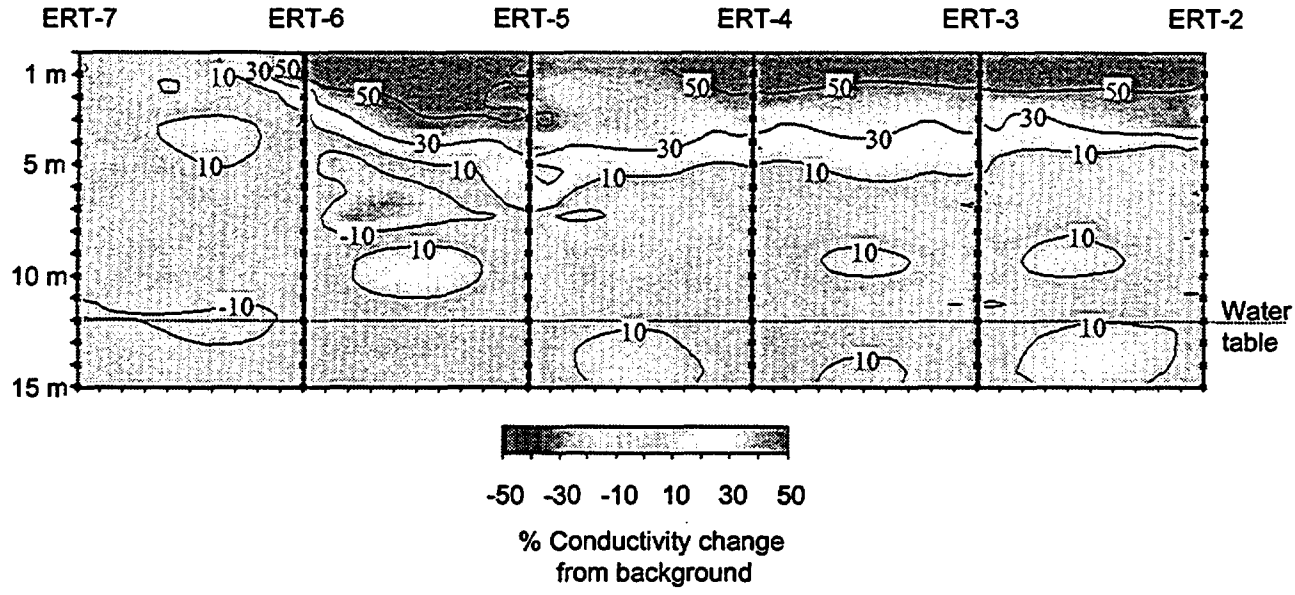

Figure 3.9-3. Inversion results for Day 18 during Experiment 1, and are shown as percent difference in conductivity from the background data set.

Table 3.9-1. Wetting front depths as interpreted using the ERT system and adjacent vertical neutron probe access tubes during Experiment 1. All values in meters.

Instrument	Day 8	Day 18†
ERT-6	1.5	1.5
access tube #421	1.0	n/a‡
ERT-5	3.0	4.5
access tube #422	>3.0	8.0
ERT-4	1.5	3.5
access tube #423	1.75	5.75
ERT-3	1.5	3.5
access tube #424	2.0	n/a
ERT-2	1.5	4.0
access tube #425	2.0	4.0

† - Neutron probe data collected on Day 17.
‡ - Wetting front depth beyond end of shallow access tubes

3.9.2 Experiment 2

No inverted data are available for Experiment 2; thus, no additional information on the ERT will be provided.

3.10 Gas Flow Studies

The results of both the pneumatic and the atmospheric pumping studies are presented as a standalone document found in Appendix C. However, we briefly summarize the findings below.

3.10.1 Pneumatic Tests

Pneumatic tests were conducted in February 1998. We measured flow rate, pressure, air temperature at the well heads and at depth, and subsurface pressures at 2.5 m depth intervals in 3 monitoring wells. Results from a typical pneumatic test are shown in Figure C-3. The initial small step increase in injection pressure (a) corresponds to the pump being switched on and the second step increase (b) corresponds to connection of the pump to the well. Pressures were highest at 5 m depth, corresponding to the injection depth, and decreased with distance from the injection well. Results of the analyses indicate that the horizontal intrinsic permeability ranged from 4.8 to 6.7 $x10^{-12}$ m^2 (equivalent to between 360 and 505 cm d^{-1} at 15.6°C). The vertical permeability ranged from 1.2 to 1.8 x 10^{-12} m^2 (equivalent to between 90 and 135 cm d^{-1}), or about 2 to 3 times less than the horizontal permeability. The range of values is within the range expected for the predominantly sandy-loam and loamy-sand soils at the site.

3.10.2 Atmospheric Pumping

The maximum pressure variation recorded at the surface during the field monitoring period was 1,000 Pa (10 mbar) in a 24 h period (Figure C-4), when the amplitude of the pressure variation at the surface (ΔP) was equal to 500 Pa and at different depths ranged from 489 to 497 Pa. The maximum differential pressures measured at the 4 different depths ranged from 3 to 11 Pa during this period, which approached the detection limits of the differential pressure transducers used to monitor these pressure fluctuations. Though these pressures resulted in an amplitude differential of very close to unity (e.g., 497 Pa / 500 Pa = 0.994), we estimated the vertical air permeability by of Equation C-4 (Appendix C), and found that the minimum vertical air permeabilities ranged from 0.6 to 0.9 $x10^{-12}$ m^2 (equivalent to between 45 and 68 cm d^{-1}) at different depths. These values of vertical permeability are similar to vertical air permeabilities estimated from the pneumatic data. Overall, we found that the attenuation of atmospheric pressure variations was very small, owing to the high permeability of the soil and the relatively shallow water table.

3.11 Transport of Bromide Using Solution Samplers

An important component of this field research was the use of a miscible tracer and salt during the irrigation phases of both experiments, and the subsequent subsurface monitoring. Bromide (as $NaBr_2$) was added to the irrigation water during Experiment 1. Soil solution samplers installed in three monitoring strategies (monitoring trench, monitoring islands, and deep boreholes) were periodically used to collect soil pore water. Monitoring wells were also used for collecting groundwater samples. Samples were transported to the laboratory and analyzed for tracer concentration. The results of the analyses are needed for estimating dispersivity and retardation factors, both important parameters for estimating the transport rates of constituents in subsurface environments. The sections below are divided according to the three strategies listed above, then subdivided according to the tracer being used. Sampling schedules are listed for each strategy for both experiments (Tables 3.11-1 and 3.11-2). Note that time will be referred to as combined time, which is continuous from the beginning of Experiment 1, through the end of Experiment 2; using this scale, Experiment 2 began on Day 219.

Subsamples of the irrigation water were collected at the header manifold immediately before the water was delivered to the individual irrigation stations. On several experimental days, we collected samples from each of the six separate stations. Figure 3.11-1 shows the results of the laboratory analyses for Experiment 1 bromide input. Numbers next to the data points represent the number of subsamples collected on days, when more than one sample was collected. Some variability in bromide concentration was caused primarily by difficulties in controlling the exact fluid volume in the mixing tanks, especially on Day 12, when water overflowed the top of the mixing tanks. The

Table 3.11-1. Schedule of soil solution sampling for three monitoring strategies. The numbers reflect the quantity of samples analyzed for bromide during Experiment 1. No samples were collected from the monitoring wells.

Time (days)	Buried Trench	Monitoring Islands	Deep Boreholes
4	0	3	0
5	0	4	0
6	0	6	0
7	2	8	0
8	2	10	0
9	3	11	0
10	4	12	0
11	5	20	0
12	5	25	0
13	6	28	0
14	7	30	0
15	9	30	0
16	11	29	13
17	11	30	14
18	11	30	9
19	11	30	16
20	10	30	17
21	11	30	18
22	11	30	18
23	10	30	16
24	11	30	18
26	10	30	18
28	10	30	18
30	10	28	18
32	10	29	18
35	9	27	23
38	11	30	24

Time (days)	Buried Trench	Monitoring Islands	Deep Boreholes
42	11	30	26
46	10	30	25
51	10	29	27
58	11	27	26
65	11	30	25
72	12	29	23
79	12	30	25
86	12	30	26
93	11	30	27
Total	300	898	488

Table 3.11-2. Schedule of soil solution sampling for four monitoring strategies. The numbers reflect only those samples analyzed for bromide during Experiment 2.

Time of Exp. 2 (days)	Combined Time (days)	Buried Trench	Monitoring Islands	Deep Boreholes	Monitoring Wells
-7	212	0	0	0	8
1	220	0	23	0	0
3	222	0	5	0	0
4	223	0	8	0	0
5	224	0	9	0	0
6	225	12	12	0	0
7	226	9	21	0	0
8	227	10	26	9	0
9	228	0	16	12	0
10	229	10	29	0	0
11	230	0	0	14	0
12	231	12	27	0	0
13	232	0	0	17	11
14	233	12	28	0	0
15	234	0	0	18	11
16	235	8	29	0	0
17	236	0	0	18	11
18	237	12	25	0	0
19	238	0	0	19	11
22	241	0	0	21	11
24	243	0	0	22	11
26	245	0	0	23	11
27	246	0	0	25	11
28	247	0	0	0	11
30	249	0	0	18	11
33	252	0	0	17	11

Time of Exp. 2 (days)	Combined Time (days)	Buried Trench	Monitoring Islands	Deep Boreholes	Monitoring Wells
34	253	0	0	0	10
35	254	0	0	16	11
36	255	0	0	0	11
37	256	0	0	17	11
40	259	0	0	17	11
41	260	0	0	0	11
44	263	0	0	17	11
48	267	0	0	0	11
51	270	0	0	17	11
55	274	0	0	16	10
58	277	0	0	0	11
65	284	0	0	12	11
140	359	0	0	0	11
202	421	0	0	0	11
Total		86	259	345	281

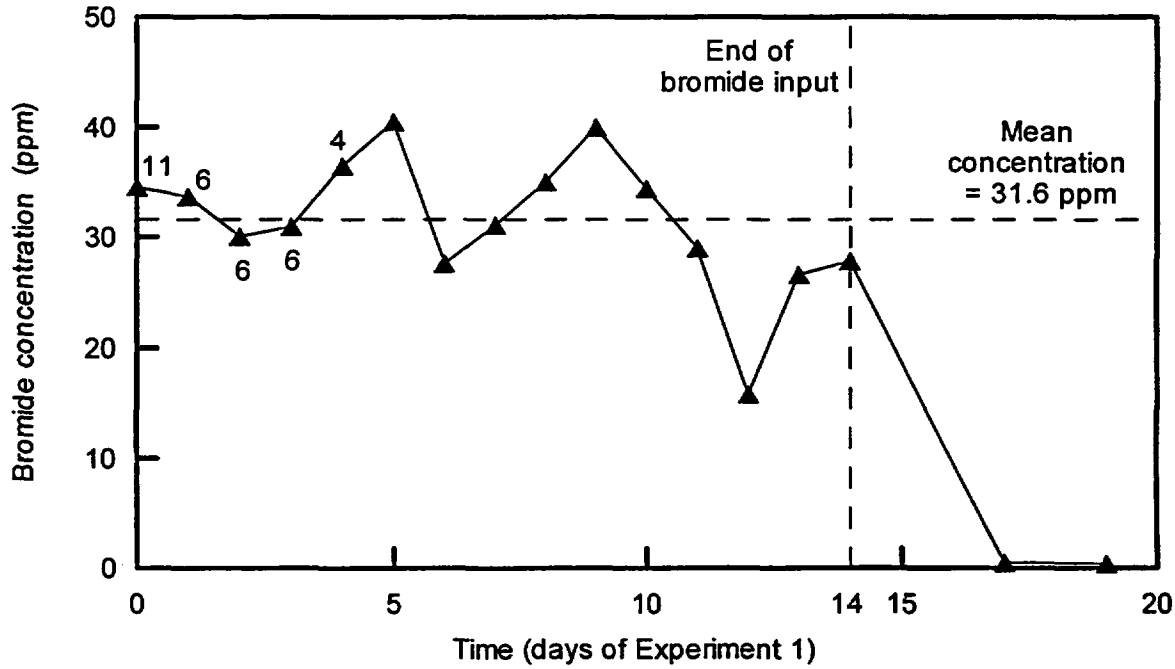

Figure 3.11-1. Bromide concentration measured from samples collected at irrigation header manifold during Experiment 1. Values are arithmetic means of multiple subsamples. Numbers on graph show the number of subsamples collected each day, when greater than one.

average concentration of 31.6 ppm is shown on the figure. We also collected subsamples of the irrigation water used during Experiment 2, and analyzed them for bromide (Figure 3.11-2) in order to quantify background concentrations. We found from analysis of 117 samples collected during the first 19 days of irrigation, that the average background level of bromide was 0.47 ppm (CV = 37.4 %). Initially, elevated concentrations could have been caused by residual bromide in the mixing tanks. However, the tanks had been flushed repeatedly to remove residual bromide, so we believe that the variability is natural and inherent in the irrigation water applied to the field.

3.11.1 Buried Trench

Using the average bromide concentration of 31.6 ppm, we calculated the relative concentration (C/C_0) of all samples analyzed. All subsequent analyses and discussions are in terms of relative concentration. Not all of the trench samplers will be represented graphically. For example, a total of 14 solution samples were collected at location 142 (2.5 m south of the irrigated plot), but because this position was outside the irrigated area, the relative concentrations were very low (maximum = 0.15, average = 0.04) throughout Experiments 1 and 2. The first sample at location 142 was collected on Day 51 (Experiment 1). The location was sampled through most of Experiment 1, and during Experiment 2. No samples were collected at location 141 (5.0 m south of the irrigated plot) during either Experiments 1 or 2.

Figures 3.11-3 through 3.11-6 show bromide breakthrough curves (BTCs) at sampling locations 143 through 153 (Y = 5 - 55 m). Breakthrough of bromide, as defined by $C/C_0 > 0.5$, was not observed for locations at the extreme northern and southern ends of the trench. In these cases (e.g., Y = 5 and 55 m), the relative concentrations were significantly below this criteria at the end of Experiment 2. At the onset of Experiment 2, small increases in relative concentrations were seen at both locations, suggesting that residual bromide was transported laterally and downward toward these samplers. Samples taken on Combined Day 237 (Experiment 2, Day 18 the last day the trench was sampled)

at the southern and northern edges of the irrigated plot show relative concentrations of 0.371 and 0.114, respectively, indicating that bromide had not been fully flushed from the edges of the plot.

Inside the irrigated plot, the breakthrough curves appear Gaussian in shape. Some variability clearly exists in the relative concentrations, but as shown in Figure 3.11-1, input concentrations varied as well. In fact, most the BTCs exhibit fluctuating concentrations after reaching relative concentrations of 1.00 or greater, somewhat similar to the pattern observed for the input concentration. For example, elevated input concentrations of bromide were recorded on Days 5 and 8 (Figure 3.11-1); the final day of bromide input (Day 14) could also be considered a peak, relative to several preceding days. By comparison, Figure 3.11-4B (location 147, Y = 25 m) shows attenuated peaks at Days 51, 65, and 86, with the final peak significantly less in magnitude than the former two, very similar to the pattern observed in the input concentration. However, no statistical analysis of the correlation between input variation and bromide concentrations in the soil at 1.5 m has been made.

Variability of soil properties leads to differences in wetting front velocities, which were observed by a variety of different measurement methods described above. Likewise, pore water or tracer velocity also will be governed by soil hydraulic properties, which vary along the trench. Therefore, the relative positions of BTCs on the time axis are expected to vary as well. Normally, the X-axis is represented in terms of dimensionless time, calculated as a function of pore volume. With Figures 3.11-3 through 3.11-6, we kept the time axis in days to minimize data manipulation. For the locations inside the plot, the sharp rise in relative concentration signaled an unambiguous breakthrough of bromide. Breakthrough of bromide occurred before the end of irrigation, relative concentrations fluctuated around unity, and then slowly tended to decrease during redistribution. Soon after the start of Experiment 2, virtually all locations experienced steep declines in concentration, as tracer-free water flushed residual bromide downward.

Though samples were collected only daily, we can estimate the time when relative concentrations exceeded 0.5. Assuming that bromide adsorption or exclusion is zero, we can calculate pore water velocities as the quotient of the breakthrough time (days), and 150 cm completion depth of the samplers. As shown in Table 3.11-3, tracer velocities vary along the trench, with the highest velocity measured for Y = 45 m, the same location where rapid flow was measured using the TDR, tensiometers, HDS units, and the neutron probe. Average velocities were calculated as 8.8

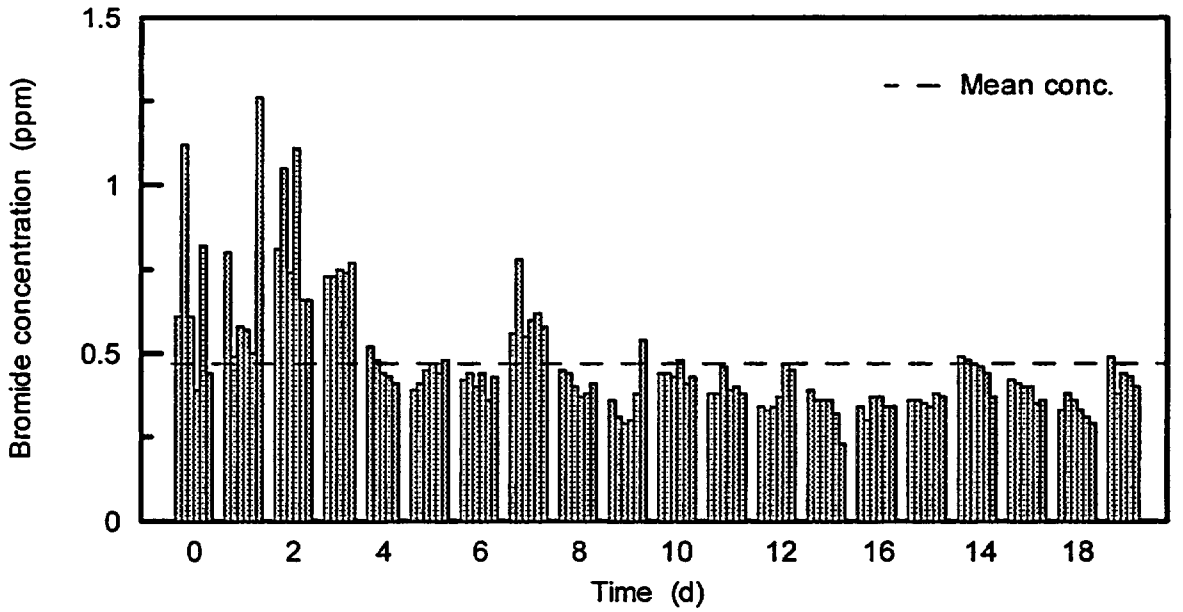

Figure 3.11-2. Bromide concentration of the irrigation water used during Experiment 2. Coefficient of variation = 37.4%.

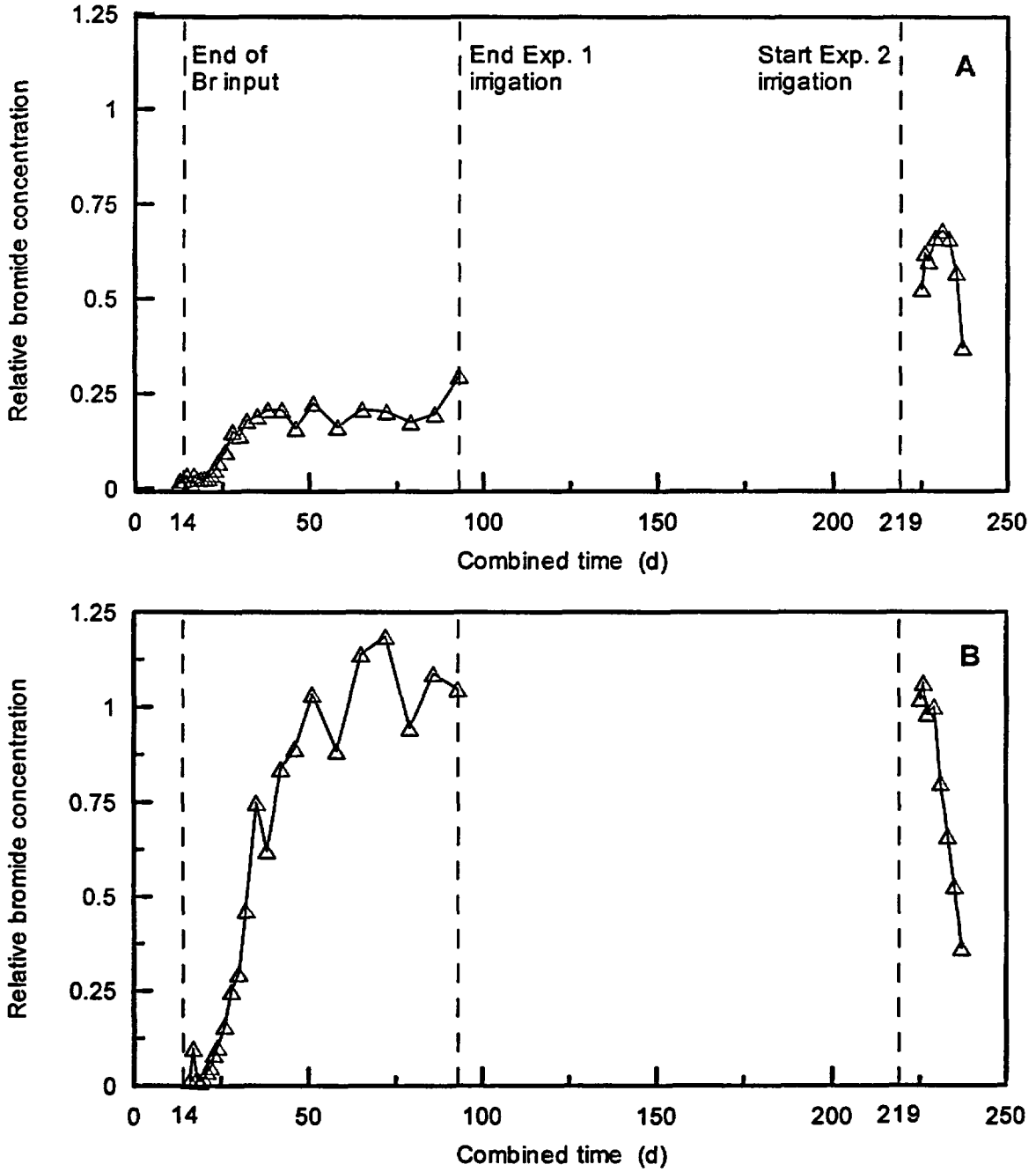

Figure 3.11-3. Relative bromide concentration from trench samplers at (A) Y = 5, (B) 10, and (C) 15 m.

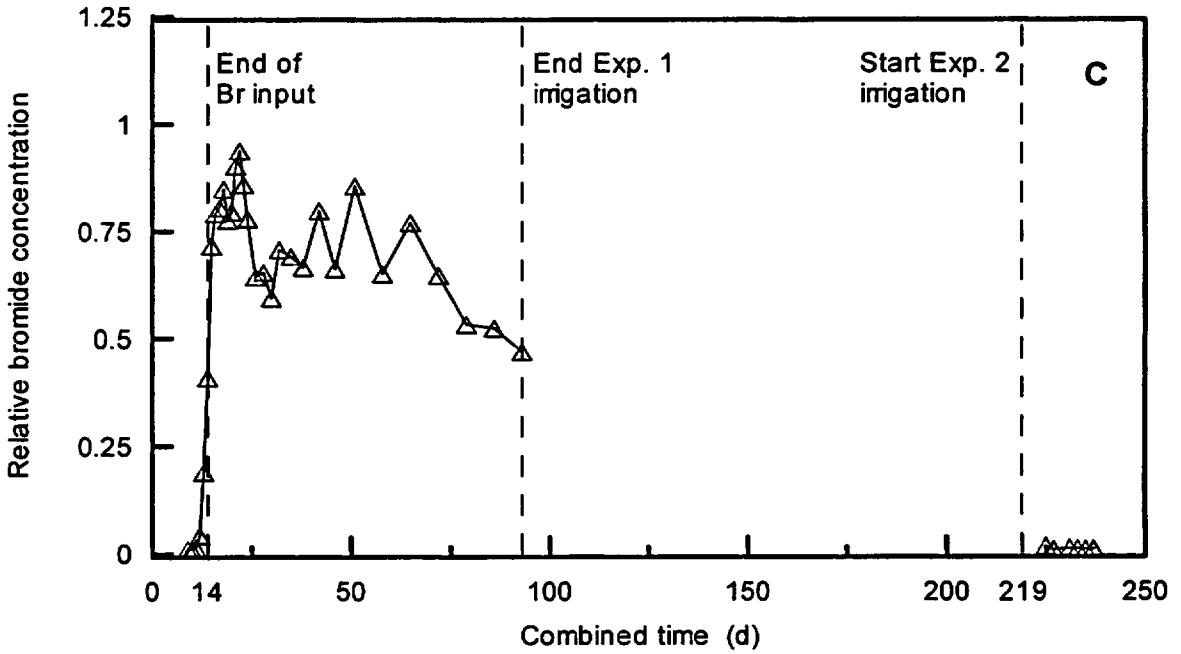

Figure 3.11-3. Relative bromide concentration from trench samplers at (A) Y = 5, (B) 10, and (C) 15 m. (Continued)

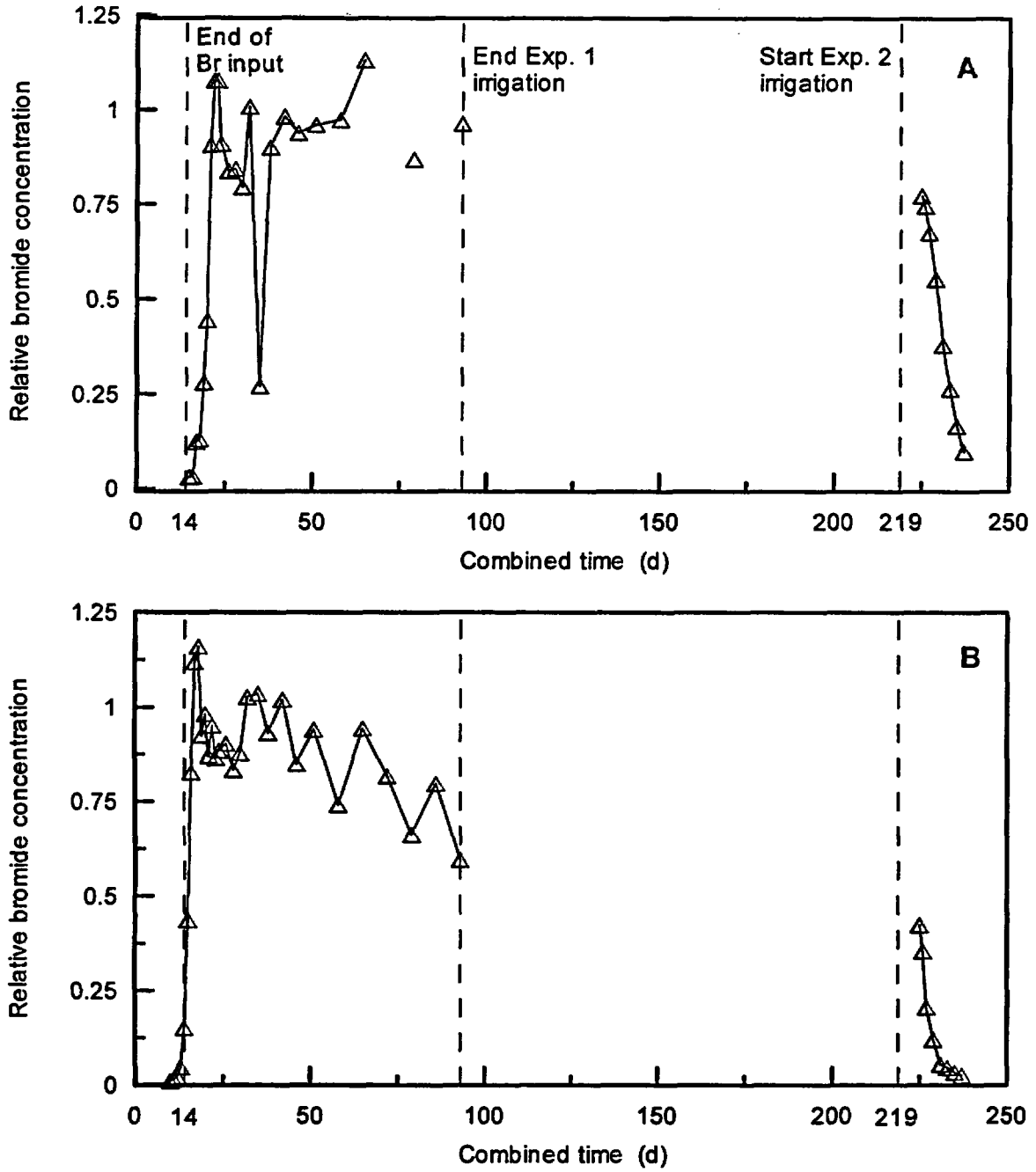

Figure 3.11-4. Relative bromide concentration from trench samplers at (A) Y = 20, (B) 25, and (C) 30 m.

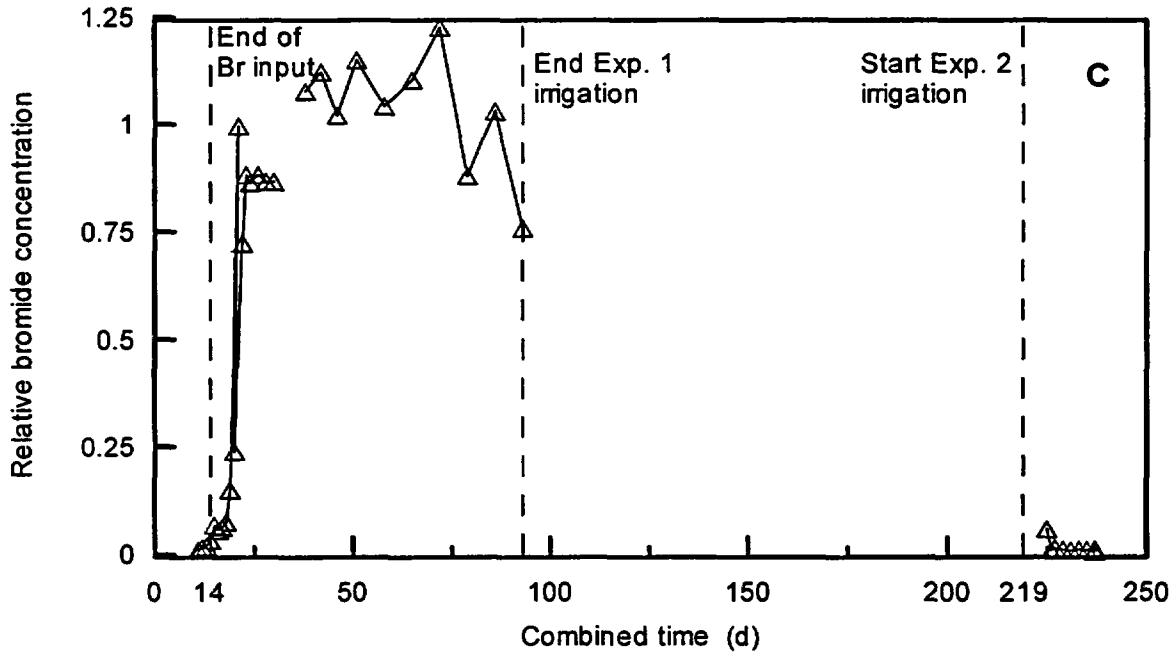

Figure 3.11-4. Relative bromide concentration from trench samplers at (A) Y = 20, (B) 25, and (C) 30 m. (Continued)

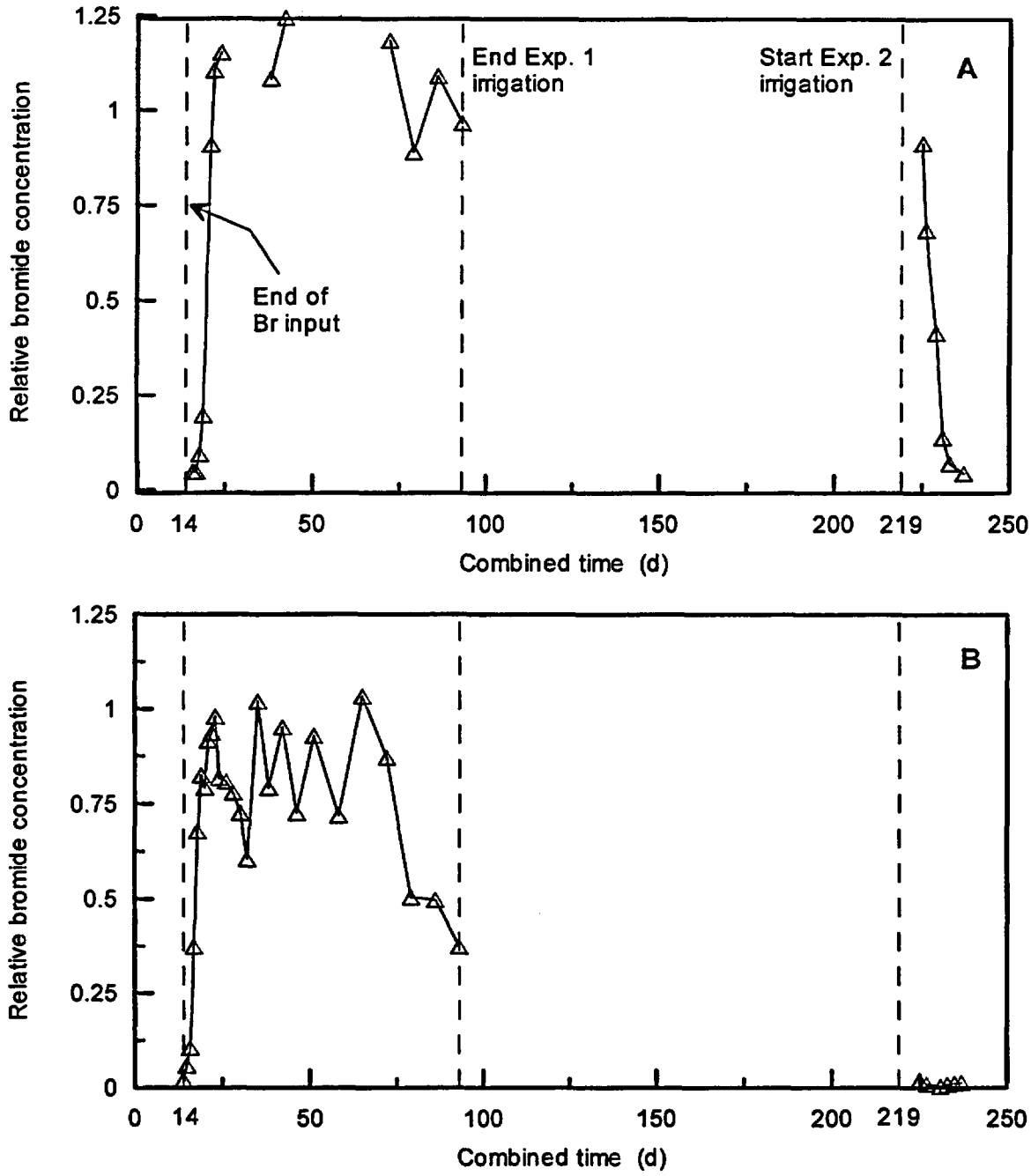

Figure 3.11-5. Relative bromide concentration from trench samplers at (A) Y = 35, (B) 40, and (C) 45 m.

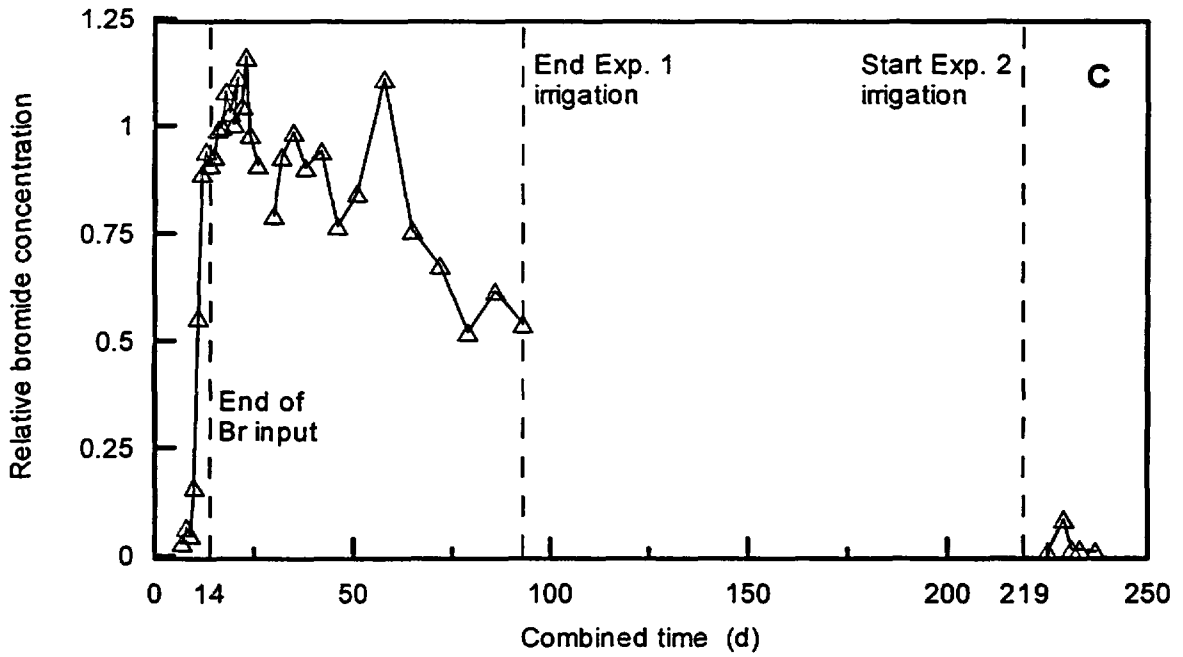

Figure 3.11-5. Relative bromide concentration from trench samplers at (A) Y = 35, (B) 40, and (C) 45 m. (Continued)

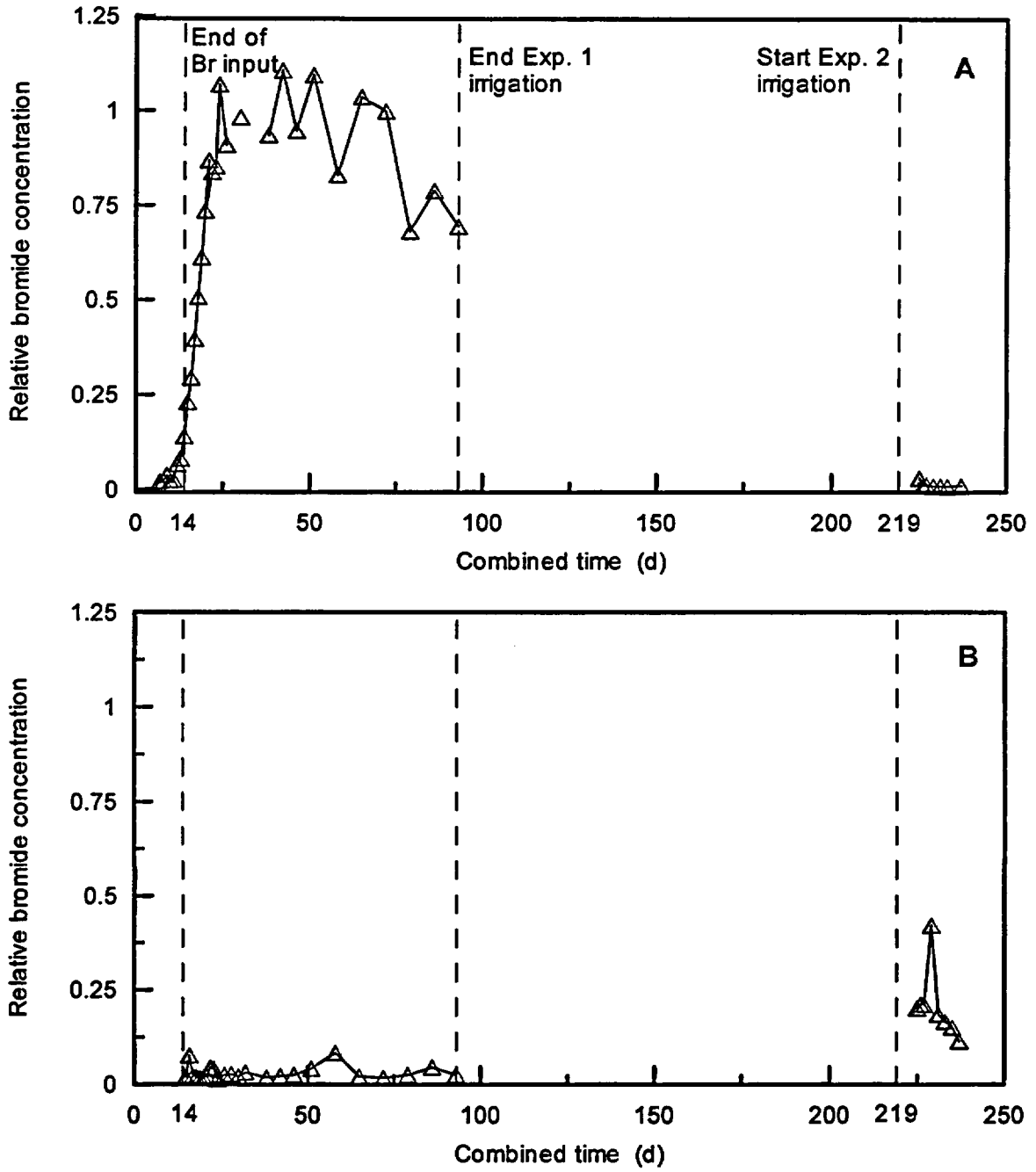

Figure 3.11-6. Relative bromide concentration from trench samplers at (A) Y = 50 and (B) 55 m.

Table 3.11-3. Estimated pore water velocity from breakthrough curves at the trench.

Location	Y-coordinate (m)	Pore water velocity estimated from BTC (cm d^{-1})	Water content based on BTC† (cm d^{-1})
143	5	n/a	n/a
144	10	4.7	0.39
145	15	10.3	0.18
146	20	7.4	0.25
147	25	9.9	0.19
148	30	7.5	0.25
149	35	7.5	0.25
150	40	8.6	0.22
151	45	14.3	0.13
152	50	8.6	0.22
153	55	n/a	n/a
Mean		8.8	0.21

† - calculated as θ = flux / pore water velocity. Flux = 1.85 cm d^{-1}

cm d^{-1}, yielding an average water content of 0.21 $m^3 m^{-3}$, certainly within the range of water contents measured using other instruments in the trench area. The slowest movement of bromide was observed at Y = 10 m, yielding an unrealistically high volumetric water content of 0.39 $m^3 m^{-3}$.

The BTCs were analyzed using the CXTFIT program (version 2.0, Toride et al., 1995). CXTFIT numerically solves the convective-dispersion equation and compares the predicted BTCs to those measured in the field. CXTFIT can be used for direct simulation, where the BTC is predicted based on user-specified parameters. It also allows for inverse simulation, so that the transport parameters (pore water velocity, dispersion coefficient, dispersivity, retardation factor) can be estimated from measured breakthrough data. Using the model in the forward mode, the model was used to predict BTCs for the following initial and boundary conditions:

$$c_i(x,0) = 0 \qquad 0 < x < \infty$$

$$c_r(0,t) = 31.6 \text{ ppm} \qquad 0 < t \leq 15 \text{ days}$$

$$\frac{\partial c_r}{\partial t}(\infty,t) = 0$$

The program was run for all solution samplers where 1) bromide breakthrough occurred before Day 23, Experiment 1; and 2) the sampler was located at least 5 m inside the irrigated area, ensuring that 1-dimensional flow occurred, which is required for proper use of the analytical solutions used in CXTFIT. A total of eight samplers were thus analyzed. Table 3.11-4 lists the resulting pore water velocities, dispersion coefficients and dispersivity values for each of the eight locations. The pore velocities were very close to the visually fitted values in Table 3.11-3. The dispersivities (α) were calculated as the quotient of the dispersion coefficient and velocity, and were within the range observed at other experiments where field scale transport behaviors were evaluated (see for example Elabd, et al., 1988, Porro et al., 1993, and Radcliffe et al., 1996).

3.11.2 Monitoring Islands

Relative bromide concentrations were plotted for the West and East sides of the South and North monitoring islands in Figures 3.11-7 through 3.11-10, respectively. Concentrations for the first 30 days of Experiment 1 are shown in graph A. The full time series of concentrations are shown in graph B, which illustrate the rapid declines in value as soon as irrigation was restarted for Experiment 2. The upper y-scale exceeds unity to show that variability in the input concentration was reflected in variability in concentration throughout the soil profile. All sampling units operated properly during the experiments.

Of the four vertical profiles available at the monitoring islands, bromide transport was quickest in the South Island, West Side, where breakthrough occurred at all six depths before the end of irrigation. Before irrigation ceased, bromide breakthrough occurred at 0.5, 1.0, and 1.5 m depth at the South Island, East Side and at both sides of the North Island, and at 2.0 m depth at the North Island, East Side. Transport rates obviously differed somewhat at the four vertical transects. For example, comparing the behavior between the West and East Sides at the South Island (with a lateral difference = 2.5 m), bromide breakthrough occurred only two days apart at the 0.5 and 1.0 m depths. However, breakthrough at 1.5 m depth differed by more than five days, which was much higher than would otherwise be indicated by the small differences in water content between 1.0 and 1.5 m depths. Large differences were also observed at other comparable depths.

Table 3.11-5 lists the results of CXTFIT analyses for all locations where breakthrough occurred while irrigation was ongoing. Similar to the criteria used for the monitoring trench, CXTFIT was not used for those locations and depths where breakthrough occurred after irrigation ended. Data in the table shows significantly higher dispersion coefficients and dispersivity at the South Island, West Side, for depths exceeding 1.0 m. Though differences in water breakthrough were small at each island, there were large differences in dispersion coefficients. Overall, BTCs were highly variable at the 1.5 m depth, perhaps a result of significant changes in texture, as well as strong calcic cementation, which were noted during drilling and excavation at or near the 1.5 m depth.

Soil layering appeared to affect breakthrough times at the North Island as well. Note for example, the differences in BTCs in Figures 3.11-9 and 3.11-10 for depths at and exceeding 2.0 m. Bromide breakthroughs at the 1.5 m depth occurred essentially at the same time, but bromide

Table 3.11-4. Transport parameters obtained using CXTFIT program for samples collected at the trench during Experiment 1.

Location	Pore water velocity fitted using CXTFIT ($cm\ d^{-1}$)	Water content based on CXTFIT results† ($m^3\ m^{-3}$)	Dispersion coefficient ($cm\ d^{-1}$)	Dispersivity (cm)
143				
144				
145	10.0	0.19	35.6	3.6
146	7.1	0.26	14.0	2.0
147	10.6	0.17	14.9	1.4
148	8.3	0.22	13.2	1.6
149	8.5	0.22	17.6	2.1
150	9.8	0.19	13.4	1.4
151	15.5	0.12	18.0	1.2
152	8.3	0.22	13.7	1.7
153				
Mean	10.0	0.19	18.1	1.9

†- calculated as θ = flux / pore water velocity. Flux = 1.85 $cm\ d^{-1}$

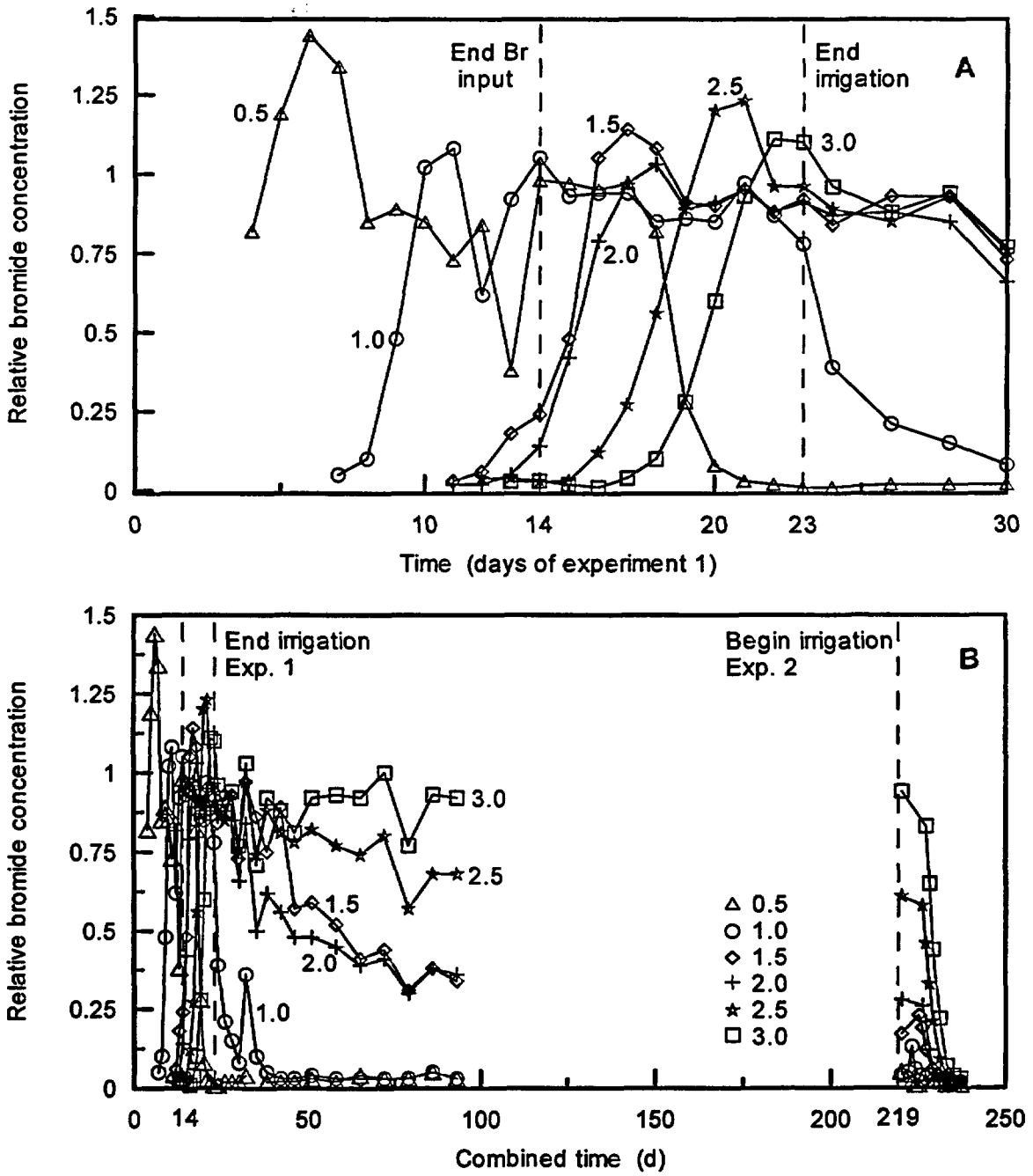

Figure 3.11-7. Relative bromide concentration during (A) Experiment 1 and (B) throughout both experiments for solution samplers installed in the South Island, West Side.

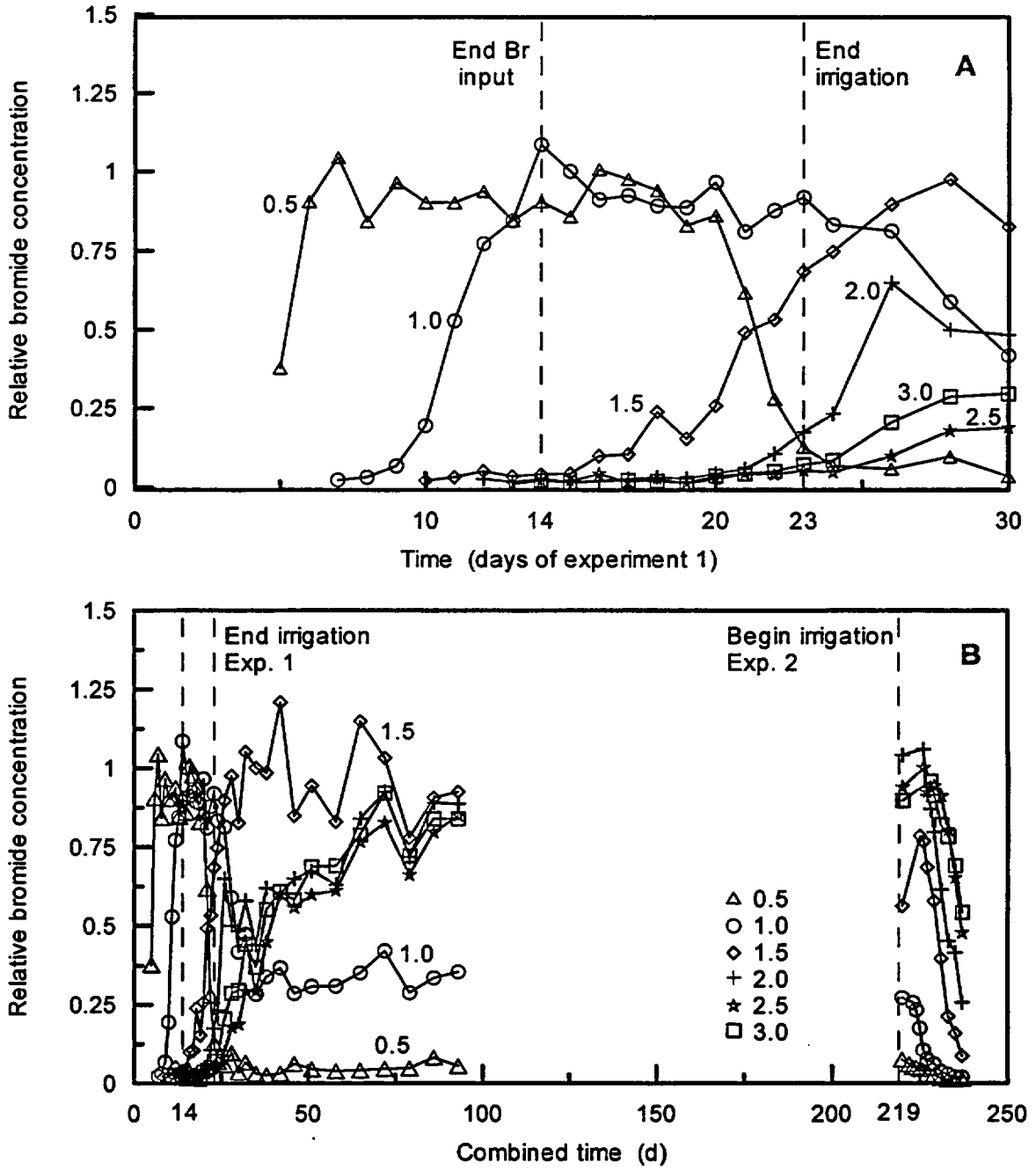

Figure 3.11-8. Relative bromide concentration during (A) Experiment 1 and (B) throughout both experiments for solution samplers installed in the South Island, East Side.

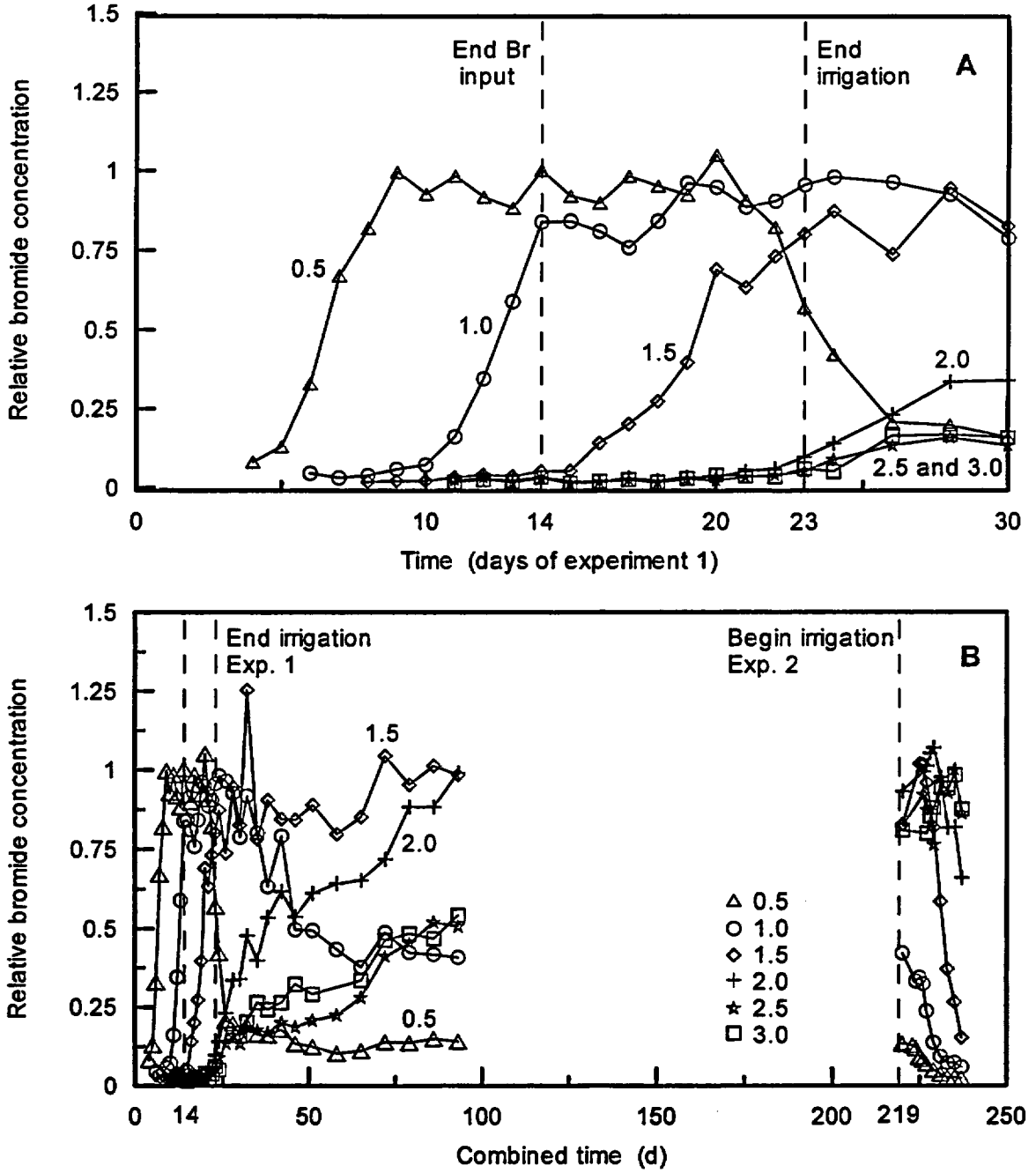

Figure 3.11-9. Relative bromide concentration during (A) Experiment 1 and (B) throughout both experiments for solution samplers installed in the North Island, West Side.

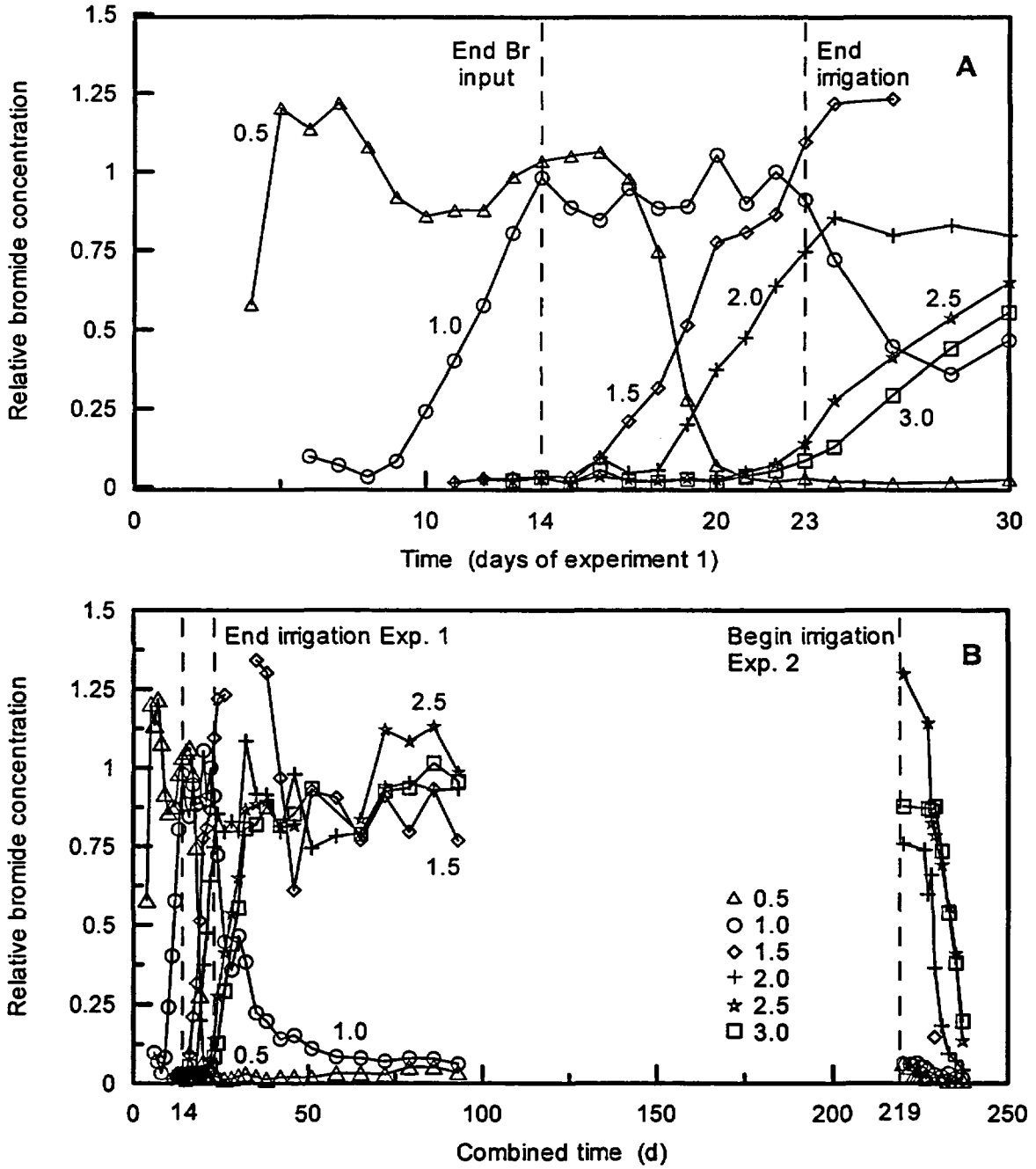

Figure 3.11-10. Relative bromide concentration during (A) Experiment 1 and (B) throughout both experiments for solution samplers installed in the North Island, East Side.

Table 3.11-5. Results of CXTFIT analyses for bromide transport data collected at the monitoring island during Experiment 1. V is pore water velocity, D is the dispersion coefficient, and α_L is the longitudinal dispersivity.

South Monitoring Island									
	West Side			East Side			North Side		
Depth (m)	V ($cm\ d^{-1}$)	D ($cm^2\ d^{-1}$)	α_L (cm)	V ($cm\ d^{-1}$)	D ($cm^2\ d^{-1}$)	α_L (cm)	V ($cm\ d^{-1}$)	D ($cm^2\ d^{-1}$)	α_L (cm)
0.5	11.4	12.8	1.1	8.4	10.2	1.2			
1.0	10.8	22.0	2.0	8.4	17.5	2.1			
1.5	9.5	35.7	3.8	7.0	11.3	1.6			
2.0	14.4	40.9	2.8				8.1	30.6	3.8
2.5	15.5	45.4	2.9						
3.0	16.0	49.2	2.9				10.6	53.1	5.0
North Monitoring Island									
	West Side			East Side			South Side		
Depth (m)	V ($cm\ d^{-1}$)	D ($cm^2\ d^{-1}$)	α_L (cm)	V ($cm\ d^{-1}$)	D ($cm^2\ d^{-1}$)	α_L (cm)	V ($cm\ d^{-1}$)	D ($cm^2\ d^{-1}$)	α_L (cm)
0.5	6.1	13.4	2.2	13.2	14.5	1.1			
1.0	8.7	10.0	1.1	9.0	17.9	2.0	5.7	25.5	4.5
1.5	7.5	7.6	1.1	7.2	33.6	4.7			
2.0				8.5	35.6	4.2	7.1	60.7	8.6
2.5									
3.0							11.0	84.1	7.7
Overall Mean	V ($cm\ d^{-1}$)		D ($cm^2\ d^{-1}$)		α_L				
	9.7		30		3.1				

did not exceed a relative concentration of 0.5 at the West Side until Days 38, 86 and 93 for depths of 2.0, 2.5, and 3.0 m depths, respectively, almost at the end of redistribution. On the East Side, however, breakthrough occurred before Day 30 at these same depths, indicating higher fluxes on the East Side of the North Island.

Bromide BTCs for solution samplers placed in the backfill material in the annular spaces around both islands are shown in Figure 3.11-11. Concentrations of bromide observed in the first several samples taken in the South Island from the 1.0 and 2.0 m depths were higher than observed in the North Island (earlier breakthrough), while the maximum concentrations at 2.0 and 3.0 m depth were up to two times the input concentration. Even though these data at first appeared to be erroneous, repeated laboratory analyses showed the concentration to be accurate. The high concentrations may possibly be explained by water evaporation that occurred around the access ports in the monitoring island itself. During the experiments, site personnel observed salt buildup occurring on the backfill material, indicating that evaporation was causing salt-laden pore water to flow laterally toward the access port, where it would evaporate and precipitate bromide salts.

3.11.3 Borehole Monitoring

Borehole monitoring points include the porous stainless steel samplers installed in individual boreholes (3, 5 and 10 m depth), as well as neutron probe access tubes that were completed with well screens at the water table adjacent to the deep solution samplers. A total of eight such wells existed at the site. Bromide concentrations for each of the sampling points are shown in Figures 3.11-12 through 3.11-20; the figures are captioned similar to the deep tensiometers, i.e., SW indicates the southwest cluster, etc. The X-scale is identical for all locations where a neutron probe access tube was located nearby, except for Figure 3.11-20, because samples were not collected after Combined Day 284. Each figure contains two graphs, one which shows Experiment 1 primarily, and a second which provides data for both experiments. Concentrations varied significantly during the early part of the experiment, in some cases, by more than 10 ppm bromide on successive sampling periods. Samples which appeared unrealistic were reanalyzed and then checked again for accuracy by use of laboratory standards; often the original analysis was correct.

Bromide breakthrough at the 3 m depth occurred at eight locations before the end of Experiment 1 irrigation (Table 3.11-6); bromide breakthrough did not occur at the NE sampling location during irrigation, though breakthrough did occur during redistribution. Relative concentrations generally hovered near or above unity during redistribution, and clearly decreased in value soon after irrigation was restarted for Experiment 2. The pore water velocity was found to be highest at the southwest portion of the plot and slower toward the eastern and northern portions. We found that breakthrough patterns generally mirrored those found from the tensiometer responses, although bromide breakthrough lagged the wetting front breakthroughs. Comparison of BTCs for the 3 m depth showed that bromide transport was less variable for the eastern sampler locations than for the western locations. Flow and transport in the western portion of the site may have been influenced by a wider pore size distribution that found in the eastern half.

Of the nine operating locations at the 5 m depth, only three recorded breakthrough before the end of irrigation during Experiment 1, and all three were located in the southwestern portion of the site. Samplers located toward the north and east did not contain bromide concentrations high enough to achieve breakthrough; in several cases, relative concentrations were not exceeded until the onset of Experiment 2, when bromide-free water was added to the plot for 33 days. Very high concentrations ($C/C_0 > 1.5$) were recorded in several sampling locations, all of which were found in the western portion of the site. Note that the rate of increase in bromide concentration was slower than observed at the 3 m depth, due to greater dispersion in the deeper soil. However, with the onset of irrigation during Experiment 2, bromide concentrations at 5 m depth were quickly reduced to near background levels. However, at two locations (see Figures 3.11-16 and 3.11-17), relative bromide concentrations increased above 0.5 after Experiment 2 irrigation began, indicating the presence of a residual bromide pulse in the shallower soil, rather than the bromide being fully mixed in the pre-existing soil water.

Very low concentrations of bromide were recorded in pore water samples collected at the 10 m depth, especially before the beginning of Experiment 2. However, concentrations at this depth were often significantly above the detection limit of the bromide analyzer (e.g., 0.2 ppm or $C/C_0 = 0.006$). For example, Figure 3.11-12 showed an increase in relative

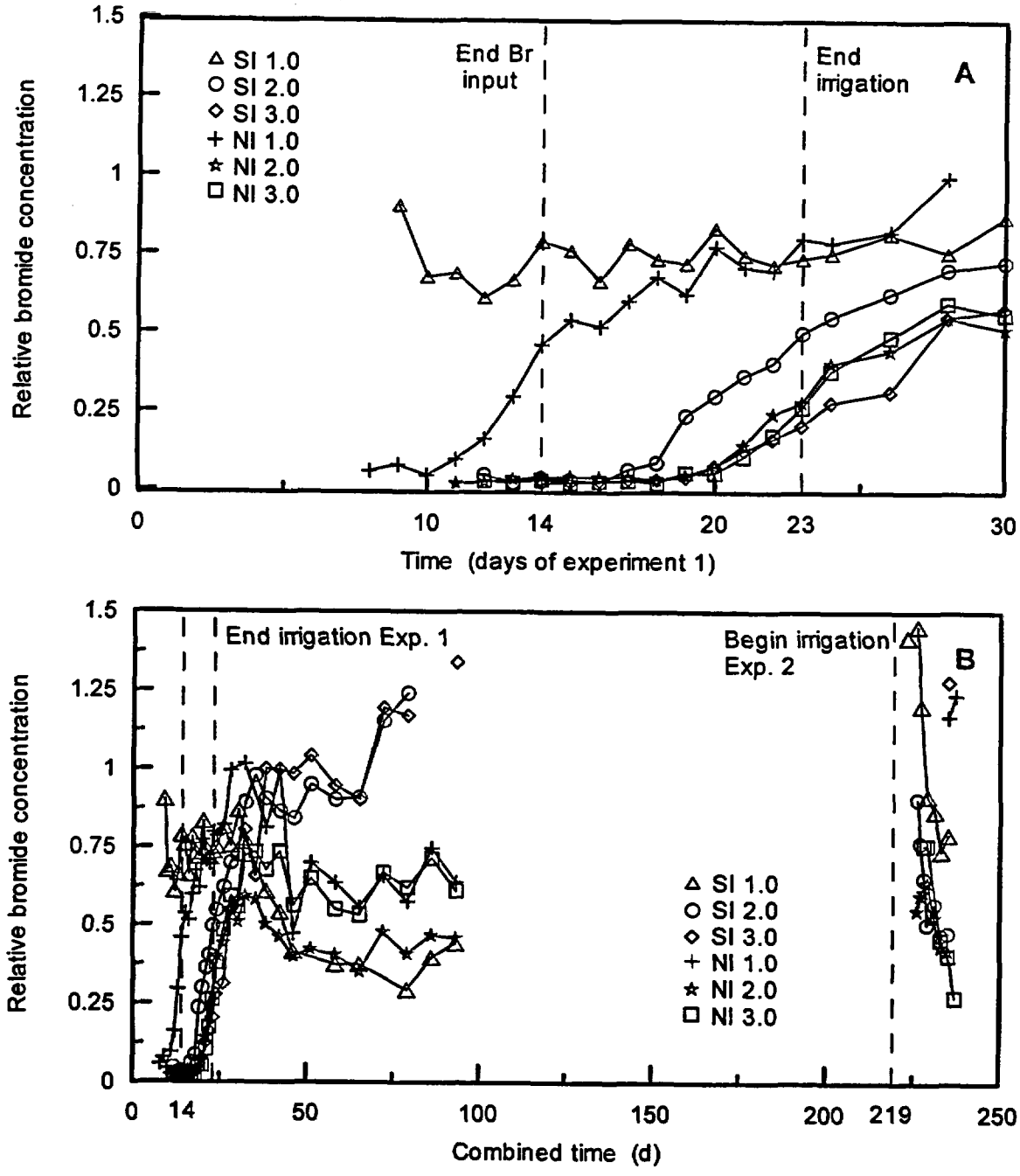

Figure 3.11-11. Relative bromide concentration during (A) Experiment 1 and (B) throughout both experiments for solution samplers installed in the annular spaces of the South and North Islands.

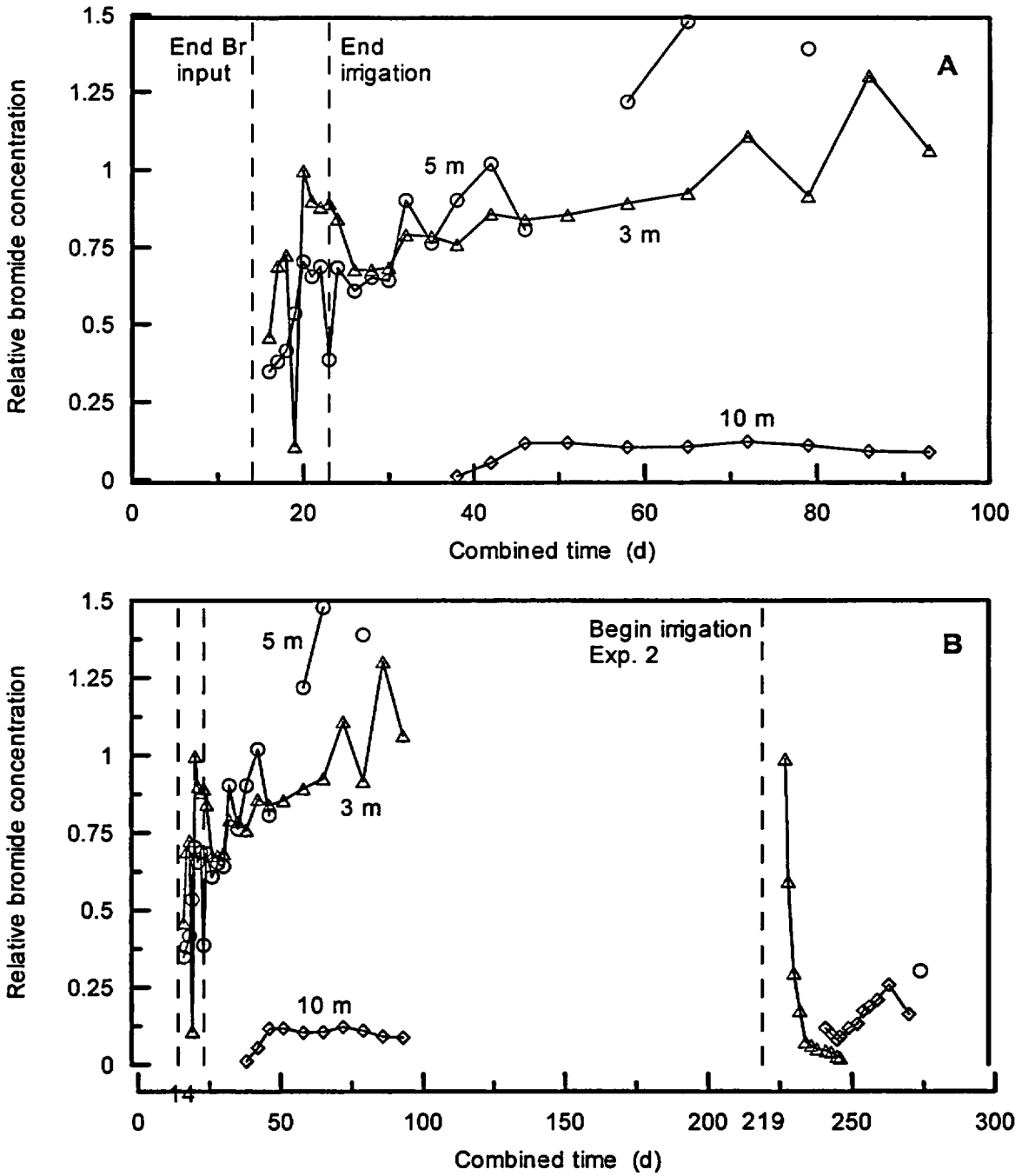

Figure 3.11-12. Bromide concentration measured for deep solution samplers located at SW corner of plot during both Experiments 1 and 2.

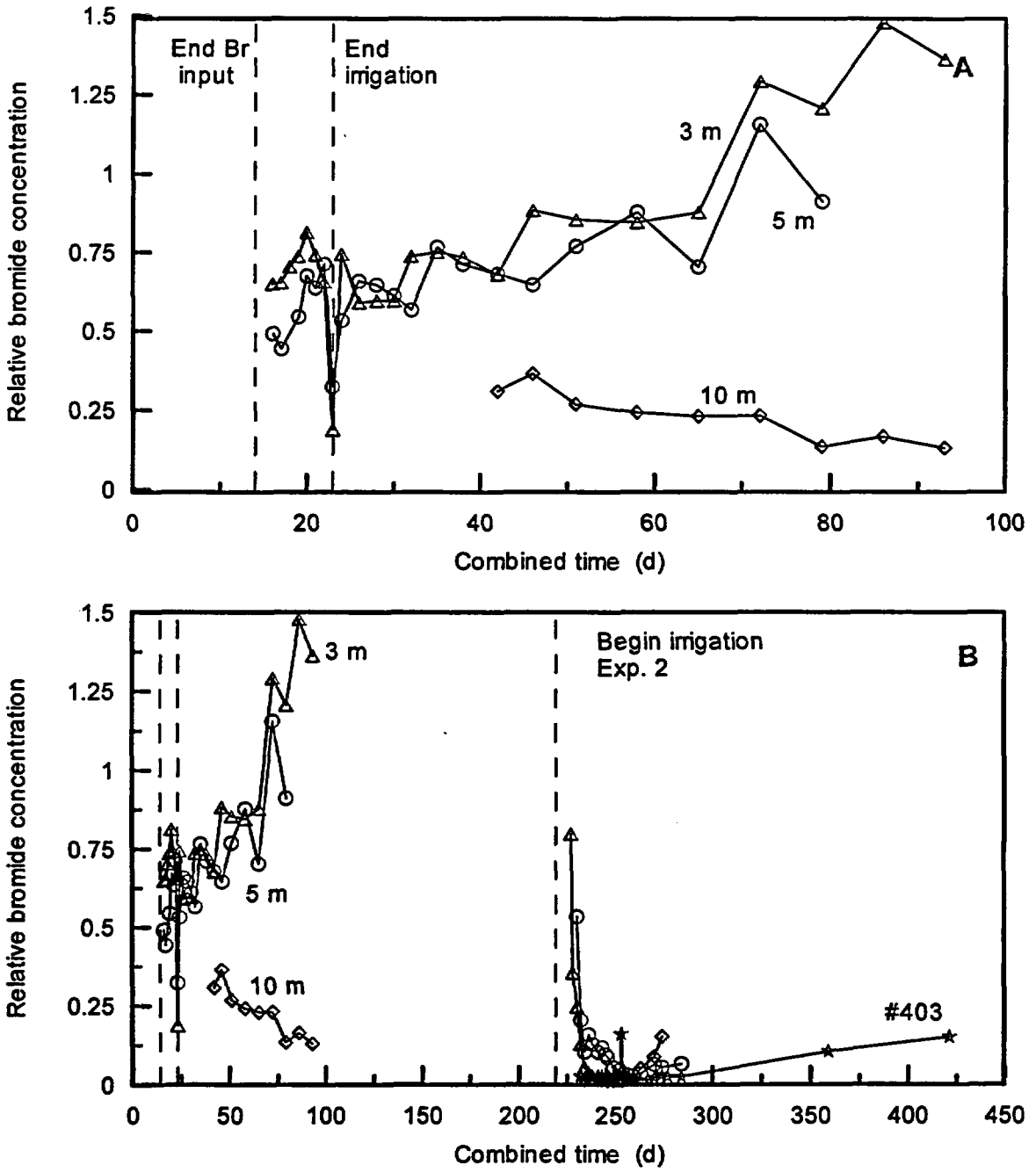

Figure 3.11-13. Bromide concentration measured for deep solution samplers located at SC section of plot during both Experiments 1 and 2. Access tube #403 is also plotted.

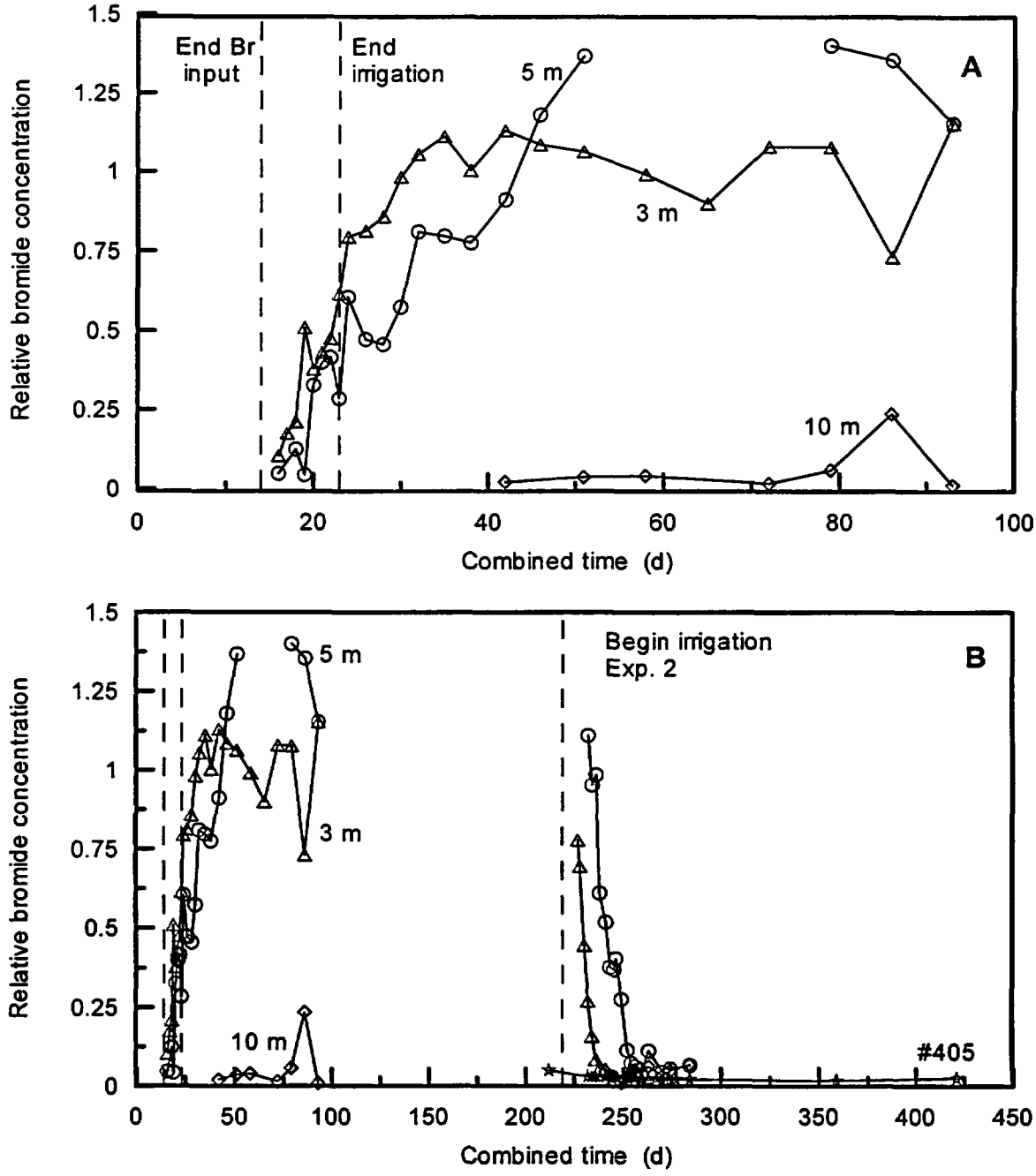

Figure 3.11-14. Bromide concentration measured for deep solution samplers located at SE section of plot during both Experiments 1 and 2. Access tube #405 is also plotted.

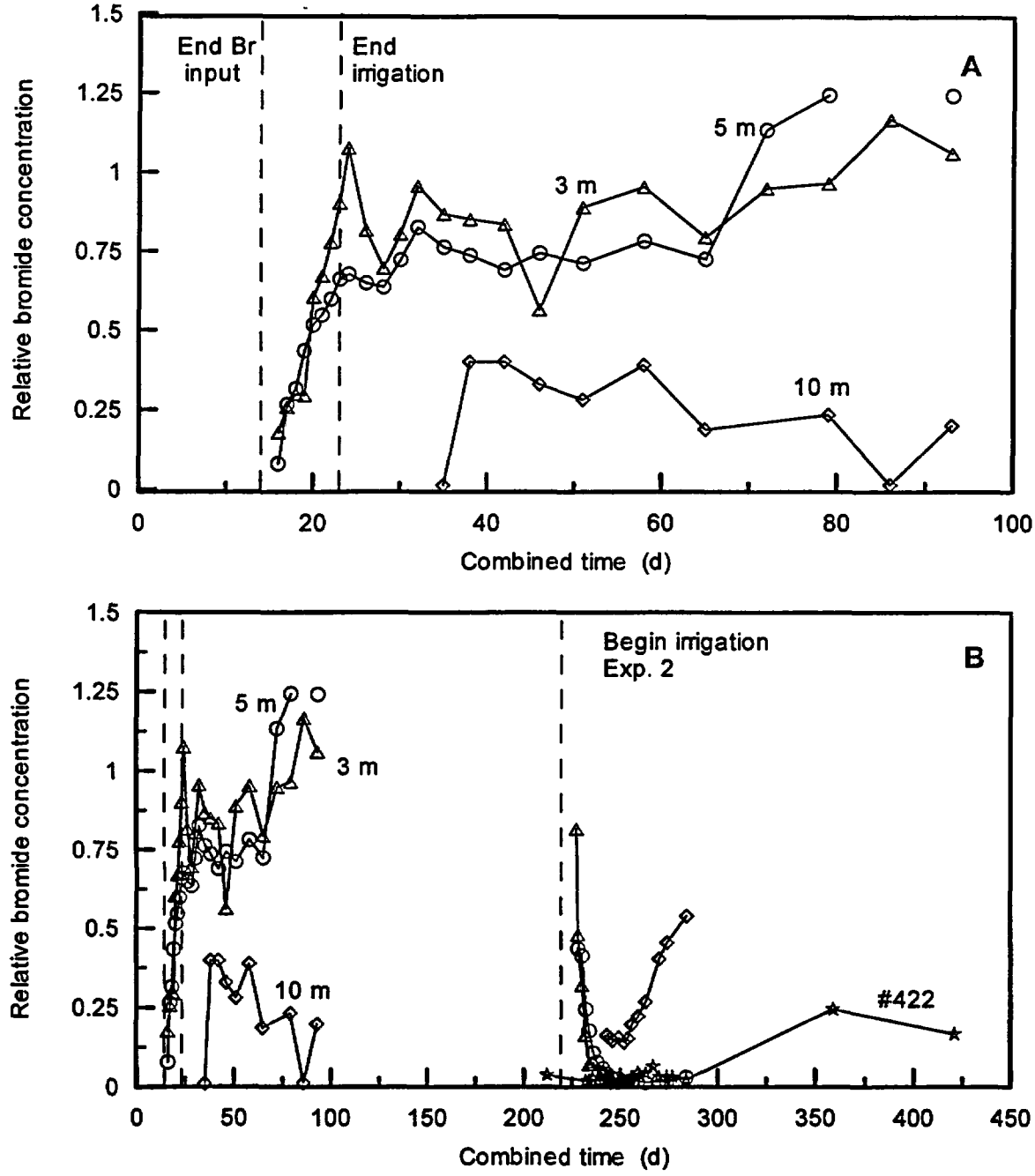

Figure 3.11-15. Bromide concentration measured for deep solution samplers located at CW section of plot during both Experiments 1 and 2. Access tube #422 is also plotted.

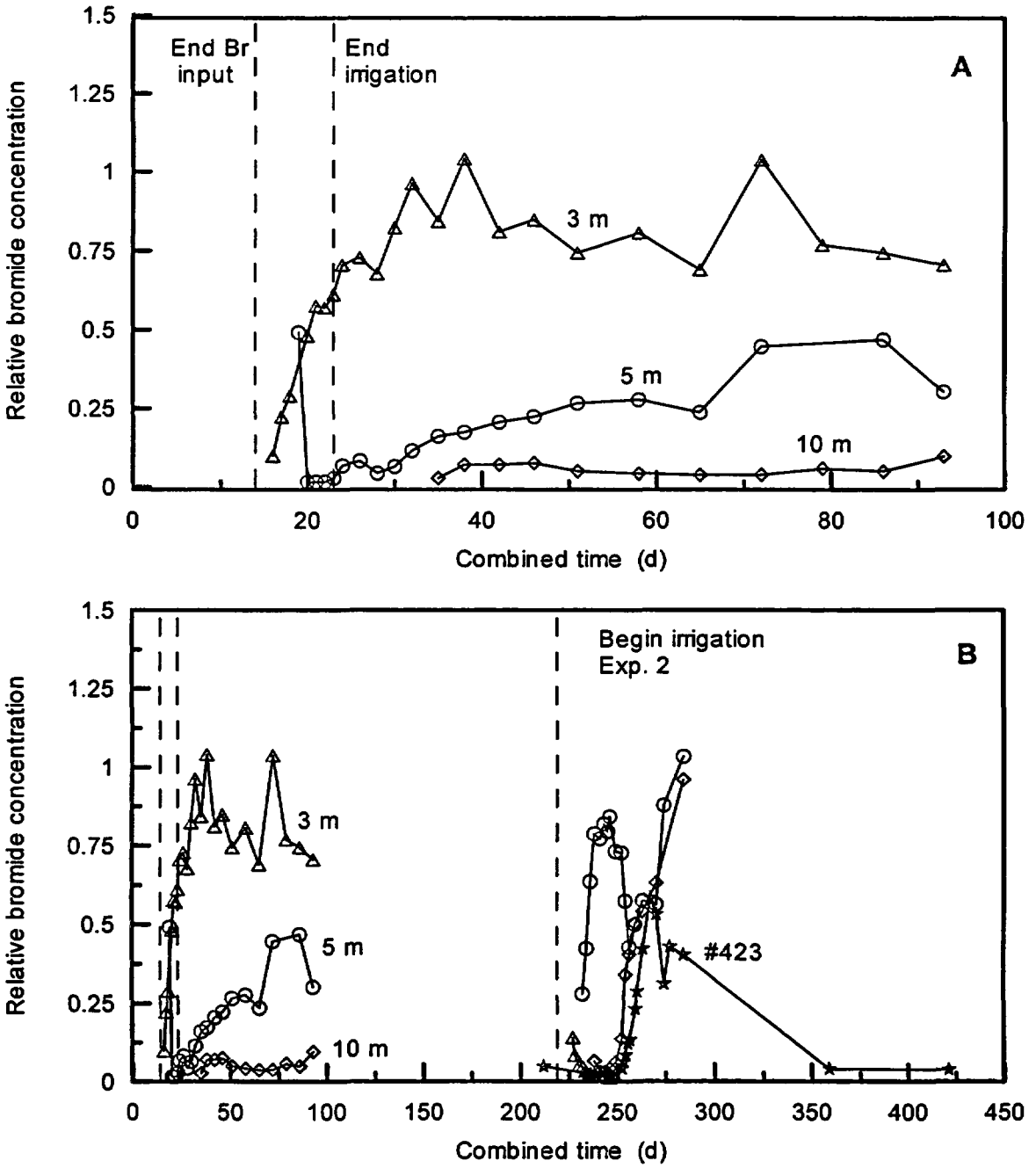

Figure 3.11-16. Bromide concentration measured for deep solution samplers located at CC section of plot during both Experiments 1 and 2. Access tube #423 is also plotted.

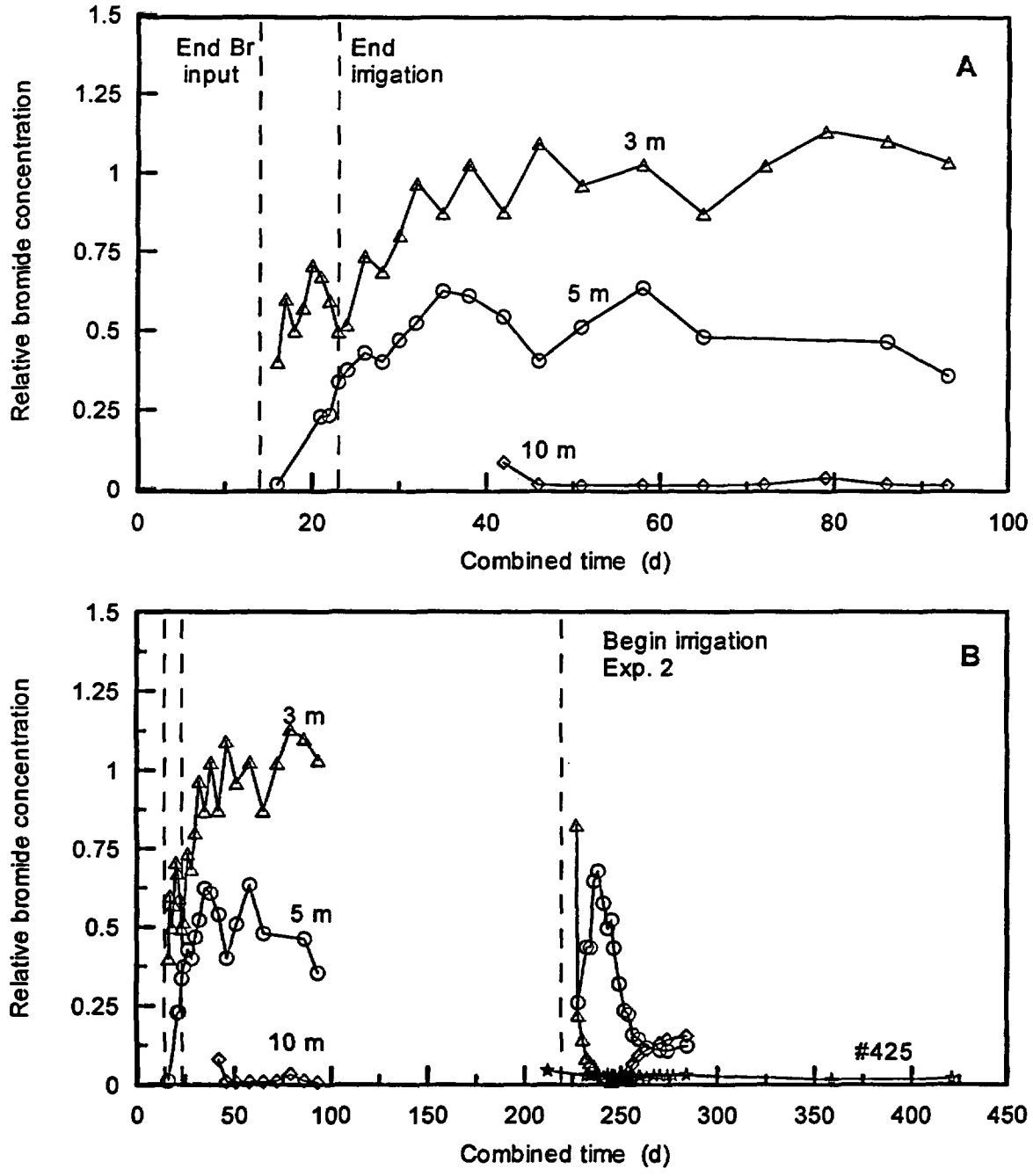

Figure 3.11-17. Bromide concentration measured for deep solution samplers located at CE section of plot during both Experiments 1 and 2. Access tube #425 is also plotted.

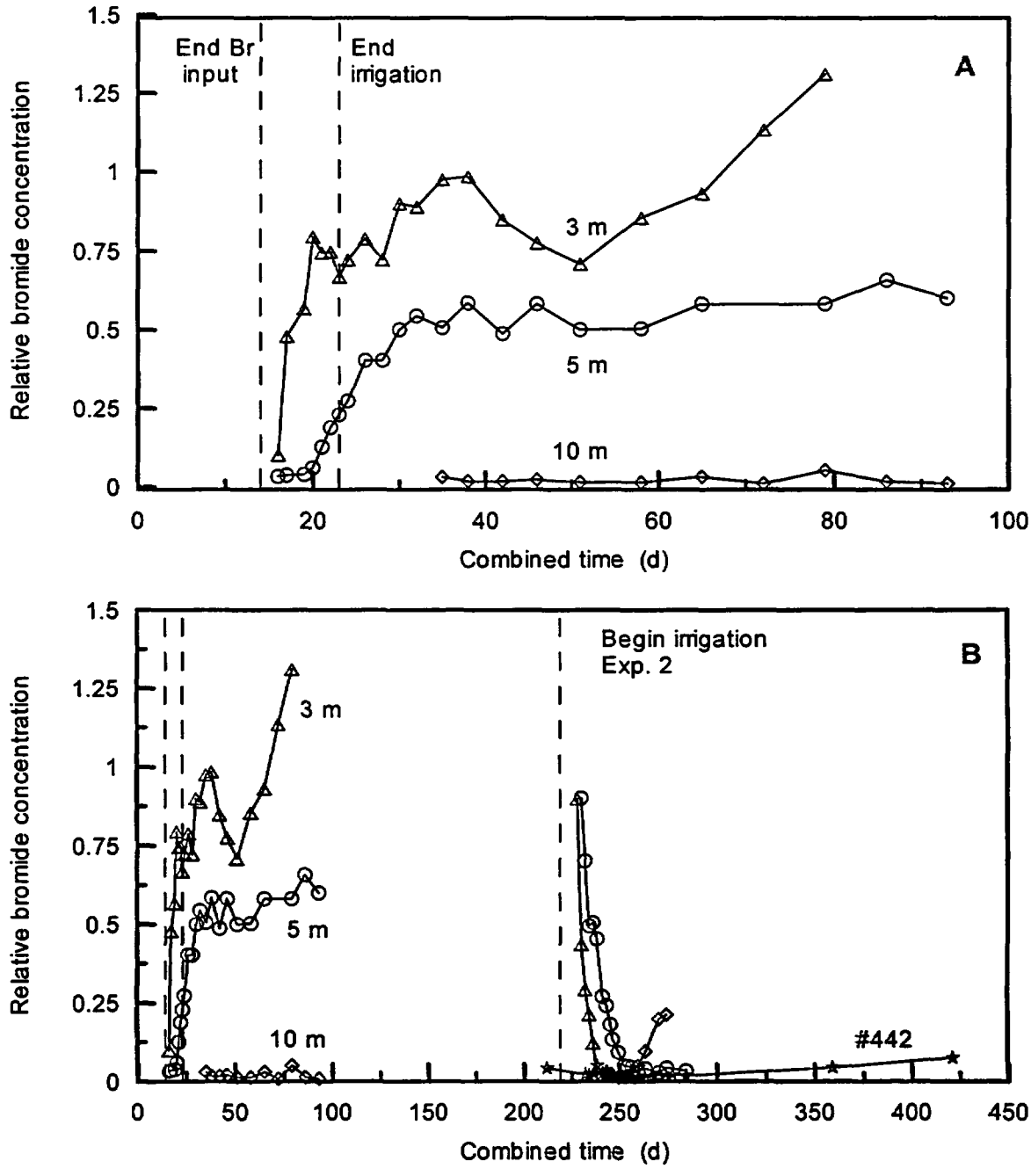

Figure 3.11-18. Bromide concentration measured for deep solution samplers located at NW section of plot during both Experiments 1 and 2. Access tube #442 is also plotted.

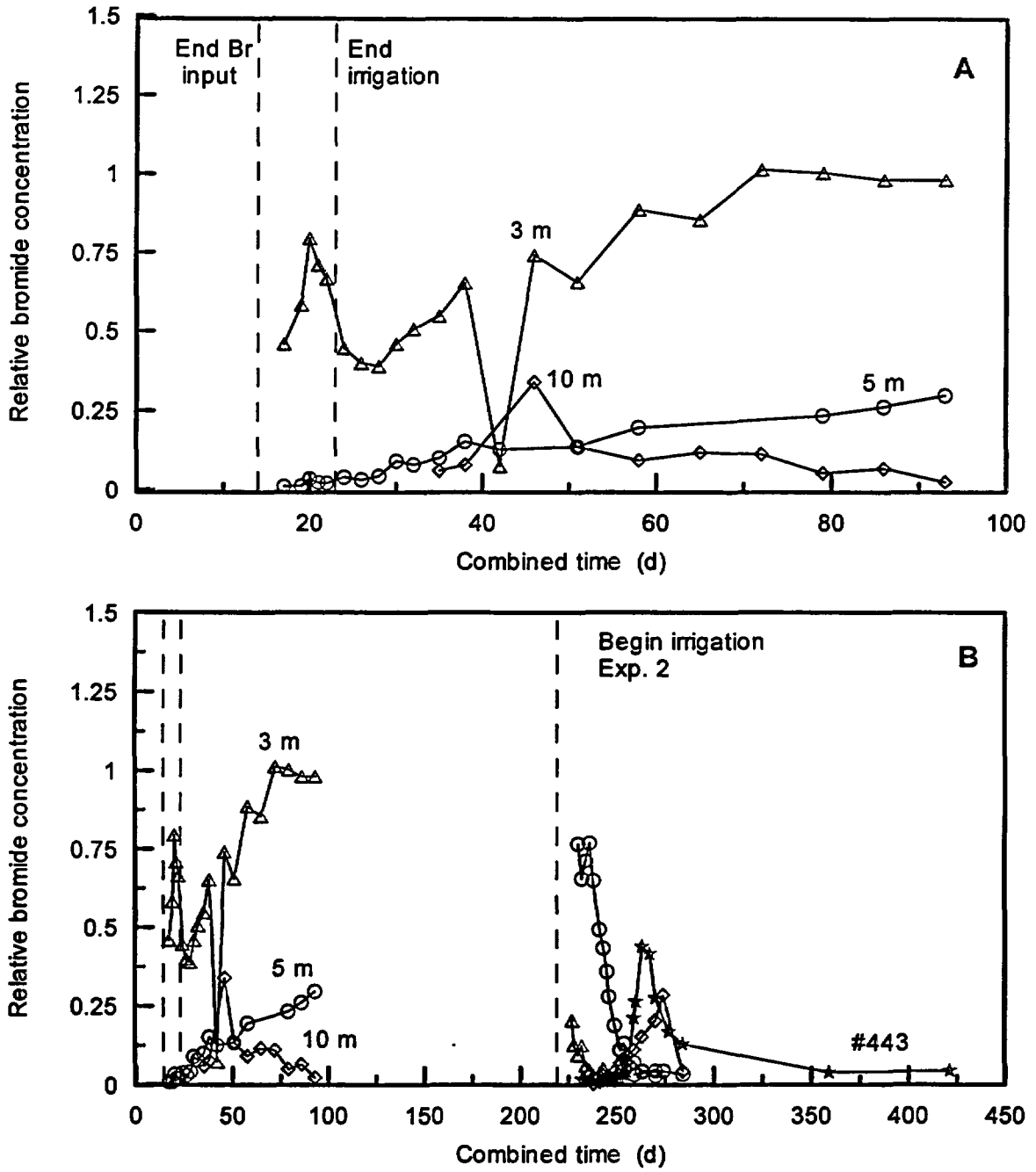

Figure 3.11-19. Bromide concentration measured for deep solution samplers located at NC section of plot during both Experiments 1 and 2. Access tube #443 is also plotted.

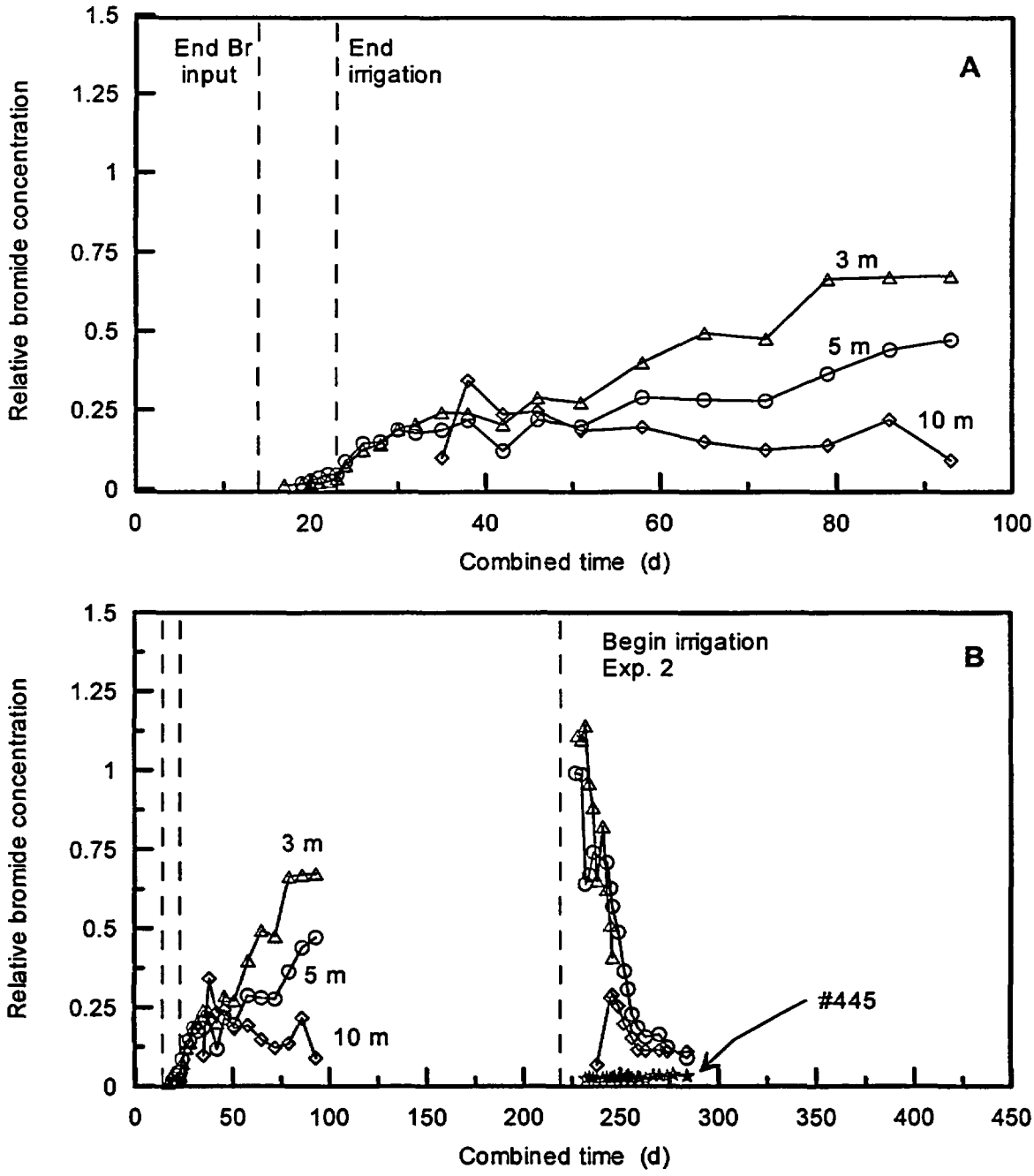

Figure 3.11-20. Bromide concentration measured for deep solution samplers located at NE section of plot during both Experiments 1 and 2. Access tube #445 is also plotted.

Table 3.11-6. Estimated breakthrough times for samples collected in deep boreholes during Experiment 1.

Location	Breakthrough time at 3 m depth (days)	Breakthrough time at 5 m depth (days)	Associated Figure
SW	15	18	3.11-13
SC	15	18	3.11-14
SE	20	25	3.11-15
CW	18	18	3.11-16
CC	20	NA†	3.11-17
CE	18	30	3.11-18
NW	17	30	3.11-19
NC	20	NA	3.11-20
NE	70	NA	3.11-21
Mean	23.6	46.4‡	

† - NA = no arrival

‡ - calculated assuming that breakthrough occurred at the end of Experiment 1.

bromide concentration at 10 m after Day 40 to levels close to $C/C_0 \approx 0.1$, which remained constant until the end of Experiment 1. On Day 44 of Experiment 2 (11 days after the end of irrigation), a peak concentration of 8.1 ppm was recorded, more than 40 times the detection limit. In several other instances (e.g., Figures 3.11-13 and 3.11-15), relative bromide concentrations approached or exceeded 0.5 during Experiment 1, leading to the possibility that fast flow paths influenced bromide transport in these areas. However, bromide concentrations increased more consistently during Experiment 2 after residual mass was flushed downward. This flushing was quite evident in Figures 3.11-15 and 3.11-16, where rapid decreases in concentration at 3 and 5 m depth led to sudden increases in concentration at 10 m. The increased concentrations at 10 m occurred only at the end of the field experiments, and thus no data were available to confirm if the relative concentrations would have continued to increase with time.

Of the deep neutron probe access tubes installed at the site, eight were installed with well screen so that ground water samples could be collected. (The access tube located at the SW monitoring cluster was installed with solid well pipe down to the final depth of 15 m.) The presence of a screened interval allowed us to directly compare bromide concentrations in ground water samples against bromide found in soil pore water, collected about 1.7 m above the water table. The access tube associated with each monitoring cluster was labeled accordingly on Figures 3.11-13 through 3.11-20. Table 3.11-7 lists the average relative bromide concentrations measured in the upper few centimeters of the groundwater during Experiment 2. Samples from two of the access tubes showed higher bromide concentrations (see Figures 3.11-16 and 3.11-19) than the others. The groundwater in these two access tubes experienced significant increases in relative concentration, indicating a definable arrival of the bulk of residual bromide, immediately after arrival at the 10 m deep solution sampler. Slight increases in relative concentration were also recorded at two other locations (#403, #422 [Figures 3.11-13 and 3.11-15]), indicating that bromide transport during Experiment 2 redistribution was still occurring. These observations indicate that neutron probe access tubes can be used as monitoring wells, with reasonable assurances, without the need to install monitoring points using the traditional construction practices (e.g., with bentonite plug and grout).

As described above, monitoring wells were constructed at the plot corners. Three of these monitoring wells were sampled during Experiment 2 and analyzed for bromide. The fourth well was not monitored during the experiment because of the installation of a pressure transducer to support the gas flow studies (only two samples were collected - Days 359 and 421). Figure 3.11-21 shows the relative bromide concentrations at boreholes #801, #802 and #804, corresponding to the SW, SE and NE corners of the plot, respectively. Because ground water flow is toward the SW corner, boreholes #802 and #804 can be considered background while #801 is considered the downgradient observation point.

No overall trend in the background concentration of bromide was apparent, though obviously the first data point, collected one week before Experiment 2 began, was higher than the average values. Some fluctuations were present, but fall within a range of $C/C_0 = \pm 0.005$, which is only $\pm$ 0.16 ppm and very close to the detection limit for the analyzer. Thus, we concluded that baseline relative concentrations for background boreholes #802 and #804 were 0.037 and 0.026, respectively. The changes in relative concentration at the downgradient observation well (e.g., #801) appeared to follow some trend from Combined Day 238 (Experiment 2, Day 19) to about Day 277, but this most likely is just natural fluctuation, especially considering that all the data fall within an envelope of 0.6 ppm. Based on a measured gradient at the site of 0.007 m/m, an assumed hydraulic conductivity of 1000 cm d^{-1}, and an assumed porosity of 0.40, we calculated the pore water velocity toward the downgradient well (e.g., velocity = K × gradient / porosity) of 18 cm d^{-1}. Hence, travel time for bromide from the center of the plot (access tube #423) to the SW corner (access tube #801), a distance of 33.6 m, is approximately 192 days. Given the increase in relative concentration at access tube #423 (Figure 3.11-16), we should see some increase in bromide at the downgradient well at some later time. Obviously, bromide concentration on Days 359 and 421 did not increase significantly, indicating that 1) dilution of the bromide pulse in the ground water reduced the concentration to baseline levels, 2) the bromide pulse did not reach the downgradient well by Day 421, or 3) borehole #801 is not located along the streamline of access tube #423. Future monitoring should help to clarify the fate of the bromide in groundwater at the site.

Table 3.11-7. Average relative bromide concentrations from groundwater samples collected at the water table.

Location	Relative Bromide Concentration
403	0.037
405	0.027
422	0.041
423	0.155
425	0.027
442	0.024
443	0.097
445	0.028
801	0.022
802	0.037
804	0.026

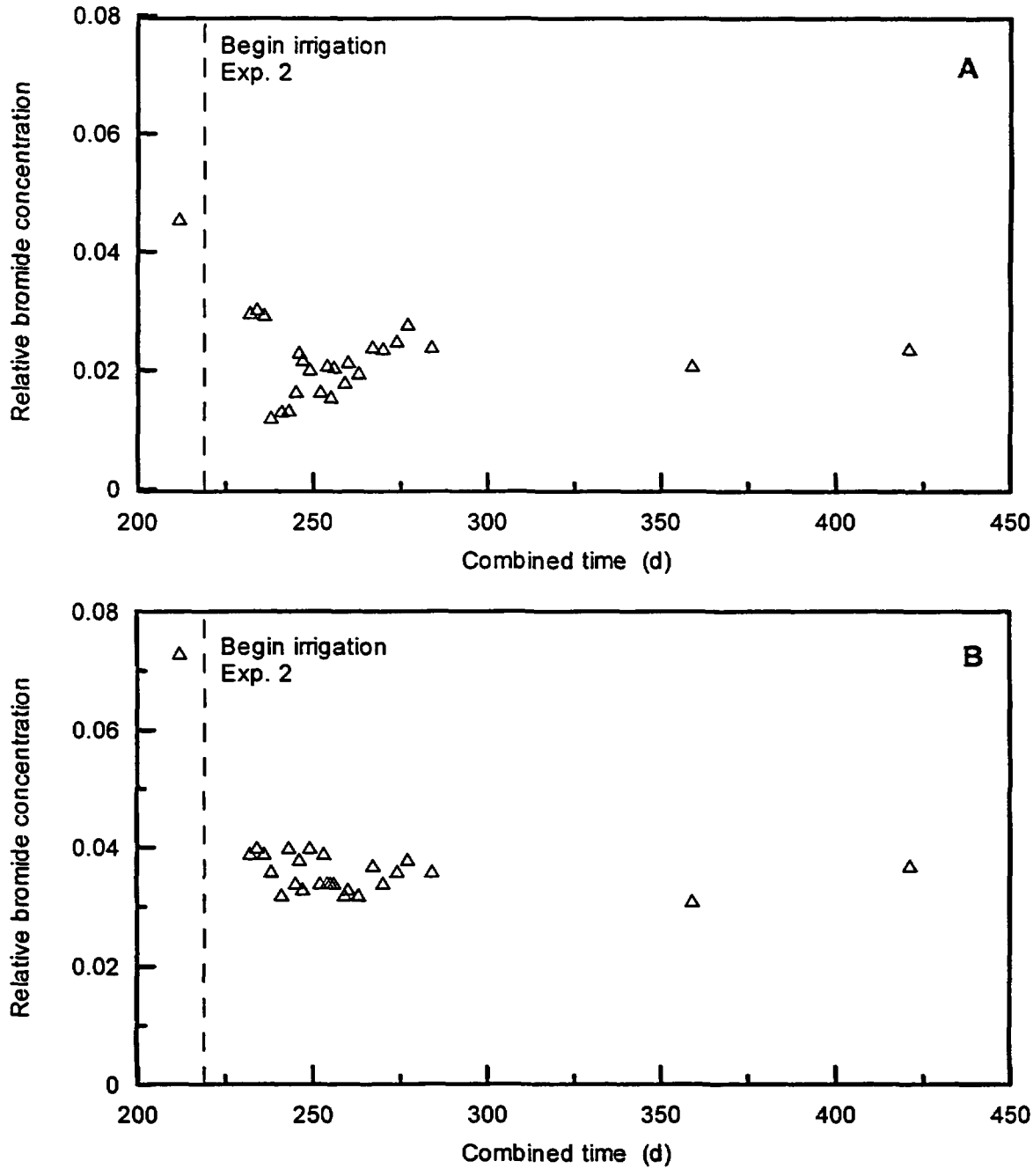

Figure 3.11-21. Relative bromide concentration during Experiment 2 from three groundwater monitoring wells located at the corners of the irrigated plot (data are unavailable for the fourth well). Wells are (A) #801 in the SW corner, (B) #802 in the SE corner, and (C) #804 in the NE corner.

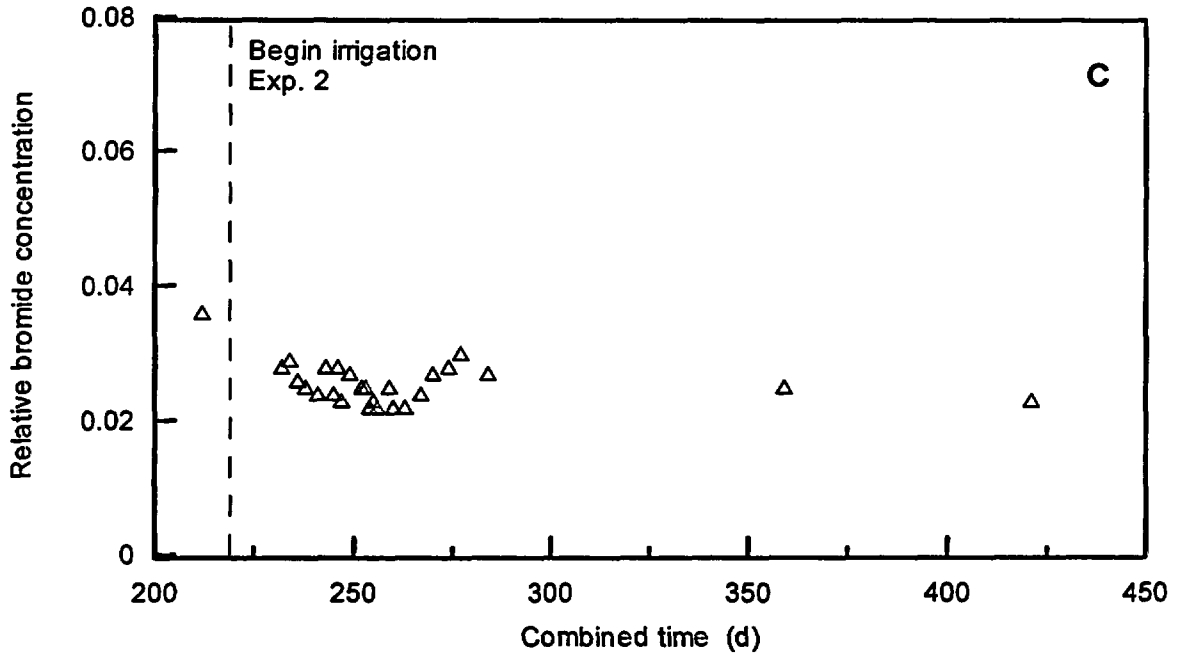

Figure 3.11-21. Relative bromide concentration during Experiment 2 from three groundwater monitoring wells located at the corners of the irrigated plot (data are unavailable for the fourth well). Wells are (A) #801 in the SW corner, (B) #802 in the SE corner, and (C) #804 in the NE corner. (Continued)

4.0 SUMMARY

The objectives for this document were to describe the activities conducted at the field site, to report on field observations during two water flow and solute transport experiments, and then to discuss some of the successes and failures of the monitoring systems that were used during the experiments.

The field design emphasized the implementation of monitoring systems to support four basic monitoring strategies. Briefly described, the Monitoring Trench strategy is a 60 m trench excavated to 1.5 m depth, into which 13 instrumentation clusters were installed at 5 m lateral spacing. The Monitoring Island strategy consists of two vertical culverts (1.55 m diameter) drilled to 3 m depth; monitoring instruments were installed radially around the islands into undisturbed soil. The Borehole Monitoring strategy utilized vertical and horizontal access tubes (120 total), into which permanently-installed (tensiometers and solution samplers) and portable sensors (neutron probe) were inserted for taking measurements. The Geophysical Monitoring strategy incorporated permanently-installed (ERT; 12 locations) and portable (EM-31, EM-38; 90 locations each) sensors for monitoring changes in bulk electrical conductivity and resistivity. Several monitoring systems could be categorized into more than one strategy, and their spatial locations at the site were designed to dovetail extensively.

The following review summarizes the results of the field implementation and Experiments 1 and 2.

4.1 Field Activities

1. A field study was designed for understanding monitoring issues at arid and humid LLW and SDMP sites. The field site was located in a semi-arid setting so that components that operate in the dry water content range could be used. However, the experimental conditions, including the use of higher flux rates and pond liner material to cover the soil surface, created a subsurface environment associated with humid sites.

2. A field site for controlled studies was established. The field site at Maricopa is perhaps the largest prescribed flux experimental site built to date. The size of the facility allowed in-depth studies to be conducted on both instrumentation and soil water movement. Major components installed at the site included:

   A. Irrigation system - The water application system consisted of mixing tanks with 50,000 liter capacity, a large capacity pump and sand filter, and a drip irrigation system with approximately 27,000 emitters.
   B. Full AC power at the site for operating a series of data loggers and cable testers necessary for site monitoring.
   C. Establishment of four monitoring strategies, including the installation of redundant monitoring systems to support them.
   D. The use of manual and automatic data collection systems, and intrusive and non-intrusive systems, all of which overlapped from one monitoring strategy to the next.

3. The approved field study design was implemented at the Maricopa site, including a significant amount of additional site development (e.g., re-installed irrigation system, added AC power). At the time of proposal development, we intended to use the existing infrastructure at the agricultural center, but soon found that most of the components would require replacement. For example, though AC power was available just west of the support zone, the amperage was insufficient to operate our instruments, and a significant level of AC noise was observed in our TDR systems. The smaller amperage was boosted by the installation of power lines from different sources, but the AC background noise could not be resolved without modifying data collection from the TDR instruments themselves.

4. Two water flow and solute transport experiments were conducted. Experiment 1 was conducted to observe water flow (average flux = 1.85 cm d^{-1} for 23 days) and solute transport (average Br^- input = 31.6 ppm for 14 days) through initially dry soil material. The focus on instrumentation was on detection of changes of a particular performance measure (e.g., water content, water tension, solute concentration). Experiment 2 was conducted using similar boundary conditions

(average water input = 1.97 cm d^{-1} for 33 days). The focus during Experiment 2 was on instrument repeatability, especially for smaller expected changes in water content.

4.2 Summary of Field Observations

1. Water movement within the plot was spatially variable during Experiment 1, due mostly to variability in the initial water content, and thus, the hydraulic conductivity. The results of both intrusive and non-intrusive instruments, many of which provided redundant measurements of performance measures, showed that 1) water movement in the western portion of the site was faster than the eastern portion, most likely due to soil texture and structure; 2) a zone of especially rapid water flow was observed at Y = 45 m, near the center of the plot on the E-W coordinate system, as confirmed using several types of instruments; and 3) the variability of water movement, as measured using neutron probe, decreased with increasing depth, when the effective thickness of the soil profile was increased.

2. Spatial variability of water movement during Experiment 2 was significantly reduced in surface soils (< 1.5 m). We found, from using HDS units in the trench, that variability was reduced from CV = 41.8 % to 4.7 % between Experiments 1 and 2, respectively. The reduced variability was observed because the flux-controlled water application led to more uniform hydraulic conductivity fields, and thus, more uniform water movement. If a flooding method of water application had been used, infiltration rates would have been highly dependent on the hydraulic conductivity of surface soils, an aspect of the field site that would be very difficult to characterize or monitor. Given that most natural infiltration occurs in non-flood conditions (e.g., rainfall rate < soil hydraulic conductivity), the boundary conditions used during the experiments are more realistic and easily monitored.

3. The irrigation system used for the experiments performed with very low variability. During initial testing of the system, we measured the Coefficient of Uniformity of about 95% on a single irrigation station of approximately 4500 drip emitters. Water application rates were thus very consistent, especially considering the complexity of the system. Given that uniformity coefficients of sprinkler irrigation systems used for similar studies (e.g., Butters, 1989) were about 80%, we believe that our application was more uniform. Though the input solute concentration varied somewhat during Experiment 1, the problem could have been resolved by installing additional sensors at the mixing tanks, and an automatic shut-off switch for the pump. These components were not installed prior to Experiment 1 because we were unaware of the potential difficulties in estimating the correct volumes of water that were required on a day-to-day basis. The variability issues became apparent only after the chemical analyses were performed. The relatively short time frame dedicated to tracer input during Experiment 2 reduced the need to retrofit the mixing tanks.

4. Implementation of large field studies requires a significant level of design and staff effort in order to achieve satisfactory results. During the design of the instrumentation, electrical wiring and plumbing systems, field personnel became mired in the details of installation, causing a much higher staff effort than was originally allocated. Budgets for monitoring programs at disposal sites must account for the fact that field installation will be very tedious; undercutting staff effort could lead to reduced vigilance during installation, causing weak links to develop in the monitoring systems. Moreover, the monitoring system needs to be carefully designed to account for longevity in the presence of potentially aggressive subsurface environments. Sufficient design factors should account for expansion of the monitoring system and the increased life span of the components.

5. The variety of monitoring systems used at the site provided a large amount of data so that technical personnel could gain a better understanding of the significance of water movement across the site. For example, after reviewing the data from Experiment 1, we noted that a zone of rapid water movement was observed at approximately Y = 45 m, near the center of the plot. Using any one monitoring system would have led us to question whether the zone was real or an artifact of field activities. However, we recorded the rapid water movement using several systems: neutron probe in both N-S horizontal access tubes, and tensiometers, TDR, and HDS units installed in the

trench at Y = 45 m. The lateral offset of these instruments was 2.5 m, and the instruments were backfilled differently. Therefore, we consider it to be only a remote possibility that the fast flow paths were caused anthropomorphic activities. These redundant measurements provided much higher confidence in our observations that a fast flow path existed at that location. Reliance on a single monitoring system would have made these observations less supportable.

4.3 Summary of Positive Aspects of Field Design and Implementation

1. As stated above, the redundancy of measurements designed into the field study allowed us to observe water arrival and redistribution with enhanced reliability because we used independently controlled measurement instruments. We consider the use of redundant monitoring systems potentially advantageous for the ability to monitor water or contaminant release from a disposal site. For example, in the monitoring trench, we used three instruments that measure soil tension as a performance measure: HDS units measure thermal diffusivity, tensiometers measure soil tension directly, and thermocouple psychrometers measure soil humidity. Each instrument has a specific range of measurement, and other limitations with respect to installation and operation, yet each ultimately measures the same performance measure. Therefore, relying on a single monitoring instrument in a field monitoring program increases the vulnerability of the program, making it susceptible to uncontrollable environmental conditions. Using several instruments reduces this susceptibility.

2. The large field size permitted the field team to study water movement not previously possible from other field experiments, especially with respect to spatial variability of water movement. Collection of additional samples (e.g., soil, water, and data) could improve the understanding of field observations during the two experiments, and thus confirm the reliability of the data.

3. The use of integrated data logging systems was, after a steep learning curve, flexible enough to allow a large number and a wide variety of sensors to be monitored simultaneously. The sensors, mostly available through a small number of vendors, were wired into a series of data loggers (models CR7 and CR10X, Campbell Scientific, Inc., Logan UT). The loggers were programmed so that adequate amounts of data were collected during and between the experiments. Though we relied on AC power to recharge the battery packs installed in the loggers, solar cells could have easily provided adequate power. These loggers, or models from other vendors, other data loggers must provide necessary data throughput and sensor ports for the wide variety of monitoring systems expected for LLW disposal sites. Moreover, the logging system must be flexible enough to expand the monitoring program with new instruments, or to contract the program by removing instruments without replacing the logger itself.

4.4 Field Problems That Led to Data Loss

1. The majority of field problems which led to lost or unreliable data were caused by faulty electrical connections between sensors and electrical leads immediately adjacent to the instrument or the nearest opening to conduit. Of the instruments used during the field research, tensiometers equipped with pressure transducers (especially in the monitoring trench and deep boreholes) were most vulnerable to faulty electrical connections because transducers were not purchased with the exact lead length, thereby requiring extra soldering and weatherproofing. When the units were placed in the humid soil environment, these connections began corroding, eventually leading to the failure of five of 19, and nine of 19 units during the water applications phases of Experiments 1 and 2, respectively. In the case of tensiometers installed in the deep boreholes, corrosion of the surface electrical connections led to data loss from six of 27, and 17 of 27 units during Experiments 1 and 2, respectively. Obviously, this would not be acceptable during long-term monitoring programs, so additional measures will be needed to reduce or eliminate the corrosion problem. Thermocouple psychrometers and HDS units, in contrast, were purchased with specific lead lengths which were estimated *a priori* by the field team. Moreover, the electrical leads were potted

directly to the sensor. The lower cost pressure transducer (e.g., $30 - $60 each) are available only with shorter, precut leads, and in some cases, without any leads. Higher cost units (closer to $500 each) can be purchased with pre-specified lengths.

2. AC power is thought to have caused significant feedback through both TDR systems at the site, requiring much longer time periods for data collection, and higher noise. The feedback was caused by a poorly grounded AC electrical system as it entered the Maricopa site. Similar feedback has been identified in other TDR systems (R. Reedy, Univ. of Texas at Austin, 1997, personal communication). The noise was manifested in a backward-moving standing wave that overwhelmed the normal waveform associated with moist soil. To account for this feedback during Experiment 1, filtering on the cable tester was maximized, but this did not completely solve the problem; thus, some data were clearly unreliable. Between Experiments 1 and 2, both TDR systems were modified so that the cable testers were electrically removed from AC power while data were collected. During periods between data collection, the AC system was used to recharge the cable tester batteries. More intensive testing of the TDR systems before the beginning of Experiment 1 would have reduced data loss.

3. It appears that the neutron probe instrument, used for the vertical access tubes, became more variable with time. We noted, for example that the Coefficients of Variation for the standard counts, taken in a borehole approximately 20 m west of the irrigated plot, were 5.1 % and 8.5 % during Experiments 1 and 2, respectively. The higher standard counts (average counts were 3.7% higher during Experiment 2) and the higher variability from one day to the next causes the count ratio to also become more variable. When looking at wetting front arrival, this variability is negligible. However, it becomes very important when calculating mass balance. It is not clear why the variability would be higher during Experiment 2, though it is possible that the lower ambient temperature may have played a role.

4. Our experiences during the field experiment indicate the strong need to dedicate at least one technical person to immediately reduce and check the incoming data for accuracy or reliability. During site planning, specific personnel were responsible for checking specific data streams, but they became overloaded during active field work. This led to a faster rate of personnel fatigue. Immediate data checking by site personnel could have been instrumental in reducing some of the data gaps that are now present in the final data base.

5. Instrument responses to added water were clearly stronger during the initial wetting from Experiment 1, than during the smaller increases in water content (and decreases in water tension) during Experiment 2. In the case of the EM method, the change in EC_a were very small and thus more affected by background noise. Other instruments were affected similarly, e.g., neutron probe. This points to the need for isolating the subsurface soil material from premature wetting before burial of waste material, especially below the disposal zone. Otherwise, instrument variability will reduce the detection sensitivity of the instrument, so that only large changes will be statistically significant.

References

Baehr, A.L. and M.F. Hult, Evaluation of unsaturated zone air permeability through pneumatic tests, Water Resour. Res., 27, 2605-2617, 1991.

Borchers, B., T. Uram, and J.M.H. Hendrickx, Tikhonov regularization of electrical conductivity depth profiles in field soils, Soil Sci. Soc. Am. J. 61, 1004-1009, 1997.

Briscoe, R.D, Thermocouple psychrometers for water potential measurements. Reprint from the Proceedings of the NATO Advanced Study Institute on 'Advanced Agricultural Instrumentation', May 27-June 9, Il Ciocco (Pisa), Italy, 1984.

Butters, G.L., W.A. Jury, and F.F. Ernst, Field scale transport of bromide in an unsaturated soil 1. Experimental methodology and results, Water Resour. Res. 25, 1575-1581, 1989.

Carneiro, C. and E. de Jong, In-situ determination of the slope of the calibration curve of a neutron probe using a volumetric technique, Soil Sci. 139, 250-254, 1985.

Carslaw, H.S. and J.C. Jaeger, *The Conduction of Heat in Solids*, 510 p, Oxford Univ. Press, London, 1959.

CATI. Performance report for irrigation equipment - drip emitters and microsprinklers. Center for Irrigation Technology Publication No. 950103. Cal. State Univ., Fresno, Fresno, California, 1995.

Cresswell, H.P., Evaluation of the portable pressure transducer technique for measuring field tensiometers, Aust. J. Soil Res, 31, 397-406, 1993.

Edwards, K.B., Air permeability from pneumatic tests in oxidized till, J. Environ. Engin., 120, 329-346, 1994.

Elabd, H., I. Porro, and P.J. Wierenga, Estimation of field transport parameters using the convection dispersion equation. *In* "International conference and workshop on the validation of flow and transport models for the unsaturated zone," P.J. Wierenga and D. Bachelet, editors, May, 1988.

Fredlund D.G. and D.K.H. Wong, Calibration of thermal conductivity sensors for measuring soil suction, Geotech. Test. J., 12, 188-194, 1989.

Grismer, M.E. K.M. Ball, and F.E. Robinson, Field-scale neutron probe calibration and variance analysis for clay soil, J. of Irrig. and Drain. Engin., 121, 354-362, 1995.

Harding Lawson & Associates, Final vadose zone and trench cap monitoring plan, proposed low-level radioactive waste disposal facility, Ward Valley, California, 1991.

Joss, C.J. and A.L. Baehr, AIR2D - A computer program to simulate two dimensional axisymmetric air flow in the unsaturated zone, *in* U.S. Geol. Survey Open File Report 97-588, 106 p, U.S. Geol. Survey, 1997.

Kozak, M.W. and N.E. Olague, Updated recommendations for low-level waste performance assessment, Proceedings of the Symposium on Waste Management at Tucson, Arizona, 371-376, 1993.

Massmann, J. and D.F. Farrier, Effects of atmospheric pressures on gas transport in the vadose zone, Water Resources Research, 28, 777-791, 1992.

McNeill, J.D., Rapid, accurate mapping of soil salinity by electromagnetic ground conductivity meters. *In* Advances in measurement of soil physical properties: Bringing theory into practice, SSSA Special Publication no. 30. Soil Sci. Soc. Am., Madison, WI, 1992.

Montgomery, D.C., *Design and analysis of experiments*, 4th edition, John Wiley and Sons, New York, NY, 1997.

National Research Council. Ward Valley: An Examination of Seven Issues in Earth Sciences and Ecology, National Academy Press, Washington, D.C., 1995.

Nilson, R.H., E.W. Peterson, K.H. Lie, N.R. Burkard, and J. R. Hearst, Atmospheric pumping: a mechanism causing vertical transport of contaminated gases through fractured permeable media, J. Geophys. Res., 96, 21933-21948, 1991.

Office of the Federal Register, Code of Federal Regulations. Title 10, Parts 51 to 199. U.S. Governmental Printing Ofc., Washington, DC, 1990.

Porro, I., P.J. Wierenga, R.G. Hills, 1993, Solute transport through large uniform and layered soil columns, Water Resour. Res., 29, 1321-1330, 1993.

Prudic, D.E., and R.G. Striegl, Tritium and radioactive Carbon (14C) analyses of gas collected from unsaturated sediments next to a low-level radioactive-waste burial site south of Beatty, Nevada, April 1994 and July 1995, *In* U.S. Geol. Surv. Open-File Report, 7 p, U.S. Geol. Surv., 1995.

Radcliffe, D.E, P.M. Tillotson, P.F. Hendrix, L.T. West, J.E. Box, E.W. Tollner, Anion transport in a Piedmont ultisol: I. Field scale parameters, Soil Sci. Soc. Am. J., 60, 755-761, 1996.

Rawlins, S.L. and G.S. Campbell, Water potential: Thermocouple psychrometry, *In*: A. Klute (ed.) Methods of soil analysis, Part 1- Physical and mineralogical methods Agron. Mono. 9, 2nd Ed., p. 597-618, ASA, Madison, WI, 1986.

Reece, C.F., Evaluation of a line heat dissipation sensor for measuring soil matric potential, Soil Sci. Soc. Am. J., 60, 1022-1027, 1996.

Rojstaczer, S. and J. P. Tunks, Field-based determination of air diffusivity using soil-air and atmospheric pressure time series, Water Resour. Res., 12, 3337-3343, 1995.

Sheets, K.R. and J.M.H. Hendrickx, Noninvasive soil-water content measurement using electromagnetic induction, Water Resour. Res., 31, 2401-2409, 1995.

Shum, E., R.J. Starmer, M.H. Young, Environmental monitoring at low-level radioactive waste disposal facilities, NUREG-1388, U.S. Nuclear Regulatory Commission, Washington, DC, 1989.

Soil Conservation Service, Soil Survey: Eastern Maricopa and Northern Pinal Counties Area, Arizona, USDA/SCS, U.S. Government Printing Office, Washington, DC., 1974.

Soil Conservation Service, Soil Survey of Pinal County, Arizona, Western Part, USDA/SCS, U.S. Government Printing Office, Washington, DC, 1991.

Striegl, R.G., D.E. Prudic, J.S. Duval, R.W. Healy, E.R. Landa, D.W. Pollock, D.C. Thorstenson, and E.P. Weeks, Factors affecting tritium and ^{14}Carbon distributions in the unsaturated zone near the low-level radioactive-waste burial site south of Beatty, Nevada, in U.S. Geological Survey Open File Report, pp. 16, U.S. Geological Survey, 1996.

Stubben, M.A. and D.J. LaBreque, 3-D ERT inversion used to monitor an infiltration experiment: In Proceedings of the symposium on the application of geophysics to engineering and environmental problems, EEGS, Chicago, Illinois, 593-602, 1998.

Toride, N., F. J. Leij, and M. Th. van Genuchten, The CXTFIT code for estimating transport parameters from laboratory or field tracer experiments, Version 2.0. Research Report No. 137, U.S. Salinity Laboratory, USDA, ARS, Riverside, California, 1995.

U.S. Dept. of Agriculture, Soil taxonomy: Washington, D.C., Soil Conservation Service, 754 p, 1975.

Vinson, J., P.J. Wierenga, R.G. Hills, and M.H. Young, Flow and transport at the Las Cruces trench site: Experiment 2b, NUREG/CR-6437, U.S. Nuclear Regulatory Commission, Washington, DC, 1997.

Weeks, E. P., Field determination of vertical permeability to air in the unsaturated zone, *In* U.S. G.S. Prof. Paper, pp. 41, U.S. Geol. Surv., 1978.

Wierenga, P.J., R.M. Hagan, and D.R. Nielsen, Soil temperature profiles during infiltration and redistribution of cool and warm irrigation water, Water Resour. Res., 6, 230-238, 1970.

Young, M.H., J.B. Fleming, P.J. Wierenga, and A.W. Warrick, Rapid laboratory calibration of TDR probes using upward infiltration, Soil Sci. Soc. Am. J., 61, 707-712, 1997.

Young, M.H., Z-Y. Zou, L.L Hofmann, and P.J. Wierenga, Neutron probe calibration using field infiltration data, Soil Sci., submitted, 1998a.

Young, M.H., P.J. Wierenga, A.W. Warrick, L.L. Hofmann, and S.A. Musil, Variability of water front velocities during field-scale infiltration experiments, Water Resour. Res. Submitted, 1998b.

Young, M.H., P.J. Wierenga, A.W. Warrick, L.L. Hofmann, S.A. Musil, B.R. Scanlon, and T.J. Nicholson, Field testing plan for unsaturated zone monitoring and field studies,

NUREG/CR-6462, U.S. Nuclear Regulatory Commission, Washington, DC, 1996.

Young, M.H., A.W. Warrick, P.J. Wierenga, and S.A. Musil, Comparing monitoring strategies at the Maricopa Site, Arizona, NUREG/CR-5698, U.S. Nuclear Regulatory Commission, Washington, DC, 1999.

Appendix A-1. Coordinates of monitoring devices at the Maricopa site

Vertical Neutron Probe Access Tubes

Number	Location	X Coordinate (m)	Y Coordinate (m)	Depth (m)
1	401	5	10	3
2	402	15	10	15
3	403	25	10	15
4	404	28	10	3
5	405	35	10	15
6	406	45	10	3
7	407	55	10	3
8	411	0	20	3
9	412	10	20	3
10	413	20	20	3
11	414	28	20	3
12	415	40	20	3
13	416	50	20	3
14	417	60	20	3
15	421	5	30	3
16	422	15	30	15
17	423	25	30	15
18	424	28	30	3
19	425	35	30	15
20	426	45	30	3
21	427	55	30	3
22	431	0	40	3
23	432	10	40	3
24	433	20	40	3
25	434	28	40	3
26	435	40	40	3
27	436	50	40	3
28	437	60	40	3
29	441	5	50	3
30	442	15	50	15
31	443	25	50	15
32	444	28	50	3

Number	Location	X Coordinate (m)	Y Coordinate (m)	Depth (m)
33	445	35	50	15
34	446	45	50	3
35	447	55	50	3
36	451	28	0	3
37	452	28	2.5	3
38	453	28	5	3
39	454	28	15	3
40	455	28	25	3
41	456	28	35	3
42	457	28	45	3
43	458	28	55	3

Time Domain Reflectometry Probes

Number	Location	X Coordinate (m)	Y Coordinate (m)	Depth (m)
1	141	30	0	1.5
2	142	30	2.5	1.5
3	143	30	5	1.5
4	144	30	10	1.5
5	145	30	15	1.5
6	146	30	20	1.5
7	147	30	25	1.5
8	148	30	30	1.5
9	149	30	35	1.5
10	150	30	40	1.5
11	151	30	45	1.5
12	152	30	50	1.5
13	153	30	55	1.5
14	201	20	18.7	0.5
15	202	20	18.7	1
16	203	20	18.7	1.5
17	204	20	18.7	2
18	205	20	18.7	2.5
19	206	20	18.7	3
20	211	22.524	18.7	0.5
21	212	22.524	18.7	1
22	213	22.524	18.7	1.5
23	214	22.524	18.7	2
24	215	22.524	18.7	2.5
25	216	22.524	18.7	3
26	221	21.262	19.462	1
27	222	21.262	19.462	2
28	223	21.262	19.462	3
29	231	18.738	20.538	1
30	232	18.738	20.538	2
31	233	18.738	20.538	3
32	241	17.476	21.3	0.5
33	242	17.476	21.3	1
34	243	17.476	21.3	1.5
35	244	17.476	21.3	2
36	245	17.476	21.3	2.5
37	246	17.476	21.3	3
38	251	20	21.3	0.5

Number	Location	X Coordinate (m)	Y Coordinate (m)	Depth (m)
39	252	20	21.3	1
40	253	20	21.3	1.5
41	254	20	21.3	2
42	255	20	21.3	2.5
43	256	20	21.3	3

Tensiometers

Number	Location	X Coordinate (m)	Y Coordinate (m)	Depth (m)
1	123	30	5	1
2	125	30	15	1
3	127	30	25	1
4	129	30	35	1
5	131	30	45	1
6	133	30	55	1
7	141	30	0	1.5
8	142	30	2.5	1.5
9	143	30	5	1.5
10	144	30	10	1.5
11	145	30	15	1.5
12	146	30	20	1.5
13	147	30	25	1.5
14	148	30	30	1.5
15	149	30	35	1.5
16	150	30	40	1.5
17	151	30	45	1.5
18	152	30	50	1.5
19	153	30	55	1.5
20	201	20	18.7	0.5
21	202	20	18.7	1
22	203	20	18.7	1.5
23	204	20	18.7	2
24	205	20	18.7	2.5
25	206	20	18.7	3
26	211	22.524	18.7	0.5
27	212	22.524	18.7	1
28	213	22.524	18.7	1.5
29	214	22.524	18.7	2
30	215	22.524	18.7	2.5
31	216	22.524	18.7	3
32	221	21.262	19.462	1
33	222	21.262	19.462	2
34	223	21.262	19.462	3
35	231	18.738	20.538	1
36	232	18.738	20.538	2
37	233	18.738	20.538	3
38	241	17.476	21.3	0.5
39	242	17.476	21.3	1

Number	Location	X Coordinate (m)	Y Coordinate (m)	Depth (m)
40	243	17.476	21.3	1.5
41	244	17.476	21.3	2
42	245	17.476	21.3	2.5
43	246	17.476	21.3	3
44	251	20	21.3	0.5
45	252	20	21.3	1
46	253	20	21.3	1.5
47	254	20	21.3	2
48	255	20	21.3	2.5
49	256	20	21.3	3
50	301	15	10	5
51	302	15	10	10
52	303	15	10	3
53	311	30	10	5
54	312	30	10	10
55	313	30	10	3
56	321	45	10	5
57	322	45	10	10
58	323	45	10	3
59	331	15	30	5
60	332	15	30	10
61	333	15	30	3
62	341	30	30	5
63	342	30	30	10
64	343	30	30	3
65	351	45	30	5
66	352	45	30	10
67	353	45	30	3
68	361	15	50	5
69	362	15	50	10
70	363	15	50	3
71	371	30	50	5
72	372	30	50	10
73	373	30	50	3
74	381	45	50	5
75	382	45	50	10
76	383	45	50	3

Heat Dissipation Sensors

Number	Location	X Coordinate (m)	Y Coordinate (m)	Depth (m)
1	141	30	0	1.5
2	142	30	2.5	1.5
3	143	30	5	1.5
4	144	30	10	1.5
5	145	30	15	1.5
6	146	30	20	1.5
7	147	30	25	1.5
8	148	30	30	1.5
9	149	30	35	1.5
10	150	30	40	1.5
11	151	30	45	1.5
12	152	30	50	1.5
13	153	30	55	1.5
14	201	20	18.7	0.5
15	202	20	18.7	1
16	203	20	18.7	1.5
17	204	20	18.7	2
18	205	20	18.7	2.5
19	206	20	18.7	3
20	211	22.524	18.7	0.5
21	212	22.524	18.7	1
22	213	22.524	18.7	1.5
23	214	22.524	18.7	2
24	215	22.524	18.7	2.5
25	216	22.524	18.7	3
26	222	21.262	19.462	1
27	224	21.262	19.462	2
28	226	21.262	19.462	3
29	232	18.738	20.538	1
30	234	18.738	20.538	2
31	236	18.738	20.538	3
32	241	17.476	21.3	0.5
33	242	17.476	21.3	1
34	243	17.476	21.3	1.5
35	244	17.476	21.3	2
36	245	17.476	21.3	2.5
37	246	17.476	21.3	3
38	251	20	21.3	0.5
39	252	20	21.3	1

Number	Location	X Coordinate (m)	Y Coordinate (m)	Depth (m)
40	253	20	21.3	1.5
41	254	20	21.3	2
42	255	20	21.3	2.5
43	256	20	21.3	3

Single Chamber Solution Samplers

Number	Location	X Coordinate (m)	Y Coordinate (m)	Depth (m)
1	141	30	0	1.5
2	142	30	2.5	1.5
3	143	30	5	1.5
4	144	30	10	1.5
5	145	30	15	1.5
6	146	30	20	1.5
7	147	30	25	1.5
8	148	30	30	1.5
9	149	30	35	1.5
10	150	30	40	1.5
11	151	30	45	1.5
12	152	30	50	1.5
13	153	30	55	1.5
14	201	20	18.7	0.5
15	202	20	18.7	1
16	203	20	18.7	1.5
17	204	20	18.7	2
18	205	20	18.7	2.5
19	206	20	18.7	3
20	211	22.524	18.7	0.5
21	212	22.524	18.7	1
22	213	22.524	18.7	1.5
23	214	22.524	18.7	2
24	215	22.524	18.7	2.5
25	216	22.524	18.7	3
26	221	21.262	19.462	1
27	222	21.262	19.462	2
28	223	21.262	19.462	3
29	231	18.738	20.538	1
30	232	18.738	20.538	2
31	233	18.738	20.538	3
32	241	17.476	21.3	0.5
33	242	17.476	21.3	1
34	243	17.476	21.3	1.5
35	244	17.476	21.3	2
36	245	17.476	21.3	2.5
37	246	17.476	21.3	3
38	251	20	21.3	0.5
39	252	20	21.3	1

Number	Location	X Coordinate (m)	Y Coordinate (m)	Depth (m)
40	253	20	21.3	1.5
41	254	20	21.3	2
42	255	20	21.3	2.5
43	256	20	21.3	3

Dual Chamber Solution Samplers

Number	Location	X Coordinate (m)	Y Coordinate (m)	Depth (m)
44	301	15	10	5
45	302	15	10	10
46	303	15	10	3
47	311	30	10	5
48	312	30	10	10
49	313	30	10	3
50	321	45	10	5
51	322	45	10	10
52	323	45	10	3
53	331	15	30	5
54	332	15	30	10
55	333	15	30	3
56	341	30	30	5
57	342	30	30	10
58	343	30	30	3
59	351	45	30	5
60	352	45	30	10
61	353	45	30	3
62	361	15	50	5
63	362	15	50	10
64	363	15	50	3
65	371	30	50	5
66	372	30	50	10
67	373	30	50	3
68	381	45	50	5
69	382	45	50	10
70	383	45	50	3

Temperature Thermocouples

Number	Location	X Coordinate (m)	Y Coordinate (m)	Depth (m)
1	104	30	10	0.05
2	106	30	20	0.05
3	114	30	10	0.1
4	116	30	20	0.1
5	124	30	10	0.25
6	126	30	20	0.25
7	144	30	10	0.5
8	146	30	20	0.5
9	164	30	10	1
10	166	30	20	1

Thermocouple Psychrometers

Number	Location	X Coordinate (m)	Y Coordinate (m)	Depth (m)
1	141	30	0	1.5
2	142	30	2.5	1.5
3	143	30	5	1.5
4	144	30	10	1.5
5	145	30	15	1.5
6	146	30	20	1.5
7	147	30	25	1.5
8	148	30	30	1.5
9	149	30	35	1.5
10	150	30	40	1.5
11	151	30	45	1.5
12	152	30	50	1.5
13	153	30	55	1.5

Surface Electromagnetic Induction

Number	Location	X Coordinate (m)	Y Coordinate (m)	Depth (m)
1	1	-15.4	-4.7	0
2	2	-6.4	-4.7	0
3	3	2.6	-4.7	0
4	4	11.6	-4.7	0
5	5	20.6	-4.7	0
6	7	38.6	-4.7	0
7	8	47.6	-4.7	0
8	9	56.6	-4.7	0
9	11	-15.4	1.3	0
10	12	-6.4	1.3	0
11	13	2.6	1.3	0
12	14	11.6	1.3	0
13	15	20.6	1.3	0
14	17	38.6	1.3	0
15	18	47.6	1.3	0
16	19	56.6	1.3	0
17	20	65.6	1.3	0
18	21	-15.4	10.3	0
19	22	-6.4	10.3	0
20	23	2.6	10.3	0
21	24	11.6	10.3	0
22	25	20.6	10.3	0
23	27	38.6	10.3	0
24	28	47.6	10.3	0
25	29	56.6	10.3	0
26	30	65.6	10.3	0
27	31	-15.4	19.3	0
28	37	38.6	19.3	0
29	38	47.6	19.3	0
30	39	56.6	19.3	0
31	40	65.6	19.3	0
32	41	-15.4	28.3	0
33	42	-6.4	28.3	0
34	43	2.6	28.3	0
35	44	11.6	28.3	0
36	45	20.6	28.3	0
37	47	38.6	28.3	0
38	48	47.6	28.3	0
39	49	56.6	28.3	0
40	50	65.6	28.3	0

Number	Location	X Coordinate (m)	Y Coordinate (m)	Depth (m)
41	51	-15.4	37.3	0
42	52	-6.4	37.3	0
43	53	2.6	37.3	0
44	54	11.6	37.3	0
45	55	20.6	37.3	0
46	57	38.6	37.3	0
47	58	47.6	37.3	0
48	59	56.6	37.3	0
49	61	-15.4	46.3	0
50	62	-6.4	46.3	0
51	63	2.6	46.3	0
52	64	11.6	46.3	0
53	65	20.6	46.3	0
54	67	38.6	46.3	0
55	68	47.6	46.3	0
56	69	56.6	46.3	0
57	70	65.6	46.3	0
58	71	-15.4	55.3	0
59	72	-6.4	55.3	0
60	73	2.6	55.3	0
61	74	11.6	55.3	0
62	75	20.6	55.3	0
63	76	29.6	55.3	0
64	77	38.6	55.3	0
65	78	47.6	55.3	0
66	79	56.6	55.3	0
67	80	65.6	55.3	0
68	81	-15.4	64.3	0
69	82	-6.4	64.3	0
70	83	2.6	64.3	0
71	84	11.6	64.3	0
72	85	20.6	64.3	0
73	86	29.6	64.3	0
74	87	38.6	64.3	0
75	88	47.6	64.3	0
76	89	56.6	64.3	0
77	90	65.6	64.3	0

Electroresistivity Borehole Tomography

Number	Location	X Coordinate (m)	Y Coordinate (m)	Depth (m)
1	7	-6	30	15
2	6	4	30	15
3	5	14	30	15
4	4	24	30	15
5	3	34	30	15
6	2	44	30	15
7	1	54	30	15
8	12	4	40	15
9	11	14	40	15
10	10	24	40	15
11	9	34	40	15
12	8	44	40	15

Appendix B-1. Collection of Soil Samples

B-1.1 Introduction

Soil samples were collected from selected boreholes and during trench construction. Samples collected from boreholes used the split-spoon sample method in conjunction with the hollow-stem auger drilling method. Soil samples collected during trench construction, and during other site activities, used either the grab (disturbed) or tube (undisturbed) method.

Sampling of unconsolidated material was performed for subsequent laboratory analysis of selected general analytes, particle size distribution, or tracer concentration. Undisturbed soil samples, collected using the tube method, were analyzed for general analytes and particle size distribution, as well as for determining hydraulic or transport parameters.

B-1.2 Material and Equipment

Grab Method

- Hand trowel
- Sample collection bag
- Alconox® detergent, if necessary
- Log book

Tube method

- Drilling equipment (supplied by the drilling contractor)
- Sample collection sleeves, acrylic or brass, 61 cm long, 2.54 cm inside diameter
- Alconox® detergent, if necessary
- End caps
- Marking pens
- Log book

Undisturbed core method

- Steel soil core sampler with female threaded bottom
- Male threaded soil core container
- Slide hammer
- Aluminum soil sleeves and spacing rings
- Chain wrench
- Putty knife
- Saran wrap and electrical tape
- Markers and labels
- Containers for soil cores

B-1.3 Procedures

Grab sampling of soil

- Choose an adequate location for collection of soil. This can be either a specific location in the open trench, or cuttings retrieved from the auger flights of the mechanical drilling rig, or from a pile of soil collected after excavation.
- Label the sample bag accordingly
- Using the hand trowel, scoop or dig up the soil and store in the sample bag.
- Seal the sample bag (or container).

Store the sample in a cooler maintained at 4°C, until transportation to the U of A campus in Tucson, AZ.
Record in the Sample Collection Logbook information on the sampling event and the sample itself, as listed in Section 3.3.

Tube Samplers

Collection of soil samples using either a split spoon sampler will be performed by the drilling contractor H-F Drilling (Phoenix, AZ). Their staff was responsible for collecting samples in depth locations specified by U of A field crews, in a manner consistent with applicable standards developed by the American Society for Testing and Materials (ASTM, Philadelphia, PA). U of A field crew, however, were responsible for several tasks that relate to collection of undisturbed soil samples. They are listed below.
Choose the depths and spatial locations for collection of soil. The locations currently chosen (at the time of this writing) are listed in Table 2.1 of this appendix.
Label the tube (or sample bag) accordingly. Prior to inserting the acrylic tubes into the split barrel sampler, marked with an indelible marker, or with tape, in such a way that the direction of sample collection will be known.
Once the sampling apparatus is assembled by the drillers, including the tube sampler, measure the total length of the drilling string, so that the exact depth of soil collection will be known and recorded.
After collection of the sample tube, check the percent recovery. This can be done visually if acrylic tubes are used. Alternatively, measure gaps of soil at either end of an opaque tube (e.g., brass, stainless steel) and assume that no gaps of soil exist inside the tube. If tubes are not used, determine percent recovery directly from amount of soil in tube.
Seal the tube with plastic end caps, and seal closed using electrical tape. This will prevent the water content of the soil sample from changing.
Store the sample away from direct sunlight until transportation to the U of A campus in Tucson, AZ.
Record in the Sample Collection Logbook information on the sampling event and the sample itself, as listed in Section 3.4.

Undisturbed Soil Core Samplers

Determine location of sample collection and mark label and logbook accordingly. Locations are listed in Table 2.
Insert tared sleeve with ring spacers on top and bottom into core sampler container.
Screw container into sampling device until snug.
Hold sampling device upright and drive container into soil with slide hammer until entire container is blow ground surface.
Turn sampling device counter-clockwise to break soil core at base of samplers, and lift up to remove assembly from ground.
Remove sample container after loosening with chain wrench.
Remove sleeve and ring spacers from containers by applying pressure to bottom of core.
Remove ring spacers making sure not to break core, leaving center soil core with rounded ends.
Use putty knife to shave ends of soil core, leaving approximately 1 cm of soil on both ends of the core.
Wrap the core in saran wrap and tape closed with electrical tape.
Place wrapped core in container, label and seal.
Keep soil core away from the direct sun, placing core in a cooler as soon as possible.

B-1.4 Logbook Entries

The following information, when appropriate, will be entered into the field notebook each time a sample is collected:

a. sample location/identifier;
b. depth at which sample was collected;

c. date and time sample was collected;
d. analyses to be performed;
e. sample lithologic description, if possible.
f. percent recovery, if appropriate;
g. any other pertinent information, such as difficulties in sampling or unusual drilling occurrences.

B-1.5 Quality Control/Quality Assurance

B-1.6 Soil Compaction During Tube Sampling

It is important to note that secondary compaction during sampling is a potential problem when using tube samplers. This problem is compounded when the sampler is driven with a hammer, as opposed to placing the sampler ahead of the bit during drilling. The undisturbed core samples that have been subjected to hammering may have incorrectly high bulk densities. Also, the depth of sampling determined for each subsample within the tube will be affected. Vinson (New Mexico State University, personal communication, 1990) found compaction to be up to 25% in some cases when using 5 foot spoon samplers inside of a hollow stem auger, making it very difficult to calculate the exact depth of collection. Very dry soils are susceptible to this problem. The depths of collection can be estimated by normalizing the recovery by the total length of the sampler. Each depth is then multiplied by the normalizing factor for that particular sampler.

B-1.7 Cross-contamination

Any equipment that could contact soil material being collected for chemical analysis, must be decontaminated prior to use. If soil material is collected in plastic sleeves, then decontamination may not be necessary since soil never comes into direct contact with components of the soil sampler. If soil can contact the sampling tool, then it should be cleaned by washing the sampling tool in tap water and Alconox® detergent, then rinsed clean with tap water. The use of solvents (e.g., alcohol, hexane) to achieve better decontamination will not be performed during this research, because 1) the majority of samples to be collected using the tube samplers will be prior to the introduction of tracers, 2) the tracers themselves are inorganic, and 3) the analytical equipment is not precise enough to warrant extra cleaning measures.

Table B-1.1. Spatial locations and depths for collection of soil using split spoon sampling

X,Y Coordinate (m)	
5, 55	
55,5	
55,55	
Depth increments	
feet	meters
0-2	0-0.6
5-7	1.52-2.31
10-12	3.05-3.66
15-17	4.57-5.18
20-22	6.10-6.71
25-27	7.62-8.23
30-32	9.14-9.75
35-37	10.67-11.28
40-42	12.19-12.80
45-47	13.72-14.33
Bottom of borehole	

Table B-1.2. Locations and numbers of replicates of undisturbed soil core samples

Locations†	Depth (m)	Replicates‡
29, 0	1.5	3
29, 2.5	1.5	3
29, 5.0	1.5	3
29, 10.0	1.5	3
29, 15.0	1.5	3
29, 20.0	1.5	3
29, 25.0	1.5	6
29, 30.0	1.5	3
29, 35.0	1.5	3
29, 40.0	1.5	3
29, 45.0	1.5	3
29, 50.0	1.5	3
29, 55.0	1.5	3
28,5.0	0.12	2
28,5.0	0.37	2
28,5.0	0.84	2
28,45.0	0.24	2
28,45.0	0.48	2

† Represented as X,Y location on the field plot. Exact locations and depths may vary somewhat, because replicate samples were collected.

‡ Replicate core samples were collected no closer than 15 cm from one another.

Appendix C-1. Estimation of Gas Permeabilities for the MEM Site

INTRODUCTION

Upward and downward migration of gases from waste-disposal facilities is a critical issue for low-level radioactive waste disposal. Gaseous radionuclides in low-level waste include H-3, C-14, and Rn-222. Upward migration of gases to the surface can be important, particularly during operation of the facility (Kozak and Olague, 1993). High tritium values (for example 1,100 TU at 24 m depth, = 162 TU at 109 m depth) have been found adjacent to the Beatty site, Nevada, that cannot readily be explained by liquid or combined liquid and vapor transport (Prudic and Striegl, 1995; Striegl et al., 1996). Because disposal practices at Beatty varied in the past and included disposal of as much as ~ 2,000 m^3 of liquid waste, further research on tritium movement at Beatty is warranted. Transport mechanisms for gases include not only diffusion but also advection. Analysis of gas transport is important at many low-level waste disposal facilities as shown by the intensive program to monitor concentrations and concentration gradients of gaseous radionuclides proposed for the California low-level radioactive waste disposal facility (Harding Lawson & Assoc., 1991). Performance assessment calculations require information on parameters related to gas transport to predict long-term migration of gases in the subsurface. The purpose of this part of the Maricopa study was to evaluate different techniques of estimating gas transport parameters and of monitoring subsurface gas migration.

Pneumatic pressure tests were conducted to estimate vertical and horizontal air permeabilities at different levels. In addition, permeabilities were calculated from atmospheric breathing data that included evaluation of subsurface response to barometric pressure fluctuations. Computer simulations suggest that air from the surface can move several meters into the ground during typical barometric pressure cycles (Massmann and Farrier, 1992). Gas ports were installed at different depths in two boreholes to evaluate atmospheric pumping. The results of this study will provide valuable information on subsurface gas transport processes and the various techniques to obtain data on parameters required for simulation of such processes. These data are required for performance assessment calculations for future.

METHODS

Theory

Advective transport of gases depends on gas permeability and the presence of a pressure gradient. Gas permeability can be estimated from (1) pneumatic tests and (2) analysis of atmospheric pumping data.

Pneumatic Tests

Pneumatic tests are widely used to evaluate gas permeability in the unsaturated zone. In pneumatic tests, air is either injected or extracted from a well, and pressure is monitored in gas ports installed at different depths in surrounding monitoring wells. Most analyses of pneumatic tests assume that the gas content (θ_G) is constant over time; that is, that there is no redistribution of water during the test.

A variety of techniques are available for analyzing pneumatic tests. The initial transient phase of the test or the steady-state portion of the test can be analyzed. The transient phase of gas tests is generally short (~ seconds to hours; Edwards, 1994) and it is sometimes difficult to collect reliable data. Most studies analyze the steady-state portion of the test. Analysis of pneumatic tests is similar to the inverse problem in well hydraulics, where permeabilities are estimated from pressure data. Various solutions for estimating gas permeability differ in terms of the boundary conditions that are assumed at the ground

surface (such as unconfined, leaky confined, and confined) and the method of solution. The lower boundary is generally assumed to be the water table or an impermeable layer. All solutions assume radial flow from a vertical well.

Steady-state and horizontally axisymmetric air flow in the unsaturated zone is described by the following equation:

$$k_r \frac{\partial^2 \phi}{\partial r^2} + \frac{k_r}{r} \frac{\partial \phi}{\partial r} + k_z \frac{\partial^2 \phi}{\partial z^2} = 0 \qquad \text{(C-1)}$$

where k_r is horizontal permeability, r is radial distance, z is depth, and $\phi = P^2$, where P is air pressure. Baehr and Hult (1991) provided analytical solutions to this equation. A computer code (AIR2D) is available that includes these analytical solutions (Joss and Baehr, 1997). Air compressibility is approximated by the ideal gas law. The pressure dependence of permeability (Klinkenberg effect) is neglected.

Analysis of Atmospheric Pumping Data

Comparison of temporal variations in gas pressure (monitored at different depths in the unsaturated zone) with atmospheric pressure fluctuations at the surface can be used to determine the minimum vertical air permeability that exists between land surface and monitoring depth (Weeks, 1978; Nilson et al., 1991).

Data analysis consists of expressing the variations in atmospheric pressure as time-harmonic functions. Attenuation of the surface waves at different depths in the unsaturated zone provides information on how well or how poorly the unsaturated sections are connected to the surface. The accuracy of the results increases with the amplitude of the surface signals.

The governing equation is:

$$\frac{\partial P}{\partial t} = \alpha \frac{\partial^2 P}{\partial z^2} \qquad \text{(C-2)}$$

where, t is time, $\alpha = \frac{kP_0}{\mu_G \theta_G}$ is the pneumatic diffusivity, k is permeability, P_0 is the mean static pressure, μ_G is the gas viscosity, and is θ_g volumetric gas content. The surface pressure varies harmonically as

$$P = P_0 + \Delta P \cos \omega t \qquad \text{(C-3)}$$

where ω is the angular frequency ($2\pi/T$) and T is the period. The water table or a low-permeability air barrier is assumed to act as a no-flow boundary. Equation 2 is solved with the above boundary conditions for the ratio of subsurface to surface pressure amplitudes (Carslaw and Jaeger, 1959 in [Nilson et al, 1991]):

$$\frac{P - P_0}{\Delta P} = \frac{\sqrt{\cosh[\sqrt{2}\lambda(1 - \frac{z}{h})] + \cos[\sqrt{2}\lambda(1 - \frac{z}{h})]}}{\sqrt{\cosh\sqrt{2}\lambda + \cos\sqrt{2}\lambda}} \qquad \text{(C-4)}$$

where $\frac{P - P_0}{\Delta P}$ is the amplitude ratio, ΔP is the pressure variation at the surface, P is the pressure at depth, P_0 is the mean pressure at the mean surface, $\lambda = h\sqrt{\frac{\omega}{\alpha}} = \sqrt{\frac{2\pi h^2}{\alpha T}}$, and h is the depth to the lower boundary or water table. Using equation 4 one solves for λ, and then calculates α and k. The ratio of the amplitude at a certain depth z compared with the amplitude at the surface can be obtained graphically or by using time series analysis (Rojstaczer, 1995).

Materials And Methods

A total of six boreholes were drilled for the soil gas studies at the Maricopa site. Four boreholes were drilled outside the irrigated plot for pneumatic pressure tests. The other two boreholes were used to monitor subsurface gas pressures in response to barometric pressure fluctuations, one inside (MAM1) and the other outside (MAM2) the irrigated plot.

Four boreholes were drilled to conduct pneumatic pressure tests. An injection/extraction borehole (designated MI1) was drilled to 5 m depth, and 3 monitoring boreholes (designated MP1, MP2, and MP4) to 10 m depth at distances of 1, 2, and 4 m from the injection/extraction borehole. Sediment samples were collected at 0.3 m intervals to total depth for texture and water content analyses in all boreholes. A PVC screen (5 cm diameter with 0.25 mm slots) was installed at the base of the injection/extraction well (MI1). A PVC pipe of similar diameter was used to connect the screen to the surface. Sand (20/40) was used to complete the boreholes around the screens and the remainder of the borehole was completed with grout to land surface. Gas ports were installed at 2.5 m intervals in each of the monitoring boreholes. The gas ports consisted of 3 mm copper tubing at the desired test depth with a 3 cm slotted section at the base. Sand was used to complete the borehole surrounding the screened intervals. Thermistors were placed at each depth in MP2 to record temperature fluctuations during testing All grout used was pounded into the borehole in dry form. The powdered material was then set up in-situ.

The pneumatic tests were conducted using a high volume, low pressure blower to inject/extract air into MI1. A ROTRON Model EN6F5L blower was used with a 1.80 m section of flexible hose (5 cm diameter) attached to a 3 m section of pipe to establish laminar flow. At the end of the pipe a thermistor, a flow meter, and a 15 psi pressure transducer were used to measure the air temperature, flow rate, and injection pressure respectively. A second section of flexible hose connected the pipe to the PVC well head on MI1. A Campbell CR10X data logger was used to monitor pressures and temperatures. A Campbell AM416 Multiplexer was used to switch between the 12 pressure transducers (4 units in each of the 3 boreholes) and 4 thermistors used during testing. Data required for analysis included flow rate from the air pump, temperature and pressure of injected or extracted air, pressure at all monitored depths in all monitored boreholes, and temperature measurements from one borehole. Injection tests were conducted at 5, 10, 15 and 20 Pa. Two tests were run at each injection pressure. Each test was run until no observable change occurred in the farthermost pressure transducer (MP4, 10 m depth).

The monitoring atmosphere boreholes (i.e. MAM1 and MAM2) were drilled using a hollow stem auger (diameter: 18.4 cm [7.25 inch]) to a depth of 11 m. Soil samples were collected at 0.3 m depth intervals for analysis of texture and water content. Bulk density samples were collected at 0.9 to 1.5 m depth intervals. Gas ports, consisting of slotted stainless steel screens (2.54 cm outside diameter, 30 cm long), were installed at 2.5 m intervals to 10 m. A YSI thermistor was installed with each gas port to monitor temperature change at depth. The gas ports were connected to the surface using nylon tubing (0.635 cm outside diameter). The borehole was backfilled with sand 13 cm below and above the screens and a 50:50 sand/bentonite mixture to form a seal and to prevent preferential flow in the borehole.

The data logging system consisted of a Campbell Scientific CR10X data logger that controlled solenoid valves, a pressure transducer, a barometer, and thermistors. Each gas port was connected to a dedicated solenoid valve. An extra solenoid valve was included to use as an atmospheric vent. The solenoid controlled flow to a common manifold measured with a single differential pressure transducer (Model 239, SETRA, Acton, MA) at the surface. The solenoid valves were opened and closed by a Campbell CD16AC switching unit which received commands from the CR10X. A Setra 270 Barometer was included to monitor barometric pressure fluctuations. Surface and subsurface gas pressures and temperatures were logged every 15 min to evaluate attenuation and phase lag of pressure fluctuations with depth.

RESULTS AND DISCUSSION

Soil Texture and Water Content

Soil texture is coarse grained (Figure C-1, Table C-1). Gravel content ranged from 0 to 37%. High gravel content was found generally at depths > 5 m in all MP profiles. Mean sand content ranged from 71 to 79%. The dominant textures ranged from gravely sand, sand, loamy sand, and sandy loam. Water content ranged from 0.03 to 0.34 g g^{-1}. Mean water contents ranged from 0.08 to 0.12 g g^{-1} in the various profiles. There was no systematic variation in water content with depth. Variations in water content were generally not related to textural variations.

Pneumatic Tests

Pneumatic tests were conducted in February 1998. The relative locations of the injection and monitoring wells are shown in Figure C-2. We monitored the flow rate, pressure, and temperature of the air at the well head, and subsurface pressures at 2.5 m depth intervals in 3 monitoring wells at distances of 1 m (MP1), 2 m (MP2) and 4 (MP4) from the injection well and temperatures at the monitoring well. Results from a typical pneumatic test are shown in Figure C-3. The initial small step increase in injection pressure (a) corresponds to the pump being switched on and the second step increase (b) corresponds to connection of the pump to the well. Pressures were highest at 5 m depth which corresponds to the injection depth and decreased with distance from the injection well. Pressures at all other monitoring points were much lower. The transient portion of the tests was very short (~ minutes). The steady state data were analyzed using the analytical solutions in the AIR2D code (Baehr and Hult, 1991). The upper boundary was assumed to be open to the atmosphere and the lower boundary is the water table at 11.2 m depth. Input data for the AIR2D simulations are presented in Table C-2. Results of the analyses indicate that the horizontal permeability ranged from 4.8 to 6.7 x10^{-12} m^2 (4.2 to 7.2 darcies, Table C-3). Results from duplicate tests conducted at similar injection pressures were similar. The vertical permeability ranged from 1.2 to 1.8 x 1000^{-12} m^2 and was 2 to 3 times less than the horizontal permeability. The permeability anisotropy is attributed to layering of the sediments.

Atmospheric Pumping

The maximum pressure variation recorded at the surface was 1,000 Pa (10 mbar) in a 24 h period (Figure C-4). This surface pressure variation was attenuated with depth. During high atmospheric pressure periods, the differential pressure at depth is negative, meaning a lower pressure at depth and during low atmospheric pressure periods differential pressure is positive, meaning a higher pressure at depth. Equation C-4 was used to solve for permeability. The amplitude of the pressure variation at the surface (ΔP) was equal to 500 Pa and at different depths ranged from 489 to 497 Pa. The maximum differential pressures measured at the different depths ranged from 3 to 11 Pa for this period which approaches the limits of the differential pressure transducer used to monitor these pressure fluctuations (Figure C-5). Because attenuation of the pressure signal with depth was negligible, the amplitude ratio is close to 1. Equation 4 was solved iteratively, and λ was estimated by minimizing the difference between the measured and calculated amplitude ratio. In order to calculate permeability from λ a value of 0.2 was used for volumetric air content. Minimum vertical air permeabilities ranged from 0.6

to 0.9 x10^{-12} m^2 (0.6 to 0.9 darcies) at different depths. These values of vertical permeability are similar to vertical air permeabilities estimated from the pneumatic data.

Sensitivity analyses were conducted to evaluate the atmospheric pumping technique for estimation of minimum vertical air permeabilities under different conditions. Variations in the ratio of the subsurface to the surface P amplitudes for different permeabilities and water table depths were calculated by modifying equation C-4. A ratio of 1 indicates no pressure attenuation. These analyses indicate that the attenuation factor is negligible in high permeability media if the water table is shallow (~ 10 m; Figure C-6a). Decreasing the permeability increases the pressure attenuation. Increasing the depth to the water table also increases the pressure attenuation. The combination of high permeability and shallow water table at this site results in negligible attenuation of barometric pressure fluctuations with depth.

CONCLUSIONS

The site is characterized by coarse grained sediments with mean water contents of ~ 0.1 g g^{-1}. Pneumatic tests resulted in horizontal permeabilities that ranged from 1 to 2 x 10^{-12} m^2. Horizontal permeabilities exceeded vertical permeabilities by a factor of 2 to 3 which is consistent with the layering of the sediments at this site. Vertical permeabilities estimated from atmospheric pumping data were similar to those calculated from the pneumatic tests. The high permeabilities and shallow water table at this site result in negligible attenuation of surface pressure fluctuations with depth which is consistent with theory.

Table C-1. Soil moisture and texture by depth for boreholes.

Well ID	Depth (m)	θ_g	Gravel (%)	Sand (%)	Silt (%)	Clay (%)	Soil Texture
MI1	0.34	0.05	2	67	15	16	Sandy Loam
	0.85	0.08	2	64	19	16	Sandy Loam
	1.52	0.11	1	66	26	8	Sandy Loam
	2.87	0.11	0	85	11	4	Loamy Sand
	3.08	0.11	3	82	11	5	Loamy Sand
	3.32	0.11	0	84	12	5	Loamy Sand
	3.69	0.13	0	89	6	5	Sand
	3.99	0.11	29	57	11	4	Gravelly Muddy Sand
	4.33	0.10	2	64	19	16	Sandy Loam
	4.57	0.10	3	65	18	15	Sandy Loam
	4.79	0.10	1	64	28	7	Sandy Loam
	5.15	0.18	0	64	29	7	Sandy Loam
	Mean	0.11	4	71	17	9	
MP1	0.24	0.03	3	68	18	13	Sandy Loam
	0.88	0.09	1	62	22	15	Sandy Loam
	1.19	0.10	2	67	28	4	Sandy Loam
	1.46	0.08	11	64	18	7	Gravelly Muddy Sand
	1.80	0.07	0	82	14	4	Loamy Sand
	1.89	0.07	0	93	6	1	Sand
	2.16	0.05	0	88	9	3	Sand
	2.35	0.06	0	54	40	6	Sandy Loam
	2.71	0.10	0	84	12	4	Loamy Sand
	3.05	0.12	0	73	23	4	Sandy Loam
	3.28	0.09	0	69	26	5	Sandy Loam
	3.63	0.12	1	91	7	1	Sand
	3.99	0.13	3	92	5	1	Sand
	4.19	0.09	1	92	6	1	Sand
	4.54	0.09	3	90	6	2	Sand
	4.91	0.13	10	87	2	1	Gravelly Sand
	5.18	0.08	12	86	1	1	Gravelly Sand
	5.70	0.21	19	77	3	2	Gravelly Sand
	6.37	0.24	15	82	3	1	Gravelly Sand
	6.74	0.07	14	79	6	2	Gravelly Sand
	7.04	0.06	14	82	3	2	Gravelly Sand
	7.35	0.04	36	60	3	2	Sandy Gravel
	7.35	0.05	10	82	5	4	Gravelly Sand
	7.65	0.04	1	67	21	12	Sandy Loam
	8.46	0.03	3	79	12	7	Loamy Sand
	8.81	0.04	11	75	10	5	Gravelly Muddy Sand
	9.17	0.05	7	80	8	5	Gravelly Muddy Sand
	9.37	0.06	31	60	6	4	Muddy Sandy Gravel
	9.68	0.04	37	56	6	2	Muddy Sandy Gravel
	9.78	0.03	0	67	29	4	Sandy Loam
	10.09	0.06	0	63	31	6	Sandy Loam
	Mean	0.08	8	76	12	4	
MP2	0.34	0.06	1	70	16	14	Sandy Loam
	0.63	0.05	2	66	19	14	Sandy Loam

Well ID	Depth (m)	θ_g	Gravel (%)	Sand (%)	Silt (%)	Clay (%)	Soil Texture
	0.94	0.08	2	67	21	11	Sandy Loam
	1.12	0.08	2	49	40	10	Loam
MP2	1.49	0.08	4	64	28	5	Sandy Loam
	1.86	0.06	0	78	16	6	Loamy Sand
	2.16	0.06	1	70	20	10	Sandy Loam
	2.41	0.05	0	84	11	5	Loamy Sand
	2.47	0.04	0	87	10	4	Loamy Sand
	2.71	0.04	0	82	15	3	Loamy Sand
	3.08	0.15	0	67	29	4	Sandy Loam
	3.28	0.15	0	84	14	2	Loamy Sand
	3.63	0.12	1	94	3	2	Sand
	3.89	0.12	6	90	3	1	Gravelly Sand
	4.54	0.11	6	94	-1	0	Gravelly Sand
	4.60	0.11	4	93	2	2	Sand
	5.21	0.12	8	82	8	2	Gravelly Muddy Sand
	6.45	0.15	10	89	1	0	Gravelly Sand
	6.74	0.34	9	86	5	1	Gravelly Sand
	6.93	0.12	0	94	5	1	Sand
	7.24	0.05	26	70	3	1	Gravelly Sand
	7.35	0.06	27	70	2	1	Gravelly Sand
	7.65	0.04	17	76	5	3	Gravelly Sand
	7.85	0.02	16	77	5	2	Gravelly Sand
	8.15	0.11	1	66	22	11	Sandy Loam
	8.56	0.04	3	62	21	14	Sandy Loam
	8.90	0.04	2	79	13	7	Loamy Sand
	9.17	0.07	15	70	9	6	Gravelly Muddy Sand
	9.48	0.06	13	79	4	4	Gravelly Sand
	9.68	0.05	27	67	3	3	Gravelly Sand
	10.03	0.05	18	75	4	4	Gravelly Sand
	10.39	0.04	0	53	38	9	Sandy Loam
	Mean	0.08	7	76	12	5	
MP4	0.53	0.07	3	67	20	11	Sandy Loam
	0.88	0.09	1	66	20	14	Sandy Loam
	1.45	0.12	3	74	17	7	Sandy Loam
	1.49	0.10	0	65	22	13	Sandy Loam
	2.36	0.05	5	86	7	3	Sand
	2.71	0.14	0	74	19	7	Sandy Loam
	3.41	0.09	0	70	24	6	Sandy Loam
	4.24	0.11	0	62	34	4	Sandy Loam
	5.21	0.10	0	91	7	1	Sand
	6.02	0.18	5	91	2	2	Gravelly Sand
	6.31	0.10	4	70	23	4	Sandy Loam
	6.92	0.22	9	77	9	6	Gravelly Muddy Sand
	7.28	0.07	0	92	6	2	Sand
	7.85	0.04	21	76	3	1	Gravelly Sand
	8.20	0.04	12	79	7	3	Gravelly Muddy Sand
	8.76	0.11	0	59	27	14	Sandy Loam
	9.07	0.07	0	65	24	11	Sandy Loam
	9.68	0.04	8	84	5	4	Gravelly Sand
	9.98	0.07	10	57	26	7	Gravelly Muddy Sand
	Mean	0.10	4	74	16	6	

Well ID	Depth (m)	θ_g	Gravel (%)	Sand (%)	Silt (%)	Clay (%)	Soil Texture
MAM1	0.53	0.05	2	64	18	17	Sandy Loam
	0.88	0.11	1	58	24	18	Sandy Loam
	1.55	0.12	6	81	4	9	Gravelly Muddy Sand
	2.35	0.09	30	64	4	2	Gravelly Sand
	2.62	0.03	0	69	24	7	Sandy Loam
	3.22	0.06	19	67	11	3	Gravelly Muddy Sand
	4.30	0.05	0	56	36	8	Sandy Loam
	5.14	0.13	2	90	7	2	Sand
	6.13	0.15	3	93	3	1	Sand
	7.28	0.26	0	61	34	5	Sandy Loam
	7.83	0.07	0	95	4	1	Sand
	8.15	0.05	7	90	2	1	Gravelly Sand
	8.76	0.27	0	61	20	19	Sandy Loam
	9.07	0.06	2	78	11	10	Sandy Loam
	9.78	0.04	14	82	1	3	Gravelly Sand
	Mean	0.10	6	74	13	7	
MAM2	0.64	0.07	2	63	17	19	Sandy Loam
	1.45	0.10	24	63	7	7	Gravelly Muddy Sand
	1.75	0.10	0	86	10	4	Loamy Sand
	2.36	0.07	0	96	2	1	Sand
	2.67	0.09	0	75	20	5	Loamy Sand
	3.38	0.08	0	76	19	4	Loamy Sand
	4.24	0.11	0	88	7	4	Sand
	5.21	0.09	19	78	2	2	Gravelly Sand
	6.08	0.16	1	95	2	3	Sand
	6.93	0.15	25	72	2	1	Gravelly Sand
	7.24	0.08	2	87	5	6	Sand
	7.85	0.04	0	94	3	3	Sand
	8.15	0.04	22	73	3	2	Gravelly Sand
	8.76	0.05	1	77	12	11	Sandy Loam
	9.07	0.09	1	72	18	10	Sandy Loam
	9.72	0.05	12	65	11	12	Gravelly Muddy Sand
	10.12	0.05	9	76	8	6	Gravelly Muddy Sand
	Mean	0.08	7	79	9	6	

Table C-2. Input data for air permeability estimation using AIR2D

Extraction Air Pressure (kPa)	5	5	10	10	15	15	20	20
Number of Pressure Transducers	12	12	12	12	12	12	12	12
Air Temperature (°C)	20	20	20	20	20	20	20	20
Soil Temperature (°C)	27.4	28.1	35.7	33.8	35.7	38.0	41.4	41.9
Measured Air Flow Rate (cm^3/sec)	3554	3296	4757	5361	4757	6396	5706	5704
Pressure 1 (D_h=1m, Z=2.5m) (kPa)	0.086	0.086	0.157	0.158	0.247	0.247	0.336	0.336
Pressure 2 (D_h=1m, Z=5m) (kPa)	1.256	1.295	2.404	2.434	3.707	3.706	4.809	4.713
Pressure 3 (D_h=1m, Z=7.5m) (kPa)	0.079	0.079	0.169	0.169	0.259	0.241	0.349	0.349
Pressure 4 (D_h=1m, Z=10m) (kPa)	0.059	0.059	0.112	0.095	0.059	0.041	0.041	0.041
Pressure 5 (D_h=2m, Z=2.5m) (kPa)	0.070	0.070	0.124	0.124	0.213	0.195	0.249	0.249
Pressure 6 (D_h=2m, Z=5m) (kPa)	0.589	0.589	1.078	1.097	1.737	1.736	2.313	2.282
Pressure 7 (D_h=2m, Z=7.5m) (kPa)	0.072	0.072	0.162	0.162	0.252	0.234	0.341	0.341
Pressure 8 (D_h=2m, Z=10m) (kPa)	0.049	0.049	0.085	0.085	0.121	0.121	0.175	0.193
Pressure 9 (D_h=4m, Z=2.5m) (kPa)	0.066	0.066	0.084	0.084	0.137	0.137	0.173	0.173
Pressure 10 (D_h=4m, Z=5m) (kPa)	0.182	0.164	0.362	0.362	0.561	0.561	0.741	0.741
Pressure 11 (D_h=4m, Z=7.5m) (kPa)	0.067	0.067	0.139	0.121	0.194	0.193	0.248	0.266
Pressure 12 (D_h=4m, Z=10m) (kPa)	0.049	0.031	0.085	0.085	0.103	0.103	0.174	0.192
Estimated anisotropy ratio (k_r/k_z)	3.6	4.9	4	3.6	3.51	3.53	3.5	3.61
Estimated horizontal permeability ($X10^{-12}$ m^2)	6.90	7.50	5.60	5.90	5.20	4.95	3.80	3.65

Table C-3. Estimated air permeability with pneumatic testing data using AIR2D

Injection Air Pressure (kPa)	5	5	10	10	15	15	20	20
Number of Pressure Transducers	12	12	12	12	12	12	12	12
Mass Flow (g/s)	4.41	4.09	6.10	6.91	9.07	8.57	7.90	7.73
Horizontal Permeability ($X10^{-12}$ m^2)	6.71	6.56	5.44	5.73	5.05	4.81	3.32	3.55
Vertical Permeability ($X10^{-12}$ m^2)	1.81	1.93	1.32	1.55	1.26	1.19	9.23	8.60
Anisotropy Ratio (k_r/k_z)	3.70	3.40	4.12	3.70	4.01	4.04	3.60	4.13
Mean of Error in Pressure ($X10^{-4}$)	9.32	4.11	2.43	2.79	5.08	5.22	6.76	6.54
Standard Deviation in Pressure ($X10^{-4}$)	9.85	1.27	1.42	1.46	1.66	1.74	2.95	2.27

Table C-4. Vertical permeability estimated from atmospheric pumping data

z (m)	z/h	Amplitude ratio	λ	k ($X10^{-12}$ m^2)
2.5	0.2232	0.9934	0.596610	0.93191
5.0	0.4464	0.9892	0.617777	0.86916
7.5	0.6696	0.9800	0.707350	0.66297
10.0	0.8929	0.9780	0.722725	0.63507

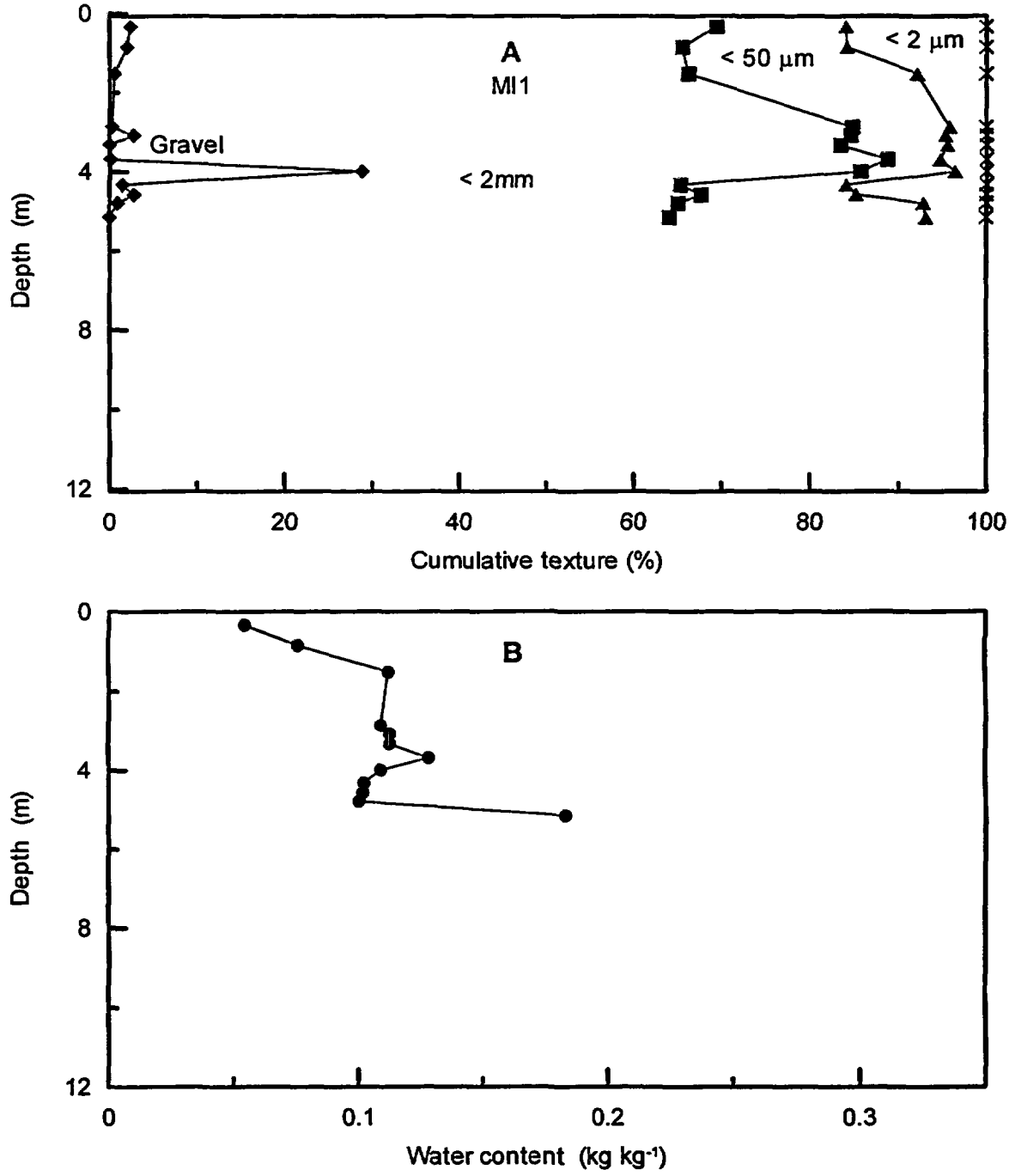

Figure C-1. Cumulative soil texture and water content in samples from boreholes drilled for pneumatic testing [MI1 (A and B), MP1 (C and D), MP2 (E and F), and MP4 (G and H)] and from boreholes drilled for monitoring atmospheric pumping [MAM1 (I and J) and MAM2 (K and L)]. Note that the gravel, sand, silt and clay percentages sum to 100%, unlike the USDA convention of reporting gravel separately.

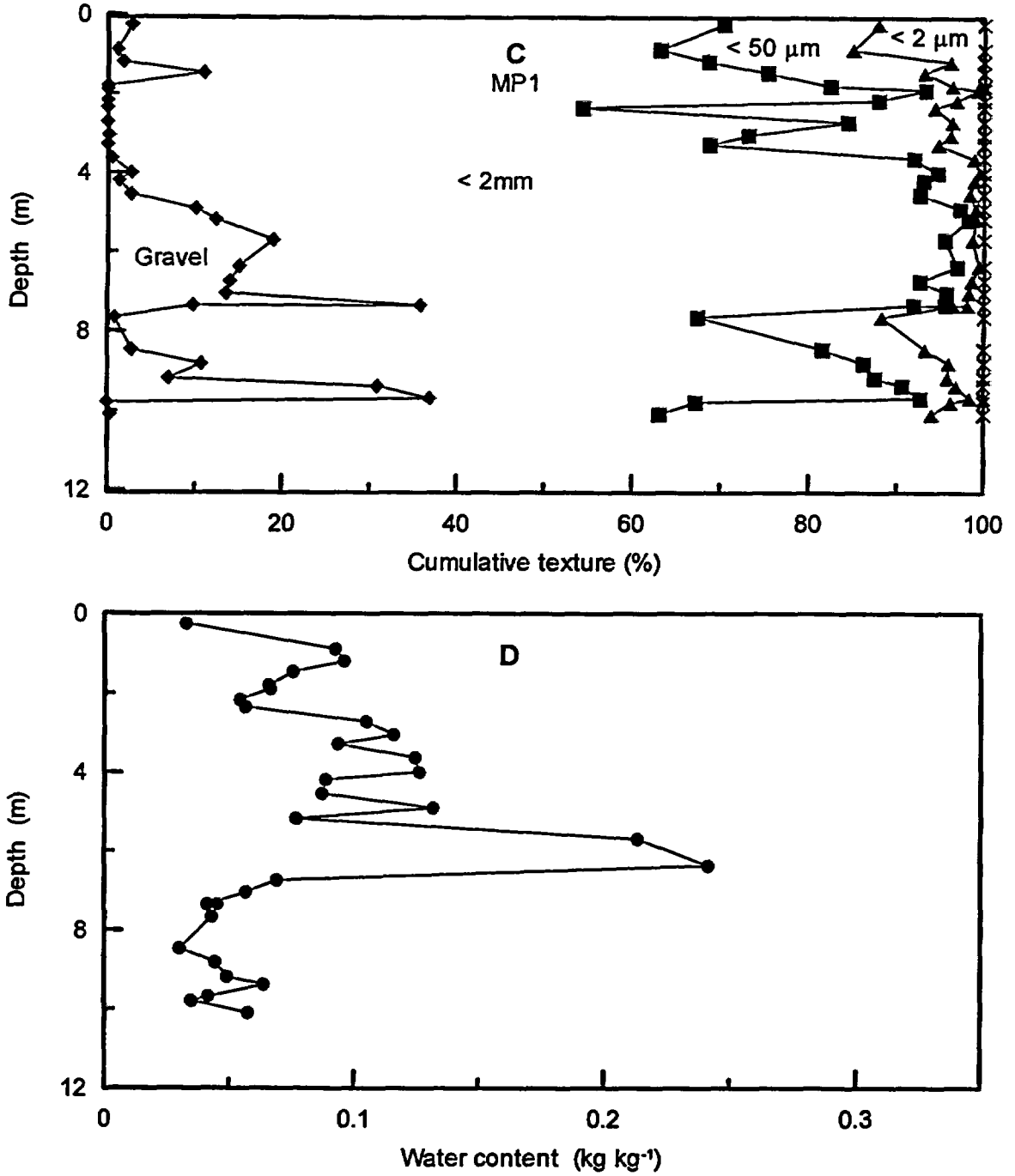

Figure C-1. Cumulative soil texture and water content in samples from boreholes drilled for pneumatic testing [MI1 (A and B), MP1 (C and D), MP2 (E and F), and MP4 (G and H)] and from boreholes drilled for monitoring atmospheric pumping [MAM1 (I and J) and MAM2 (K and L)]. Note that the gravel, sand, silt and clay percentages sum to 100%, unlike the USDA convention of reporting gravel separately. (Continued)

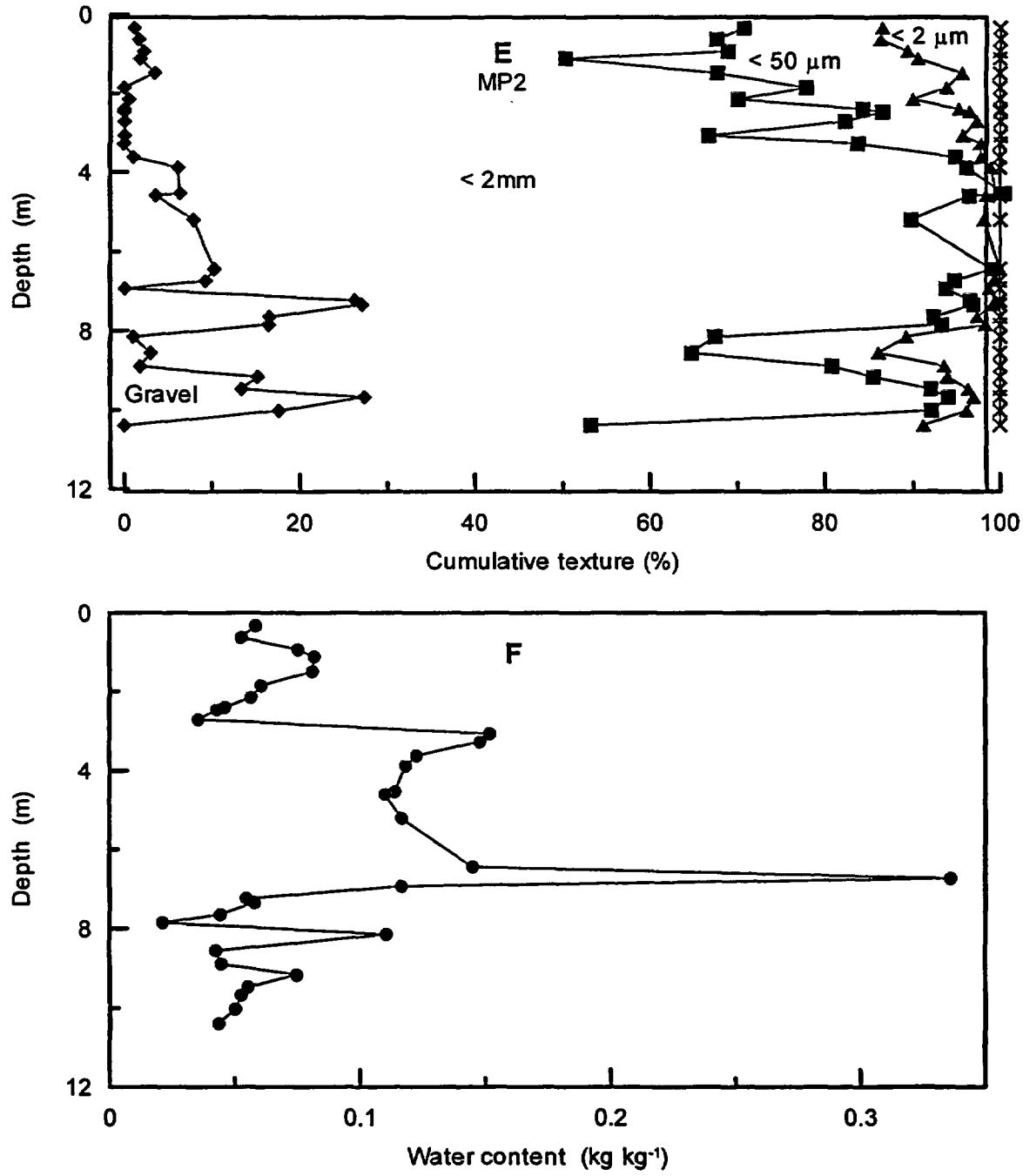

Figure C-1. Cumulative soil texture and water content in samples from boreholes drilled for pneumatic testing [MI1 (A and B), MP1 (C and D), MP2 (E and F), and MP4 (G and H)] and from boreholes drilled for monitoring atmospheric pumping [MAM1 (I and J) and MAM2 (K and L)]. Note that the gravel, sand, silt and clay percentages sum to 100%, unlike the USDA convention of reporting gravel separately. (Continued)

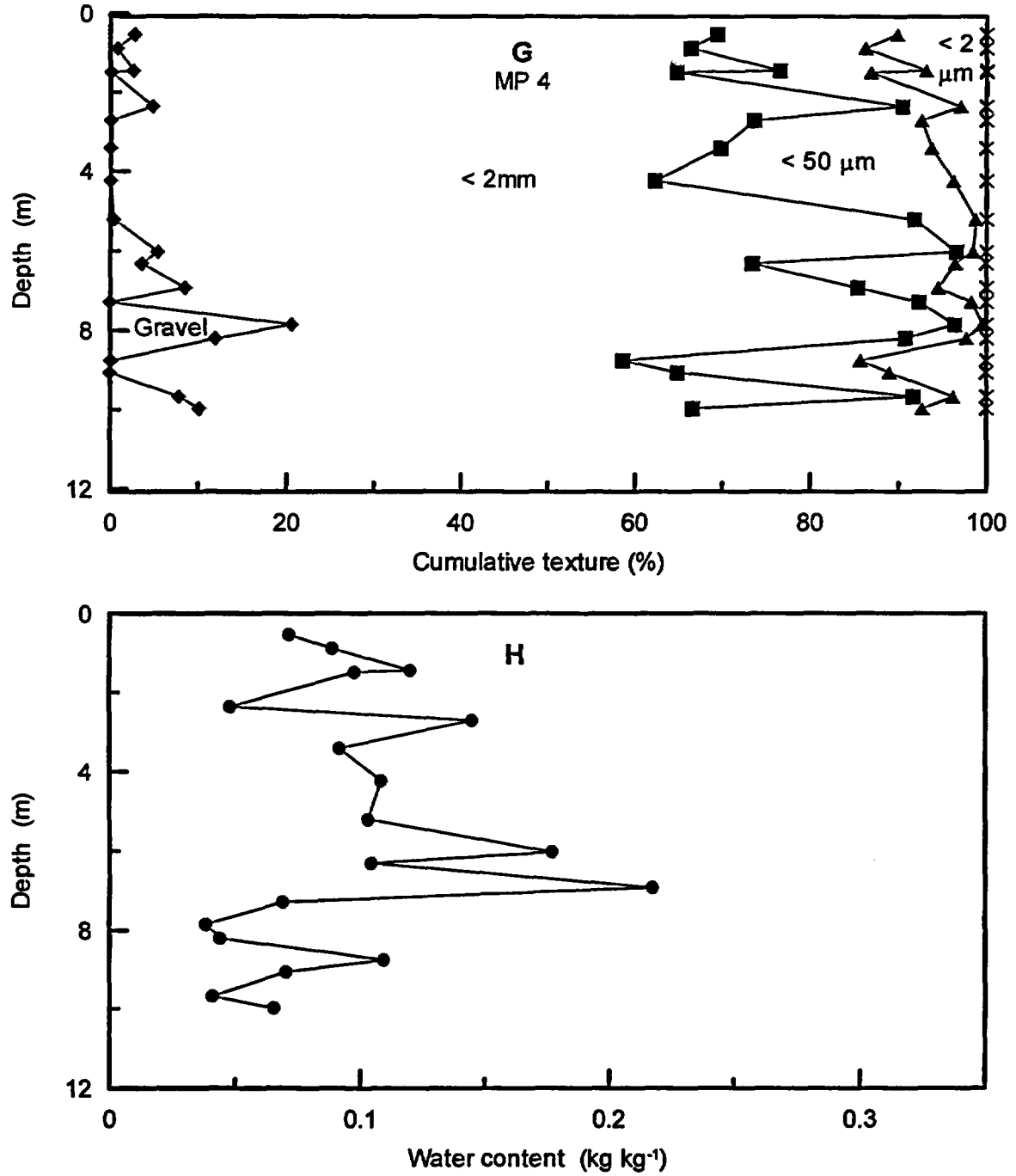

Figure C-1. Cumulative soil texture and water content in samples from boreholes drilled for pneumatic testing [MI1 (A and B), MP1 (C and D), MP2 (E and F), and MP4 (G and H)] and from boreholes drilled for monitoring atmospheric pumping [MAM1 (I and J) and MAM2 (K and L)]. Note that the gravel, sand, silt and clay percentages sum to 100%, unlike the USDA convention of reporting gravel separately. (Continued)

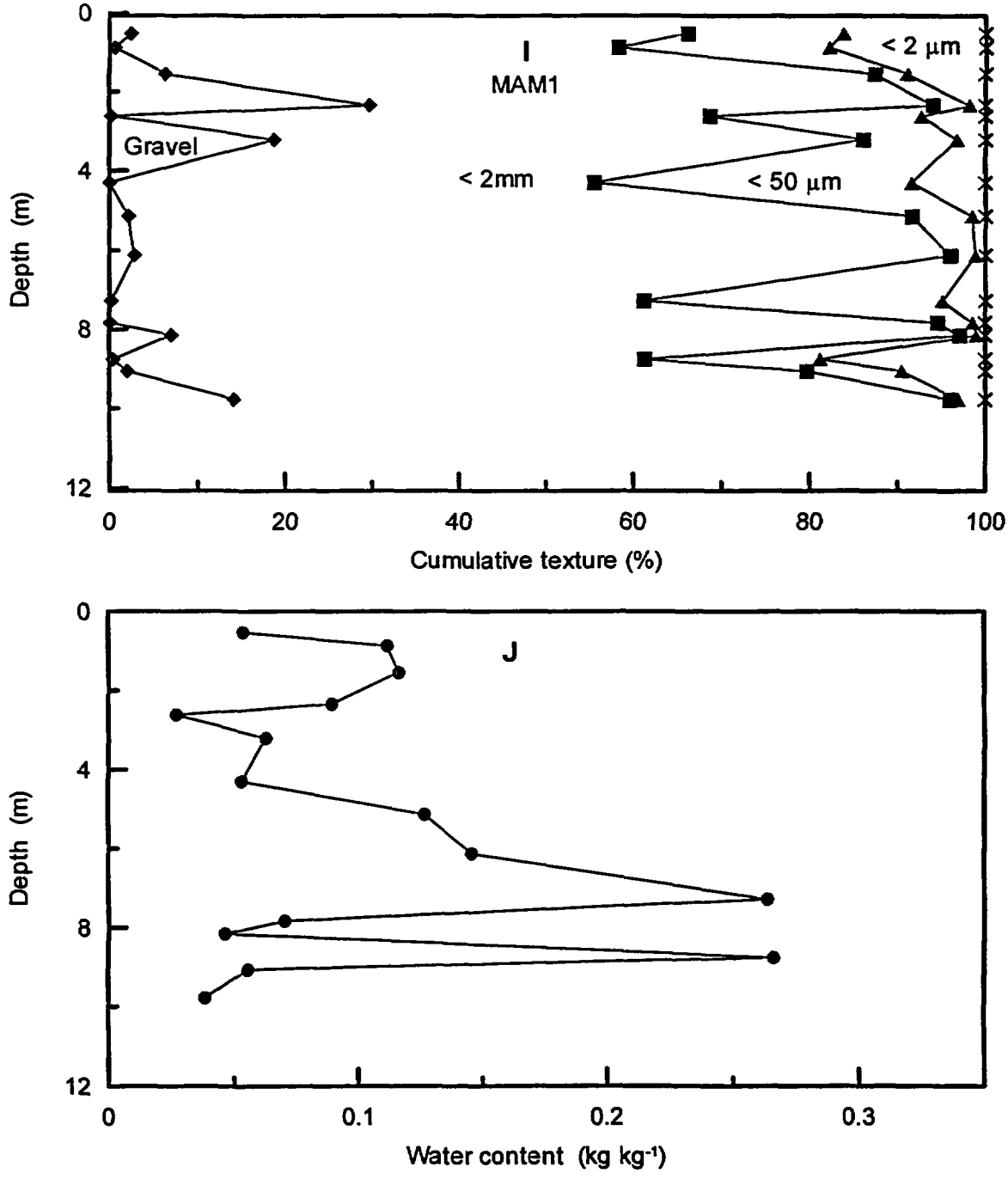

Figure C-1. Cumulative soil texture and water content in samples from boreholes drilled for pneumatic testing [MI1 (A and B), MP1 (C and D), MP2 (E and F), and MP4 (G and H)] and from boreholes drilled for monitoring atmospheric pumping [MAM1 (I and J) and MAM2 (K and L)]. Note that the gravel, sand, silt and clay percentages sum to 100%, unlike the USDA convention of reporting gravel separately. (Continued)

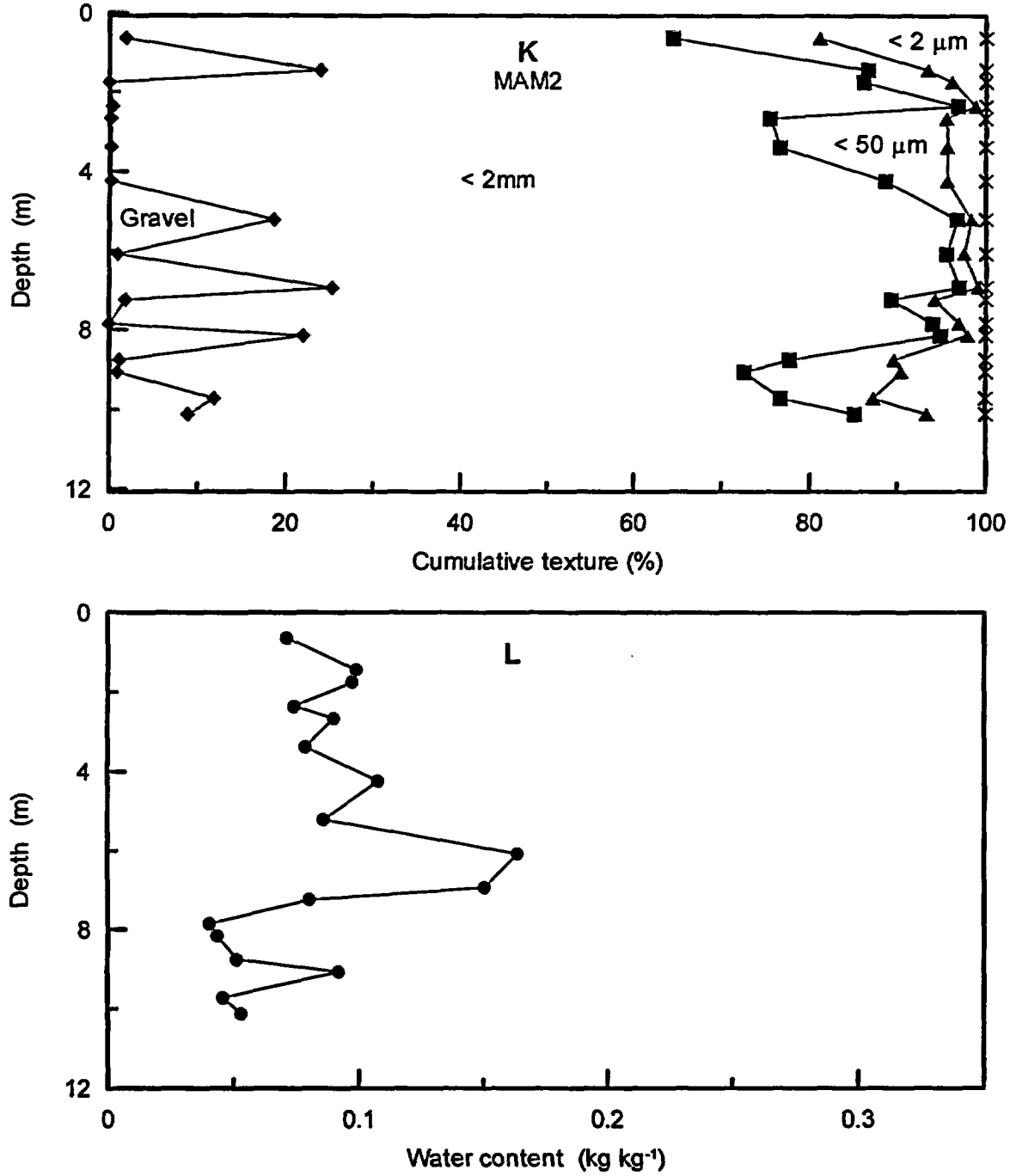

Figure C-1. Cumulative soil texture and water content in samples from boreholes drilled for pneumatic testing [MI1 (A and B), MP1 (C and D), MP2 (E and F), and MP4 (G and H)] and from boreholes drilled for monitoring atmospheric pumping [MAM1 (I and J) and MAM2 (K and L)]. Note that the gravel, sand, silt and clay percentages sum to 100%, unlike the USDA convention of reporting gravel separately. (Continued)

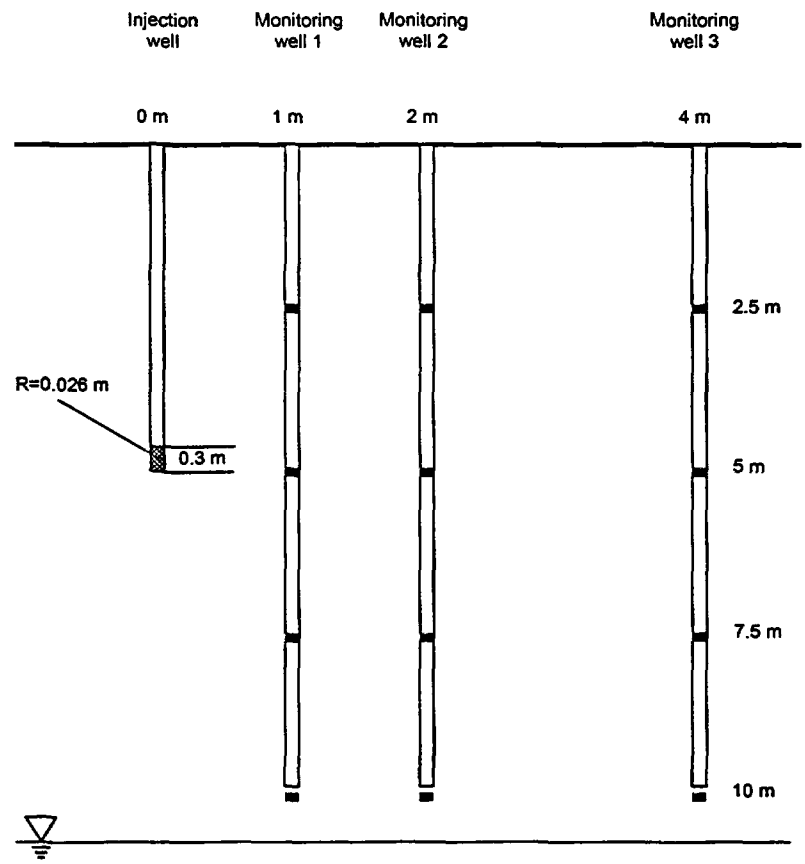

Figure C-2. Cross section of wells used in pneumatic tests.

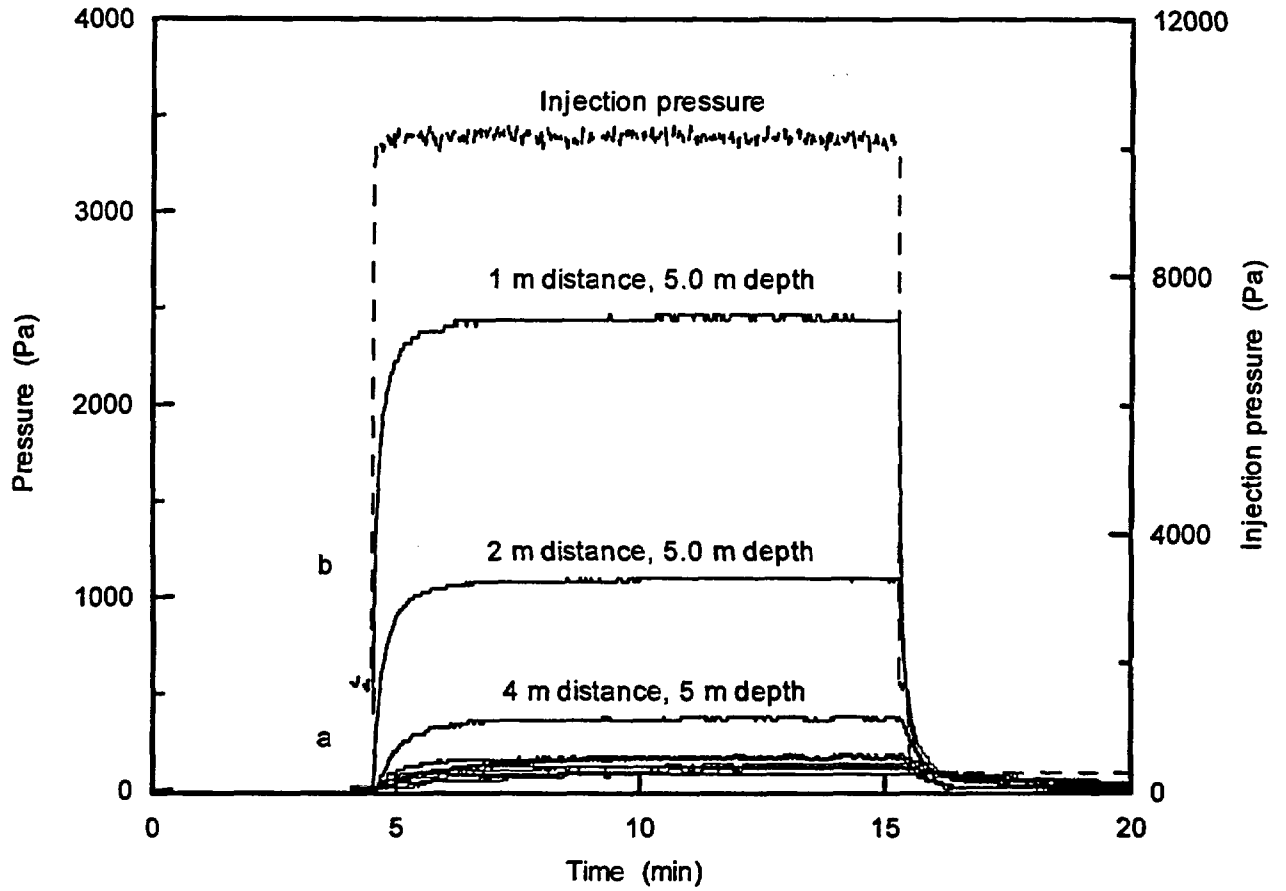

Figure C-3. Injection pressure and pressures in monitoring wells during a typical pneumatic test.

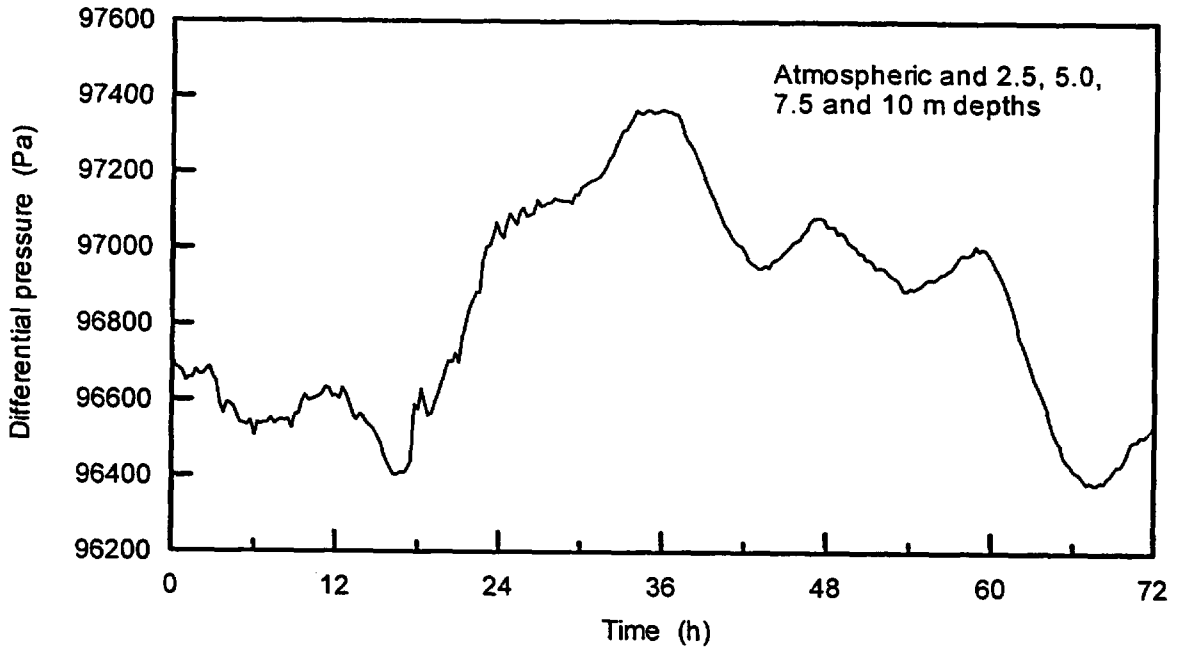

Figure C-4. Surface and subsurface monitoring pressures in monitoring well MAM1 outside the irrigated plot from 9/25/98 through 9/27/98. No differences are seen for measurements 2.5, 5.0, 7.5 and 10 m depths.

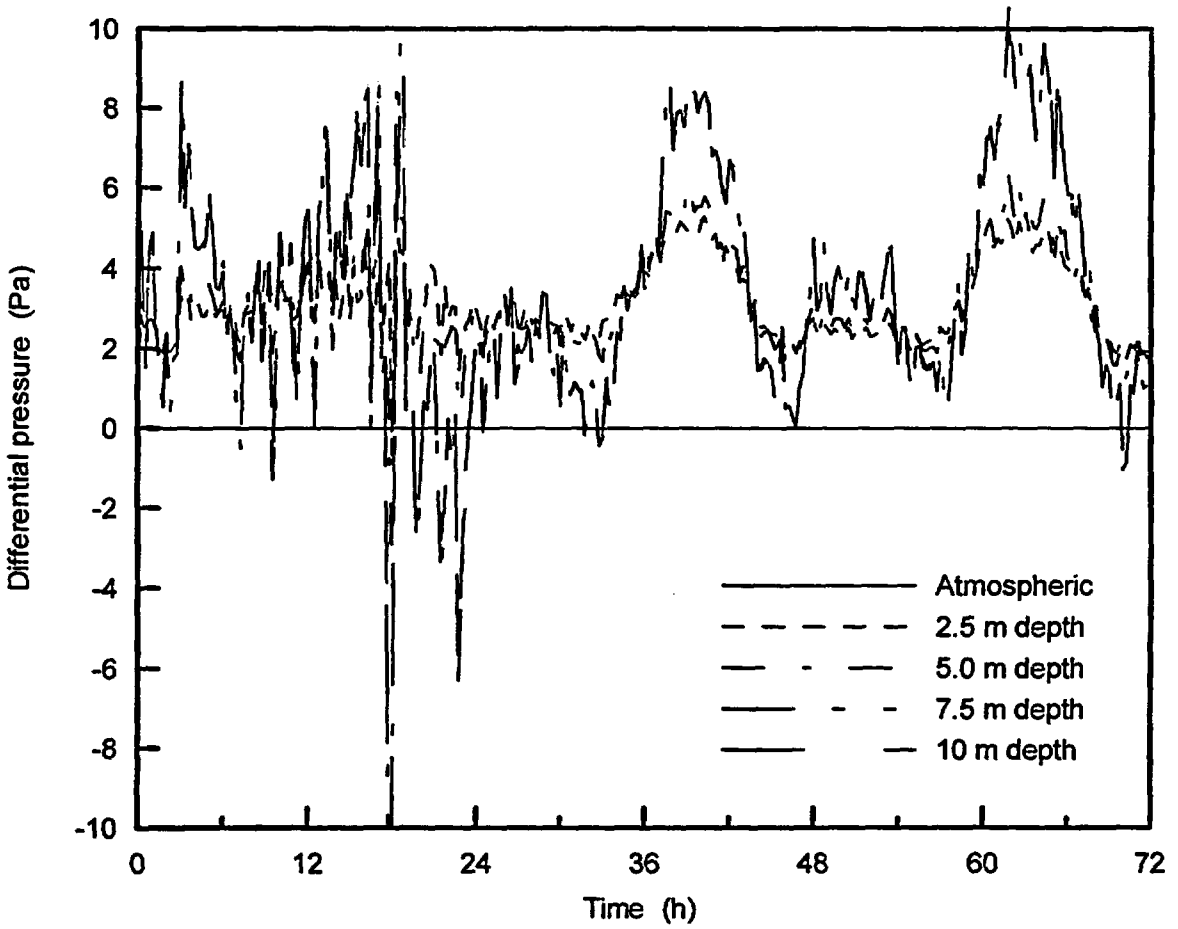

Figure C-5. Differential pressure at different depths from 9/25/98 through 9/27/98.

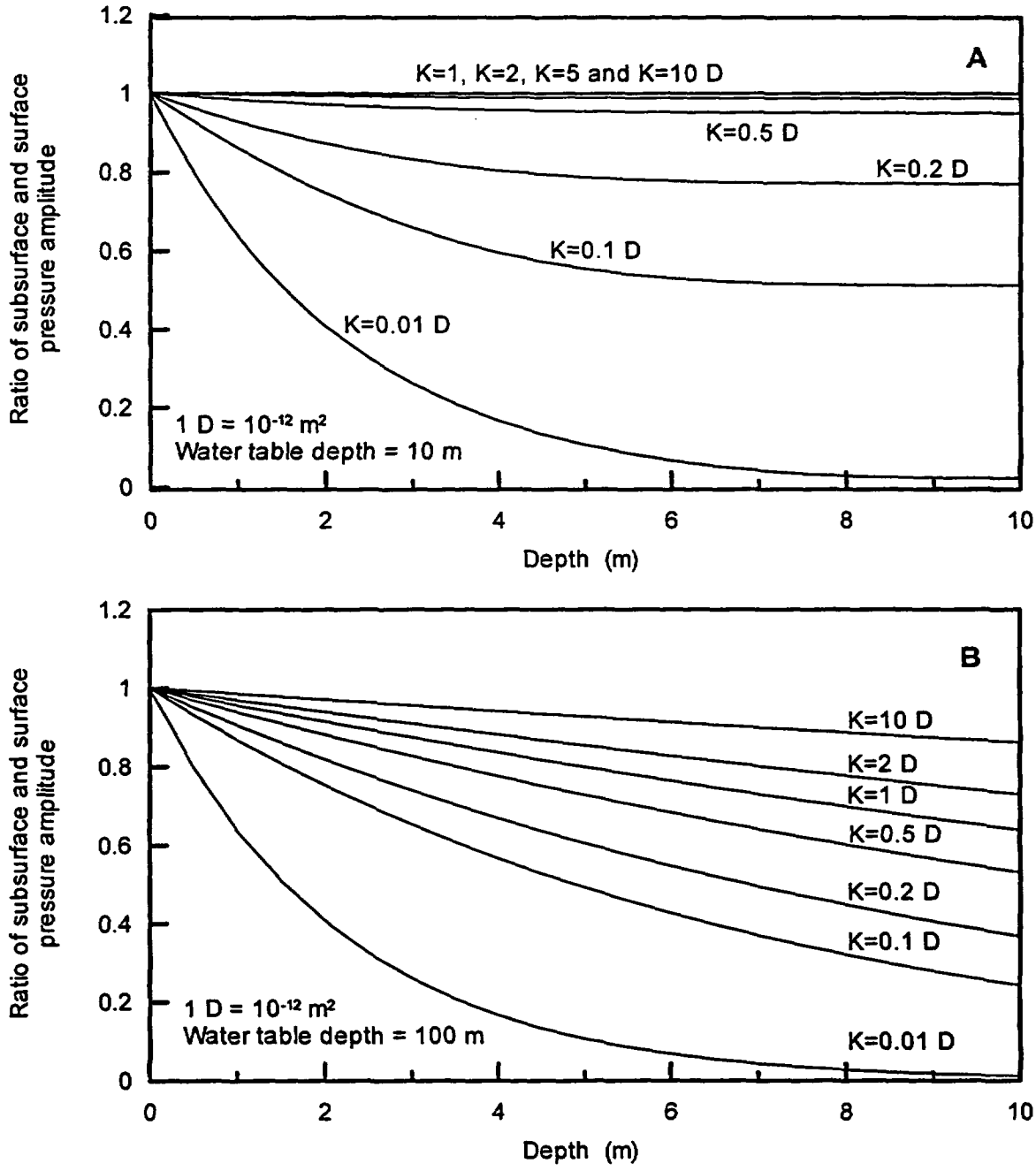

Figure C-6. Sensitivity of the pressure amplitude ratio to variations in permeability at water table depth (A) 10 m and (B) 100 m.

NRC FORM 335 (2-89) NRCM 1102, 3201, 3202

U.S. NUCLEAR REGULATORY COMMISSION

BIBLIOGRAPHIC DATA SHEET

(See instructions on the reverse)

1. REPORT NUMBER (Assigned by NRC, Add Vol., Supp., Rev., and Addendum Numbers, if any.)

NUREG/CR-5694

2. TITLE AND SUBTITLE

Results of Field Studies at the Maricopa Environmental Monitoring Site, Arizona

3. DATE REPORT PUBLISHED

MONTH	YEAR
June	1999

4. FIN OR GRANT NUMBER

JCN W6151

5. AUTHOR(S)

M.H. Young, P.J. Wierenga, A.W. Warrick, L.L. Hofmann, S.A. Musil, M. Yao, C.J. Mai, Z. Zou, and B.R. Scanlon

6. TYPE OF REPORT

Technical

7. PERIOD COVERED *(Inclusive Dates)*

04/95 - 02/99

8. PERFORMING ORGANIZATION - NAME AND ADDRESS *(If NRC, provide Division, Office or Region, U.S. Nuclear Regulatory Commission, and mailing address; if contractor, provide name and mailing address.)*

Department of Soil, Water and Environmental Science
University of Arizona
Tucson, AZ 85721

Bureau o f Economic Geology
University of Texas at Austin
Austin, TX 78713

9. SPONSORING ORGANIZATION - NAME AND ADDRESS *(If NRC, type "Same as above"; if contractor, provide NRC Division, Office or Region, U.S. Nuclear Regulatory Commission, and mailing address.)*

Division of Risk Analysis and Applications
Office of Nuclear Regulatory Research
U.S. Nuclear Regulatory Commission
Washington, DC 20555-0001

10. SUPPLEMENTARY NOTES

T.J. Nicholson, NRC Project Manager

11. ABSTRACT *(200 words or less)*

The purpose of this study was to evaluate issues related to alternative monitor ing strategies for sites containing low level radioactive wastes, consisting of a theoretical evaluation of monitoring strate gies and field studies. This NUREG/CR reports on the field activities and the results of the field experiments. The field si te, located at the Maricopa Agricultural Center (Maricopa, AZ) was designed for conducting controlled water flow and solute tra nsport studies, and for testing the strengths and weaknesses of four monitoring strategies designated as Monitoring Trench, M onitoring Island, Borehole Monitoring, and Geophysical Monitoring. Field instrumentation was extensive. Two experiments were conducted from Spring 1997 - Summer 1998, using a controlled drip-irrigation system for uniform application of wat er and solute. Water movement across the plot was spatially variable during Experiment 1, due mostly to variability in the in itial water content, and thus, the soil's hydraulic properties. Spatial variability of water movement was significantly reduced in surface soils (<1.5 m) between Experiments 1 and 2 (CV reduced from 41.8 % to 4.7 %). The flux-controlled water application led to more uniform hydraulic property fields, and thus, more uniform water movement. Most of the monitoring systems performe d well during the field experiments. An extensive data set was compiled and found useful for comparing monitoring strat egies and model testing.

12. KEY WORDS/DESCRIPTORS *(List words or phrases that will assist researchers in locating the report.)*

Hydrology
Borehole Monitoring
Field Experiments
Geophysical Monitoring
Instrumentation
Monitoring Islands
Monitoring Strategies
Monitoring Trenches
Solute Transport
Subsurface Monitoring
Unsaturated Zone
Vadose Zone Monitoring

13. AVAILABILITY STATEMENT

unlimited

14. SECURITY CLASSIFICATION

(This Page) unclassified

(This Report) unclassified

15. NUMBER OF PAGES

16. PRICE

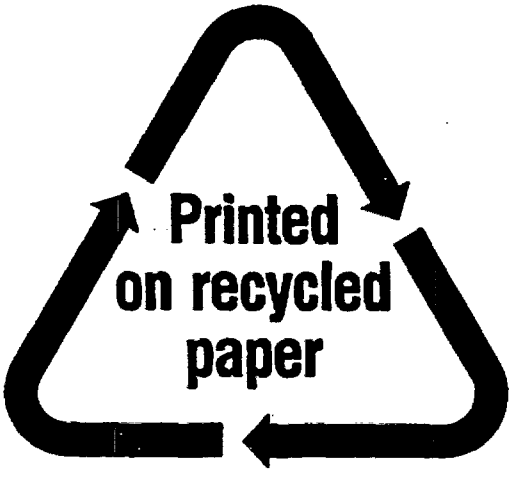

Federal Recycling Program

UNITED STATES
NUCLEAR REGULATORY COMMISSION
WASHINGTON, DC 20555-0001

OFFICIAL BUSINESS
PENALTY FOR PRIVATE USE, $300

SPECIAL STANDARD MAIL
POSTAGE AND FEES PAID
USNRC
PERMIT NO. G-67